1968-03

A study of the burning rates of composite solid propellants in acceleration fields.

Sturm, Edward John

Monterey, California. Naval Postgraduate School

A STUDY OF THE BURNING RATES OF COMPOSITE SOLID PROPELLANTS IN ACCELERATION FIELDS

EDWARD JOHN STURM

A STUDY OF THE BURNING RATES OF COMPOSITE SOLID PROPELLANTS IN ACCELERATION FIELDS

by

Edward John Sturm
Lieutenant, United States Navy
B.S., The Ohio State University, 1960

Submitted in partial fulfillment of the
requirements for the degree of
DOCTOR OF PHILOSOPHY
from the
NAVAL POSTGRADUATE SCHOOL
March 1968

ABSTRACT

The average burning rates of a series of composite solid propellants were measured in acceleration fields up to 1000 G using a combustion bomb mounted on a centrifuge. The propellants were burned at constant pressures of 500, 1000, and 1500 psia. Specially prepared motors allowed the study of the effect of simultaneous erosive and acceleration induced burning rate increases.

The burning rates of both the non-metallized and the majority of the metallized propellants were found to depend on acceleration. The effect of acceleration was found to depend on the basic burning rates of the propellants and the aluminum and oxidizer particle sizes and weight precentages. The burning rates of two very fast burning rate propellants were found to be essentially independent of acceleration. The erosion sensitivity of a propellant was found to decrease with increasing acceleration.

A model was developed which successfully correlates the experimental results obtained for the non-metallized propellants. The experimental results for the metallized propellants could not be correlated by either of two models proposed by other investigators. This result indicates that a more complex model is required to explain the observed acceleration effects for metallized propellants.

TABLE OF CONTENTS

CHAPTER		PAGE
I.	INTRODUCTION	19
II.	EXPERIMENTAL EQUIPMENT AND PROCEDURES	22
	Equipment	22
	Experimental procedures	39
III.	PROPELLANTS AND DATA REDUCTION	43
	Propellants	43
	Data reduction	55
IV.	EXPERIMENTAL RESULTS AND DISCUSSION	65
	Non-metallized propellants	66
	Metallized propellants	82
	Fast burning rate propellants	153
	Erosive burning rate propellants	157
V.	A MODEL FOR NON-METALLIZED PROPELLANTS	168
VI.	METALLIZED PROPELLANT CONSIDERATIONS	194
VII.	CONCLUSIONS	205
REFERENCES		209
APPENDIX I		212
APPENDIX II		214
APPENDIX III		217
APPENDIX IV		224

LIST OF TABLES

TABLE		PAGE
I.	Summary of Timing Wire Data for Aluminized P413 Propellant	99
II.	Erosive Burning Data	160
III.	Non-Metallized Propellant Data	185
IV.	Propellant Comparison.	186

LIST OF PLATES

PLATE		PAGE
1.	76 Inch Diameter Centrifuge	23
2.	Centrifuge Engine Control Console	24
3.	Centrifuge Instrumentation Control Console	26
4.	Centrifuge Nitrogen Charging Station	27
5.	Centrifuge Rotor Assembly	28
6.	Combustion Bomb-Surge Tank System	29
7.	Strand Holders Used in Burning Rate Experiments	31
8.	Strand Holder and Bomb Assembly	33
9.	Erosive Motor Mount Used in Erosive Burning Rate Experiments	34
10.	Pressure Sensing and Recording Circuit	36
11.	Ignition, Timing, and Continuity Test Circuits	38
12.	Ammonium Perchlorate Size Distributions	44
13.	-65/+80 Ammonium Perchlorate Size Distribution	45
14.	H-5 Aluminum Powder Size Distribution	47
15.	H-30 (-325) Aluminum Powder Size Distribution	48
16.	T-61 (-325) Alumina Size Distribution	49
17.	Motor Used in Erosive Burning Experiment	53
18.	Typical Pressure-Time Trace for Strand Experiment	57
19.	Black Powder Pressure-Time Trace with Isolation Valve Open	58
20.	Black Powder Pressure-Time Trace with Isolation Valve Closed	58
21.	Propellant Strand Length Versus Elapsed Burn Time for P401 Propellant	60
22.	Propellant Strand Length Versus Elapsed Burn Time for P411 Propellant	61
23.	Propellant Strand Length Versus Elapsed Burn Time for P413 Propellant	62

LIST OF FIGURES

FIGURE		PAGE
1.	Burning Rate Ratio Versus Acceleration for Propellant P410	68
2.	Burning Rate Ratio Versus Acceleration for Propellant P411	69
3.	Burning Rate Ratio Versus Acceleration for Propellant P420	70
4.	Burning Rate Ratio Versus Acceleration with Acceleration Vector Directed out of Propellant Surface	72
5.	Burning Rate Ratio Versus Acceleration as a Function of Initial Propellant Temperature for Propellant P410. .	74
6.	Comparison of Burning Rate Ratio Versus Acceleration for Three Non-Metallized Propellants at 500 psia.	75
7.	Comparison of Burning Rate Ratio Versus Acceleration for Three Non-Metallized Propellants at 1000 psia	76
8.	Burning Rate Ratio Versus Acceleration for Propellant P401 at 500 psia.	83
9.	Burning Rate Ratio Versus Acceleration for Propellant P401 at 1000 psia	84
10.	Burning Rate Ratio Versus Acceleration for Propellant P412 at 500 psia.	85
11.	Burning Rate Ratio Versus Acceleration for Propellant P412 at 1000 psia	86
12.	Burning Rate Ratio Versus Acceleration for Propellant P413 at 500 psia.	87
13.	Burning Rate Ratio Versus Acceleration for Propellant P413 at 1000 psia	88
14.	Burning Rate Ratio Versus Acceleration for Propellant P414 at 500 psia.	89
15.	Burning Rate Ratio Versus Acceleration for Propellant P414 at 1000 psia	90
16.	Burning Rate Ratio Versus Acceleration for Propellant P415 at 500 psia.	91
17.	Burning Rate Ratio Versus Acceleration for Propellant P415 at 1000 psia	92

FIGURE PAGE

18. Burning Rate Ratio Versus Acceleration for Propellant P421 at 500 psia. 93

19. Burning Rate Ratio Versus Acceleration for Propellant P421 at 1000 psia 94

20. Burning Rate Ratio Versus Acceleration for Propellant P423 at 500 psia. 95

21. Burning Rate Ratio Versus Acceleration for Propellant P423 at 1000 psia 96

22. Comparison of Burning Rate Ratio Versus Acceleration for Five Metallized Propellants at 500 psia 100

23. Comparison of Burning Rate Ratio Versus Acceleration for Five Metallized Propellants at 1000 psia. 101

24. Residue Mass Versus Acceleration for Propellant P412. . 104

25. Residue Mass Versus Acceleration for Propellant P413. . 105

26. Residue Mass Versus Acceleration for Propellant P414. . 106

27. Residue Mass Versus Acceleration for Propellant P415. . 107

28. Residue Mass Versus Acceleration for Propellant P421. . 108

29. Residue Mass Versus Acceleration for Propellant P423. . 109

30. Comparison of Residue Mass Versus Acceleration for One Inch Strand Lengths 110

31. Burning Rate Versus Acceleration for Six Aluminized Propellants at 500 psia 111

32. Burning Rate Versus Acceleration for Five Aluminized Propellants at 1000 psia. 112

33. Burning Rate Ratio and Aluminum Retention Ratio Versus Acceleration for P412 Propellant. 116

34. Burning Rate Ratio and Aluminum Retention Ratio Versus Acceleration for P413 Propellant. 117

35. Burning Rate Ratio and Aluminum Retention Ratio Versus Acceleration for P415 Propellant. 118

36. Burning Rate Ratio and Aluminum Retention Ratio Versus Acceleration for P421 Propellant. 119

37. Burning Rate Ratio and Aluminum Retention Ratio Versus Acceleration for P423 Propellant. 120

FIGURE PAGE

38. Extinguished Propellant Surface. 124

39. Closeup View of Extinguished Propellant Surface. 125

40. Burning Rate Versus Acceleration for Second Increment of Strand Length at 500 psia 128

41. Burning Rate Versus Acceleration for Second Increment of Strand Length at 1000 psia. 129

42. Average Residue Mass in Second Increment of Strand Length at 500 psia 130

43. Average Residue Mass in Second Increment of Strand Length at 1000 psia. 131

44. Comparison of Burning Rate Ratio Versus Acceleration for Propellants Containing Aluminum and Aluminum Oxide at 500 psia. 135

45. Comparison of Burning Rate Ratio Versus Acceleration for Propellants Containing Aluminum and Aluminum Oxide at 1000 psia 136

46. Comparison of Residue Mass Versus Acceleration for Propellants Containing Aluminum and Aluminum Oxide . . 137

47. Comparison of Solids Retention Ratio Versus Acceleration for Propellants Containing Aluminum and Aluminum Oxide 138

48. Burning Rate Ratio Versus Acceleration as a Function of Initial Propellant Temperature for Propellant P413. 140

49. Predicted Burning Rate Ratio Versus Acceleration Ratio for Two Particle Size Distribution 145

50. Geometry of Glick's Analytical Model 149

51. Burning Rate Ratio Versus Acceleration for Propellant 2A 154

52. Burning Rate Ratio Versus Acceleration for Propellant J6 155

53. Burning Rate Versus Distance from Fore End of Erosive Motor. 158,159

54. Comparison of Burning Rate Versus Distance from Fore End of Erosive Motor 161

55. Erosive Burning Rate Ratio Versus Mass Flux as a Function of Acceleration Level 164

FIGURE PAGE

56. Erosive Constant K Versus Burning Rate 166

57. Phalanx Flame at Steady State. 170

58. Critical Particle Diameter Versus Acceleration 175

59. Values of J Versus Critical Particle Diameter. 181

60. Comparison of Theory with Experiment for P410 Propellant 189

61. Comparison of Theory with Experiment for P411 Propellant 190

62. Comparison of Theory with Experiment for P420 Propellant 191

63. Comparison of Agglomerate and Ram Geometrical Effects. . 196

64. The Agglomerate Heat Transfer Model. 218

TABLE OF SYMBOLS

Latin Symbols

a	Acceleration
a_o	Standard acceleration of gravity
A	Constant
A_i	Interaction area; defined by Equation 8 (Figure 50)
A_s	Area swept by a pit on the propellant surface; defined by Equation 10 (Figure 50)
b_1, b_2	Constants
B	Mass flux per unit port area; defined by Equation I-4.
c	Subscript denoting conditions which result in a particle of mass mean size being retained on the propellant burning surface
C, C_1	Constants
dA	Area element of conical pit surface (Figure 63a)
dA_p	Projected area element of conical pit surface (Figure 63a)
d_{f_v}	Characteristic dimension of a pocket of fuel vapor
d_p	Diameter of an oxidizer particle
d_{p_c}	Diameter of an oxidizer particle of critical size
D	Diffusion coefficient
$\dot{E}_r$	Energy rate required to increase the burning rate above the base rate
$\dot{E}_s$	Energy rate supplied to the propellant surface by metal combustion
f	Fraction of combustion energy release transferred to the propellant surface
F_b	Body force
F_d	Drag force
G	Acceleration in gravitational units a/a_o

h_c	Energy released by combustion of AP oxidizer particles
h_v	Energy required to heat and vaporize a unit mass of propellant
H	Fraction of the metal additive that is agglomerated and consumed by combustion on the propellant surface
H^*	Fraction of the metal additive on the sides of a pit that is agglomerated and burned; defined by Equation 16
J	Fraction of small AP oxidizer particle mass released by decomposition on the propellant surface
K, K_1	Constants
K_{ag}	Thermal conductivity of an agglomerate
K_g	Thermal conductivity of propellant gas phase
L	Propellant strand length
L^*	Energy transferred to propellant surface per unit mass of aluminum particle burned
L_1	Length of a nominal 1.0 inch long strand
L_2	Length of a nominal 2.25 inch long strand
m	Mass
$\dot{m}_a$	Rate of metal addition to an aluminum agglomerate; defined by Equation 11
m_{r_1}	Residue mass of a nominal 1.0 inch long strand
m_{r_2}	Residue mass of a nominal 2.25 inch long strand
$m_{r_{1-2}}$	Average residue mass present on the surface of a strand during the second increment of strand burning; defined by Equation 3
M	Molecular weight
n	Constant
N_s	Number of pits per unit area of the mean propellant surface
p	Pressure
$\dot{q}_a$	Heat transfer rate through an agglomerate
$\dot{q}_{prop}$	Heat transfer rate to the propellant surface without the interposition of an agglomerate between the surface and the flame zone

r	Burning rate with acceleration
r_a	Rate an agglomerate proceeds into the solid phase of the propellant
r_e	Erosive burning rate
r_o	Burning rate without acceleration
$r_{x=o}$	Burning rate at the fore end of an erosive motor
r_1	Average burning rate of a nominal 1.0 inch long strand
r_2	Average burning rate of a nominal 2.25 inch long strand
r_{1-2}	Average burning rate for the second increment of strand length; defined by Equation 2
R	Universal gas constant
t	Time
T	Temperature
T_g	Mean temperature of the gas phase
T_o	Initial propellant temperature
V_g	Mean velocity of the combustion products away from the propellant surface
W_m	Propellant metal loading weight percentage
W_o	Propellant small AP oxidizer loading weight percentage
x	Distance from fore end of an erosive motor
y	Distance above the propellant burning surface

Greek Symbols

α	Constant in erosive burning rate ratio equation; defined by Equation 19
β	Pitting parameter $(N_s \pi \xi_a^2)^{-1} \cos \theta_c$
ΔH_c	Lower heating value for the combustion of the metal agglomerate in the products of combustion of the binder and oxidizer
$\Delta \dot{Q}$	Heat transfer to the propellant surface; defined by Equation 27

$\Delta\rho$	Characteristic density difference between the fuel and oxidizer particles
ε	Erosive burning ratio $r_e/r_{x=o}$
η	$W_o\ h_c/h_v$
θ_c	Semi-vertex angle of a conical pit in the burning surface (Figure 50)
μ_g	Viscosity of the propellant gas phase
ξ_a	Radius of an agglomerate (Figure 50)
ξ_{p_c}	Radius of a particle of critical size
ξ_{p_m}	Radius of a particle of mass mean size
Π	Propellant parameter, $W_m\ \Delta H_c/2h_v$
ρ_a	Density of an agglomerate
ρ_g	Mean density of the gas phase
ρ_p	Density of an AP oxidizer particle
ρ_s	Density of the solid propellant phase
σ	Standard deviation
τ_b	Burning time of an aluminum particle
Φ	Angle between the acceleration vector and the normal to the propellant burning surface (Figure 50)

ACKNOWLEDGMENTS

The assistance of several persons was necessary to successfully complete the work reported here. The author wishes to express his appreciation to: Mr. James Diebold of the Naval Weapons Center and Messrs. Len Caveny and B. K. Hodge of the Thiokol Chemical Corporation for supplying the propellants; Mr. James Crump of the Naval Weapons Center for photographing the propellants; Mr. Melvin Lucy of NASA Langley for supplying the extinguished propellant slabs; Mr. Cecil Gordon for his assistance with the installation of the centrifuge instrumentation; Miss Sherrie May and Mr. Pat Hickey for the graphics work; and Mr. Ted Dunton for his advice and help with the construction of the erosive motors.

The author is particularly indebted to: his wife, Annette, for assistance in the preparation of the manuscript and her patience and understanding during the period of this work; Mr. Edward Michelson for his assistance with the conduct of the experiments; and his advisor and teacher, Dr. Roy Reichenbach, for his guidance during the course of the experimental program and his help in the reporting of the work.

CHAPTER I

INTRODUCTION

Currently there are a number of applications in which the solid internal burning grain of a rocket motor is subjected to an acceleration force directed into the propellant burning surface. Three typical applications are: spin stabilized flight of rocket propelled vehicles, rocket assisted flight of gun launched artillery shells, and maneuvering flight of rocket propelled vehicles. The inflight performance of motors used in these applications has been found to vary considerably from the static performance of the motors. Typically, motor inflight performance is characterized by shorter burn times, higher chamber pressures, and lower total impulses [1,2].[1]

It is known that the radial acceleration imposed on the burning surface of these propellants causes the propellant burning rate to increase [3]. The degradation of motor performance has been attributed in part to this acceleration induced change in propellant burning rate. Several experimental investigations have been conducted to gain an insight into the mechanisms which control the observed burning rate increase. The review and abstracting of material pertinent to the effects of acceleration on solid propellant performance are presented in References 4 and 5.

Post-fire inspections of motors containing metallized propellants have revealed the presence of metal and/or metal oxide residue in the motor cases. Generally the amount of residue increased with acceleration and typically comprised 10 to 18 per cent of the initial

---

[1] Numbers in brackets refer to References listed on page 209.

metal content of the propellant for radial accelerations of the order of 150 G [1]. The propellant burning rate and the retention of metal and/or metal oxide are interrelated since the propellant burning mechanism is altered if hot metal and/or metal oxide particles remain on the burning surface, and the retention of metal and/or metal oxide is dependent on the mass flux of combustion products away from the burning surface.

In a spinning rocket motor that portion of the propellant grain nearest the nozzle end of the motor (the aft end of the motor) will experience an increased burning rate not only from the acceleration induced effect but also from the effect caused by the flow of hot gases generated by the burning propellant at the head end (or fore end) of the motor. This increase in propellant burning rate observed in the presence of a high velocity gas flow parallel to the propellant surface is called erosive burning. The relative importance of the acceleration induced and erosive induced effects at various acceleration levels was not known prior to this investigation.

Although progress has been made toward an understanding of some aspects of burning rate augmentation in acceleration fields, it was believed that additional experimental studies with well controlled propellant parameters would be valuable. A series of propellants was formulated to assist in the determination of the importance of some of the propellant parameters that could be controlled to minimize the effects of acceleration.

The objectives of this investigation were three-fold. The first objective was to obtain the quantitative effect of acceleration on the burning rate of the series of propellants as a function of propellant composition, acceleration level, pressure level, initial propellant

temperature, and time. The second objective was to obtain quantitative information on the amount of metal and/or metal oxide residue retained in the motor case as a function of propellant composition, acceleration level, pressure level, and propellant burning rate. The third objective was to ascertain the relative importance of acceleration induced and erosive burning induced increases in the propellant burning rate as a function of acceleration level.

Conventional strand burning techniques in conjunction with a centrifuge were used to study the effect of acceleration alone on the propellant burning rate. The study of the relative importance of the acceleration induced and erosive burning induced increases in burning rate was accomplished by using specially prepared motors in which the propellant grain was subjected simultaneously to erosive burning effects and an acceleration field directed normal to the propellant surface.

In Chapter II is presented a discussion of the centrifuge and associated equipment and the experimental techniques utilized in this study. The propellant formulations, the preparation of propellant strands, the erosive motor fabrication, and the method of data reduction are presented in Chapter III. In Chapter IV the experimental results are presented and discussed. The pertinent theoretical models are described and evaluated in light of the experimental results. A mathematical model for non-metallized propellants is developed and discussed in Chapter V. Chapter VI contains a discussion of some theoretical considerations relating to the acceleration induced burning rate augmentation of metallized propellants. Recommendations for future work are also presented.

CHAPTER II

EXPERIMENTAL EQUIPMENT AND PROCEDURES

I. EQUIPMENT

General

The burning rate experiments were conducted at the Naval Postgraduate School's Centrifuge Test Facility. The facility consisted of a 76 inch diameter centrifuge, two remote control consoles, and a nitrogen charging station.

The centrifuge, shown in Plate 1, was installed in an experimental test cell at the school's rocket laboratory. It was designed by Anderson [3,6] to make possible the study of solid propellant burning rates at essentially constant pressure and acceleration levels. The propellants were burned in a strand configuration in a combustion bomb mounted on the arm of the centrifuge. A 1565 cubic inch combustion bomb and surge tank volume ensured essentially constant pressure during burning. The use of relatively short, generally 2.25 inches long, propellant strands at a centrifuge radius of 3 feet limited the total acceleration change during burning to less than 7 per cent of the original value. Moreover, the strand configuration eliminated the effects of erosive burning and the possible gaseous vortices generated in the grain port of a motor configuration. Instrumentation provided for burning rate measurement consisted of a pressure transducer to sense pressure within the combustion bomb and two timing wire circuits.

The centrifuge was powered by a conventional automobile engine. The speed of the centrifuge was controlled from the engine control console shown in Plate 2. In addition the automobile engine

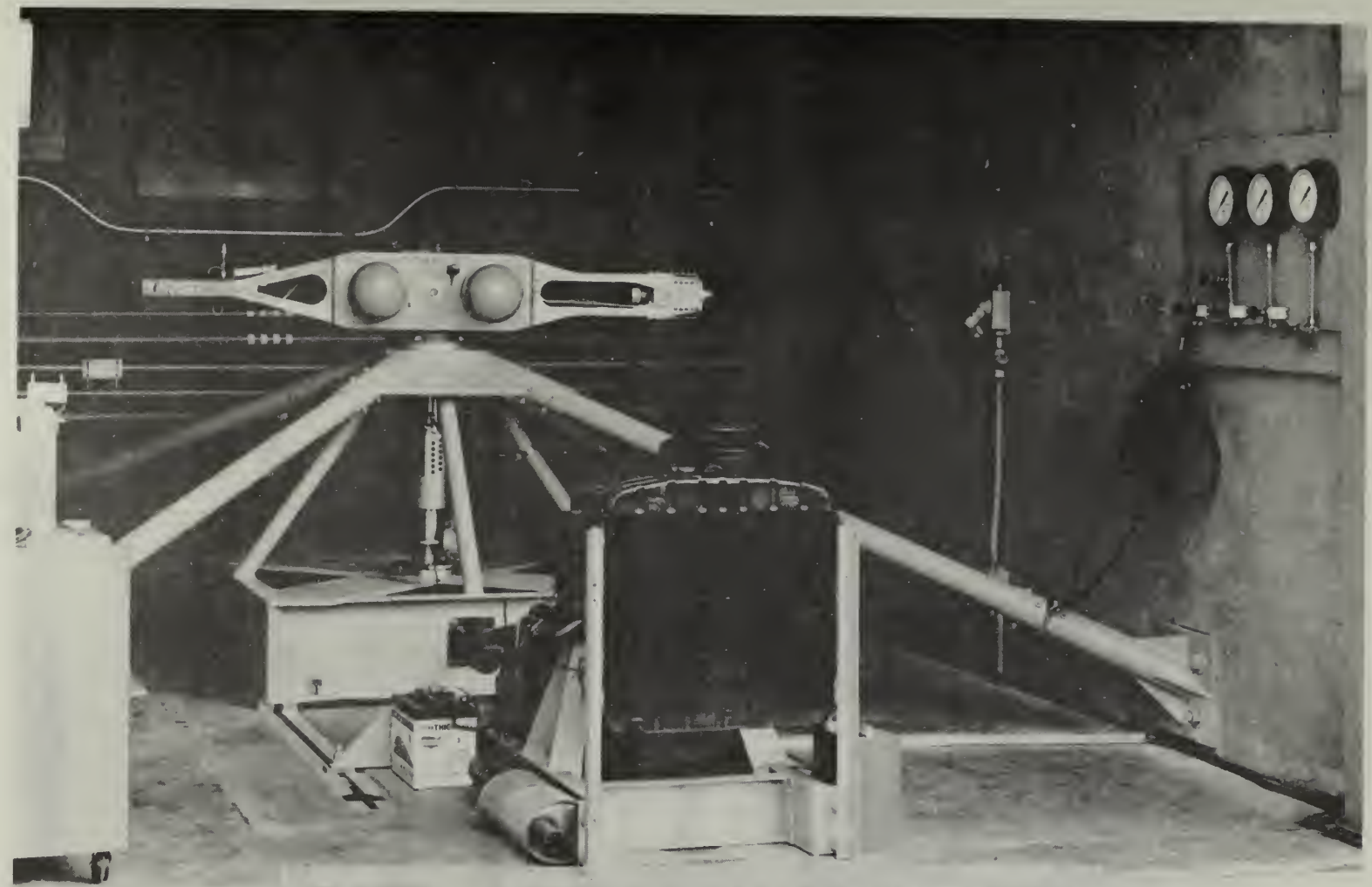

PLATE I 76 INCH DIAMETER CENTRIFUGE

PLATE 2
CENTRIFUGE ENGINE
CONTROL CONSOLE
12 VOLT
INSTRUMENTS
ENGINE
IGNITION

instrumentation was monitored at the engine control console. The burning rate instrumentation and recording equipment were controlled at the instrumentation console shown in Plate 3. The engine control console and the instrumentation console were located in the control and instrumentation room of the rocket laboratory. The combustion bomb-surge tank system could be pressurized to any level up to 3000 psia by the nitrogen charging system. The system was controlled from the nitrogen charging station shown in Plate 4.

The reader is referred to References 3 and 6 for detailed information concerning the centrifuge and related equipment. The information presented in the following paragraphs is a summary of the information contained in these references and is included for completeness and to report modifications made to the equipment.

Centrifuge

The centrifuge base structure was of a welded and bolted construction. The centrifuge shaft rotated in two bearings. The lower bearing was a SKF self-aligning double-row ball bearing, and the upper bearing was a SKF self-aligning spherical roller bearing.

The structural parts of the rotor assembly were made of aluminum and were bolted together with aircraft quality bolts. A combustion bomb, surge tanks and associated tubing, fittings and valves, pressure transducer, and counterweights were fastened to the main structural members of the rotor assembly. The rotor assembly, shown in Plate 5, was secured to the centrifuge shaft by means of a pivot pin.

The combustion bomb-surge tank system, shown schematically in Plate 6, was wholly contained in the rotor assembly. The system consisted of a 115 cubic inch stainless steel combustion bomb, two 725 cubic

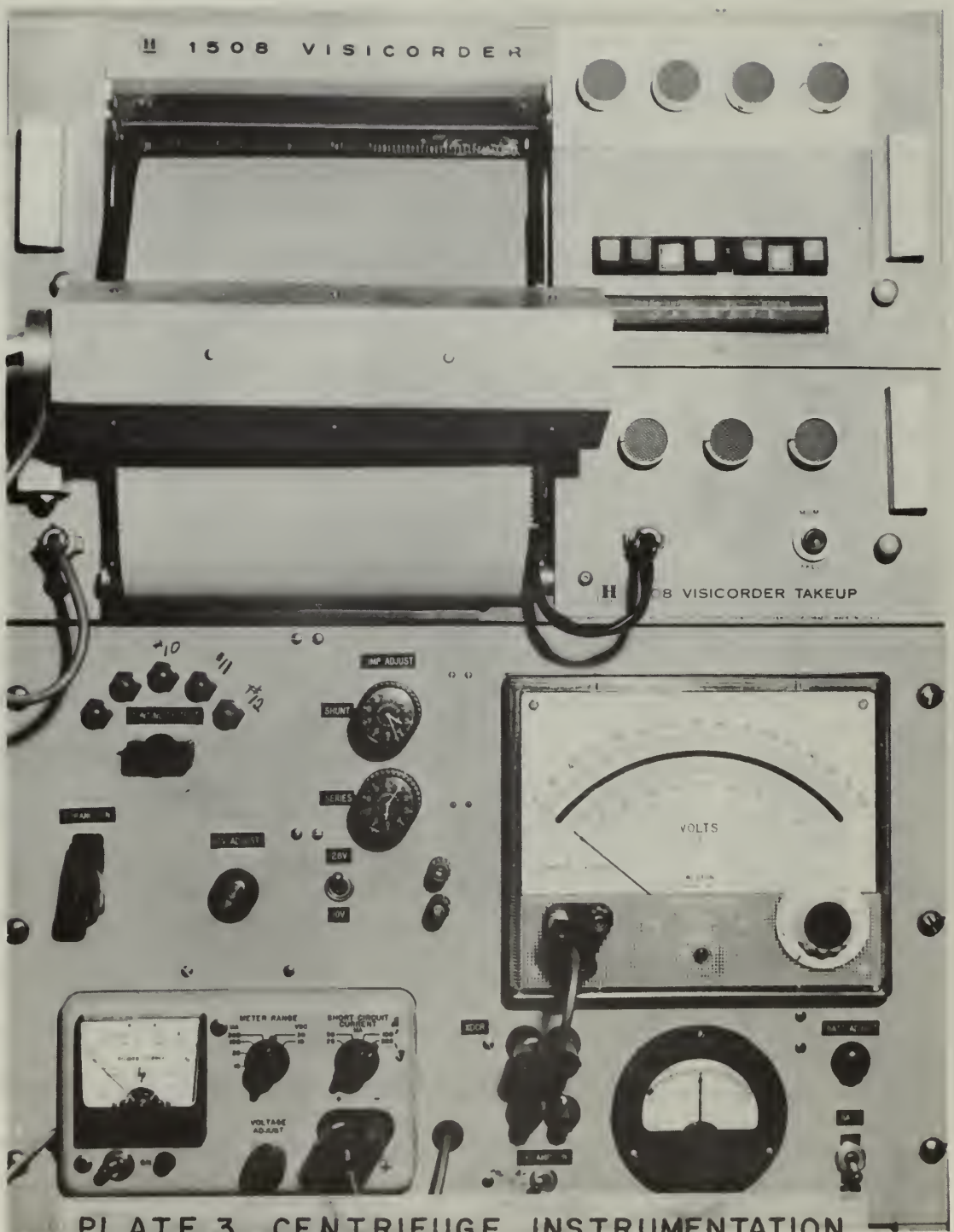

PLATE 3 CENTRIFUGE INSTRUMENTATION CONTROL CONSOLE

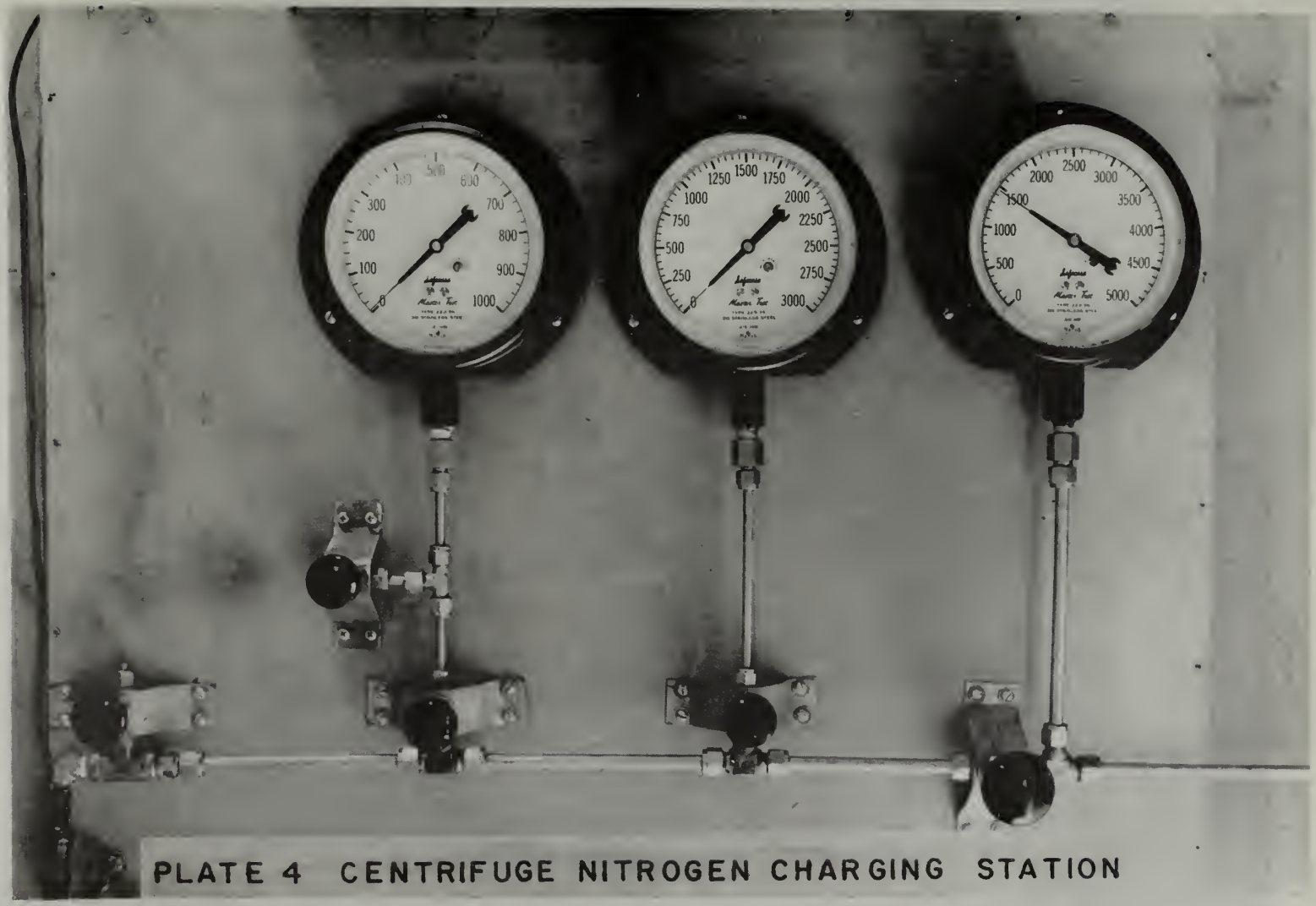

PLATE 4 CENTRIFUGE NITROGEN CHARGING STATION

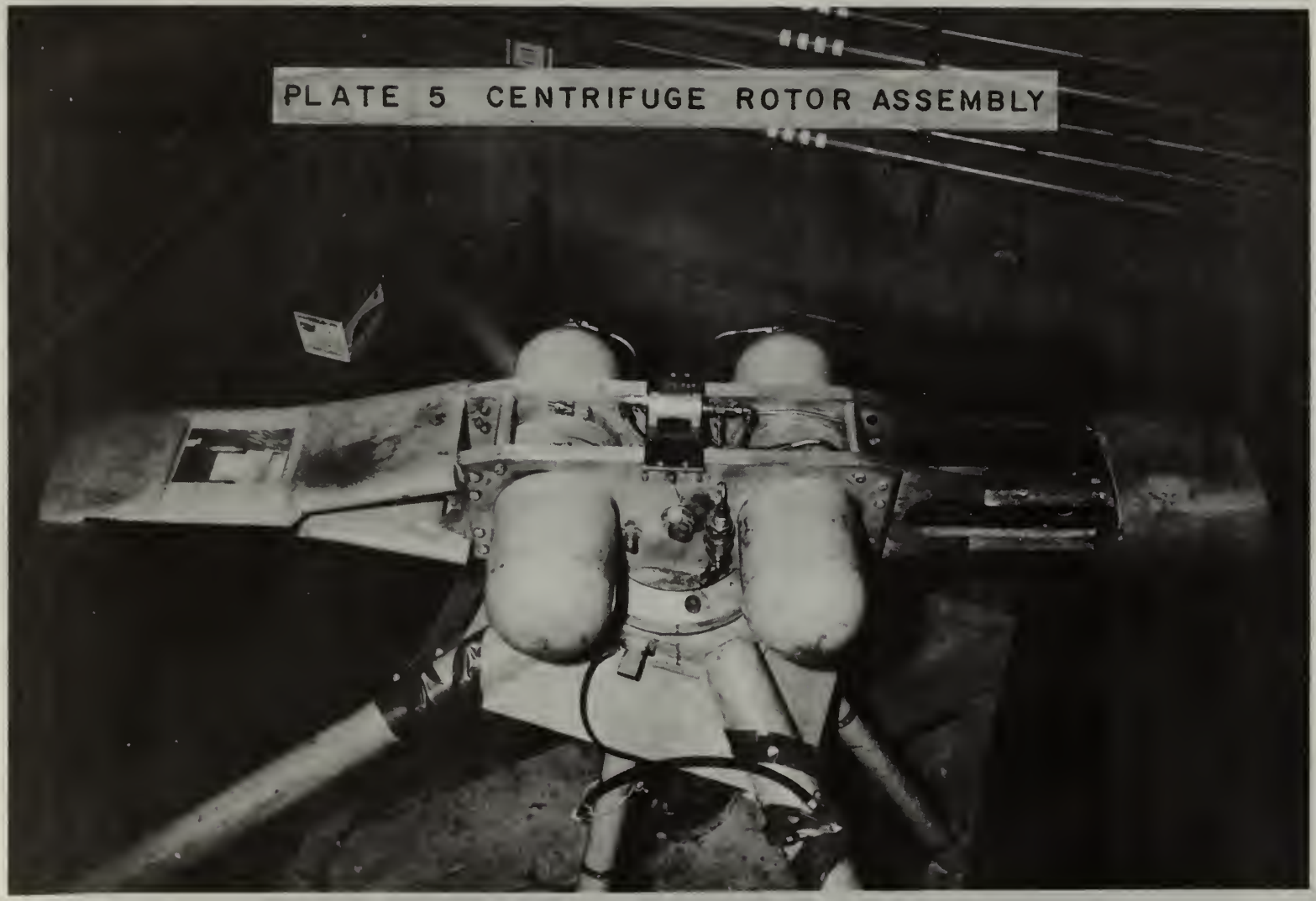
PLATE 5 CENTRIFUGE ROTOR ASSEMBLY

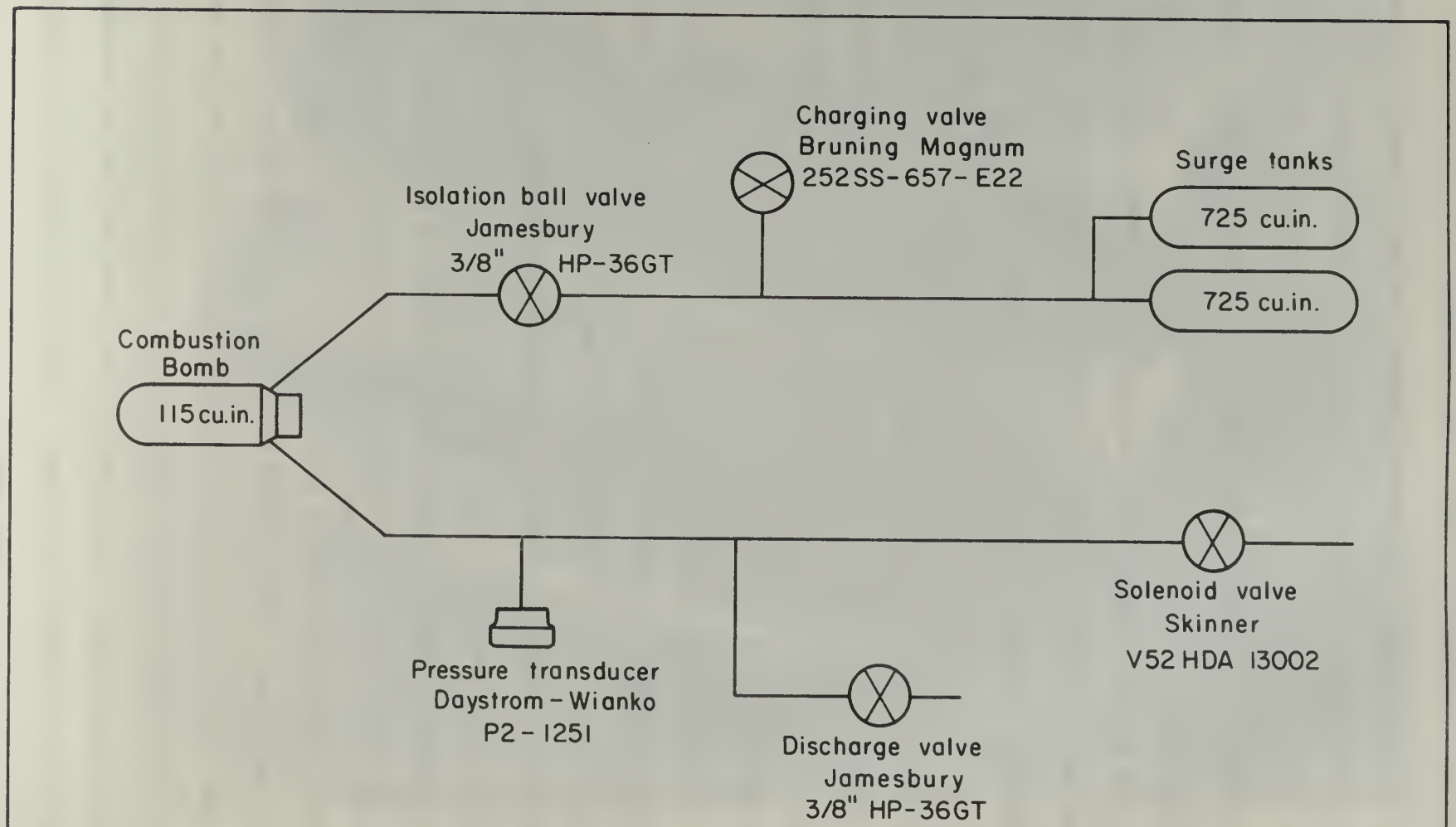

PLATE 6 COMBUSTION BOMB - SURGE TANK SYSTEM

inch 6061-T6 aluminum Navy SCUBA tanks, and associated valves and tubing. The system was pressurized through a quick disconnect fitting located between the isolation ball valve and the surge tanks. The system could be depressurized by a hand operated discharge valve or by a solenoid valve actuated by a switch on the engine control console.

Strand Holders

The strand holders, shown in Plate 7, were basically the same as those described in Reference 3. The basic components were a machined aluminum plug, a canvas phenolic slab and strand support, an insulation sheet, and a gland seal. The aluminum plug was a slip fit in the throat of the bomb, and the flared edge at the top of the plug was a metal-to-metal fit relative to the bomb throat seat. Thus the strand holder was supported in high radial acceleration fields, and extrusion of the O-ring seal was avoided.

The slab and strand support provided structural support for the propellant sample. The slab was fastened to the aluminum plug with two flat head screws, and the strand support was bonded to the slab with high temperature epoxy. Number 6-32 brass machine screws were used for ignition circuit terminals. The terminals were connected to an Amphenol plug by number 20 enameled copper magnet wire which was bonded to the back of the slab with epoxy to protect it from contact with combustion products. The canvas phenolic slab was protected from direct contact with the propellant exhaust flame by a 3/32 inch thick phenolic insulation sheet. The insulation sheet covered the entire slab and was held in place by the ignition wire terminal nuts and a number 3-48 screw near the aluminum plug. The strand holders were modified to accommodate strands equipped with timing wires. Two pairs of timing wire terminals and the necessary wiring were added.

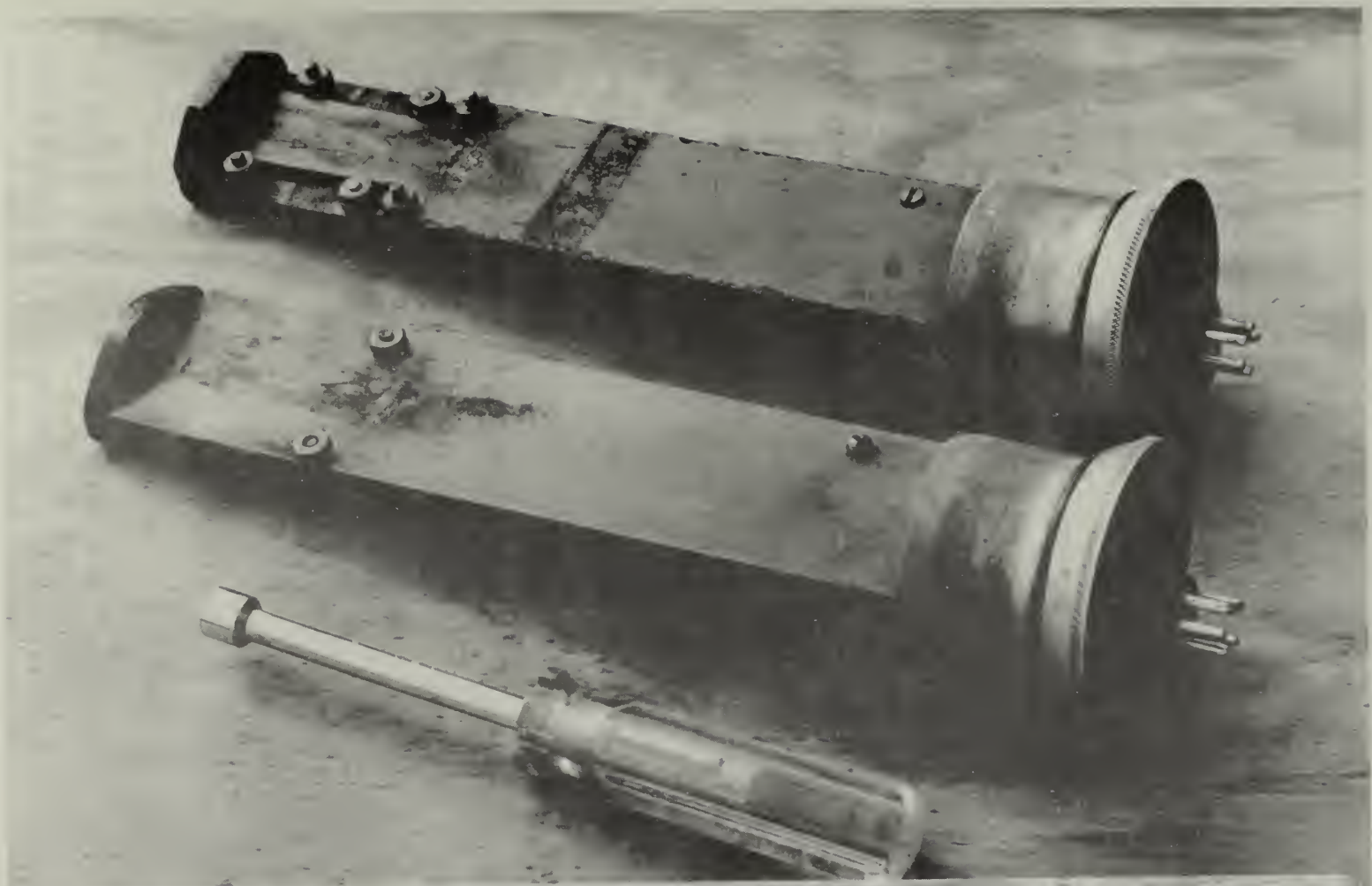

PLATE 7 STRAND HOLDERS USED IN BURNING RATE EXPERIMENTS

The propellant sample was fastened to the strand holder so that the longitudinal axis of the strand was parallel to the imposed acceleration field. The strands were generally ignited at the end of the strand facing the centrifuge axis of rotation so that the directions of strand burning and the imposed acceleration field were the same. This orientation of the acceleration field relative to the strand burning direction is defined as normal and into the propellant burning surface. A few strands were ignited at the outboard end of the strand. In this instance the strand is defined as being subjected to an acceleration field normal and away from the propellant burning surface. A strand holder in the combustion bomb with a propellant sample in the position in which it is subjected to an acceleration field normal and into the burning surface is shown schematically in Plate 8.

Erosive Motor Mount

The erosive motor mount shown in Plate 9 was designed and fabricated so that a 2.75 inch long propellant sample could be burned erosively with the acceleration vector directed normal to the propellant burning surface. The basic components of the motor holder were a machined aluminum plug, a canvas phenolic mounting plate and holder arm, and a gland seal. The aluminum plug and a gland seal were the same type as used with the strand holders.

A motor containing a propellant sample was mounted on the mounting plate equipped with six number 2-56 machine screws which served as timing and ignition circuit terminals. The plate could be rotated through a 90 degree angle. The axis of rotation was offset from the center of gravity of the motor-plate combination so that the centrifugal forces would keep the motor in a position normal to the holder arm.

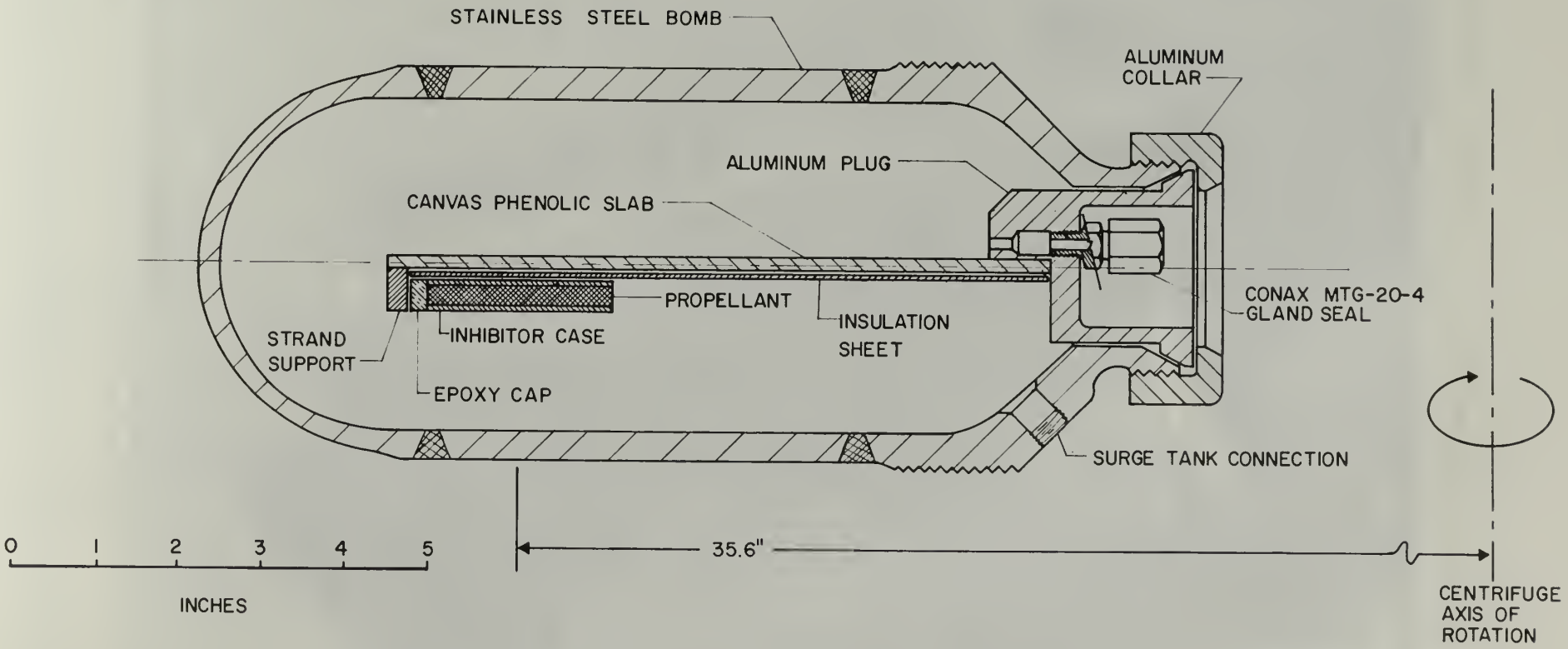

PLATE 8 STRAND HOLDER AND BOMB ASSEMBLY

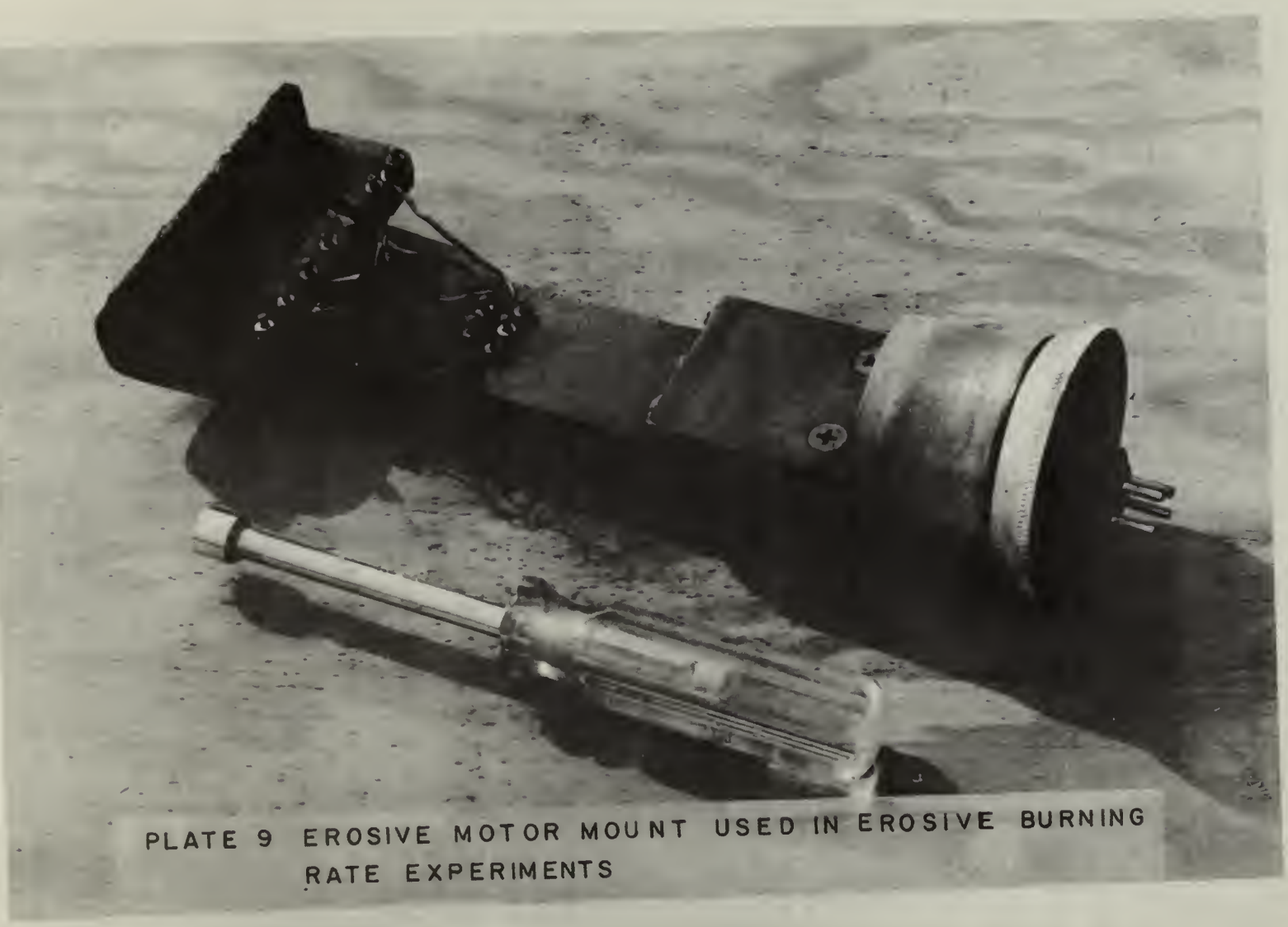

PLATE 9 EROSIVE MOTOR MOUNT USED IN EROSIVE BURNING RATE EXPERIMENTS

The mounting plate and motor were positioned parallel to the holder for insertion through the 1.875 inch diameter throat of the combustion bomb. After the motor and mounting plate had cleared the throat of the combustion bomb, they were rotated through a 90 degree angle so that the acceleration vector was directed normal to the propellant burning surface. After the motor had been fired, the motor-plate combination was rotated parallel to the holder arm and removed from the combustion bomb.

Instrumentation and Electrical

A Lebow Model 6109-12 instrumentation slip ring assembly mounted on the centrifuge shaft provided instrumentation to the rotor arm. Pressure in the combustion bomb was sensed by a Daystrom-Wiancko Type P2-1251 variable reluctance pressure transducer. The transducer was mounted on the rotor arm over the center of rotation to minimize acceleration effects. Transducer excitation voltage was provided by a Hewlett-Packard Model 721A power supply.

Pressure change in the combustion bomb was recorded on a Honeywell Model 1508 Visicorder. A bucking voltage was applied to the transducer output with a 6 volt dry cell battery and a potentiometer. The resulting small signal then went to an Astro Data Model 885 wideband differential d.c. amplifier. Amplifier output was fed to a M400-120 galvanometer in the Visicorder through signal conditioning variable resistances. These variable resistances permitted adjustment of Visicorder chart span and galvanometer damping. Zero adjustment was accomplished by adjusting the bucking voltage potentiometer setting. A schematic drawing of the pressure circuit is shown in Plate 10. A Hewlett-Packard Model 211A square wave generator was used to provide a time base on the Visicorder chart.

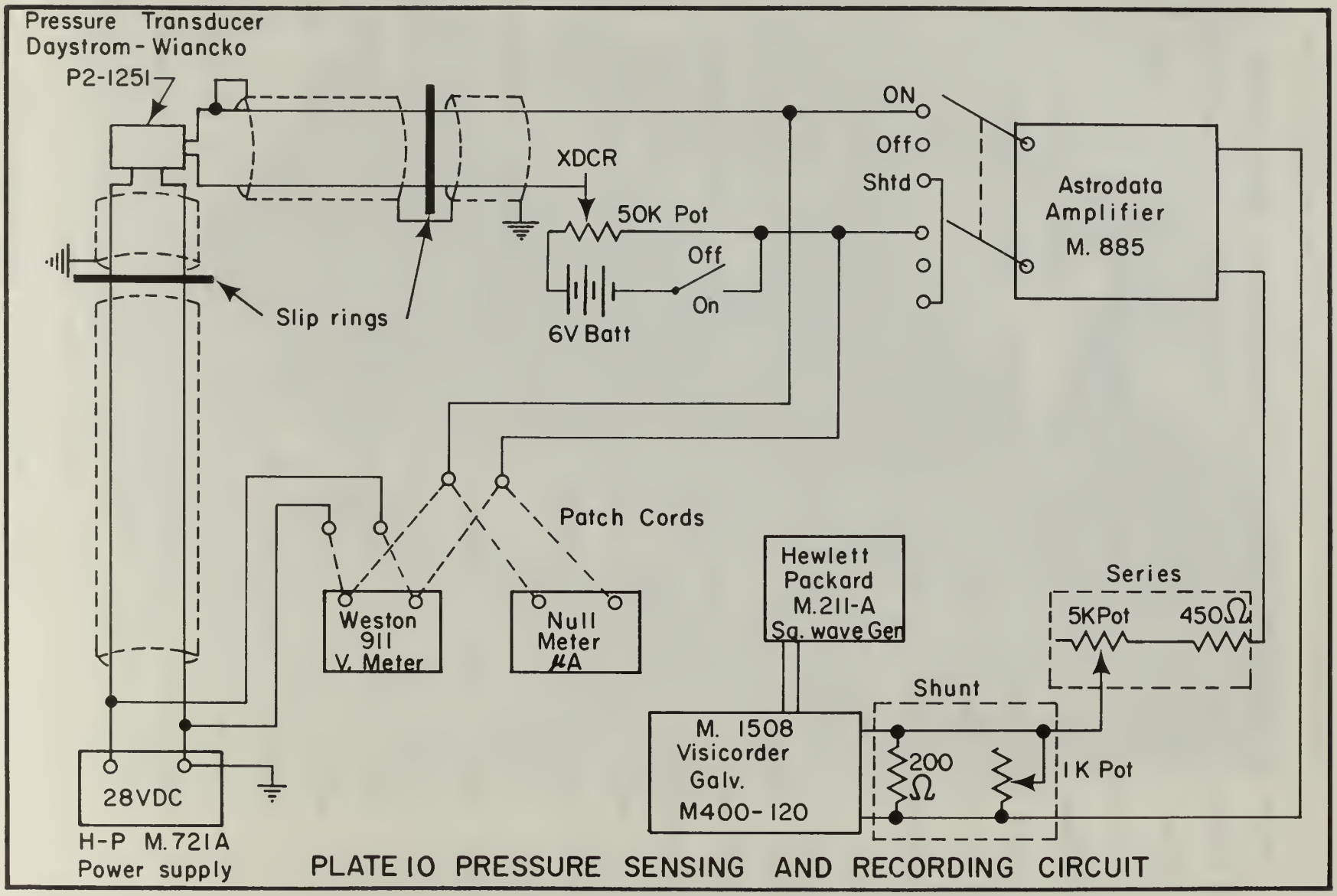

PLATE 10 PRESSURE SENSING AND RECORDING CIRCUIT

The 20 pulses per second output signal of the generator drove a M200-120 galvanometer in the Visicorder. The output of the generator was calibrated periodically with a Tektronix Type 184 time mark generator (accuracy ± 0.001 per cent).

Average burning rate of a propellant strand was calculated by dividing the initial strand length by the elapsed time of burning as determined from the pressure-time trace. Pyro-fuse timing wires (0.002 inch diameter) spaced a known distance apart were used as a secondary means of determining the burning rate. When a timing wire was intact, it closed its timing circuit which resulted in a voltage drop across a M200-120 galvanometer in the Visicorder. When a timing wire broke, it opened its timing circuit which caused a rapid deflection of the galvanometer. This deflection was recorded on the Visicorder chart. Power for the timing circuits was supplied by a 6 volt dry cell battery.

The propellant sample was ignited by means of a small amount of black powder and a number 32 nichrome wire in series with a variable resistance. The variable resistance was adjusted so that the ohmic heating of the nichrome ignition wire was sufficient to ignite the black powder without melting the ignition wire. Power was supplied from the 12 volt d.c. bus. Continuity of the ignition and timing circuits was checked by means of a rotary switch located on the instrumentation console. The rotary switch applied 6 volt d.c. power to three continuity test lamps. A schematic drawing of the ignition, timing, and continuity test circuits is shown in Plate 11.

Centrifuge rpm instrumentation consisted of a SPACO type PA-1 magnetic pickup and a Berkeley Model 5545 EPUT meter. The engine electrical system was a standard 6 volt automobile system.

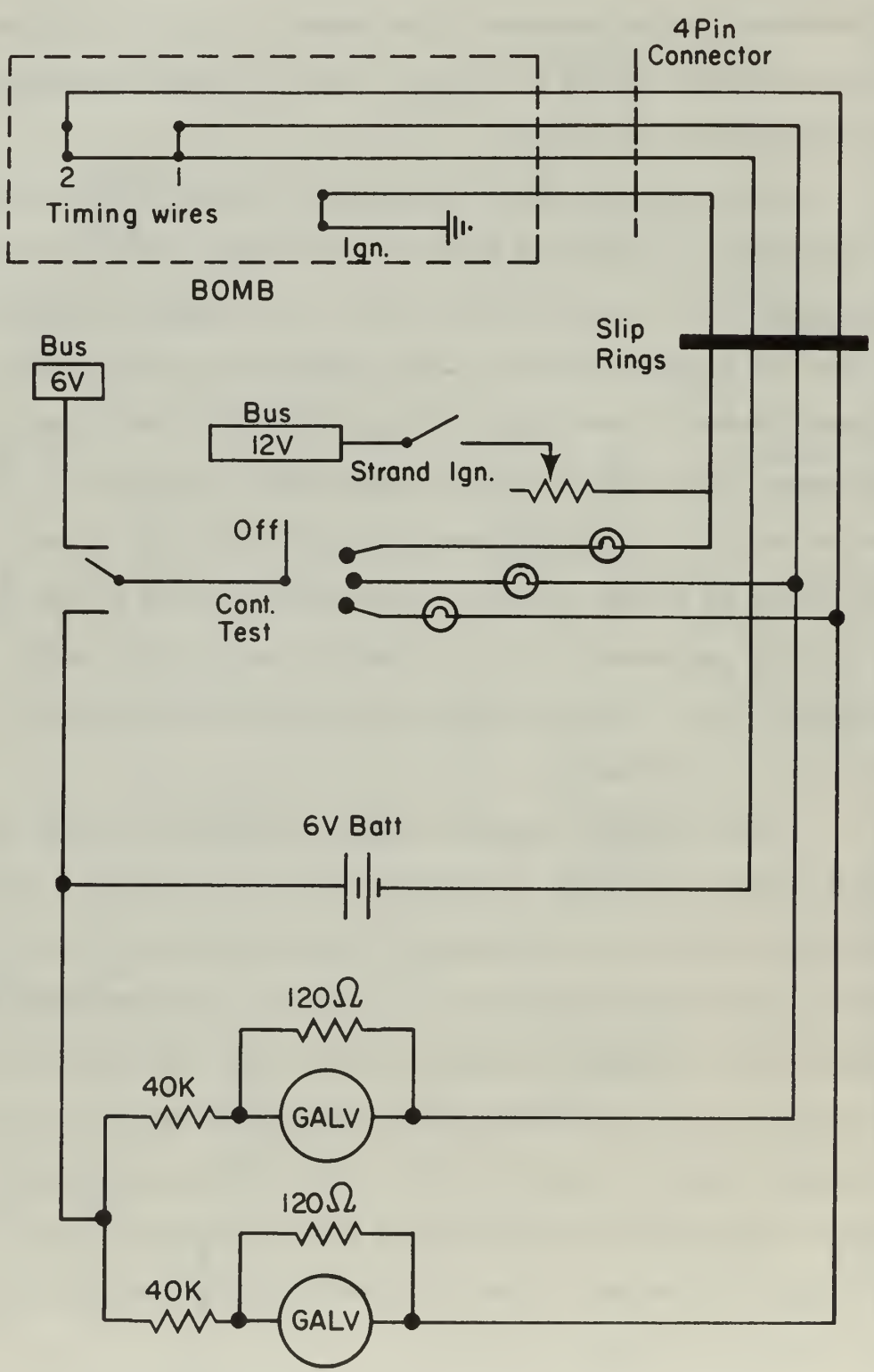

PLATE II IGNITION, TIMING, AND CONTINUITY TEST CIRCUITS

Related Systems

The nitrogen charging system consisted of a four bottle manifold, regulator, gauge panel, and flexible charging hose. On the gauge panel were mounted three Marsh Type 220-35 pressure gauges with pressure ranges of 0-1000 psig, 0-3000 psig, and 0-5000 psig. Suitable valves permitted the selection of the appropriate gauge for use in pressurizing the surge tanks and combustion bomb.

The centrifuge was powered by a 1954 Chevrolet engine with a 1950 Powerglide transmission. Power was transmitted to the centrifuge via an automobile drive shaft and a Boston VR158 spiral miter box. A double strand roller chain flex coupling transmitted the torque from the miter gear vertical output shaft to the centrifuge shaft. The engine throttle setting was controlled by an Adel ISOdraulic remote control system. The centrifuge was equipped with a hydraulically actuated disc-type brake.

II. EXPERIMENTAL PROCEDURES

General

Approximately 30 minutes prior to the first experiment of the day all instrumentation was turned on to allow for warm up and stabilization. At the end of this period the pressure transducer excitation voltage was set at 28 volts using a Weston Model 911 voltmeter. The first strand was then removed from the refrigerator-oven and placed in the combustion bomb. Continuity of the strand ignition circuit was checked. The rotor discharge valve was closed, the surge tank isolation valve opened, and the charging hose connected to the charging valve on the rotor. The charging valve at the nitrogen charging station was opened, and the surge tank-combustion bomb system was pressurized to the desired gauge pressure at the charging station.

The gauge pressure was determined in the following manner:

$$psig = psia - 15 - \Delta p + 8$$

where:

psig = gauge pressure at the charging station

psia = absolute pressure in the bomb for the burning rate experiment

15 (psia) = approximate atmospheric pressure

Δp = correction for centrifugal force (Appendix II, Reference 3)

8 (psi) = pressure differential required to unseat the rotor charging valve

After the rotor system had been charged to the desired level, the charging hose was depressurized and disconnected from the rotor charging valve. The test cell was then vacated. While the centrifuge was brought to the desired speed, the series and shunt variable resistors were adjusted to the desired values, and the transducer bucking voltage was set to position the Visicorder output near the right hand edge of the Visicorder chart. The series and shunt variable resistors were adjusted so that the expected pressure rise during propellant burning would give a Visicorder output deflection of approximately 5 inches from the start of propellant burning to propellant burnout. Chart speed was adjusted so that total burn time resulted in approximately 6 inches of chart travel.

After the centrifuge was stabilized at the desired speed the Visicorder chart was turned on and allowed to run approximately 2 seconds. Then the ignition switch on the instrumentation control console was closed until it was observed that the strand had ignited. Approximately 3 seconds after propellant burnout the Visicorder was stopped and the engine throttle closed.

The time from placement of the propellant strand in the combustion bomb until it was ignited was approximately 4 minutes. The centrifuge speed did not vary more than 2 rpm during propellant burning. At an acceleration level of 100 G a variation of 2 rpm corresponds to a variation of acceleration of ± 1.3 per cent, while at 1000 G a 2 rpm variation corresponds to a variation of only ± 0.4 per cent. While the centrifuge was decelerating, the chart was removed from the Visicorder, marked with the experiment number, and stapled to the data sheet. After the centrifuge had come to a complete stop, the arm was moved to a position where a discharge hose could be connected to the hand operated discharge valve. The surge tanks were isolated from the combustion bomb by the isolation ball valve, and the discharge valve was opened. This depressurized the combustion bomb and allowed removal of the strand holder.

An industrial vacuum cleaner was used to purge and cool the combustion bomb between experiments. The vacuum cleaner was allowed to run approximately 2 minutes. While the vacuum cleaner was running, the inhibitor case was removed from the strand holder. The case was retained for later examination of combustion residues. The strand holder was cleaned in cold water and allowed to dry. The vacuum cleaner suction hose was removed from the bomb, and preparations were made for the next experiment.

Elevated Initial Propellant Temperature Experiments

The majority of propellant strands were burned at 20 °C. Those propellant strands which were burned at elevated initial temperatures were conditioned at that temperature for 24 hours in a refrigerator-oven. After all preparations for an individual experiment were made, the

propellant sample was removed from the oven, inserted in the combustion bomb, and ignited after being brought to the desired acceleration level. Ignition of an individual strand was effected at 3.5 minutes ± 5 seconds after removal from the conditioning oven.

Propellant Ignition and Ignition Wire Placement

As mentioned previously the strands were ignited with black powder and a nichrome resistance wire. Approximately 50 mg of FFFg black rifle powder granules were used to coat the ignition surface of the strand and make contact with the nichrome wire. A small amount of LePage's Model (A) Airplane cement thinned with acetone was used to adhere the black powder granules to each other and the propellant surface.

The nichrome ignition wire was attached to the ignition terminals on the strand holder. The mid-span of the ignition wire was laid in a recessed notch filed in the propellant inhibiting case approximately 3/32 inch from the propellant surface. This was done to avoid the difficulty Anderson [3] experienced with broken ignition wires falling onto the burning surface of the propellant. The use of the variable resistance in series with the ignition wire as described previously and the recessed notch in the inhibitor case eliminated the problem of ignition wire breakage.

CHAPTER III

PROPELLANTS AND DATA REDUCTION

I. PROPELLANTS

Propellant Formulations

A parametric series of ten composite propellants was prepared by the Naval Weapons Center (N.W.C.), China Lake, California. All ten formulations contained spherical ammonium perchlorate oxidizer (AP) and PBAN binder. Various amounts of either spheroidal aluminum powder (Al) or ground tabular alumina (Al_2O_3) were added to the metallized propellants. The weight ratio of AP to PBAN in every formulation, including the metallized formulations, was constant at 79 parts AP to 21 parts PBAN.

The AP size distributions were made as narrow as possible to enable the study of the effect of oxidizer particle size on burning rate augmentation. Three different AP particle size distributions were prepared by ro-tapping "as received" American Potash and Chemical Corporation TRONA AP through appropriate Tyler screens. A distribution having a mass mean diameter (mmd) of 200 microns (μ) was obtained by screening through Tyler screens number 65 (210 μ) and number 80 (177 μ). A second distribution having a mmd of 94 μ was obtained by screening through Tyler screens number 150 (105 μ) and number 170 (88 μ). A third distribution having a mmd of 68 μ was obtained by screening the AP through Tyler screens number 170 (88 μ) and number 200 (74 μ). The particle size distributions are shown in Plates 12 and 13.

Originally it was planned to make the propellants with unimodal AP distributions. Attempts to mix unimodal formulations proved

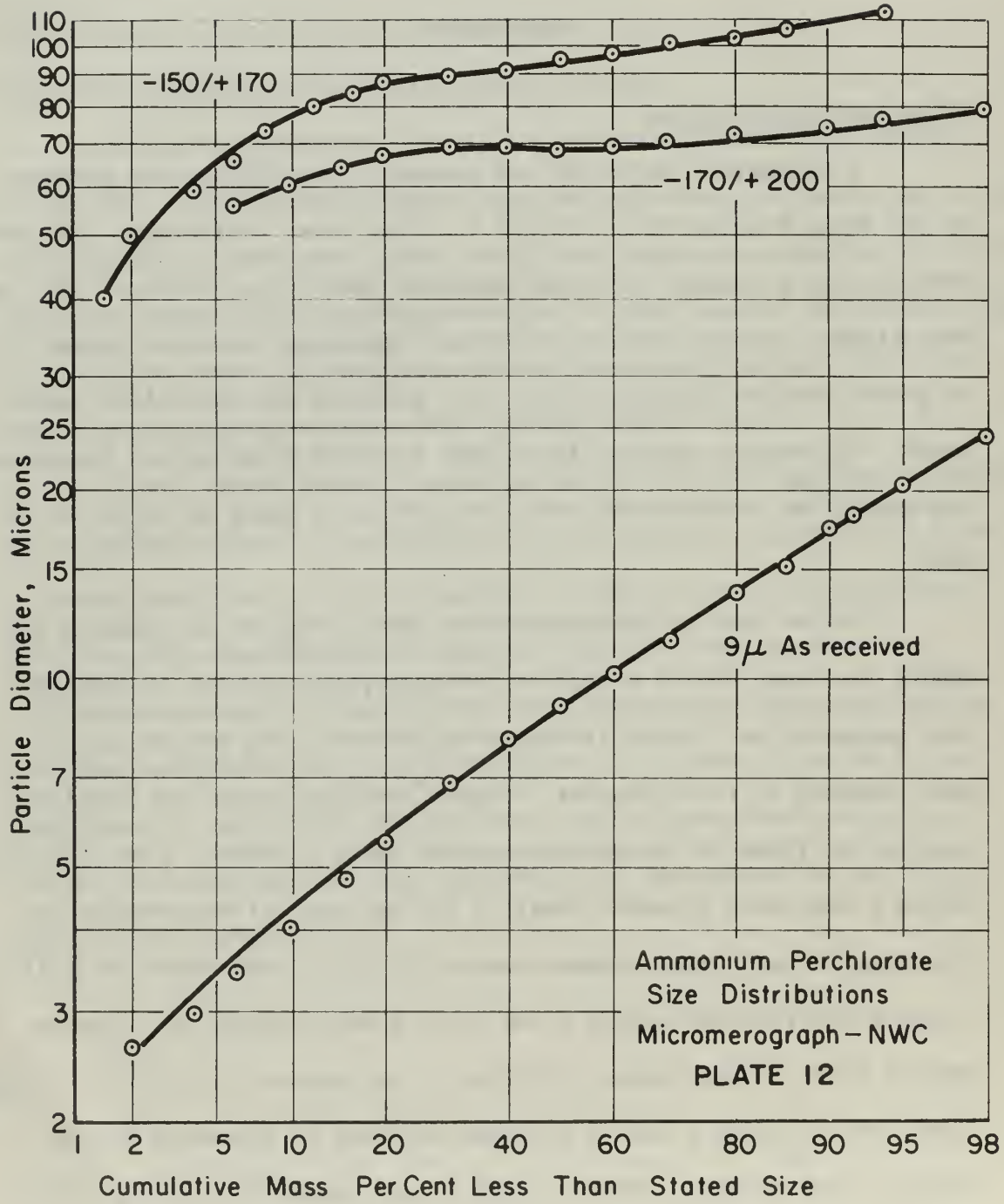
110
100
90
80
70
60
50
40
30
25
20
15
10
7
5
3
2
-150/+170
-170/+200
9μ As received
Particle Diameter, Microns
1
2
5
10
20
40
60
80
90
95
98
Cumulative Mass Per Cent Less Than Stated Size
Ammonium Perchlorate
Size Distributions
Micromerograph – NWC
PLATE 12

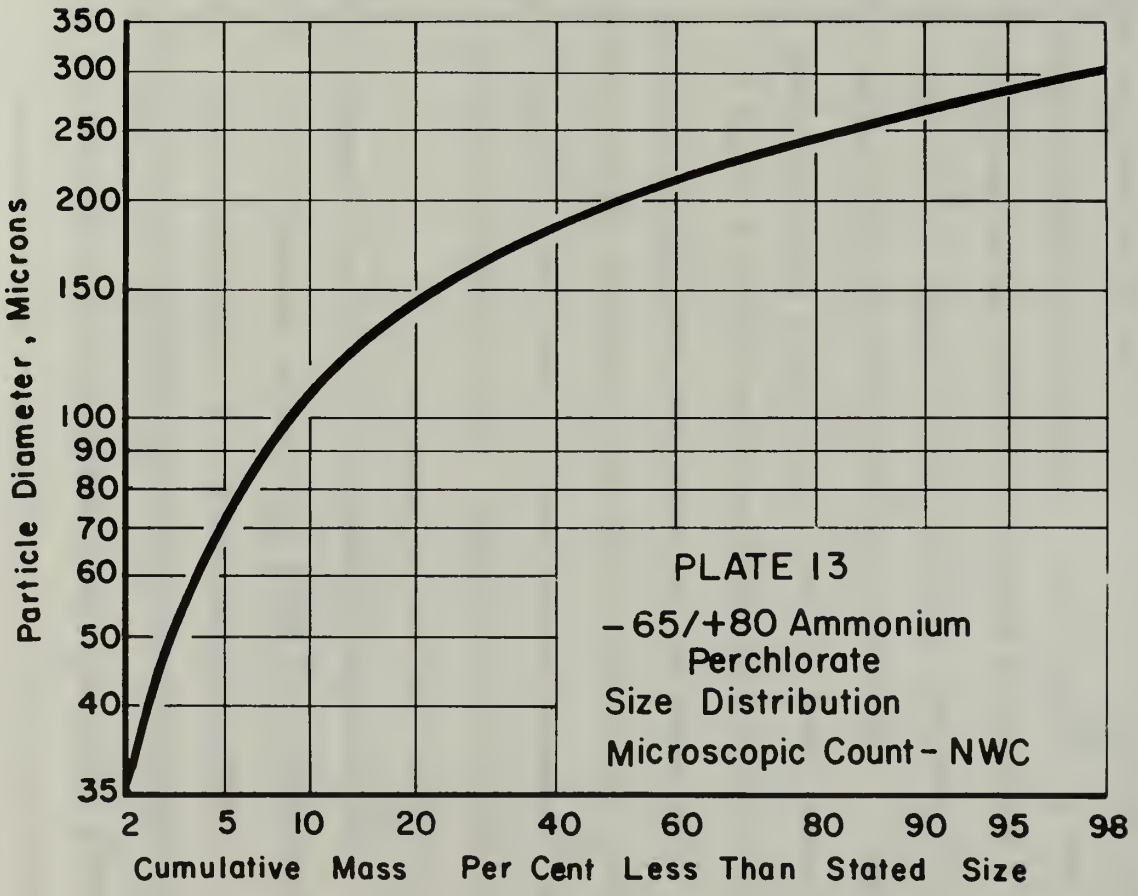
Particle Diameter, Microns
350
300
250
200
150
100
90
80
70
60
50
40
35
2
5
10
20
40
60
80
90
95
98
Cumulative Mass Per Cent Less Than Stated Size
PLATE 13
-65/+80 Ammonium Perchlorate
Size Distribution
Microscopic Count - NWC

unsuccessful. The propellants were very dry, were porous throughout, and did not burn well. One formulation, the P401 mix, did process well and was investigated. The remainder of the propellants in the parametric series contained bi-modal AP distributions.

The coarse grind AP used in the bi-modal propellants was either the 200 μ mmd material or the 94 μ mmd material. In all the bi-modal propellant mixes the fine grind AP was American Potash "as received" 9 μ mmd material. The size distribution is shown in Plate 12.

The aluminum additives used were Valley Metallurgical H-5 and H-30 spheroidal powders. The H-5 powder, 10.6 μ mmd, was used "as received." The H-30 powder was passed through a number 325 (44 μ) Tyler screen which yielded a distribution with a 28 μ mmd. The Al particle size distributions are shown in Plates 14 and 15.

One propellant was formulated with aluminum oxide as the additive. The aluminum oxide was prepared by passing Aluminum Company of America ground tabular alumina T-61 -325 mesh through a number 325 (44 μ) Tyler screen. The resulting particle size distribution, shown in Plate 16, had a mmd of 9.3 μ.

The propellant formulations in the basic parametric series were designated by a three digit number preceded by a P. This was done to facilitate discussion in the following sections. The propellant containing the 68 μ mmd AP was designated P401. The propellants containing 94 μ mmd AP were designated as the P410 series; those containing 200 μ mmd AP were designated the P420 series.

The specific propellant formulations are shown in Appendix IV. The appendix can be folded out to facilitate reference to the specific propellant formulations while simultaneously viewing the experimental results to be presented in Chapter IV.

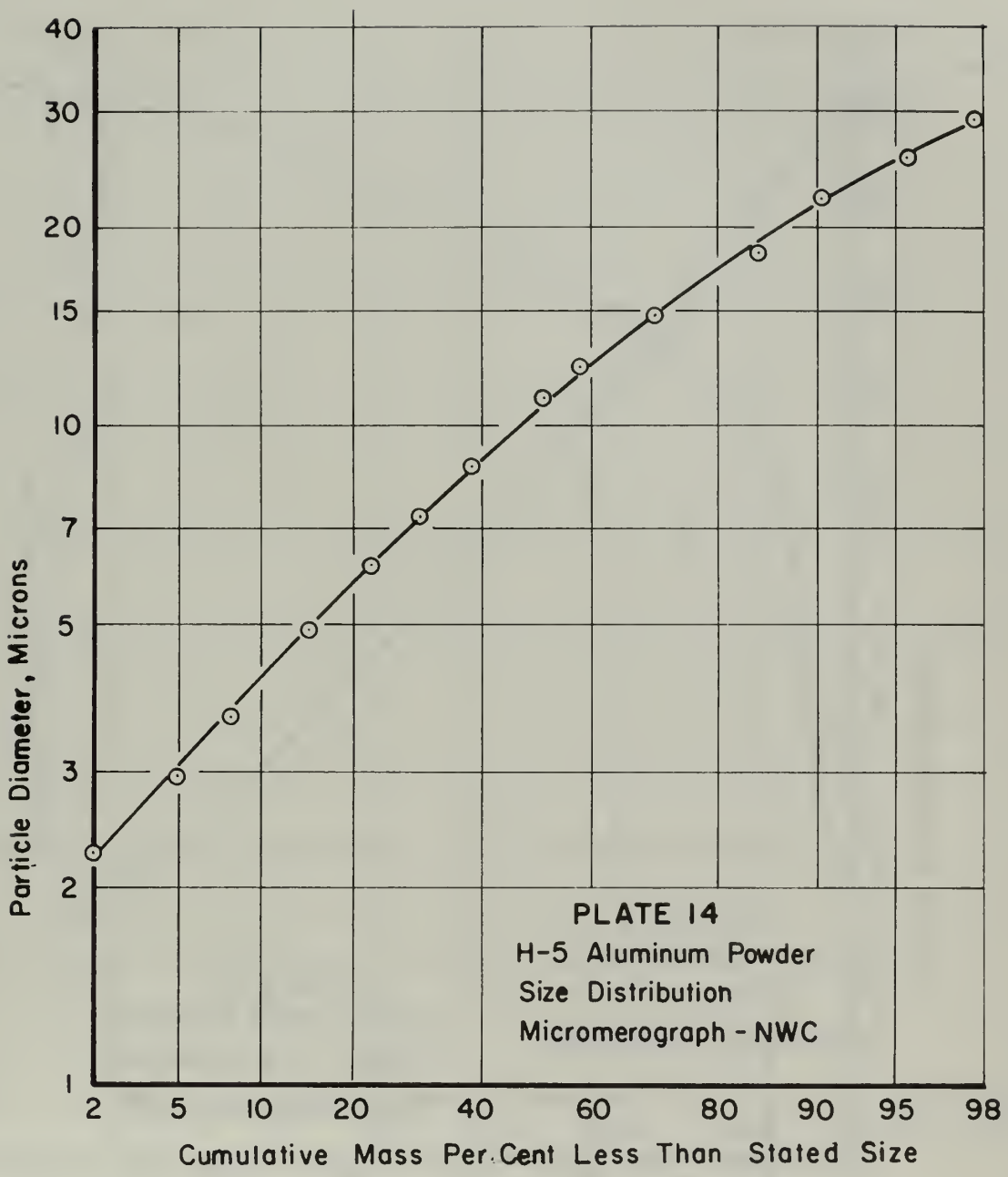
40
30
20
15
10
7
5
3
2
1
Particle Diameter, Microns
2
5
10
20
40
60
80
90
95
98
Cumulative Mass Per Cent Less Than Stated Size
PLATE 14
H-5 Aluminum Powder
Size Distribution
Micromerograph - NWC

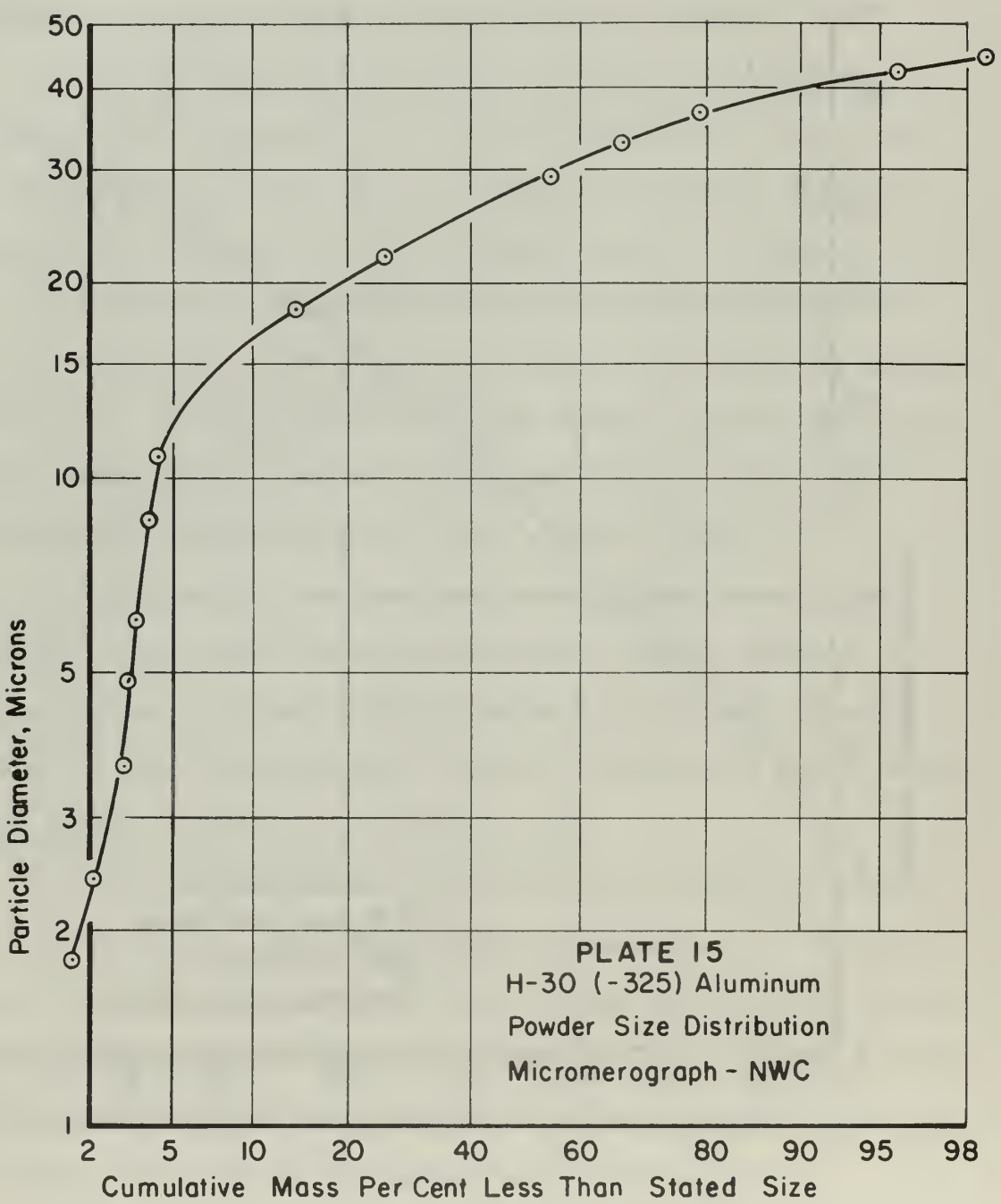
50
40
30
20
15
10
5
3
2
1
Particle Diameter, Microns
2
5
10
20
40
60
80
90
95
98
Cumulative Mass Per Cent Less Than Stated Size
PLATE 15
H-30 (-325) Aluminum
Powder Size Distribution
Micromerograph - NWC

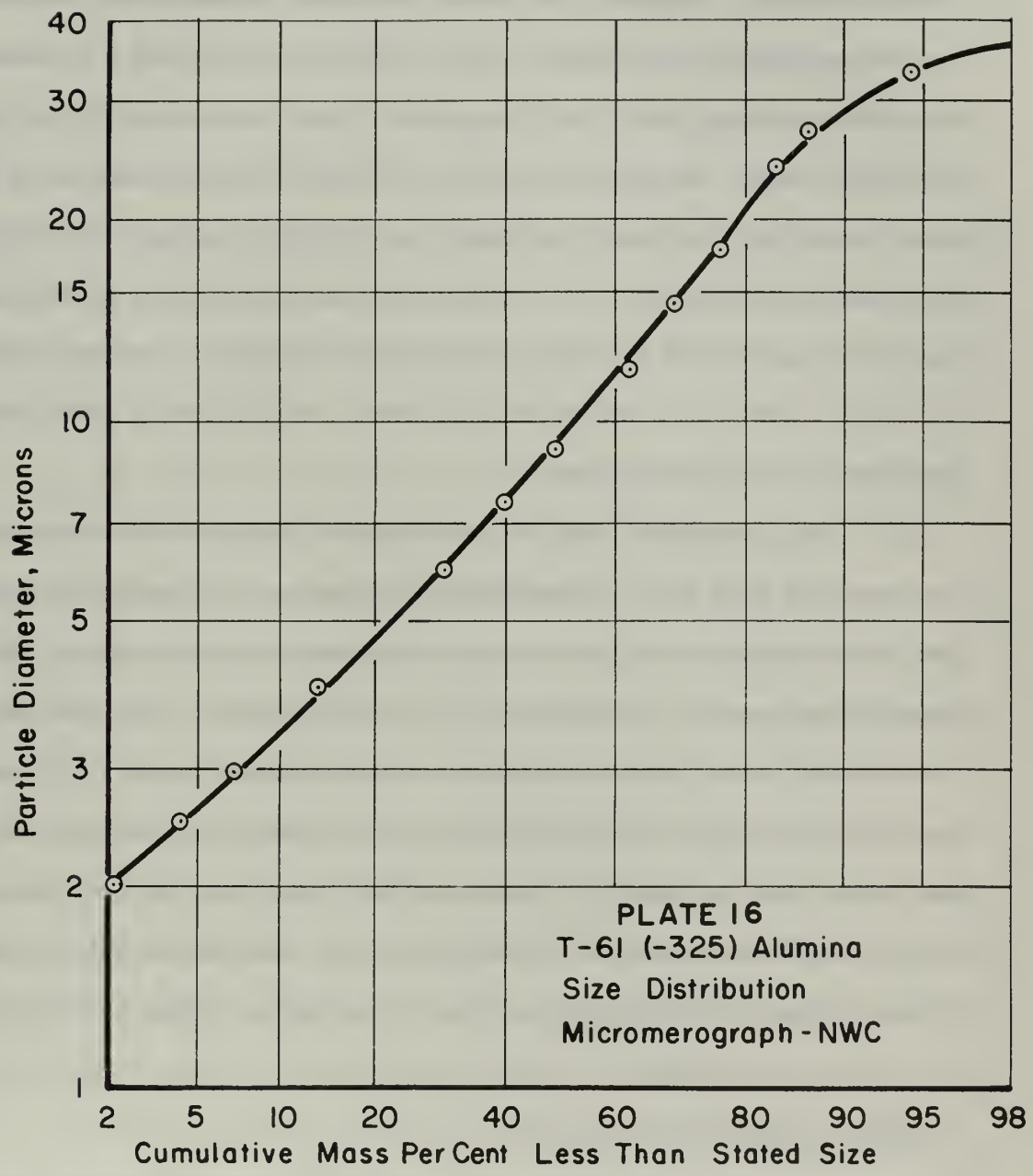
40
30
20
15
10
7
5
3
2
1
Particle Diameter, Microns
2
5
10
20
40
60
80
90
95
98
Cumulative Mass Per Cent Less Than Stated Size
PLATE 16
T-61 (-325) Alumina
Size Distribution
Micromerograph - NWC

Two fast burning rate propellants were supplied by the Thiokol Chemical Corporation, Huntsville, Alabama. A detailed description of the propellants is not possible because of security classification considerations. However, the propellants can be described in the following qualitative manner. The propellants contained a bi-modal AP oxidizer distribution. The fine grind AP particle distribution had a very small mmd. The larger grind AP particle distribution had a somewhat larger mmd, but qualitatively this distribution would be considered as a small mmd distribution. Both propellants contained a high percentage of "as received" Valley Metallurgical spheroidal aluminum powder. The binder used was a hydrocarbon polymer, and a burning rate catalyst was used in the formulations.

The propellant used in the erosive burning rate experiments was supplied by N.W.C., China Lake, California. The propellant chosen for the erosive burning rate experiments was typical of aluminized propellants used in current solid propellant motors. The specific formulation was: carboxy-terminated polybutadiene binder, 13.5 per cent; tri-modal AP oxidizer, 69.5 per cent; and H-5 aluminum, 17.0 per cent. The tri-modal AP consisted of 25 per cent 10 μ, 50 per cent 200 μ, and 25 per cent 600 μ mmd particles. The mmd of the tri-modal AP was 195 μ (micromerograph). The H-5 aluminum powder had a mmd of 7.1 μ (micromerograph).

Propellant Strand Preparation

All propellant mixes were cast in blocks and then machined into strands. The propellant strands in the basic parametric series were 0.2 inch x 0.2 inch x 5 inches long. The Thiokol propellant strands were 0.25 inch x 0.25 inch x 5 inches long. After the propellant strands were received, they were x-rayed using a Norelco Search Ray

x-ray machine to check for voids. Approximately 2 per cent of all propellants were rejected on the basis of x-rays.

The propellant strands were spirally wound with heavy-duty household string and placed in a mold for application of the inhibiting material. The inhibitor used on the strands was an unsaturated polyester resin cured with a peroxide. The resin used was Selectron 5119 (Pittsburg Plate Glass Co.). The curing agent was a 50 per cent solution of methyl ethyl Keytone peroxide in dimethyl phthalate ("Garox" Ram Chemical Co., Gardena, California). The ratio used was 96 per cent Selectron to 4 per cent curing agent. The inhibitor was cured at room temperature.

The propellant strands were cut to the desired length on a bandsaw after the inhibitor case had cured. After each strand was given an identification number and measured with a micrometer, a cap of inhibiting material was cast on one end of each sample. Thus each strand was enclosed in a small end burning motor with a port to throat area ratio of one. The inhibitor cases were 0.5 inch x 0.5 inch in cross-section. The strands were prepared with a rigid inhibitor and end closure to provide mechanical support for the visco-elastic propellant in the anticipated high acceleration environment and to retain any residue that might remain at the end of burning. A strand enclosed in its inhibitor case is shown schematically in Plate 8.

Those propellant strands which were to be used with timing wires were drilled with a number 72 (0.025 inch diameter) drill. The distance from the ignition end of the propellant strand to the timing wires was measured to the nearest 0.01 inch. As mentioned previously, the use of timing wires was the secondary means of determining burning

rate. This method was not preferred because of the excessive propellant sample preparation time, the void that had to be made in the propellant sample to accommodate the wire, and the effect the combustion of the timing wire might have had on propellant combustion. However, timing wires were used approximately once every thirtieth experiment as a check on the pressure-time trace method of determining burning rate.

The strands were stored in a hazard-safe oven at ambient temperature. Samples of the particular propellant being investigated were stored in a refrigerator-oven at a specified temperature within ± 1° C.

Erosive Motor Fabrication

Plate 17 is a schematic drawing of a motor designed to enable a sample of propellant to be burned erosively. The motor was built around a 0.375 inch x 0.375 inch x 2.75 inch propellant sample. The basic components of the motor were two motor side plates, a channeled top plate, a fore end closure, and a cast laminating resin bottom plate.

The two 0.125 inch x 0.5 inch x 3 inch canvas phenolic motor side plates were secured to opposite sides of the propellant strand with RTV-102 silicone rubber (General Electric Co.). The bottoms of the motor side plates were flush with the bottom of the propellant sample. The aft ends of the motor side plates were flush with the aft end of the propellant sample.

A 0.025 inch diameter hole was drilled through each of the motor side plates after the RTV rubber had cured. The holes, through which a nichrome ignition wire was threaded, were located at the fore end of the motor flush with the top of the propellant sample.

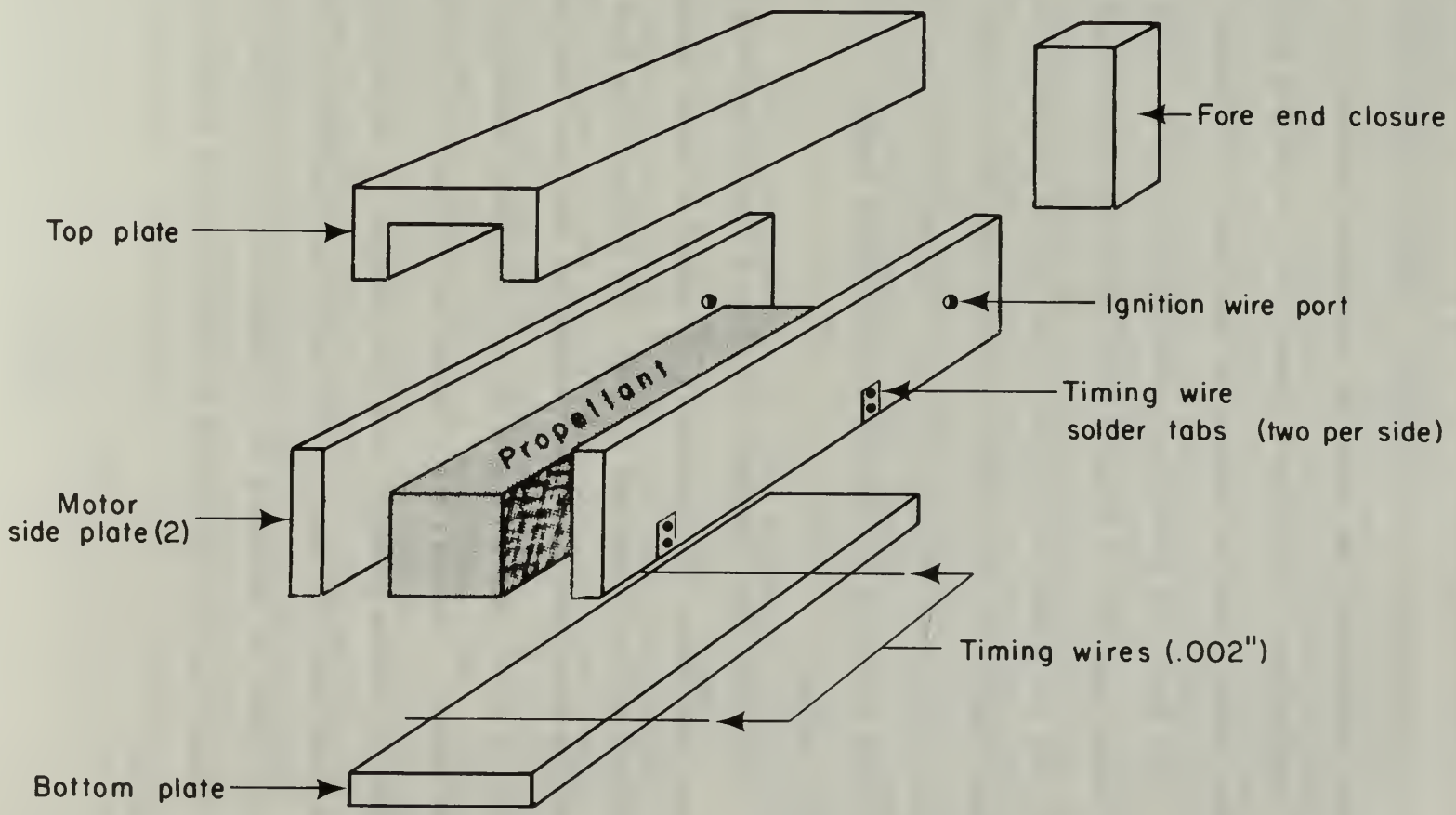

PLATE 17 MOTOR USED IN EROSIVE BURNING EXPERIMENT

Approximately 5 mg of Holex 14 ignitor moistened with a small amount of acetone was painted on the top surface of the propellant sample for its entire 2.75 inch length. Holex 14 (Holex, Inc., Hollister, California) was chosen as the ignitor because of its fast linear burning rate. Experiments showed that the entire length of the propellant sample could be ignited in less than 0.025 second.

The motor top plate was a piece of 0.625 inch x 0.30 inch x 3 inch canvas phenolic in which a 0.375 inch wide channel had been milled. The top plate was secured to the top of the motor side plates with high temperature epoxy (APCO 210 resin and 180 hardener). The motor side plates and top plate formed a channel 0.3 inches high x 0.375 inches wide over the top of the propellant sample for its entire 2.75 inch length.

Two 0.002 inch diameter Pyro-fuse timing wires were then placed flush with the bottom of the propellant strand at known distances from the fore end of the propellant strand. The timing wires were soldered to soldering tabs which had been cemented to the motor side plates. The 0.375 inch x 0.375 inch fore end of the propellant sample was inhibited with RTV rubber. The fore end closure, a 0.25 inch x 0.375 inch x 0.675 inch piece of canvas phenolic, was then secured to the motor side plates and top plate with APCO epoxy. The motor was completed by casting a 0.125 inch layer of Westglass 1013 laminating resin (Western Fibrous Glass Products Co.) on the bottom of the propellant strand and motor side plates.

II. DATA REDUCTION

Determination of the Acceleration Field

At a constant centrifuge rpm the acceleration field imposed on the propellant had two components: a radial component dependent on the angular velocity and the radial distance to the propellant surface, and a vertical component due to the earth's gravitational field. With the centrifuge at rest the acceleration was vertical and directed downward. At high centrifuge rpm the acceleration direction was nearly horizontal. The lowest acceleration level at which the centrifuge was operated during the course of this investigation was 15 times the standard acceleration of gravity. The contribution of the vertical component to the total acceleration was negligible at this acceleration level. Hence the acceleration field imposed on the propellant was assumed to be horizontal and equal to the radial component.

The radius used in determining the radial acceleration was the radial distance to the mid-point of the propellant sample. A 1.0 inch canvas phenolic spacer was inserted between the cap end of a 1.0 inch strand and the strand support on the strand holder. This was done to position the ignition end of the strand at the same radial position as the ignition circuit terminals. The cap end of a 2.0 inch strand was positioned directly against the strand support. Thus for a 1.0 inch strand (mid-point of the strand located at a radius of 35.1 inches) the centrifuge rpm for a given acceleration was slightly higher than for a 2.0 inch strand (mid-point of the strand located at a radius of 35.6 inches).

Determination of Strand Burning Rates

Burning rates of propellants equipped with timing wires were easily determined by dividing the distance between the timing wires by the elapsed time indicated on the Visicorder chart.

A typical pressure-time trace is shown as Plate 18. Approximately 0.1 seconds after the ignition switch on the instrumentation console was closed, a well defined spike appeared on the chart. Approximately 0.15 seconds after the start of the spike the pressure began to rise until propellant burnout. The pressure rise was caused by the addition of the propellant strand mass to the mass of the nitrogen gas contained in the combustion bomb-surge tank system and the increase in the thermal energy of these gases due to strand combustion. The pressure rise varied with strand length and was approximately 7 psi per inch of strand length. The pressure decay after propellant burnout was attributed to the cooling of the gases in the bomb-surge tank system. The use of the pressure-time trace to determine burning rate required interpretation of the positions on the pressure-time trace which corresponded to propellant ignition and burnout. These positions were ascertained in the following manner.

Experiments were conducted to determine the burning time and pressure-time history of a nominal 50 mg black powder ignition charge. The black powder was placed on the cap end of a spent inhibitor case and ignited with a nichrome wire positioned in the same manner as for normal strand ignition. Four experiments were conducted with the centrifuge at rest. Two experiments were made with the surge tank isolation valve open. The pressure-time trace had the shape shown in Plate 19. There was an initial spike followed by an oscillating

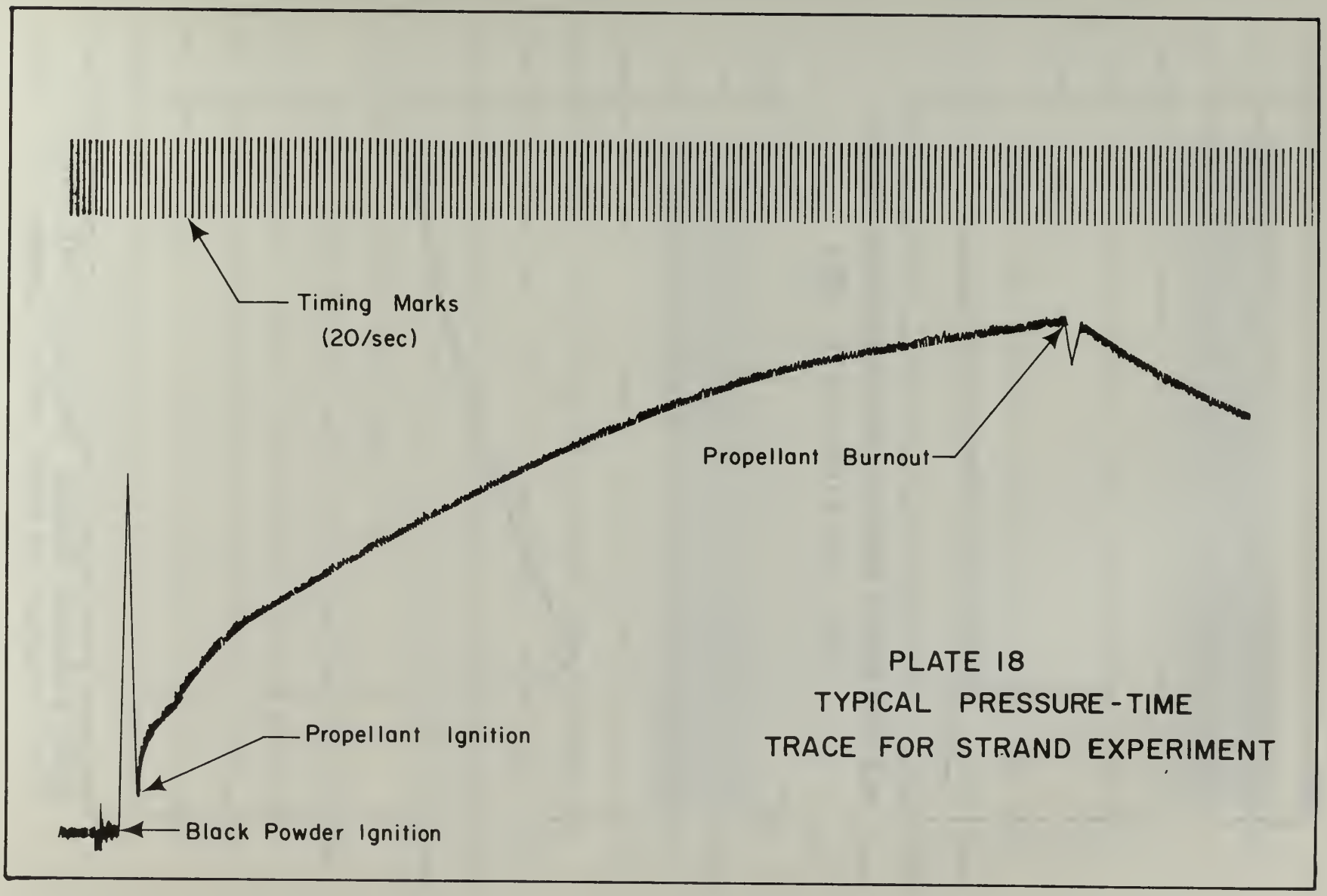

PLATE 18
TYPICAL PRESSURE-TIME
TRACE FOR STRAND EXPERIMENT

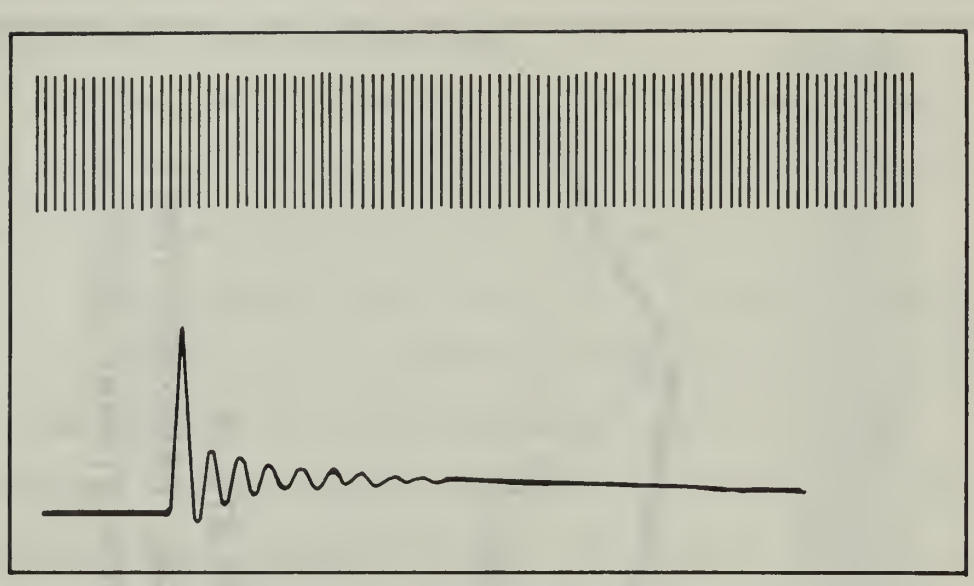

PLATE 19 BLACK POWDER PRESSURE-TIME TRACE
WITH ISOLATION VALVE OPEN

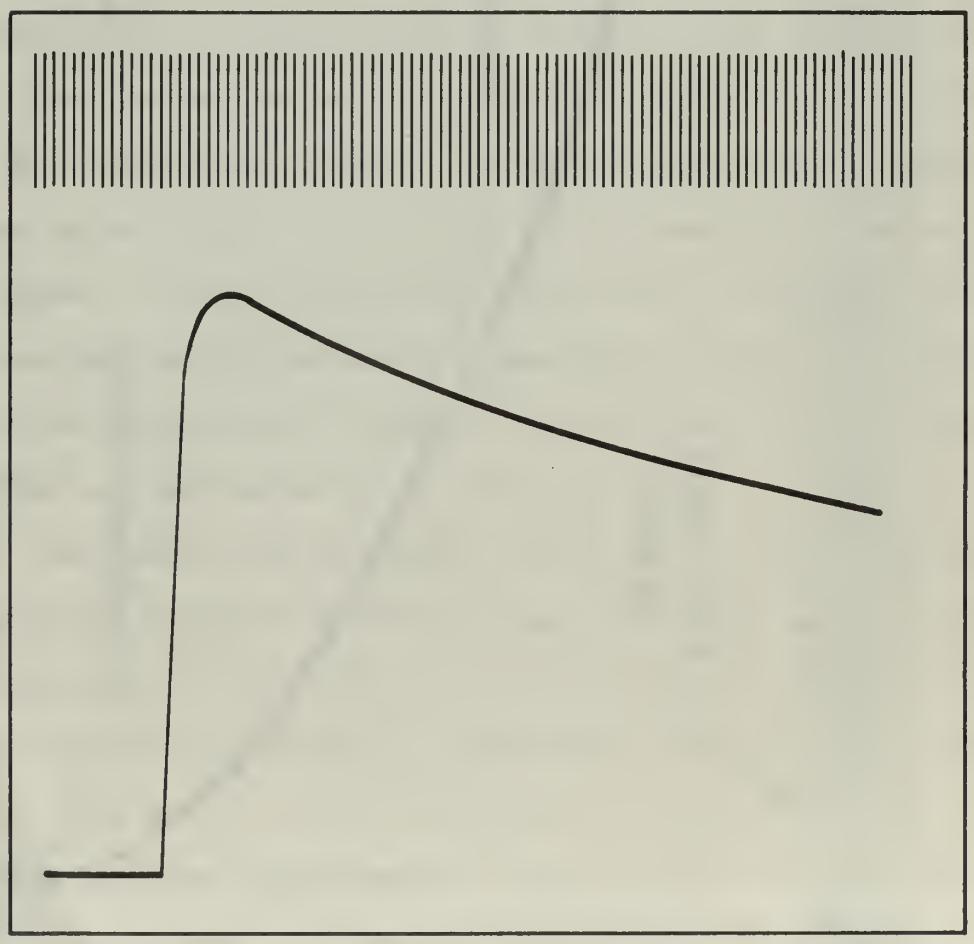

PLATE 20 BLACK POWDER PRESSURE-TIME TRACE
WITH ISOLATION VALVE CLOSED

pressure with a frequency of approximately 6.5 hertz. The spike obtained for the burning of black powder alone corresponded in shape and duration to the spike obtained when the propellant strand was ignited with black powder. The duration of black powder burning could not be determined because of the oscillatory behavior of the pressure-time trace.

The surge tank isolation valve was closed for the next two experiments. The shape of the pressure-time trace was quite different as is shown in Plate 20. There was a very rapid pressure rise followed by a rounded top and subsequent pressure drop. The absence of a pressure oscillation suggested that the oscillations were caused by the dynamic response of the surge tank-combustion bomb system. It was assumed that the black powder burned for an elapsed time corresponding to the time from the beginning of the pressure rise until the maximum pressure was reached. The average burning time obtained from the two experiments made with the surge tanks isolated from the combustion bomb was 0.28 seconds. Since it is reasonable to assume that propellant ignition occurred during the combustion of the black powder charge, it was concluded that propellant ignition took place within 0.28 seconds after the black powder charge began to burn.

Least square fits were made to the burning rate data obtained from various length strands of three different types of propellant. The propellant strands were burned at 0 G and 500 psia. The results are shown in Plates 21, 22, and 23. The ordinate is the propellant strand length, and the abscissa is the time from ignition of the black powder charge (i.e., the start of the spike) to propellant burnout. The assumption was made that the burning rate of each

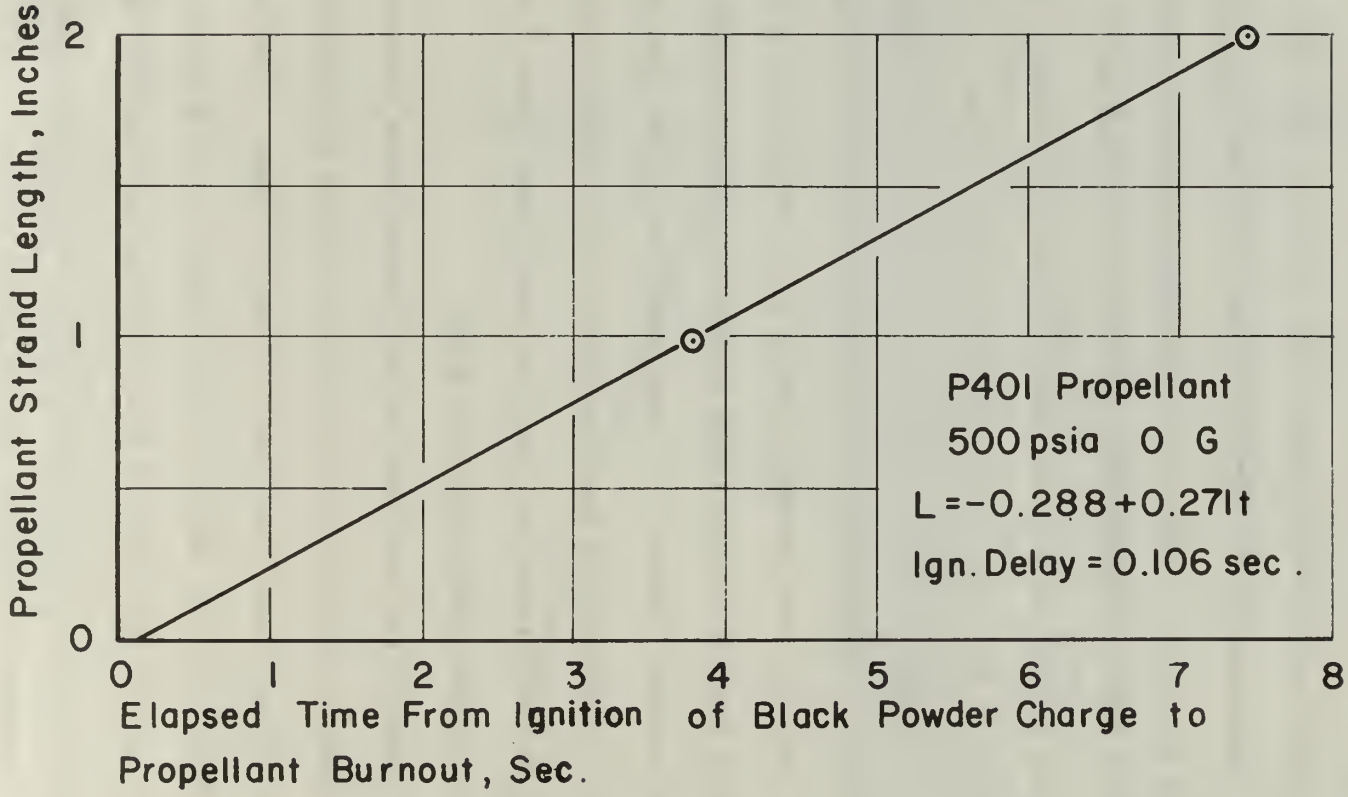

PLATE 21 PROPELLANT STRAND LENGTH VERSUS ELAPSED BURN TIME FOR P401 PROPELLANT

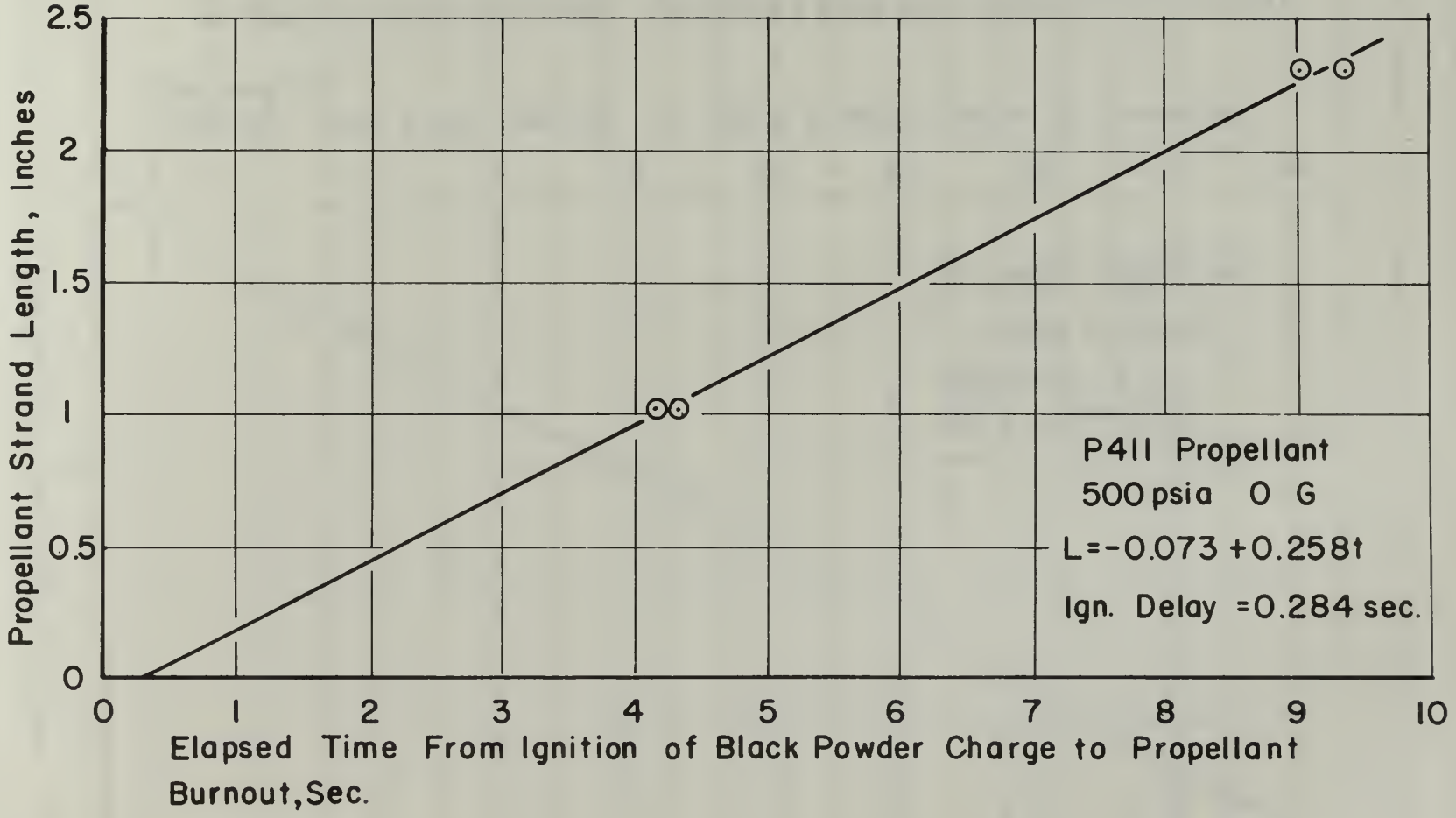

PLATE 22 PROPELLANT STRAND LENGTH VERSUS ELAPSED BURN TIME FOR P411 PROPELLANT

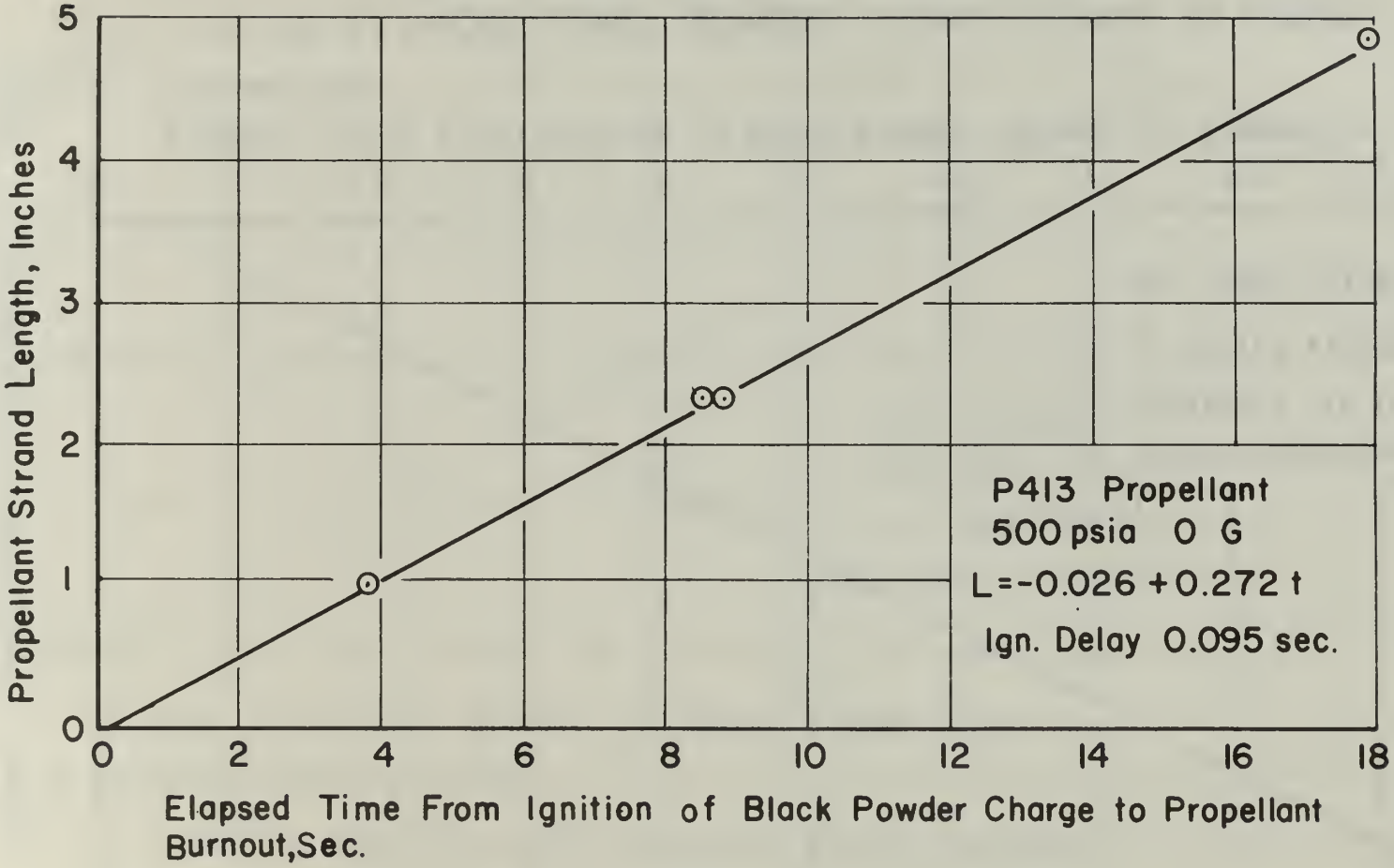

PLATE 23 PROPELLANT STRAND LENGTH VERSUS ELAPSED BURN TIME FOR P413 PROPELLANT

propellant was independent of strand length. The point where the least squares curve crossed the abscissa then represented the propellant ignition delay. The average ignition delay for the three propellants was 0.162 seconds.

An ignition delay time of 0.162 seconds was in good agreement with the commencement of the pressure rise after the spike attributed to the start of black powder combustion. Based on the above observations it was concluded that propellant ignition corresponded to the start of the pressure rise after the spike caused by the ignition of the black powder charge.

Propellant burnout was easier to deduce. Timing wires placed at the cap end of several propellant strands prior to casting on the end cap confirmed that the abrupt end of the pressure rise corresponded to propellant burnout. The oscillation in the pressure-time trace immediately after propellant burnout was attributed to the dynamic response of the surge tank-combustion bomb combination. The pressure-time trace of a propellant strand burned with the surge tanks isolated from the combustion bomb did not possess this oscillation. Experiments were made to determine the response of the surge tank-combustion bomb system to an impulsive depressurization. The system was found to have a natural frequency of approximately 6.5 hertz. The frequency of the oscillation after propellant burnout was also approximately 6.5 hertz.

The primary means of determining average propellant burning rate utilized the pressure-time trace and the propellant strand length. The burning times of the propellant strands were at least 2 seconds. The uncertainty in the elapsed time of strand burning was the result of two factors: 1) the uncertainty in the position on the pressure

time trace which corresponded to propellant strand ignition, and 2) the uncertainty in the measurement of elapsed time between the positions selected as propellant ignition and propellant burnout. These two uncertainties were judged to be ± 0.08 and ± 0.0125 seconds respectively. The propellant strands were at least 1.0 inch long and were measured to within ± 0.002 inch. Hence the probable uncertainty in the burning rate measurement is within ± 4.1 per cent.

Erosive Burning Rates

The pressure-time traces of the erosive burning propellants showed a very rapid and continuous pressure rise. Ignition of the fore end of the propellant strand was assumed to take place at the beginning of this pressure rise. A motor equipped with a timing wire positioned at the aft end of the propellant strand and across its top surface was used to determine the time required to establish combustion over the entire length of the propellant strand. The average rate of combustion initiation along the top surface of the propellant was determined to be 127 inches/second. This lengthwise ignition propagation rate was taken into account in determining the average burning rate at positions removed from the fore end of the strand. Generally this correction amounted to a change of approximately 1.0 per cent in the propellant burning rate.

CHAPTER IV

EXPERIMENTAL RESULTS AND DISCUSSION

General

The results of the experimental program are presented in this chapter. Also included is an evaluation, in light of the experimental results obtained during the course of this investigation, of the theoretical analyses of Glick [7,8] and Crowe and Willoughby [9] for the acceleration induced burning rate changes of non-metallized and metallized propellants. The results and discussion are arranged in four sections. The first section presents the experimental results for the three non-metallized propellants in the basic parametric series and an evaluation of Glick's analysis [7]. The second section presents the results for the seven metallized propellants in the basis parametric series. In addition, the analysis by Crowe and Willoughby [9] and the modification to the analysis by Glick [8] are discussed. The third section presents the results for the fast burning rate Thiokol propellants. Contained in the fourth section are the results for the erosive burning experiments.

The burning rate data are presented as either the absolute burning rate, in inches/second, versus acceleration or the burning rate ratio versus acceleration. The burning rate ratio is defined as the burning rate at a given acceleration divided by the burning rate of the propellant at 0 G acceleration. The 0 G burning rate used to form the burning rate ratio was the average value obtained from a minimum of three experiments. Each strand burning rate datum point at a given acceleration represents the result of one experiment. Thus,

to achieve a plot of burning rate or burning rate ratio versus acceleration at a given pressure, a series of at least eleven experiments was conducted. The curves drawn through the data points are only to be considered indicative of the trend in the experimental data points and are drawn to aid in comparison of the different propellants. Where it is considered that one curve will fit two sets of data points, as in Figure 1, the data points are indicated by two different symbols which are defined in the legend of the figure.

The data obtained from weighing the amount of residue retained in the inhibitor cases of the metallized propellants are presented for a particular propellant as a function of pressure, strand length, and acceleration level. The residue was generally in a single piece having a cross-sectional area equal to the cross-sectional area of the corresponding propellant strand. The residue was easily removed from the inhibitor case after the case was cut in two pieces about a half inch from the cap end of the case. The residue mass was weighed on a Mettler automatic laboratory balance.

The erosive burning data are presented as burning rate versus distance from the fore (or head) end of the motor as a function of acceleration. Only one propellant and one pressure level, 500 psia, was investigated.

I. NON-METALLIZED PROPELLANTS

Experimental Results

Three non-metallized propellants P410, P411, and P420 were investigated at pressures of 500 and 1000 psia. Unless indicated otherwise, the acceleration vector was directed normal and into the

propellant burning surface. Plots of burning rate ratio versus acceleration for each of these propellants are presented in Figures 1, 2, and 3. The data presented in these figures indicate that each of the propellants exhibited an increase in burning rate when subjected to an acceleration field normal and into the burning surface.

The acceleration dependent burning rate behavior of these propellants can be described qualitatively as: 1) a low acceleration range in which the propellants experience no burning rate increase over the 0 G burning rate, 2) an intermediate acceleration range in which the propellants exhibit an increase in burning rate with increasing acceleration level, and 3) a high acceleration range in which the propellants burn at acceleration independent burning rates as great as 60 per cent higher than their 0 G burning rates. This constant high acceleration burning rate will be referred to as the limit burning rate. The acceleration level at which a given propellant began to exhibit increases in burning rate could be determined only approximately because of the scatter in the burning rate values obtained from one strand to the next. The scatter obtained in three 0 G burning rate experiments about the average burning rate values was ± 1.0 per cent for P410, ± 2.0 per cent for P411, and ± 4.0 per cent for P420. This scatter is attributed in part to the experimental error and in part to the inherent non-uniformities in the propellant composition from one strand to the next.

At a pressure of 500 psia propellants P410 and P420 exhibited burning rates greater than their 0 G burning rates at accelerations greater than 50 G and 40 G respectively. When the pressure was raised to 1000 psia these propellants exhibited increased burning rates at an acceleration level of approximately 25 G. In the case of propellant

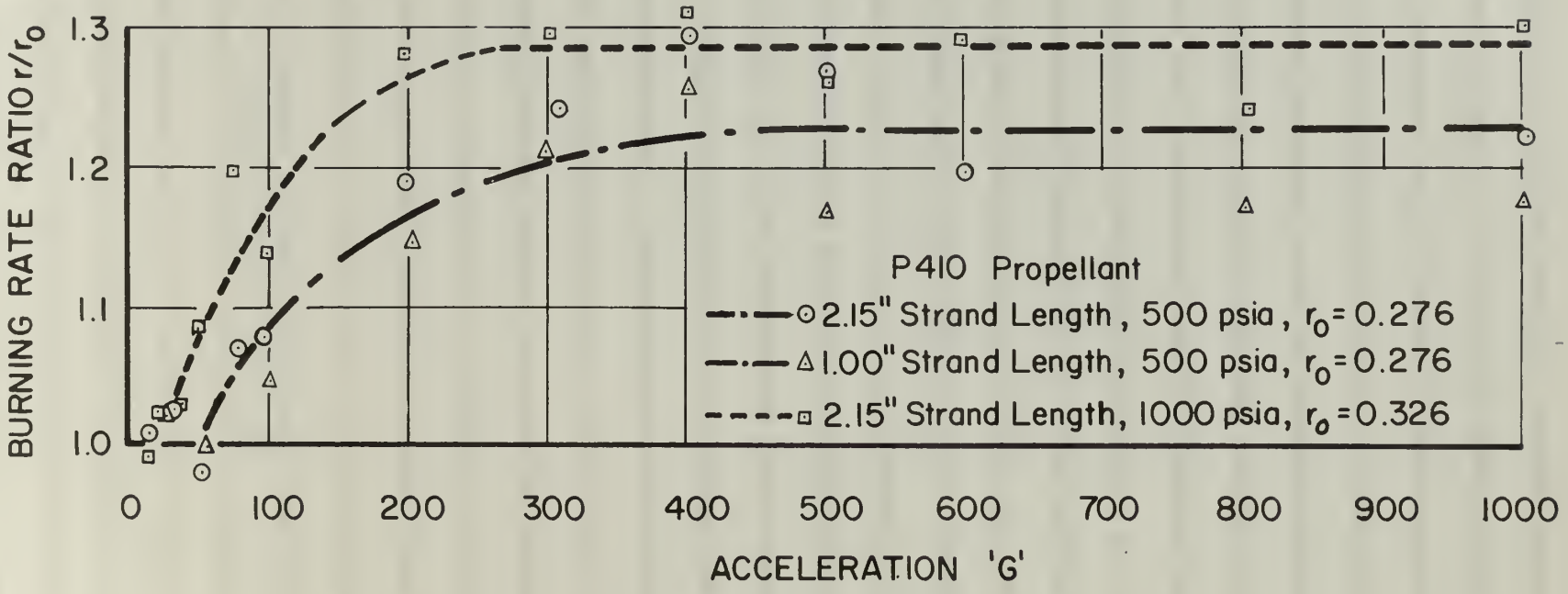

FIGURE I BURNING RATE RATIO VERSUS ACCELERATION FOR PROPELLANT P410

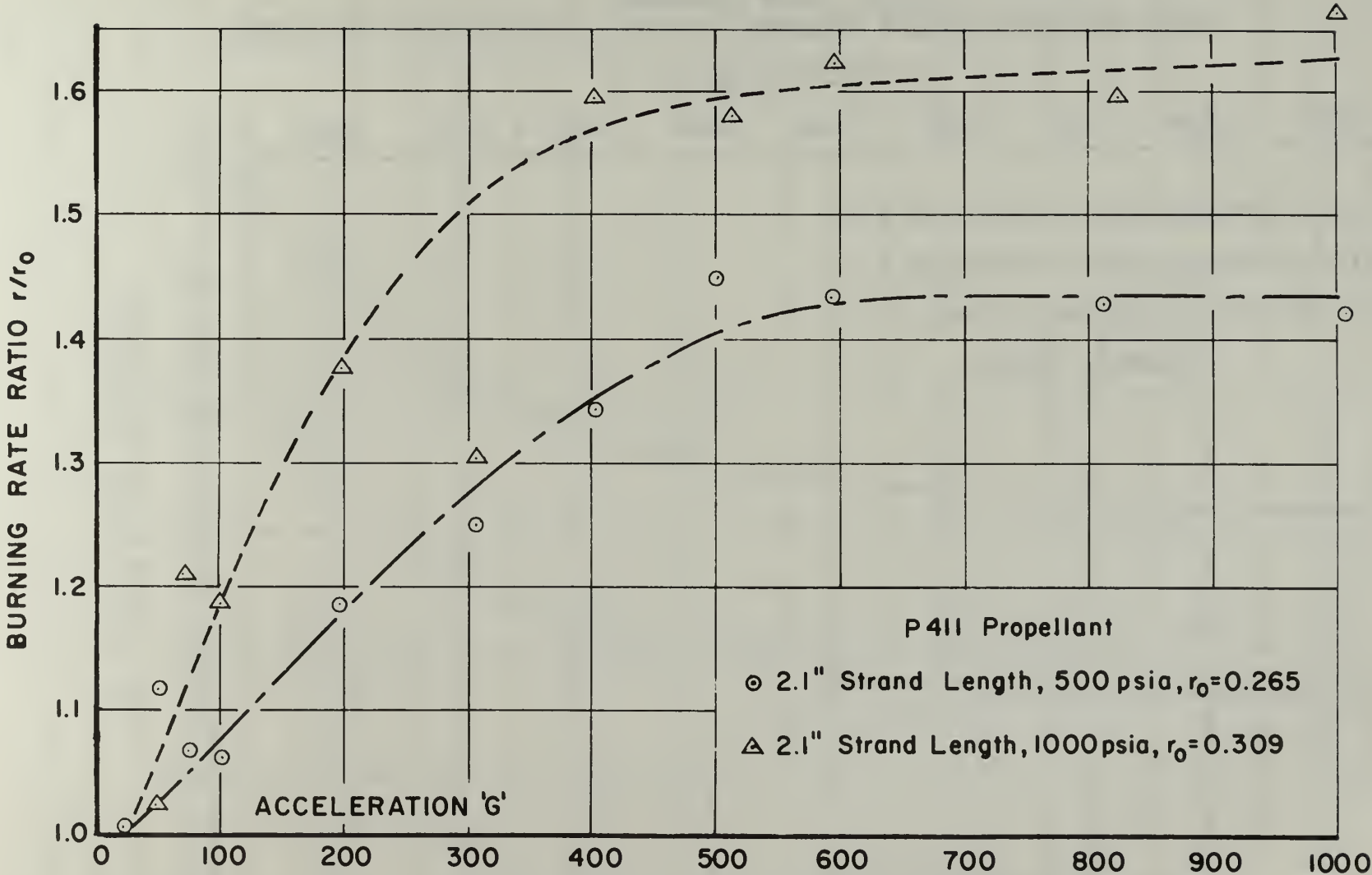

FIGURE 2 BURNING RATE RATIO VERSUS ACCELERATION FOR PROPELLANT P411

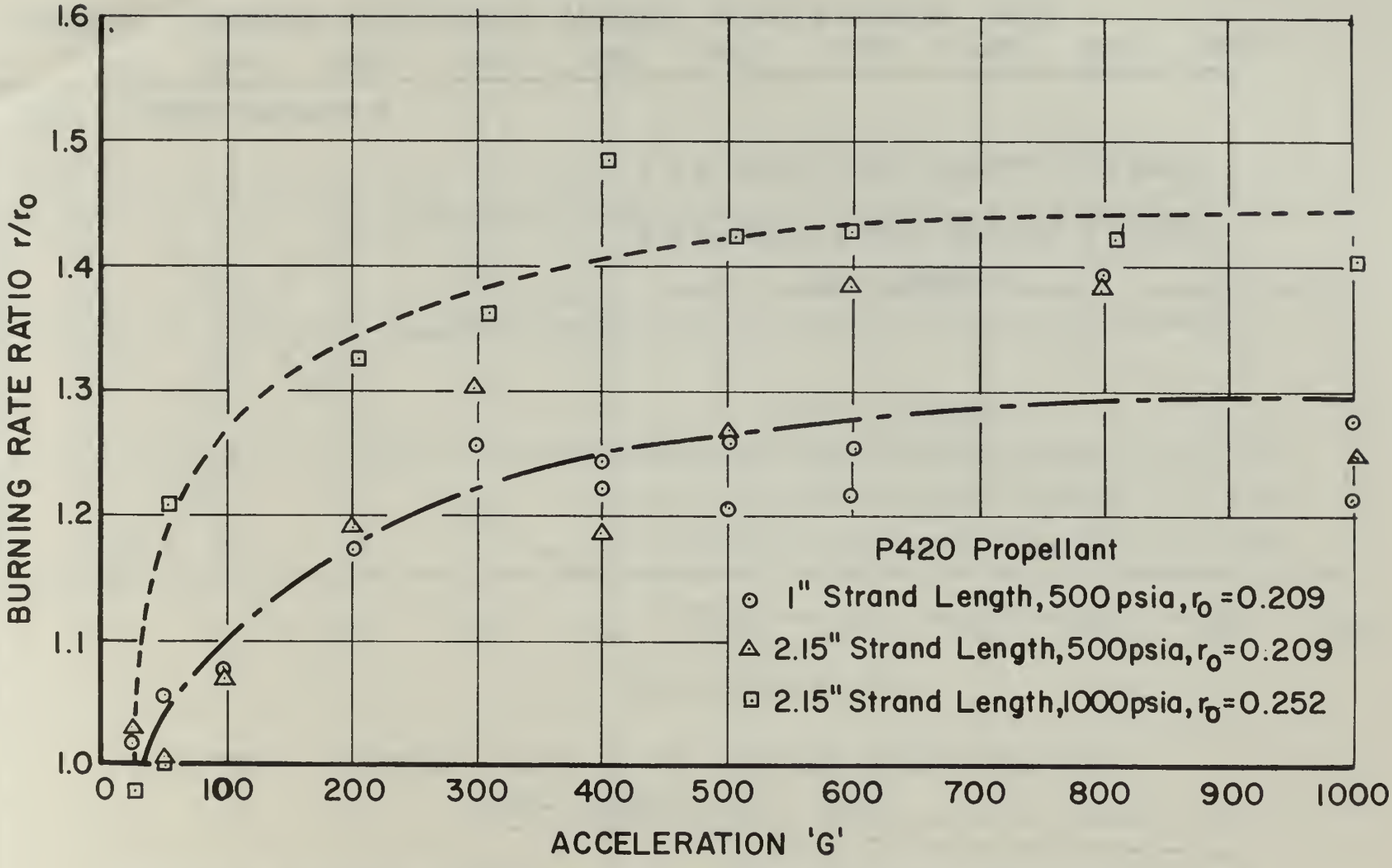

FIGURE 3 BURNING RATE RATIO VERSUS ACCELERATION FOR PROPELLANT P420

P411 the burning rate started to increase at an acceleration level of approximately 25 G independent of the pressure level. Thus, although the acceleration levels are only approximate, it was found that increasing the pressure generally decreased the acceleration level at which the propellants started to exhibit increased burning rates.

The data in Figures 1, 2, and 3 indicate that each of the three propellants reached its constant high acceleration limit burning rate at a somewhat lower acceleration level when the pressure was increased from 500 to 1000 psia. Additionally, when the pressure was increased from 500 to 1000 psia, each of the three propellants exhibited a higher limit burning rate ratio. Thus, increasing the pressure level resulted in: 1) commencement of burning rate increases at lower acceleration levels, 2) achievement of a constant limit burning rate value at a lower acceleration level, and 3) a higher limiting value of burning rate ratio.

Two different strand lengths of propellants P410 and P420 were investigated at 500 psia. As can be seen from Figures 1 and 3, there is no consistent variation in burning rate ratio with the different strand lengths. The scatter in the burning rate data at all acceleration levels is of the same order as the scatter in the 0 G burning rate data. Thus it appears that for these non-metallized propellants the burning rate in an acceleration field is independent of time.

Figure 4 contains data obtained for propellants P411 and P420 burned with the acceleration vector directed normal and out of the burning surface. These propellants were found to exhibit no change in burning rate with accelerations as high as 1000 G. The small deviations from the 0 G burning rate are at most 4.5 per cent and are of the order of the scatter in the 0 G burning rates of P411 (± 2.0 per cent) and P420 (± 4.0 per cent).

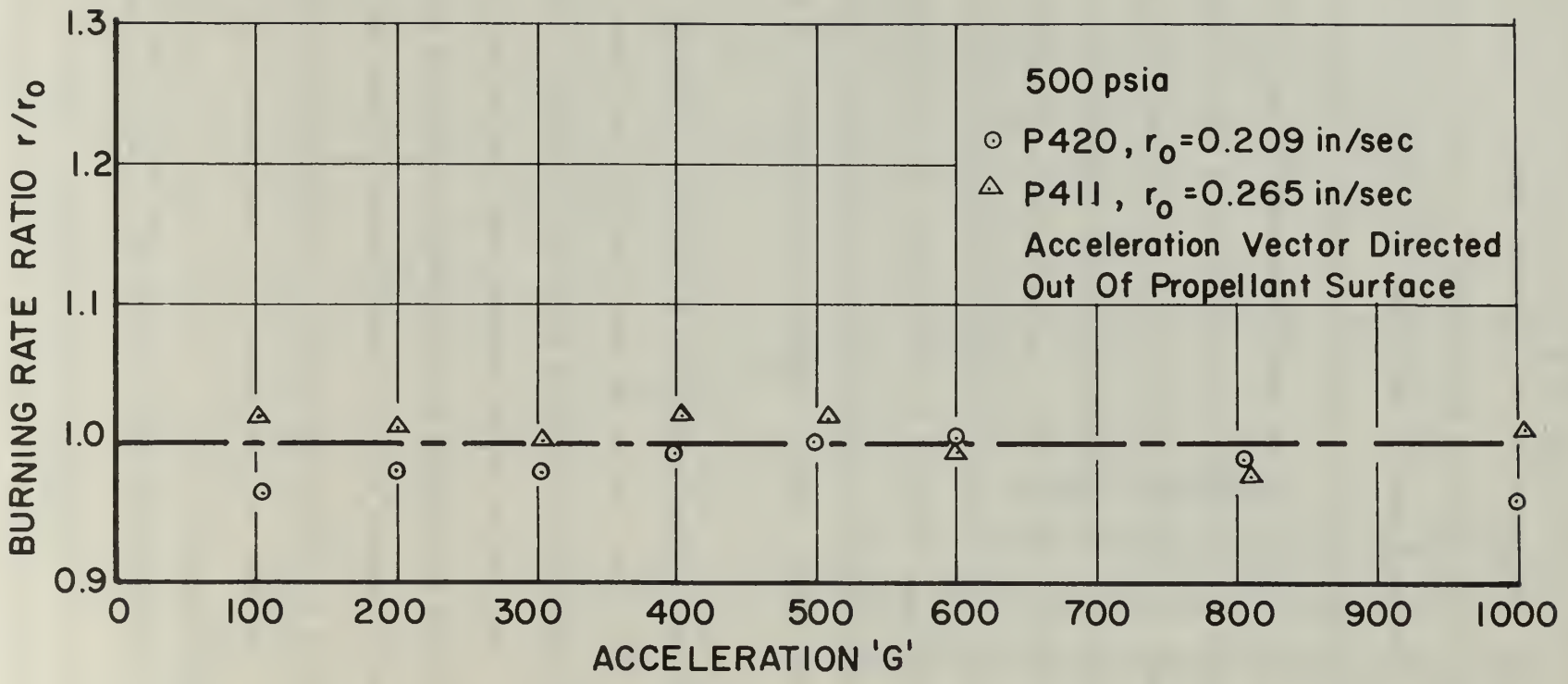

FIGURE 4 BURNING RATE RATIO VERSUS ACCELERATION WITH ACCELERATION VECTOR DIRECTED OUT OF PROPELLANT SURFACE

Figure 5 contains data which resulted from experiments in which the initial temperature of propellant P410 was 54° C. The data indicate that increasing the initial temperature of the propellant causes the burning rate ratio to depart from unity at a lower acceleration level. Higher initial propellant temperature also resulted in a higher limiting value of burning rate ratio as the acceleration level was increased beyond 400 G.

In Figures 6 and 7 are presented the smooth curves for the three propellants at 500 and 1000 psia respectively. These figures show the quantitative differences in burning rate ratio versus acceleration. The acceleration range below 150 G will be considered first. At 500 psia the burning rate ratios of all three propellants were found to be nearly equal. There were measurable differences in the burning rate at 1000 psia. Propellant P420 (largest average mmd AP) exhibited the greatest sensitivity to acceleration.[2] Propellant P411 (smallest average mmd AP) was not as sensitive to acceleration as was P420 but was more sensitive than P410 (intermediate average mmd AP).

There were definite and consistent differences in the burning rate ratios of these propellants at acceleration levels greater than 150 G. Propellant P411 exhibited the greatest sensitivity to acceleration at both pressure levels. Similarly at both pressure levels propellant P410 exhibited the least sensitivity to acceleration. Propellant P420 at 500 psia showed about the same sensitivity to acceleration as did the P410 propellant at 500 psia. Propellant P420 at 1000 psia had values of burning rate ratio midway between those of P410 and

---

[2]When the size and weight percentages of both the fine and coarse AP particles in the three non-metallized propellants are considered, propellant P420 is found to have the largest average mmd AP; propellant P411, the smallest average mmd AP; and propellant P410, an intermediate value.

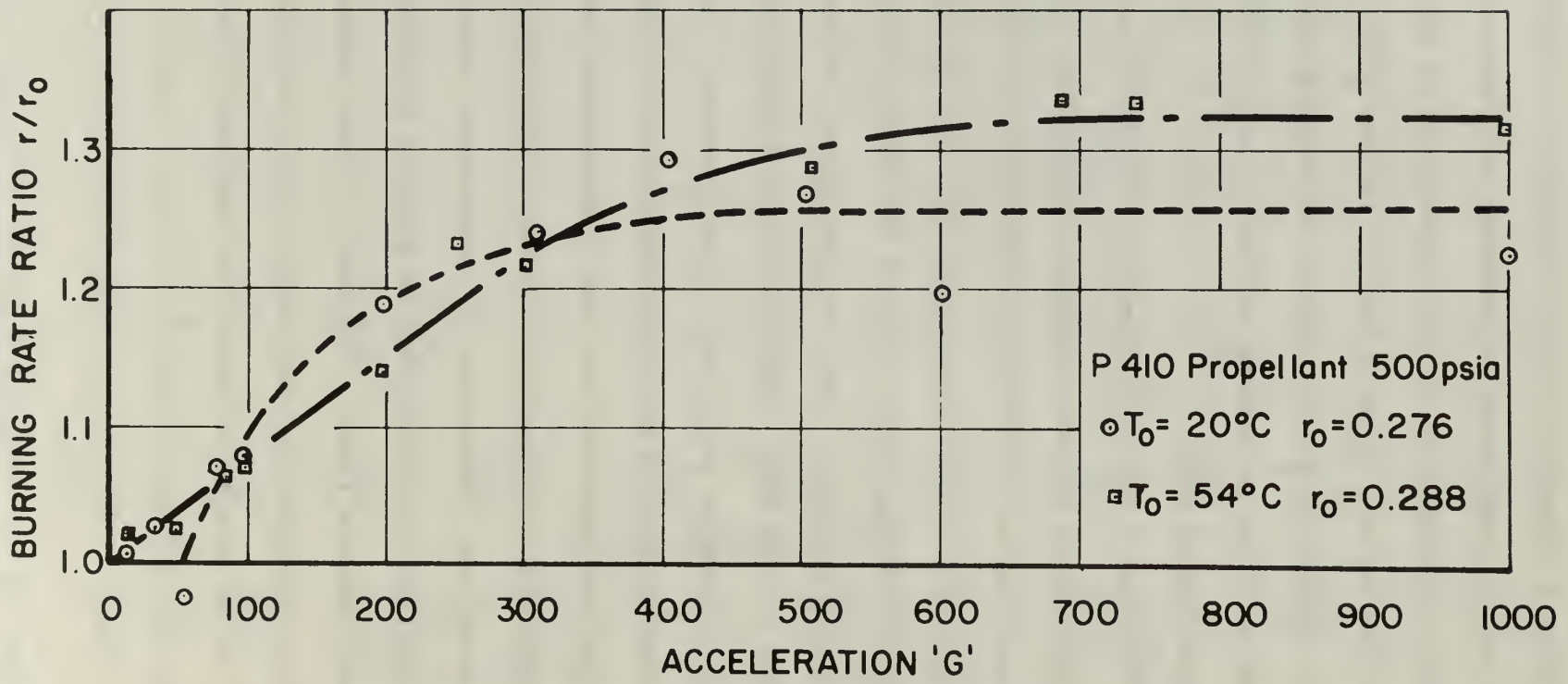

FIGURE 5 BURNING RATE RATIO VERSUS ACCELERATION AS A FUNCTION OF INITIAL PROPELLANT TEMPERATURE FOR PROPELLANT P410

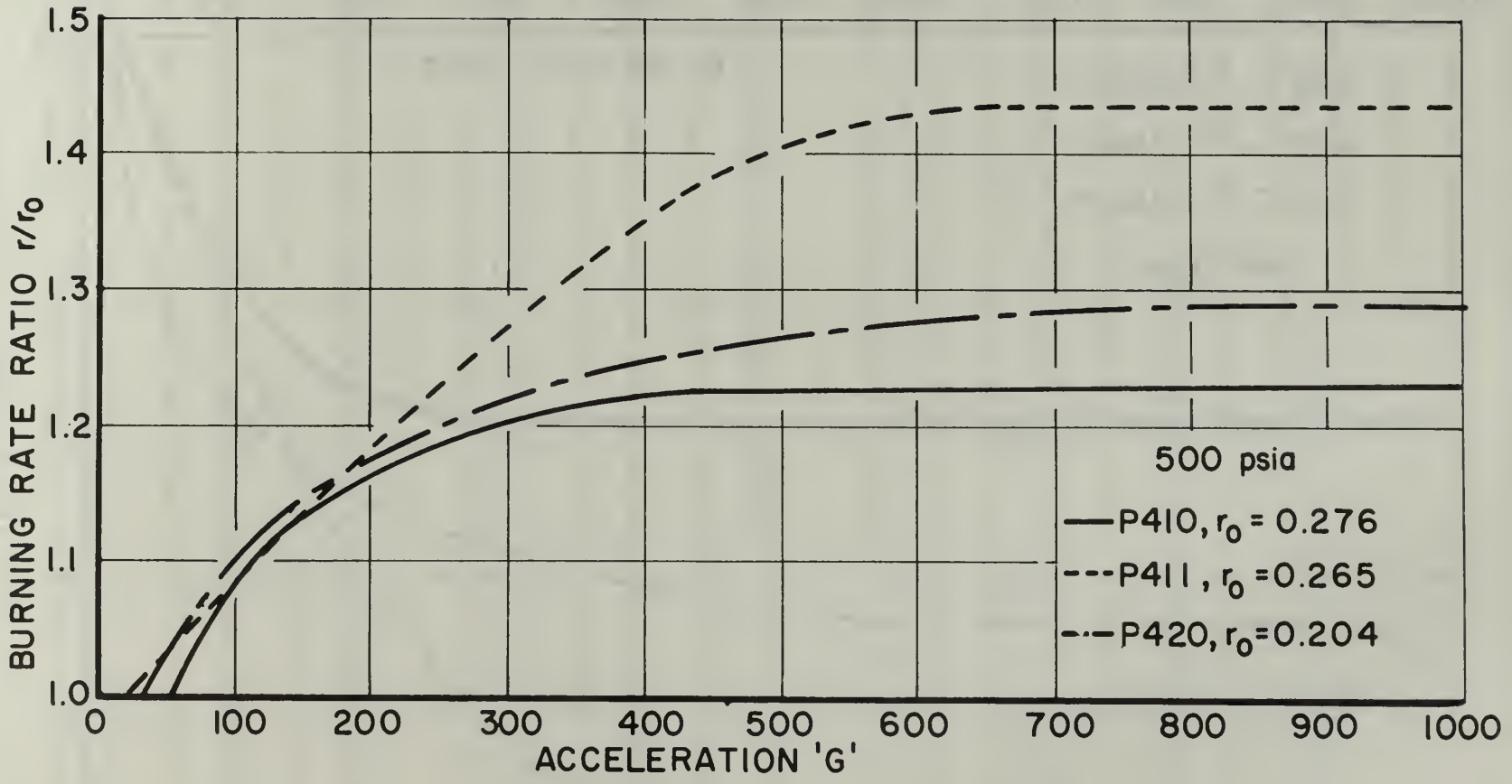

FIGURE 6 COMPARISON OF BURNING RATE RATIO VERSUS ACCELERATION FOR THREE NON-METALLIZED PROPELLANTS AT 500 PSIA

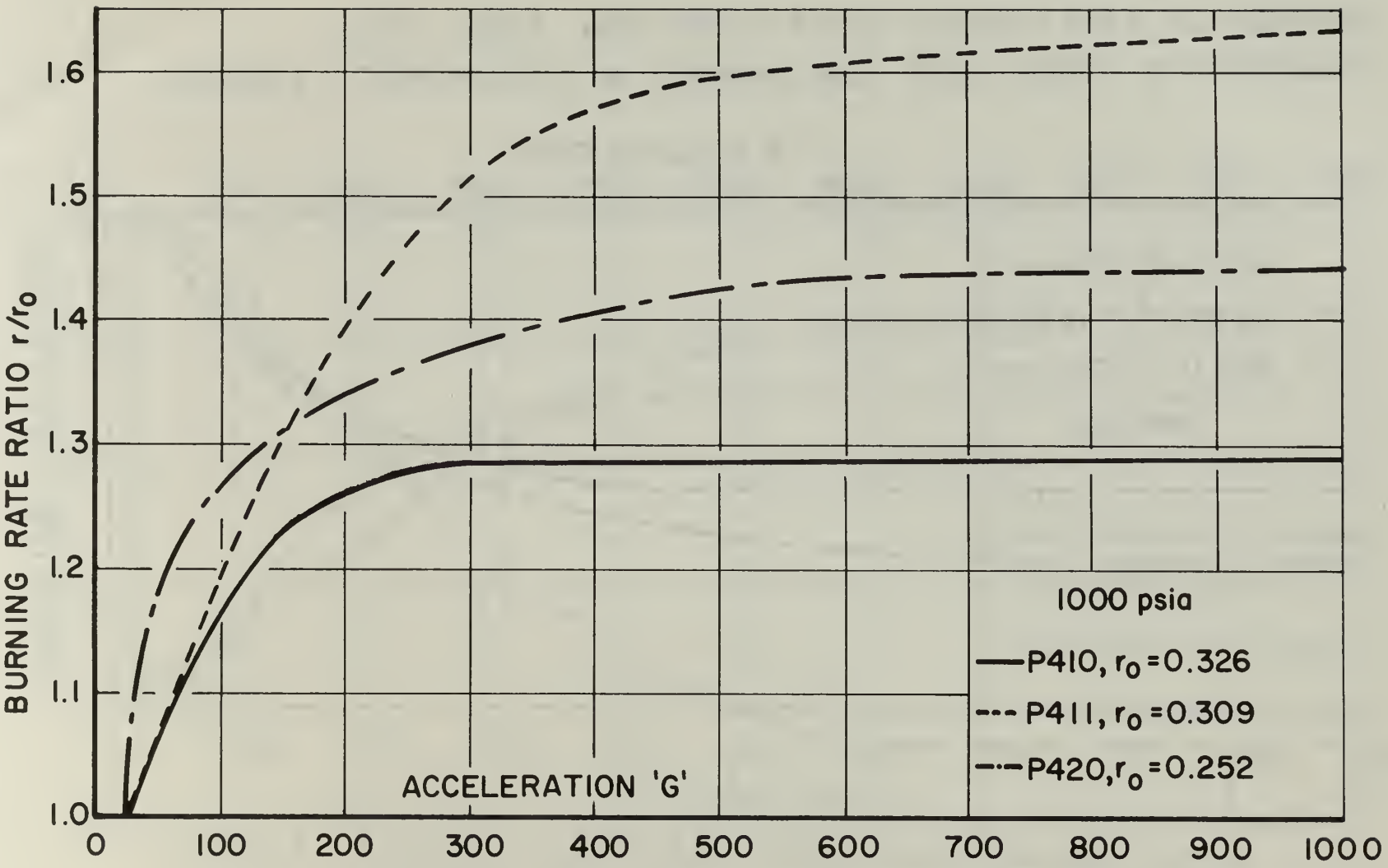

FIGURE 7 COMPARISON OF BURNING RATE RATIO VERSUS ACCELERATION FOR THREE NON-METALLIZED PROPELLANTS AT 1000 PSIA

P411 at 1000 psia. The relative sensitivity to acceleration of these propellants will be discussed further in Chapter V.

The spent inhibitor case of every non-metallized propellant strand was examined after each series of experiments. The cases of those strands which were burned with the acceleration vector directed into the propellant burning surface were found to contain a small amount of black powdery residue on the sides of the inhibitor case. The amount of black residue seemed to decrease with acceleration and did not accumulate in the bottom of the inhibitor case. The cases of those strands which were burned with the acceleration vector directed away from the burning surface contained a very small amount of the black powdery residue, just enough to blacken the sides of the inhibitor cases.

Comparison of Experiment with Glick's Theory

In this section is presented a brief description of Glick's theoretical analysis [7] of the acceleration induced burning rate increase of non-metallized propellants. Glick's analysis is based on an extension of Summerfield's [10] granular diffusion flame model. Detailed descriptions of Summerfield's and Glick's models can be obtained from the cited references.

Briefly stated, Summerfield's model assumes that propellant burning rate is controlled by the rate of energy feedback from the gas phase combustion zone to the propellant surface. Summerfield conceived the combustion zone as an aggregation of fuel vapor pockets surrounded by oxidizer vapor, or vice versa. It was assumed that the mass of each pocket was related directly to the size of the parent oxidizer particles but not to the pressure. At high pressures the

rate controlling mechanism was assumed to be the diffusion of fuel and oxidizer species into the combustion regions around each fuel (or oxidizer) pocket. The propellant burning rate was shown to be inversely proportional to the flame height which in turn was found to be inversely proportional to the one-third power of the pressure at the high pressure limit.

Glick extended the model to account for the acceleration induced buoyancy forces acting on what he assumed were fuel pockets surrounded by a sea of less dense oxidizer vapor. When the acceleration vector is directed into the propellant burning surface, the motion of the fuel pockets away from the propellant burning surface is retarded. In addition a relative velocity between the fuel pockets and the surrounding oxidizer vapor enhances the interdiffusion of fuel and oxidizer vapors. As a result, the fuel in the fuel pockets is combusted nearer the regressing propellant surface providing a higher energy flux back to the propellant surface which results in an increased overall burning rate.

When the acceleration vector is directed away from the propellant burning surface the fuel pocket lifetime is again shortened by the enhancement of fuel and oxidizer vapor interdiffusion. However, the velocity of the fuel pocket away from the propellant surface is increased. The net effect of these two distinct effects will depend on their relative magnitudes.

Glick's analysis yields an expression which can be used to predict the burning rate ratio as a function of both the direction and magnitude of the applied acceleration force. The expression

reduces to the following form when the acceleration is directed normal and into the propellant burning surface.

$$\frac{r}{r_o} = C\frac{\rho_g\, a\, \Delta\rho\, d_{f_v}^2}{\mu_g\, r_o\, \rho_s} + \left[\left\{ C\frac{\rho_g\, a\, \Delta\rho\, d_{f_v}^2}{\mu_g\, r_o\, \rho_s} \right\}^2 + 0.28 \left\{ \frac{\rho_g\, a\, \Delta\rho\, d_{f_v}^3}{\mu_g^2} \right\}^{\frac{1}{2}} \times \left\{ \frac{\mu_g}{\rho_g D} \right\}^{.35} + 1 \right]^{\frac{1}{2}} \qquad (1)$$

where:

r = burning rate with acceleration (cm/sec)

r_o = burning rate without acceleration (cm/sec)

C = constant

ρ_g = gas phase density (gm/cm^3)

a = acceleration (cm/sec^2)

$\Delta\rho$ = density difference between fuel and oxidizer vapors (gm/cm^3)

d_{f_v} = characteristic dimension of a pocket of fuel vapor (cm)

μ_g = gas viscosity (gm/cm sec)

ρ_s = solid phase propellant density (gm/cm^3)

D = binary diffusion coefficient for fuel and oxidizer species (cm^2/sec)

Equation 1 predicts that the burning rate ratio 1) is independent of time, 2) will increase at a given acceleration with increasing pressure, 3) will depart from unity as acceleration is increased from 0 G, 4) will decrease with decreasing fuel vapor pocket size, and 5) will be decreased by increasing the 0 G burning rate of the propellant (i.e., by adding burning rate catalysts or increasing the initial temperature of the propellant).

The first two conclusions are supported by the results obtained during this experimental investigation. The burning rate was not found

to depend on time as evidenced by the data presented in Figures 1 and 3 for two different strand lengths. As shown in Figures 1, 2, and 3, increasing the pressure resulted in an increased burning rate ratio at all acceleration levels as predicted by the model.

The last three predictions are not supported by the experimental data. First, as noted previously the burning rate did not immediately increase as the acceleration was increased from 0 G. Second, the analysis predicts that decreasing the fuel pocket dimension will decrease the acceleration sensitivity of the propellant. This is not in agreement with the experimental evidence as the following considerations indicate. In the Summerfield and Glick models the size of the fuel pockets is assumed to be dependent on the size of the parent oxidizer particles in the solid phase of the propellant. Decreasing the mean size of the oxidizer particles will decrease the fuel pocket size. Reference to the propellant formulations presented in Appendix IV for propellants P410, P411, and P420 indicates that propellant P411 has the smallest size mean oxidizer particles and thus should have the smallest size fuel vapor pockets. A similar line of reasoning indicates that propellant P420 should have the largest size fuel vapor pockets. Thus Glick's model predicts that the acceleration sensitivity of these propellants should be as follows: P420 should have the greatest sensitivity to acceleration, P411 should have the least sensitivity to acceleration, and P410 should have a sensitivity somewhere between that of P420 and P411. Reference to Figures 6 and 7 indicates that this is not the case. The order of increasing sensitivity was found to be: P410, P420, and P411. The failure of Glick's analysis to predict the relative sensitivity of these propellants is judged the most serious shortcoming of the model.

Finally, increasing the initial temperature of propellant P410 from 20° to 54° C resulted in the O G burning rate increasing from 0.276 to 0.288 inches/second (approximately 4.0 per cent). The analysis predicts that this increase in O G burning rate should have the effect of decreasing the acceleration sensitivity of the propellant. The data in Figure 5 do not confirm this but suggest the propellant became more sensitive to acceleration.

Basic to Glick's model is the assumption that the imposed acceleration field acts on the density inhomogeneities of the gas phase to produce a relative velocity between the fuel pockets and the surrounding oxidizer rich AP decomposition products. It is interesting to note that in a standard acceleration environment the gaseous fuel and oxidizer species are accelerated at a rate of approximately 1000 G as they traverse the distance between the solid propellant surface and the flame zone.[3] This inherent acceleration is as great as the largest externally imposed acceleration levels used during the course of this investigation. It would appear that an analysis of a model based on the establishment of an external acceleration induced relative velocity between reacting species should account for the inherent acceleration forces acting on the gas phase. The analysis does not account for this inherent acceleration.

Although the analysis of the proposed model correctly predicts the steady-state and pressure dependent behavior of the propellant, it fails to predict other important experimentally determined aspects of

---

[3]This results from heating the combustion gases from the surface temperature to the flame temperature in a distance equal to the flame zone thickness.

the behavior of the propellants. This failure to do so casts doubt on the validity of the model. An analysis is presented in Chapter V which can be used successfully to predict the experimental observations obtained during the course of this investigation.

II. METALLIZED PROPELLANTS

Experimental Results

Six propellants in the parametric series contained aluminum powder as the additive: P401, P412, P413, P415, P421, and P423. One propellant, P414, contained aluminum oxide as the additive. In much of the following discussion all seven of these propellants will be considered metallized propellants for convenience of presentation.

These seven propellants were investigated at pressures of 500 and 1000 psia. The experiments were all conducted with the acceleration vector directed normal and into the propellant burning surface. Plots of burning rate ratio versus acceleration for these propellants are presented in Figures 8 through 21. The data are arranged such that for each propellant there results two figures. One figure contains the data obtained at 500 psia for a given propellant, and the other figure, the data for 1000 psia. For most of the propellants two different strand lengths were investigated. Each figure contains the data for both strand lengths.

The value of r_o used to form the burning rate ratio was the average of four burning rates obtained at 0 G, two burning rates measured with 1.0 inch strands and two rates measured with the longer length strands. The scatter at 500 psia in the 0 G burning rates for the seven propellants was: P401, ± 1.1 per cent; P412, ± 1.9 per cent;

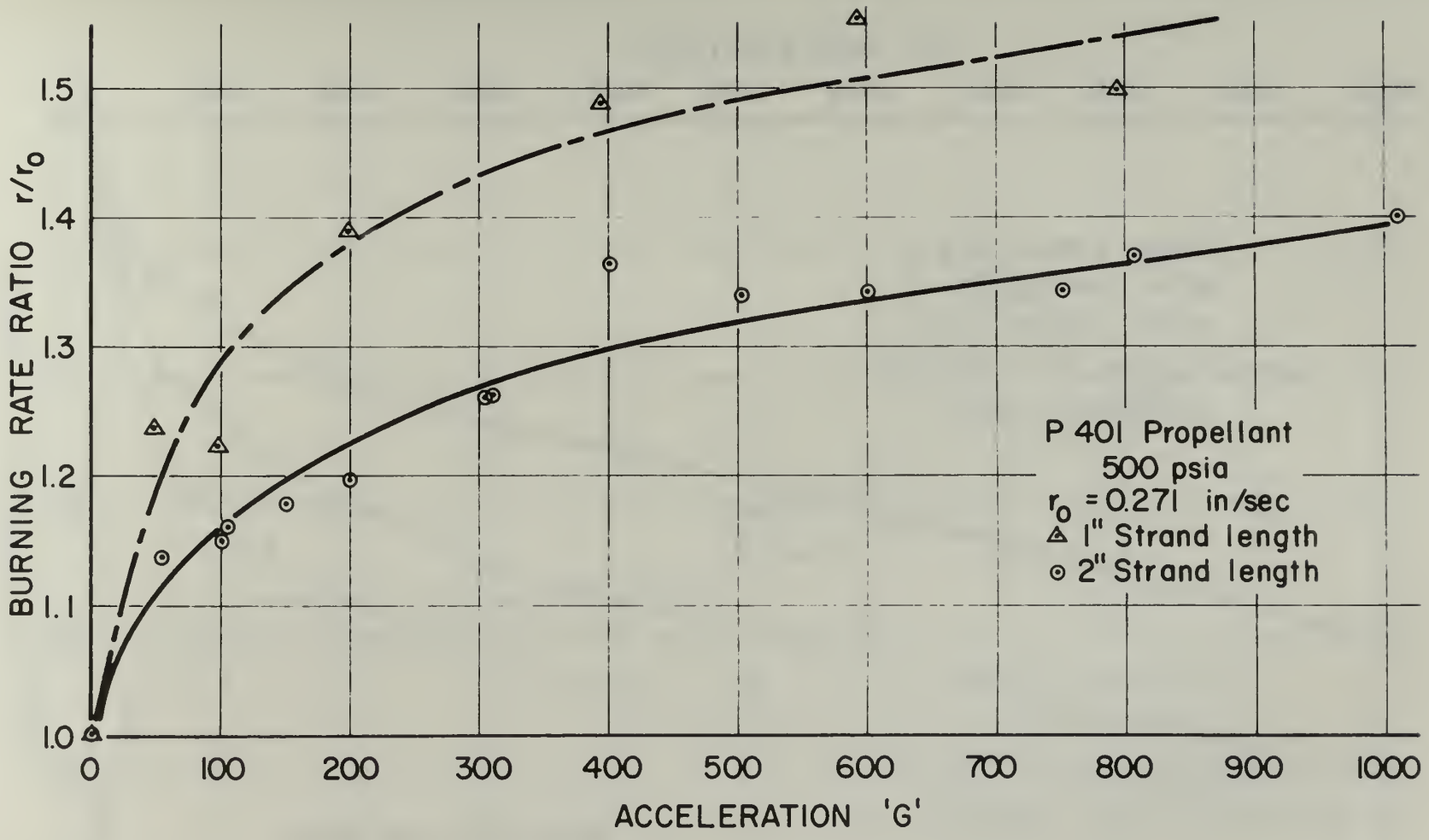

FIGURE 8 BURNING RATE RATIO VERSUS ACCELERATION FOR PROPELLANT P401 AT 500 PSIA

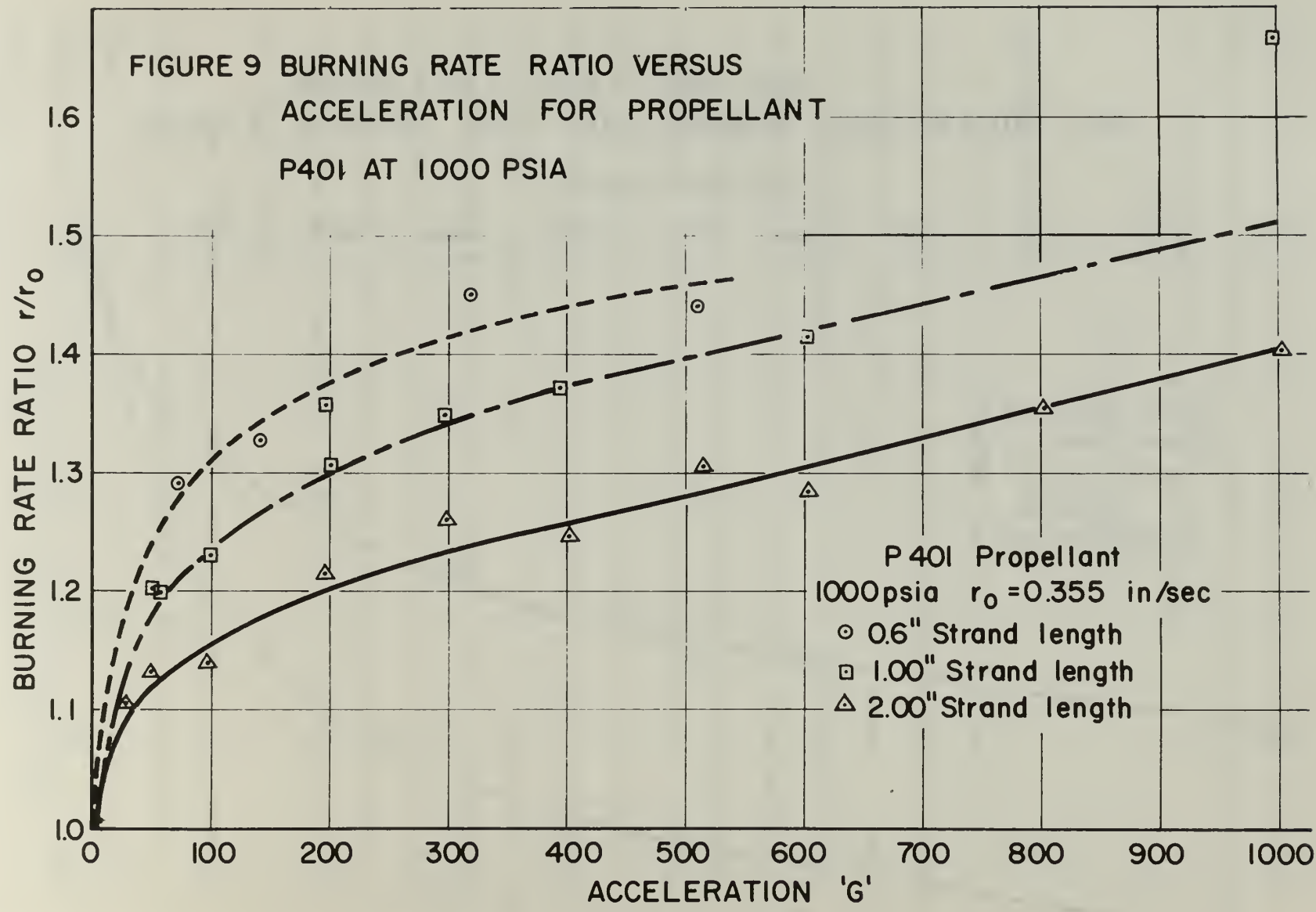
FIGURE 9 BURNING RATE RATIO VERSUS ACCELERATION FOR PROPELLANT P401 AT 1000 PSIA
BURNING RATE RATIO r/r0
1.0
1.1
1.2
1.3
1.4
1.5
1.6
0
100
200
300
400
500
600
700
800
900
1000
ACCELERATION 'G'
P 401 Propellant
1000psia r0 =0.355 in/sec
0.6" Strand length
1.00" Strand length
2.00" Strand length

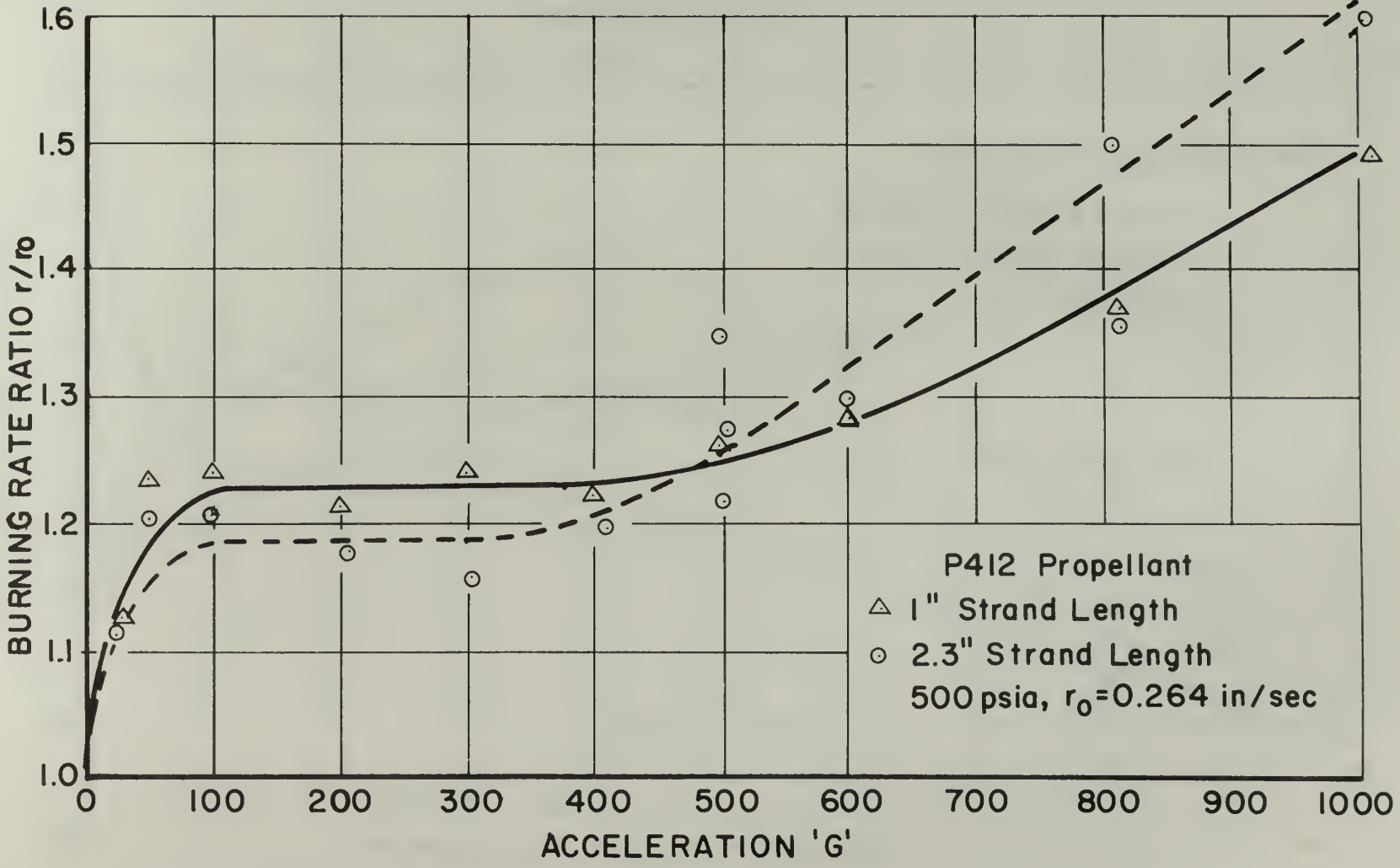

FIGURE 10 BURNING RATE RATIO VERSUS ACCELERATION FOR PROPELLANT P412 AT 500 PSIA

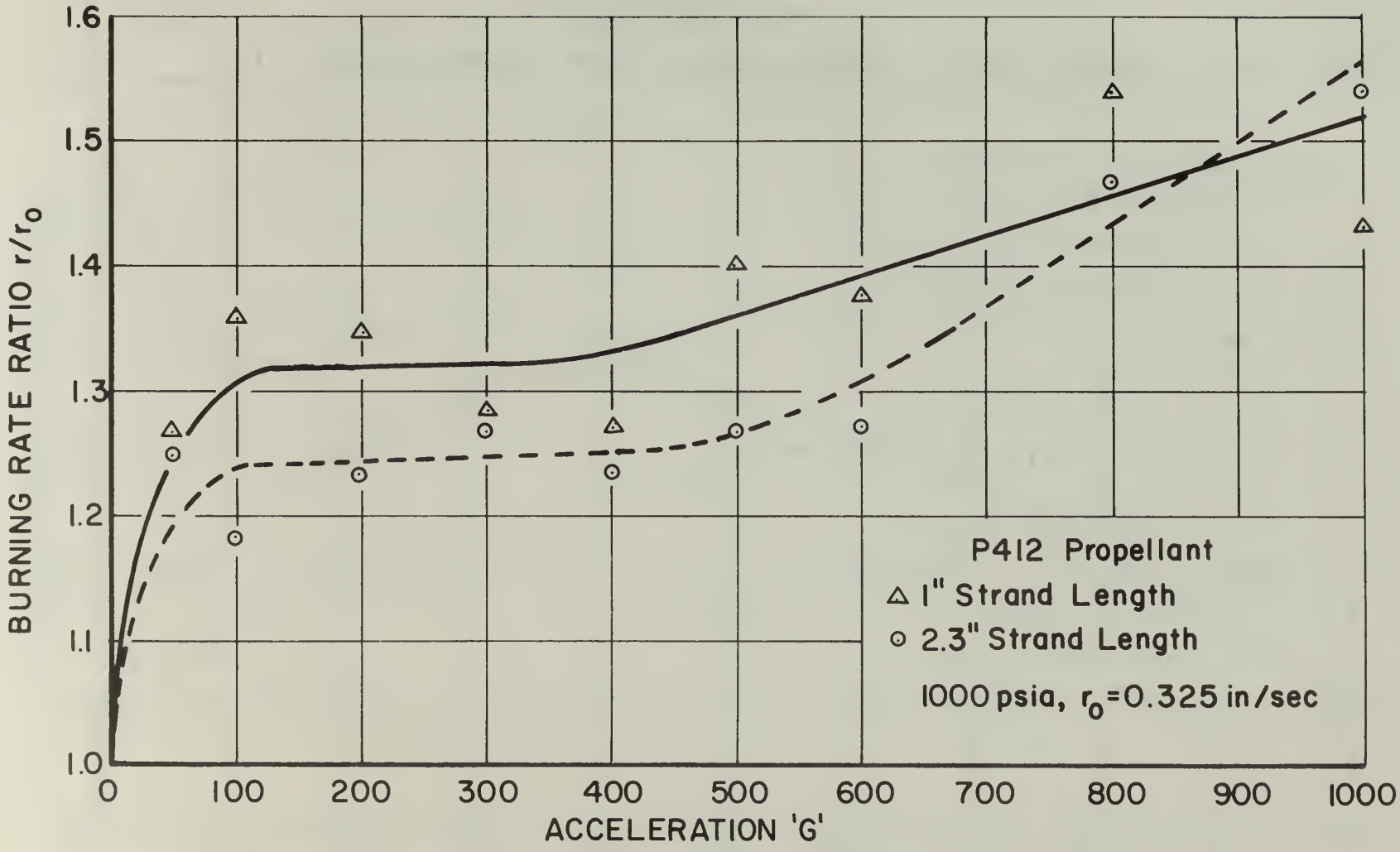

FIGURE 11 BURNING RATE RATIO VERSUS ACCELERATION FOR PROPELLANT P412 AT 1000 PSIA

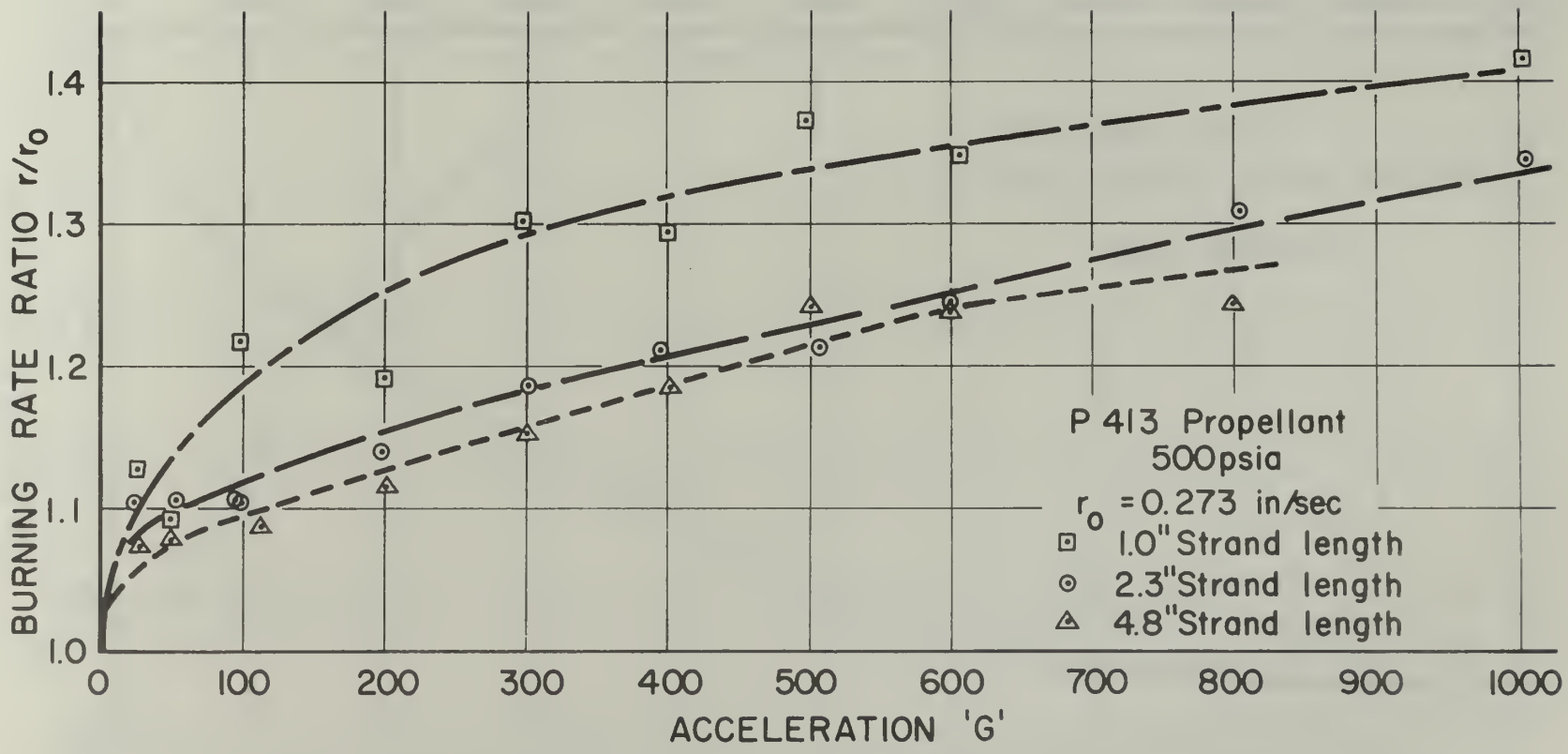

FIGURE 12 BURNING RATE RATIO VERSUS ACCELERATION FOR PROPELLANT P413 AT 500 PSIA

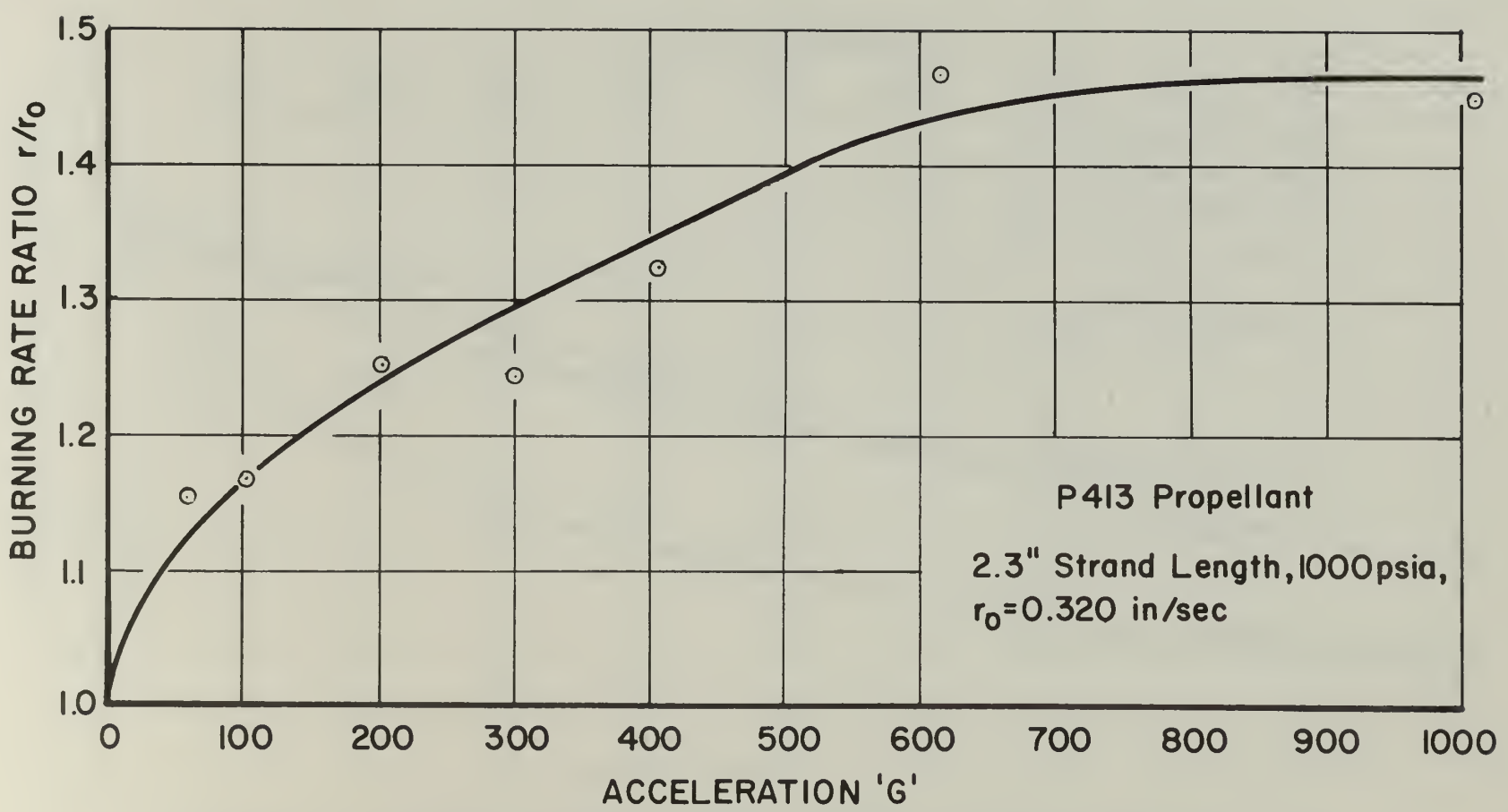

FIGURE 13 BURNING RATE RATIO VERSUS ACCELERATION FOR PROPELLANT P413 AT 1000 PSIA

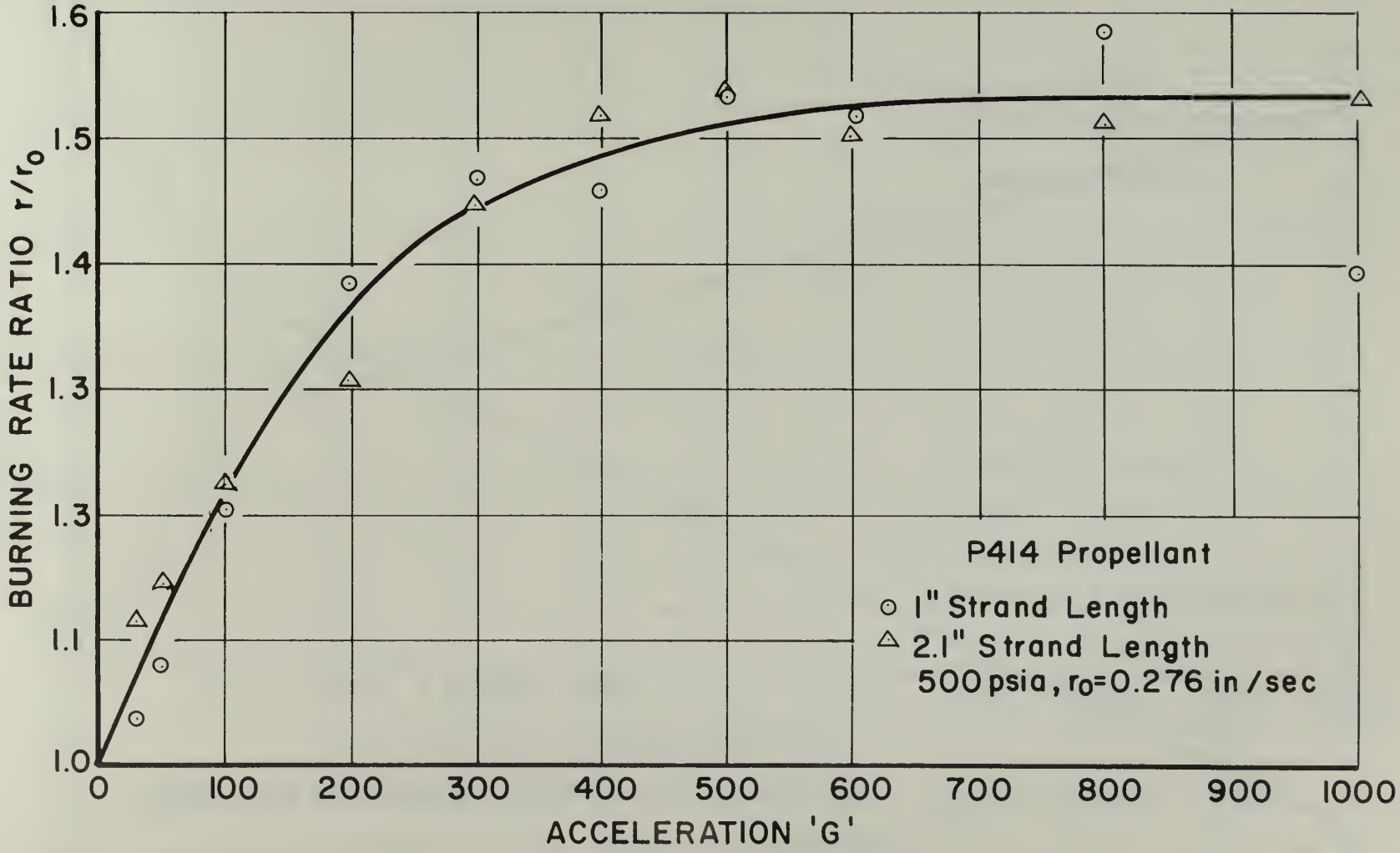

FIGURE 14 BURNING RATE RATIO VERSUS ACCELERATION FOR PROPELLANT P414 AT 500 PSIA

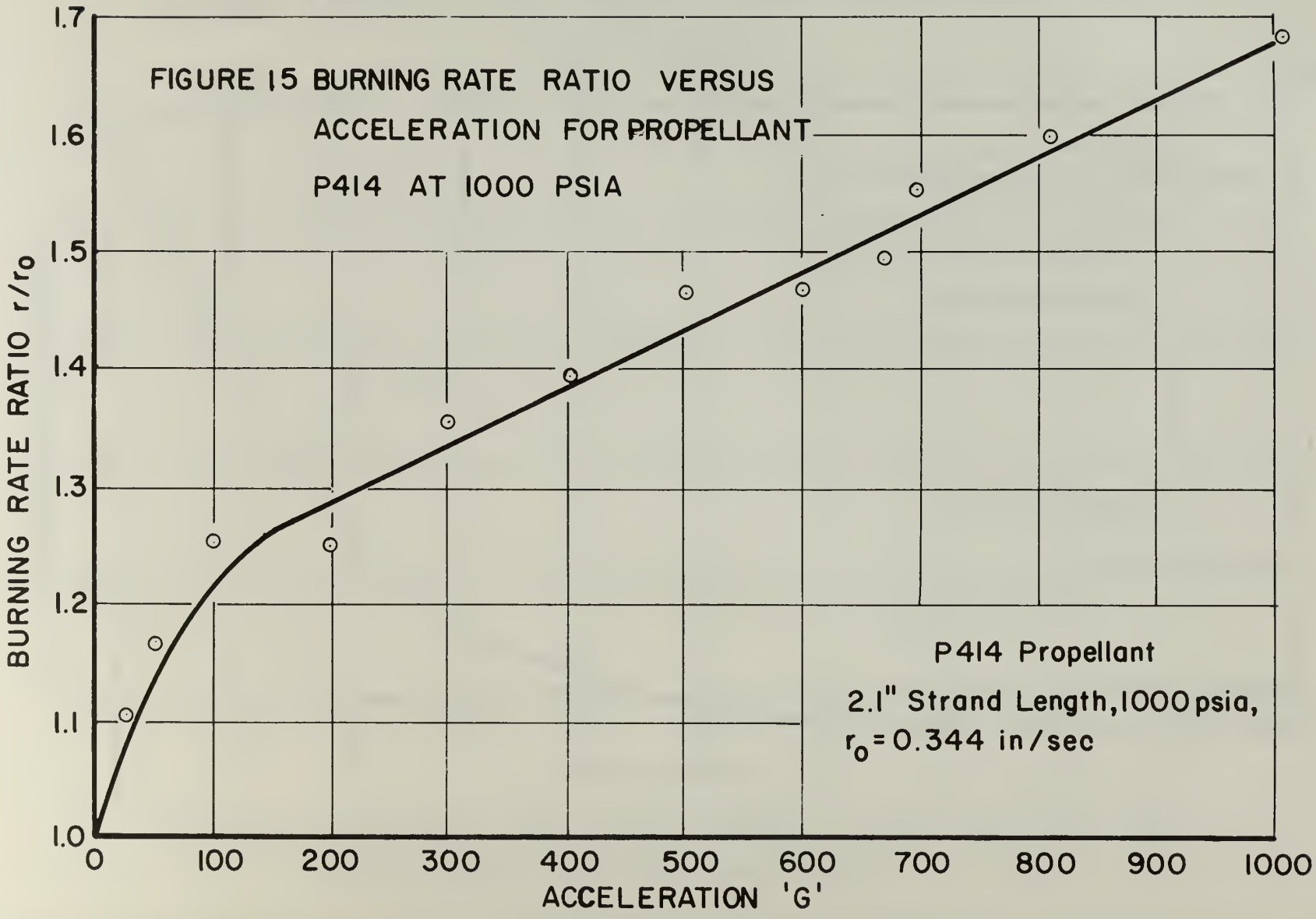
FIGURE 15 BURNING RATE RATIO VERSUS ACCELERATION FOR PROPELLANT P414 AT 1000 PSIA
BURNING RATE RATIO r/r0
1.0
1.1
1.2
1.3
1.4
1.5
1.6
1.7
0
100
200
300
400
500
600
700
800
900
1000
ACCELERATION 'G'
P414 Propellant
2.1" Strand Length, 1000 psia,
r0 = 0.344 in/sec

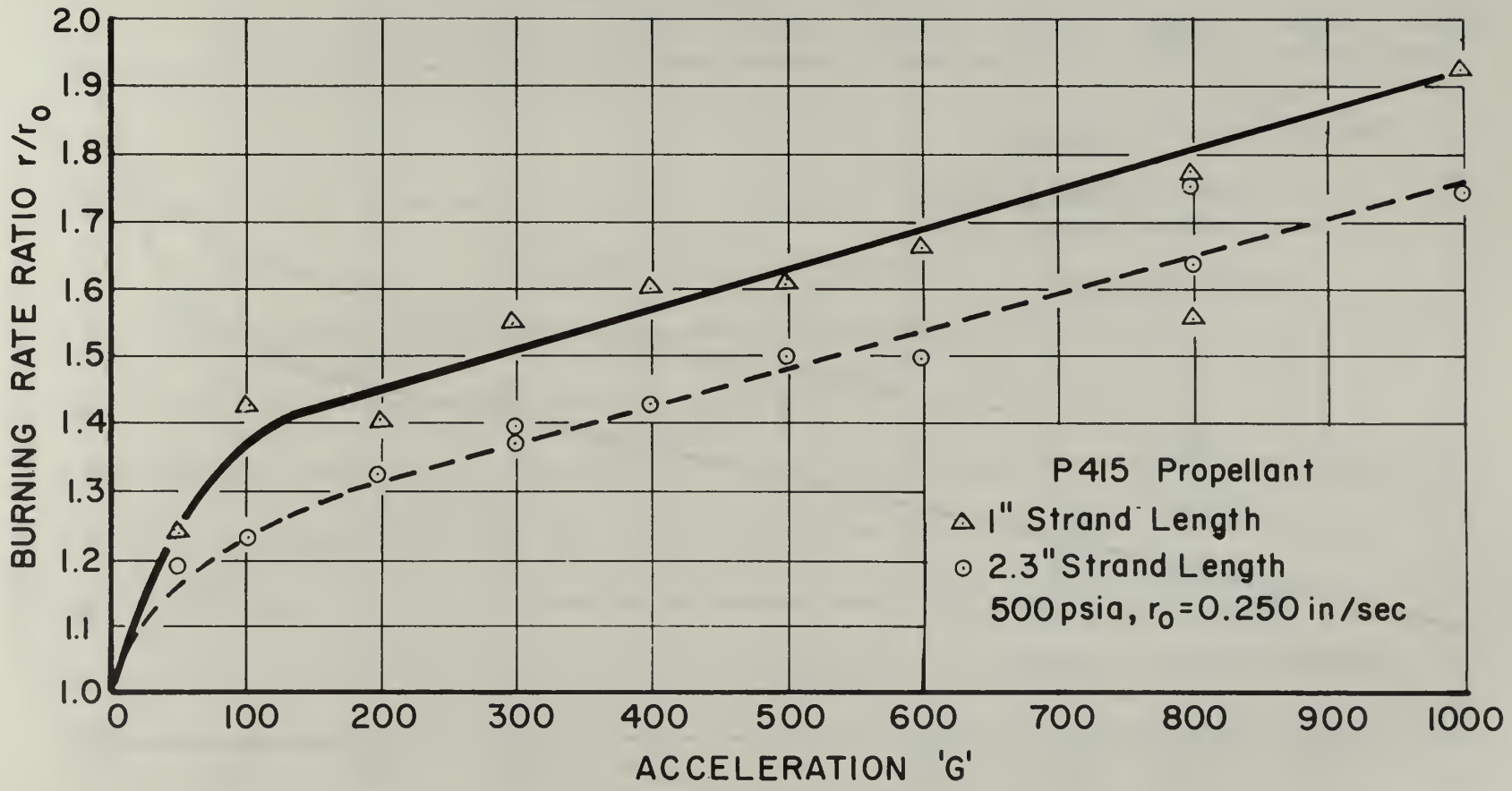

FIGURE 16 BURNING RATE RATIO VERSUS ACCELERATION FOR PROPELLANT P415 AT 500 PSIA

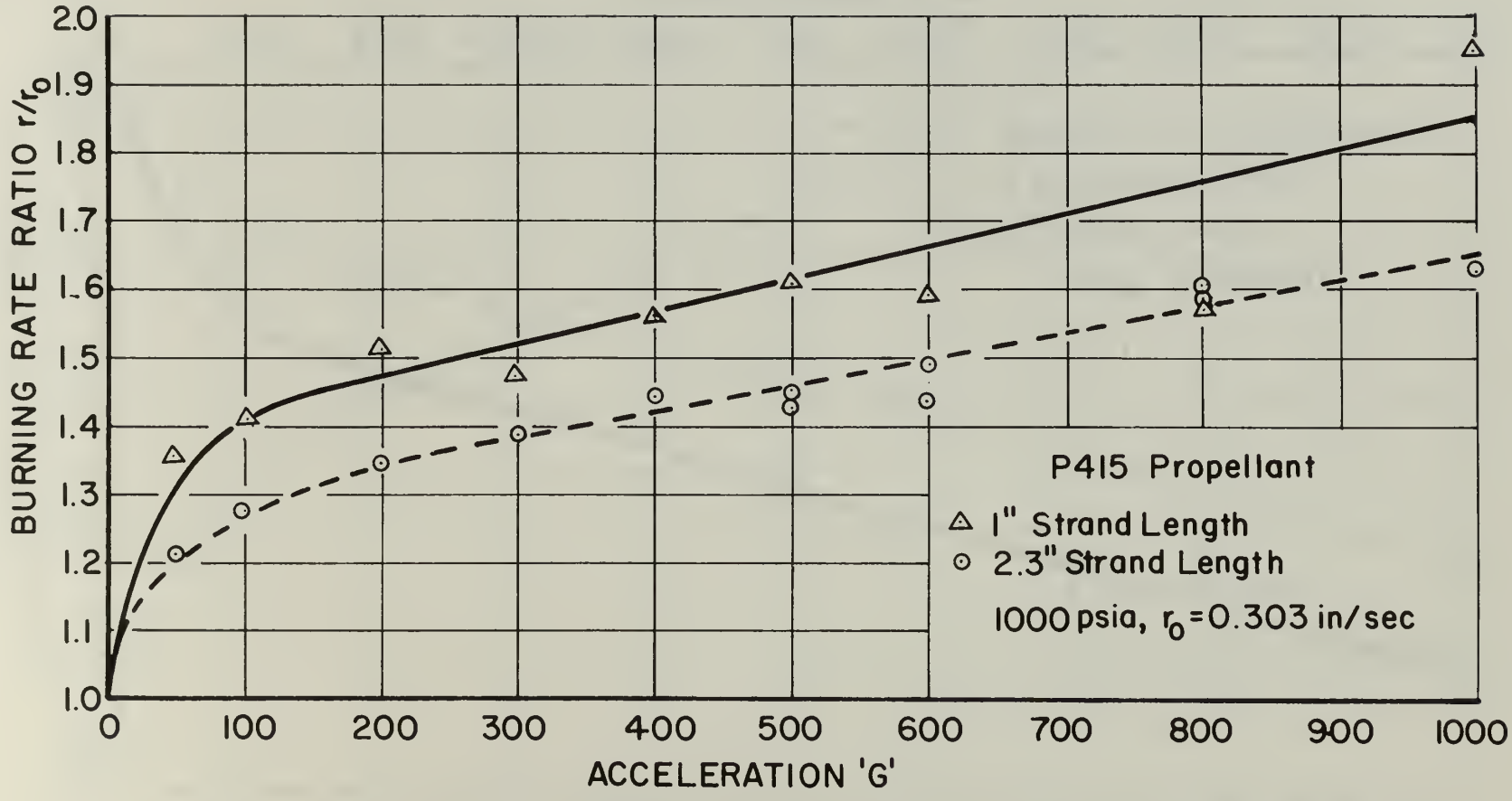

FIGURE 17 BURNING RATE RATIO VERSUS ACCELERATION FOR PROPELLANT P415 AT 1000 PSIA

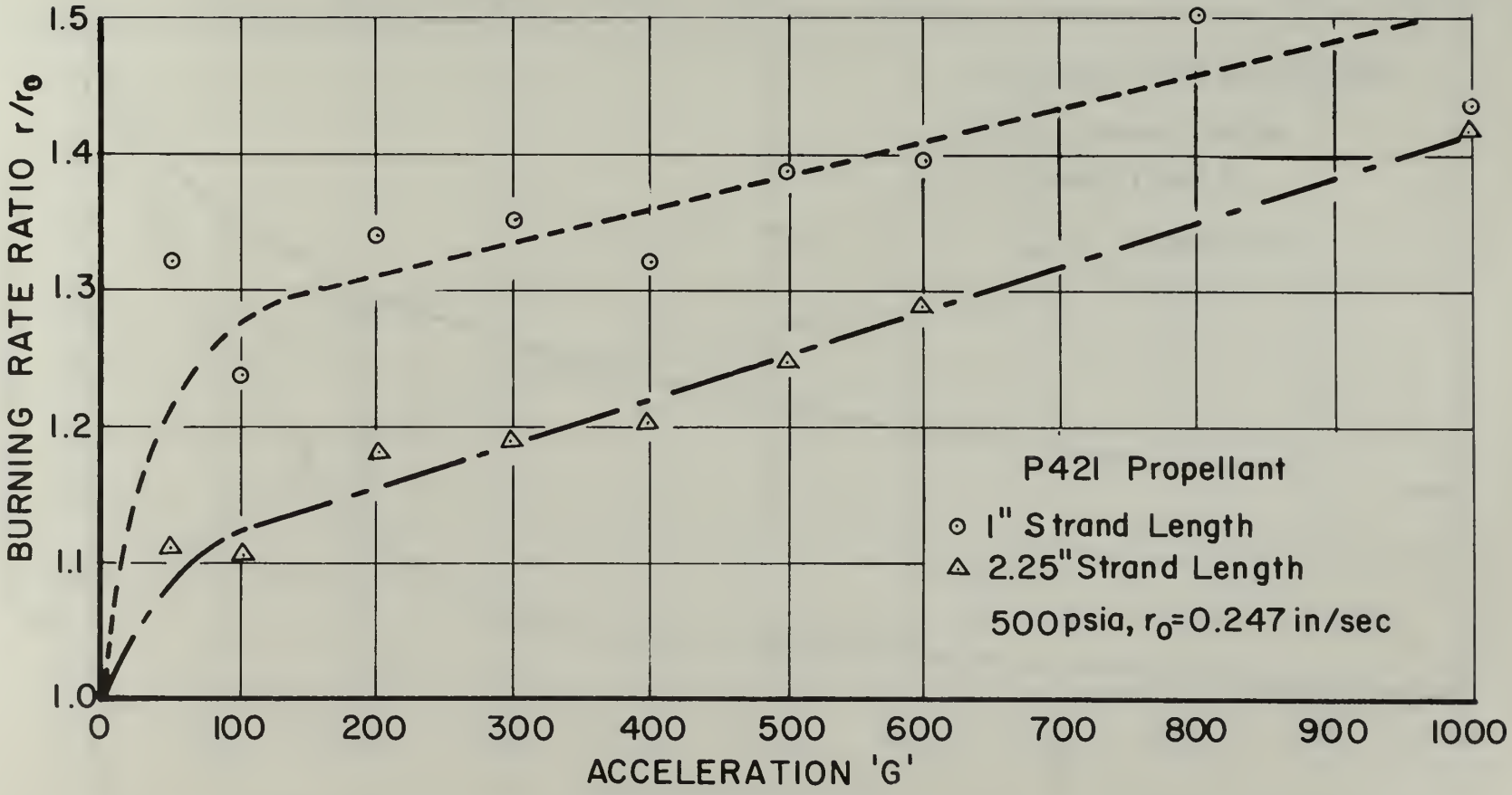

FIGURE 18 BURNING RATE RATIO VERSUS ACCELERATION FOR PROPELLANT P421 AT 500 PSIA

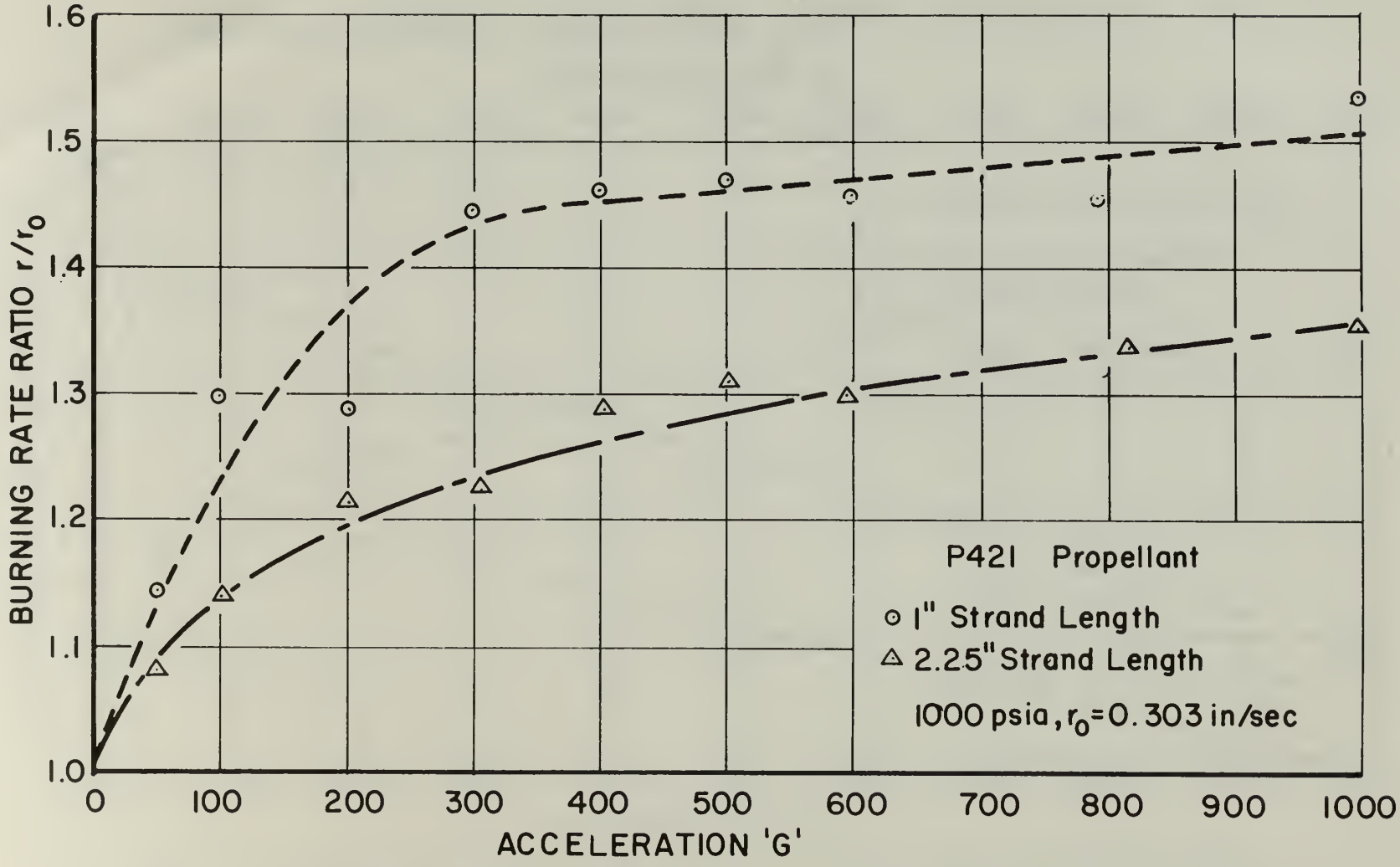

FIGURE 19 BURNING RATE RATIO VERSUS ACCELERATION FOR PROPELLANT P421 AT 1000 PSIA

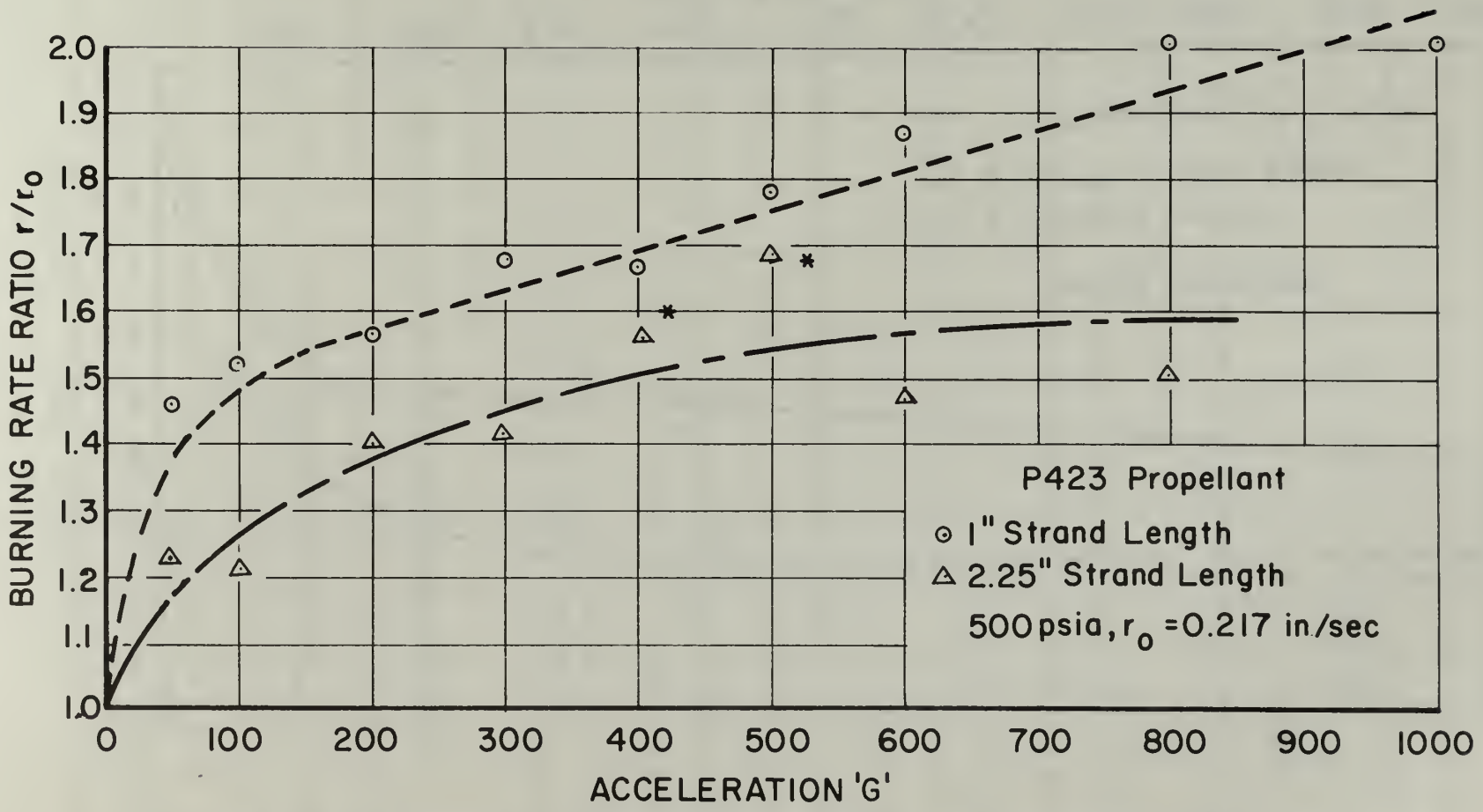

FIGURE 20 BURNING RATE RATIO VERSUS ACCELERATION FOR PROPELLANT P423 AT 500 PSIA

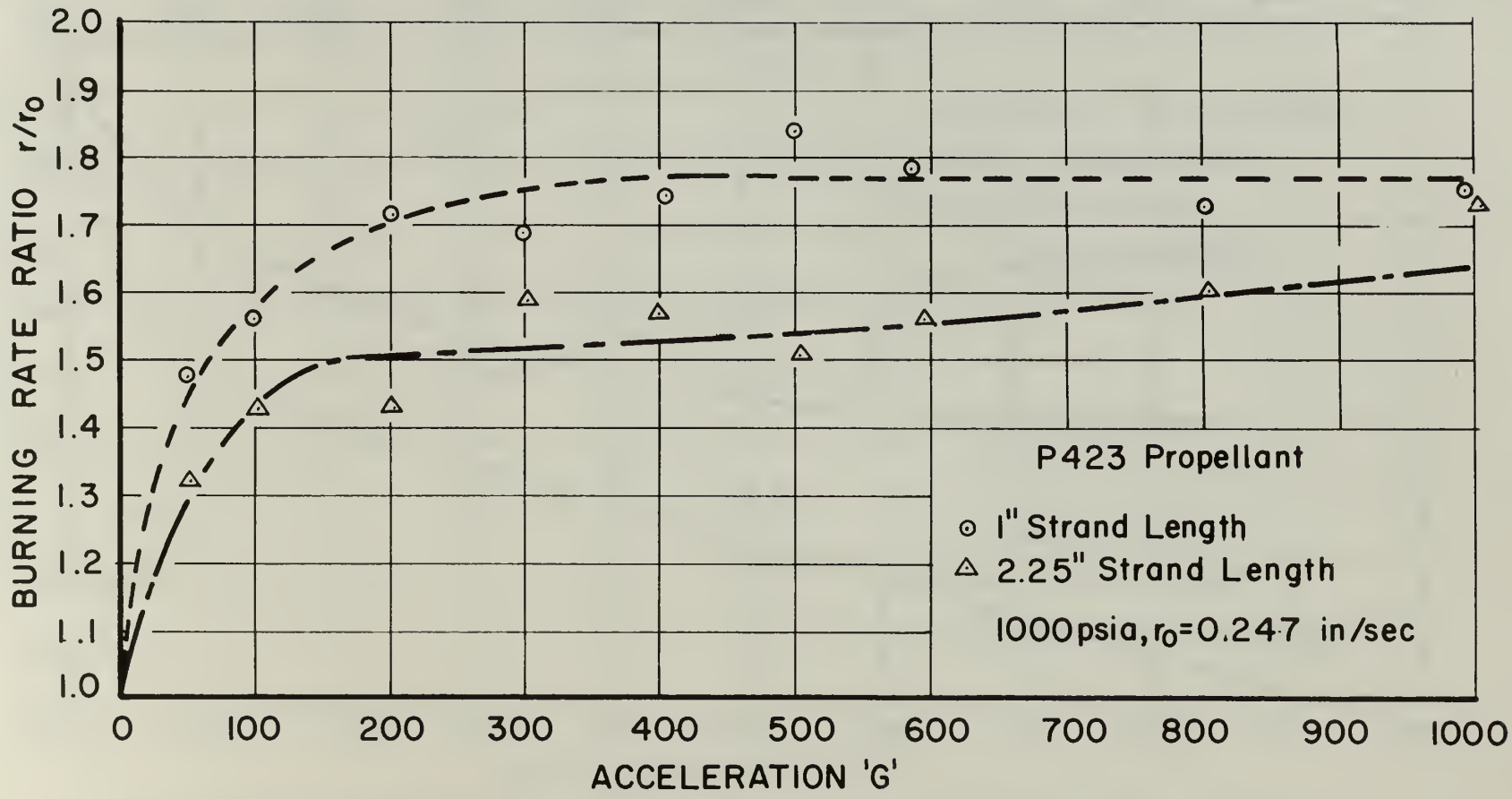

FIGURE 21 BURNING RATE RATIO VERSUS ACCELERATION FOR PROPELLANT P423 AT 1000 PSIA

P413, ± 2.9 per cent; P414, ± 2.9 per cent; P415, ± 2.8 per cent; P421, ± 1.2 per cent; and P423, ± 3.2 per cent. At 1000 psia the values were: P401, ± 2.3 per cent; P412, ± 1.5 per cent; P413, ± 0.6 per cent; P414, ± 1.0 per cent; P415, ± 1.7 per cent; P421, ± 4.3 per cent; and P423, ± 4.8 per cent. This scatter is again attributed to a combination of experimental error and the inherent non-uniformities in the propellant composition from one strand to the next.

The data in Figures 8 through 21 indicate the following general characteristics of burning rate ratio versus acceleration for all the metallized propellants: 1) Burning rate ratio increases with acceleration level commencing with one G acceleration; 2) burning rate ratio does not tend to a constant limiting value at high acceleration levels; 3) burning rate ratio for a given propellant exhibits no consistent pressure dependence (e.g., raising the pressure from 500 to 1000 psia resulted in lower burning rate ratios for P401, higher burning rate ratios for P412, P413, and P421, and no measurable change in the values for P414, P415, and P423 propellants); and 4) burning rate ratio is decreased by increasing the strand length while maintaining pressure and acceleration level constant.

There were exceptions to these general characteristics. The burning rate ratios of P413 at 1000 psia (Figure 13), P414 at 500 psia (Figure 14), and P423 at 1000 psia (Figure 21) did tend to a constant limiting value at high acceleration levels. No decrease in burning rate ratio with increasing strand length was observed for P414 (aluminum oxide additive) at 500 psia (Figure 14) or for P412 (only propellant with 5 per cent aluminum additive) at 500 psia and acceleration levels greater than 500 G (Figure 10).

The decrease in burning rate ratio with increasing strand length indicates that a strand at a given acceleration and pressure level experiences a decreasing burning rate as the strand proceeds to burn. Individual strands of P413 propellant were equipped with timing wires to verify the decrease in burning rate as burning proceeds. The data are presented in Table I. The data in the table confirm the decrease in burning rate. A probable cause for this phenomenon will be discussed later in this section.

A summary of burning rate ratio versus acceleration data for propellants P412, P413, P415, P421, and P423 is shown in Figures 22 and 23. A trend for burning rate ratio versus the 0 G burning rate of a propellant becomes evident if these propellants are divided into two groups according to the size of the coarse oxidizer particles. Consider the group P412, P413, and P415 first (coarse AP 94 μ). Propellants P412 and P413 exhibit approximately the same acceleration sensitivity and have approximately the same 0 G burning rates. Propellant P415 exhibits a higher sensitivity to acceleration than do P412 and P413 and has a lower 0 G burning rate. There exists an inverse relationship between acceleration sensitivity and 0 G burning rate. The same inverse relationship is evident for the group P421 and P423 (coarse AP 200 μ). P421 has the higher 0 G burning rate and the lower sensitivity to acceleration. However, the inverse relationship does not hold when the five propellants are considered together. As indicated by the data in Figures 22 and 23, propellants P415 and P421 have essentially equal 0 G burning rates (approximately 0.250 inches/second at 500 psia and 0.303 inches/second at 1000 psia) but quite different acceleration sensitivities (at 1000 G P415 exhibits a burning rate ratio

TABLE I

SUMMARY OF TIMING WIRE DATA FOR
ALUMINIZED P413 PROPELLANT

	Acceleration: 0 G		
Dist Int	0.00-0.64	0.64-1.66	1.66-2.306
r_o inch/sec	0.254	0.259	0.259
	Acceleration: 0 G		
Dist Int	0.00-1.00	1.00-1.91	1.91-2.298
r_o inch/sec	0.269	0.264	0.250
	Acceleration: 106 G		
Dist Int	0.00-0.24	0.24-1.39	1.39-2.301
r inch/sec	0.326	0.296	0.280
	Acceleration: 103 G		
Dist Int	0.00-0.52	0.52-1.52	1.52-2.285
r inch/sec	0.345	0.298	0.282
	Acceleration: 303 G		
Dist Int	0.00-0.27	0.27-1.01	1.01-2.309
r inch/sec	0.774	0.387	0.327
	Acceleration: 306 G		
Dist Int	0.00-0.61	0.61-1.55	1.55-2.312
r inch/sec	0.422	0.316	0.305
	Acceleration: 310 G		
Dist Int	0.00-0.97	0.97-1.61	1.61-2.285
r inch/sec	0.359	0.297	0.326
	Acceleration: 508 G		
Dist Int	0.00-0.51	0.51-1.56	1.56-2.307
r inch/sec	0.418	0.389	0.379
	Acceleration: 508 G		
Dist Int	0.00-0.74	0.74-1.69	1.69-2.300
r inch/sec	0.430	0.341	0.329
	Acceleration: 508 G		
Dist Int	0.00-0.69	0.69-2.309	
r inch/sec	0.407	0.323	

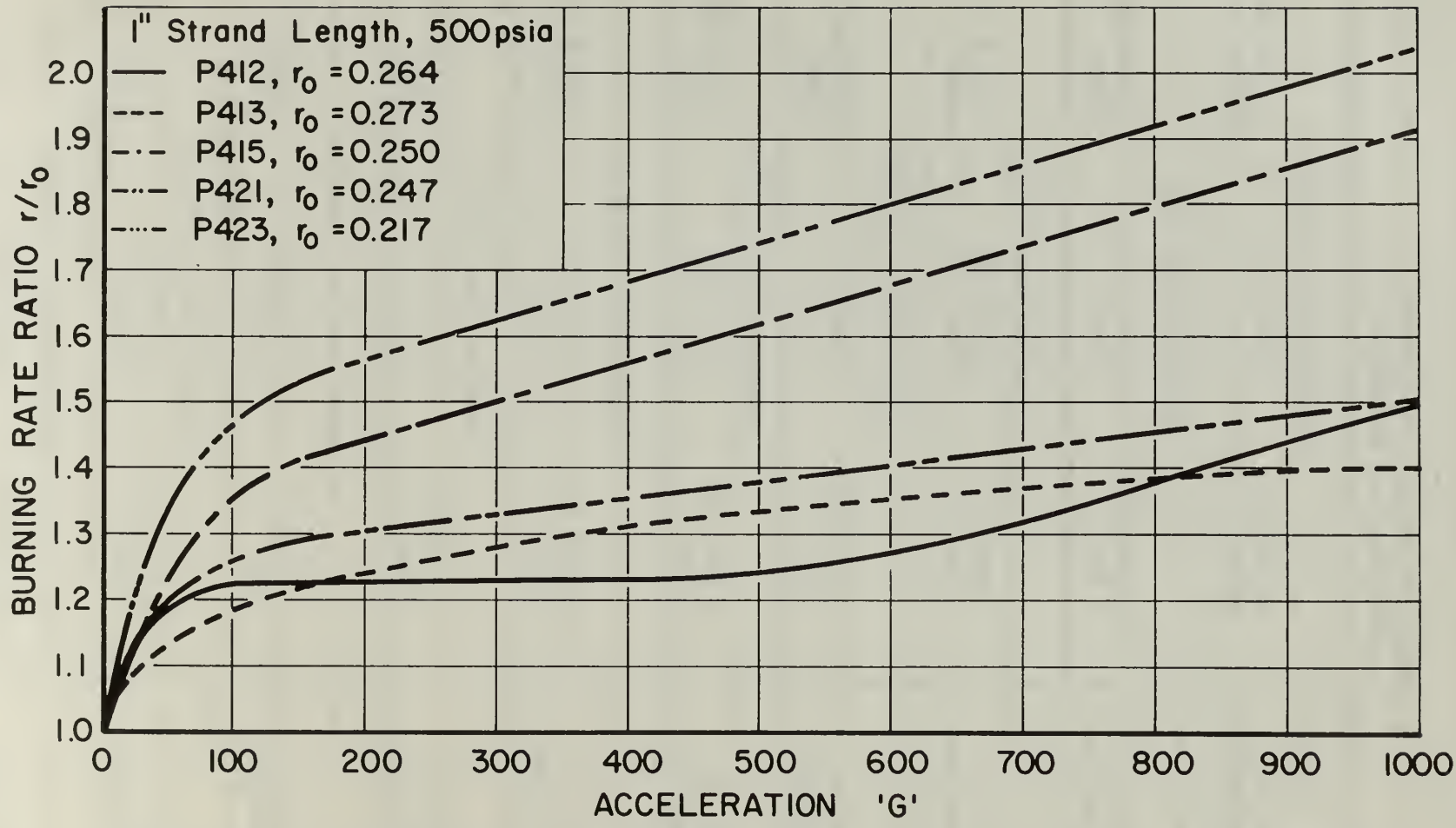

FIGURE 22 COMPARISON OF BURNING RATE RATIO VERSUS ACCELERATION FOR FIVE METALLIZED PROPELLANTS AT 500 PSIA

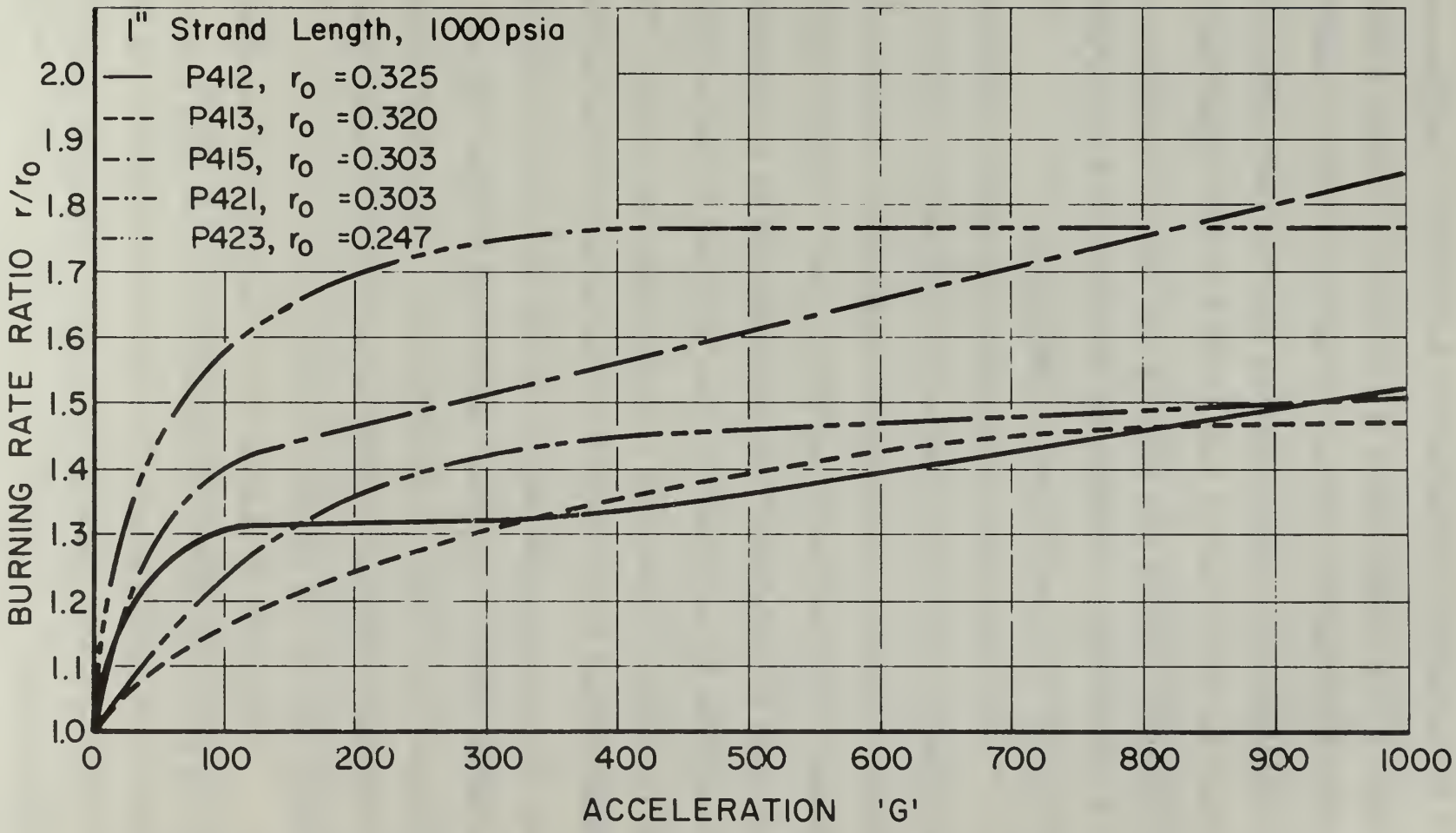

FIGURE 23 COMPARISON OF BURNING RATE RATIO VERSUS ACCELERATION FOR FIVE METALLIZED PROPELLANTS AT 1000 PSIA

of approximately 1.9, whereas P421 has a value of approximately 1.5). Based on this limited amount of information, it appears that the individual propellants in a group of propellants with the same size coarse AP particles will have acceleration sensitivities inversely proportional to the 0 G burning rate of the individual propellants. The experimental results also indicate that for two propellants with equal 0 G burning rates, the propellant with the larger coarse size oxidizer will have the lower acceleration sensitivity.

The spent inhibitor cases were examined for possible residue to ascertain the relation between the quantity and nature of the propellant residue and the propellant composition, acceleration level, pressure level, and propellant burning rate. A carbon-like residue was found on the sides of the inhibitor cases at all acceleration levels. In addition in most instances there was a metal-like cap at the bottom of the inhibitor case which could be removed in one piece. Anderson found the same type of residue cap and showed by x-ray diffraction and infrared spectrophotometer analyses that this residue was primarily aluminum oxide [3]. Northam reported that chemical analysis of residue retained in slab motor tests of aluminized propellants indicated that the amount of metallic aluminum in the residue increased from 3.4 per cent at 80 G to 6.4 per cent at 300 G [11].

The amount of aluminum and/or aluminum oxide residue retained on the propellant surface was weighed. This was done in anticipation that the propellant burning rate would be dependent on the interaction of aluminum and/or aluminum oxide residue with the propellant combustion processes.

Data on the amount of aluminum and/or aluminum oxide residue retained in the inhibitor cases as a function of acceleration are presented in Figures 24 through 29. Each figure contains data for both strand lengths and both pressure levels. Residue data for propellant P401 was not taken.

The data in Figures 24 through 29 indicate that the amount of residue for a given propellant was primarily dependent on the acceleration level and strand length. Increasing the acceleration level increased the amount of residue. The amount of residue was found to be directly proportional to the strand length for propellants P413, P414, P415 and P421 below 400 G acceleration. Approximately three times as much residue was retained in the P412 propellant inhibitor cases when the strand length was increased by a factor of 2.3. The same was true for propellant P421 above 400 G. The behavior of P423 propellant was quite different from any of the other five propellants as can be seen from the data in Figure 29. This erratic behavior of P423 will be discussed later in this section.

For propellants P412, P413, P414, and P421 the amount of residue in the inhibitor cases was independent of pressure level. Increasing the pressure resulted in more residue being retained in the inhibitor cases for propellants P415 and P423 as can be seen from Figures 27 and 29.

Figure 30 is a summary of residue data for 1.0 inch strand lengths burned at both pressure levels. A summary of burning rate versus acceleration data for 1.0 inch strand lengths is shown in Figures 31 and 32. Examination of Figures 30, 31, and 32 indicates that no consistent trend exists for the amount of residue retained and

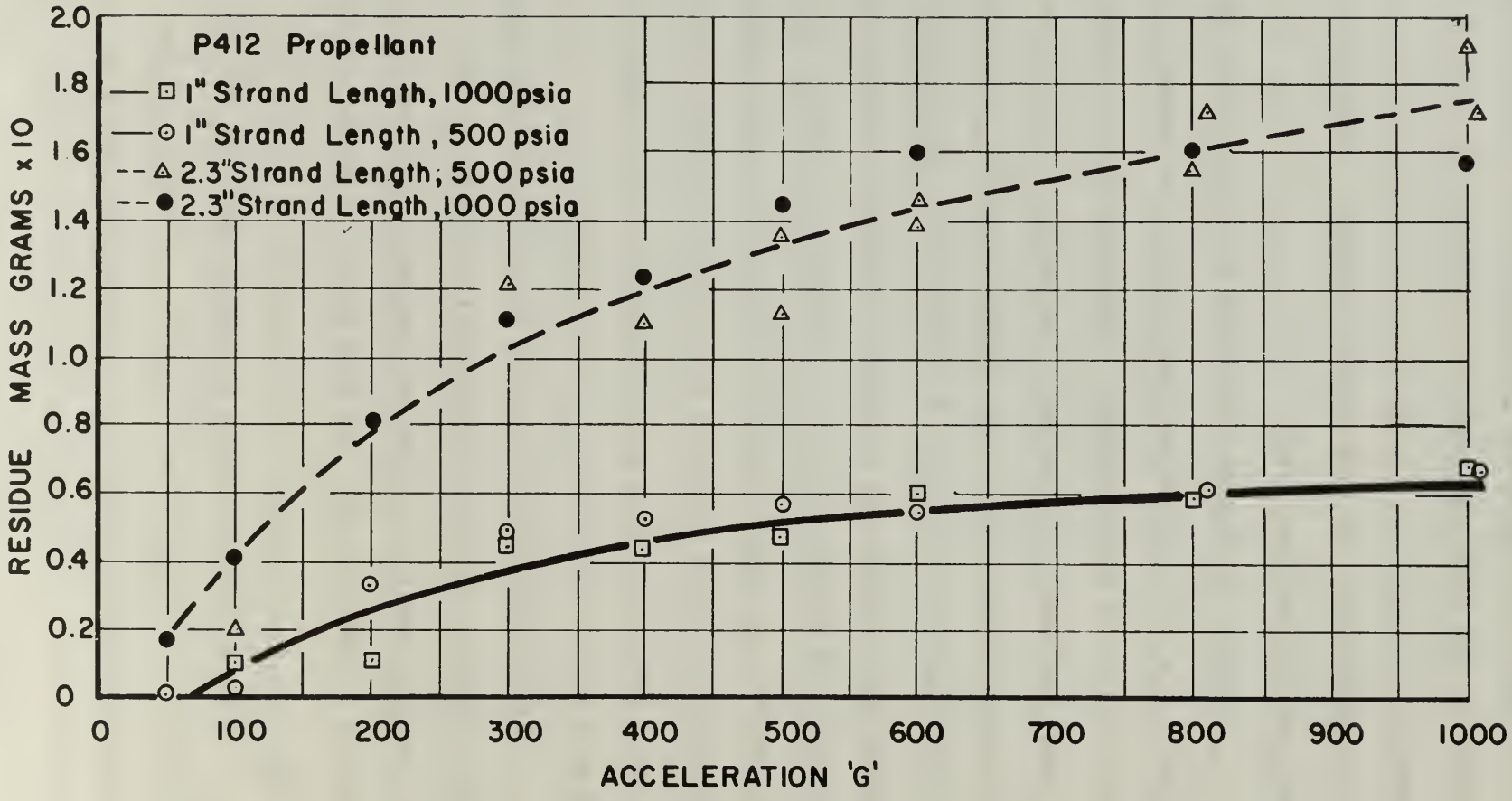

FIGURE 24 RESIDUE MASS VERSUS ACCELERATION FOR PROPELLANT P412

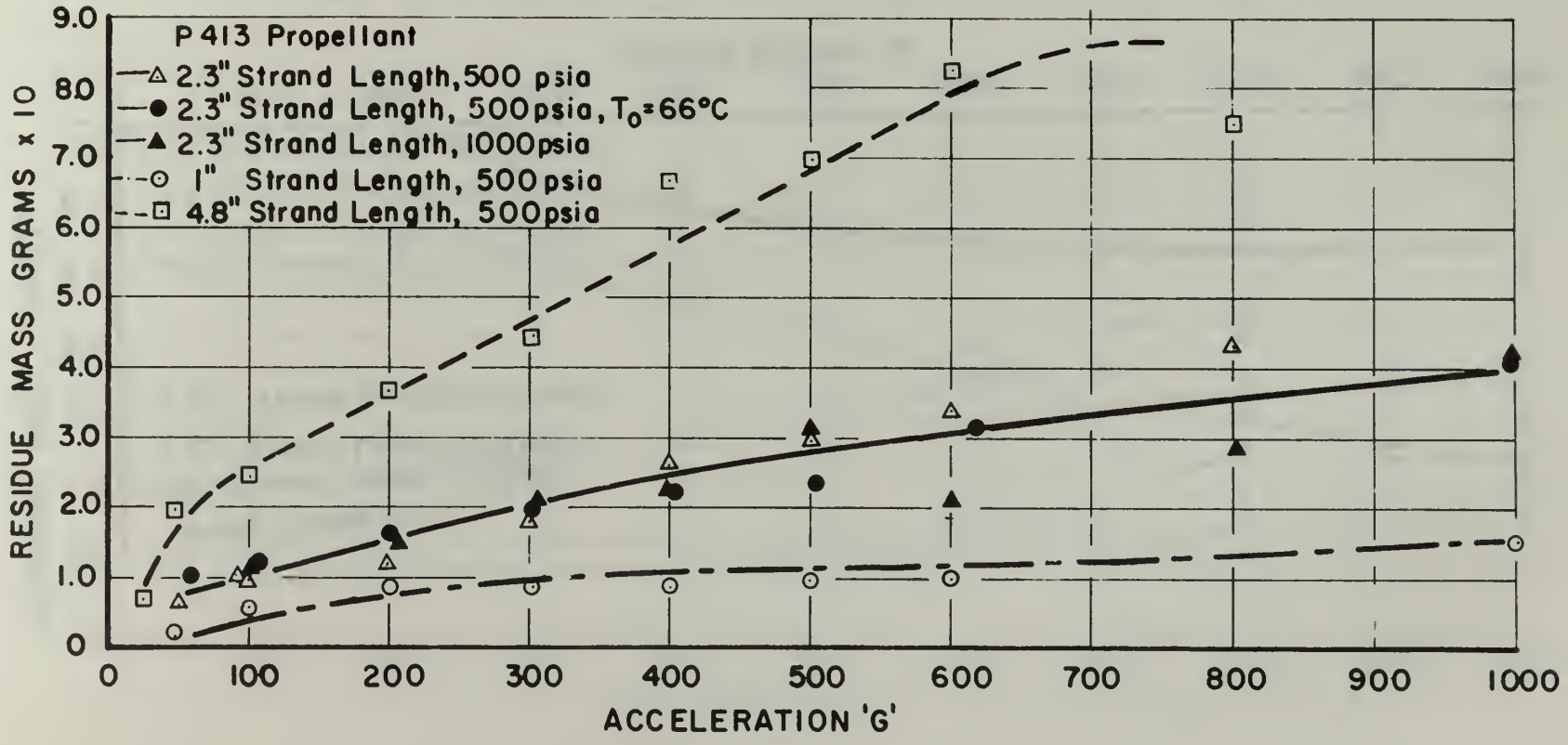

FIGURE 25 RESIDUE MASS VERSUS ACCELERATION FOR PROPELLANT P413

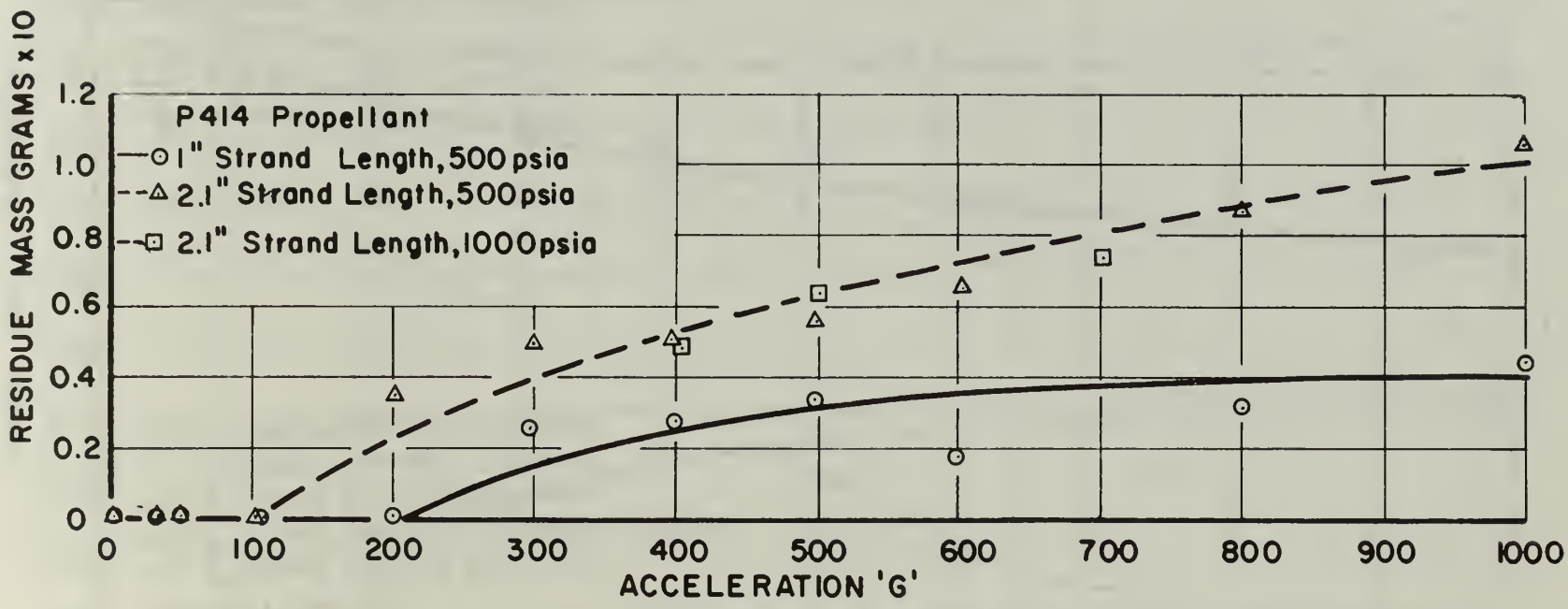

FIGURE 26 RESIDUE MASS VERSUS ACCELERATION FOR PROPELLANT P414

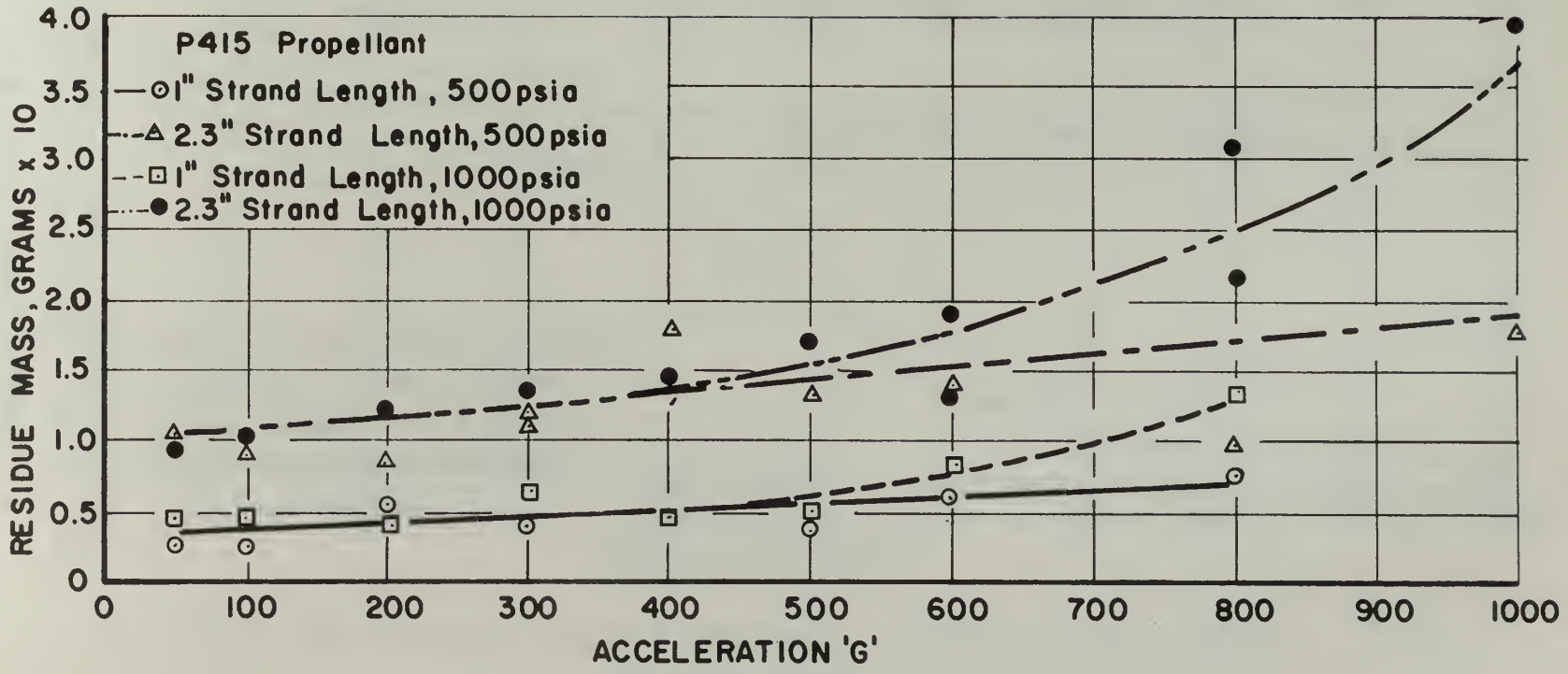

FIGURE 27 RESIDUE MASS VERSUS ACCELERATION FOR PROPELLANT P415

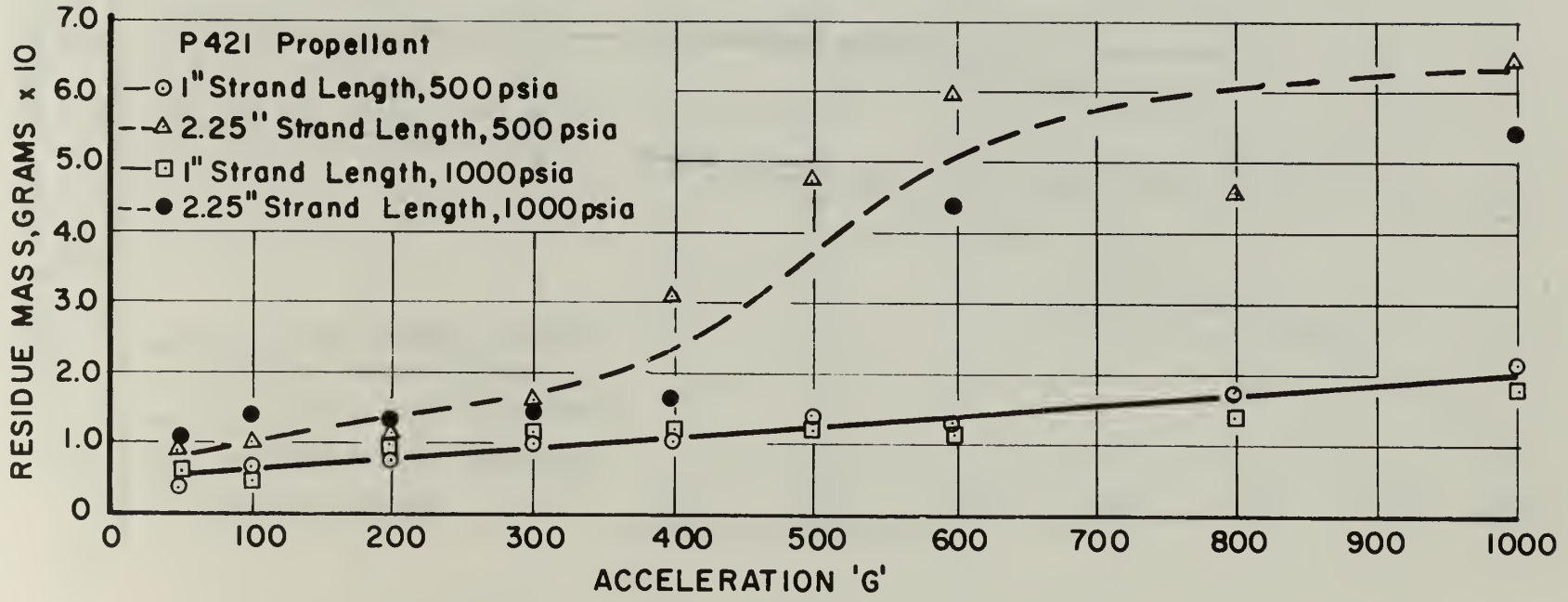

FIGURE 28 RESIDUE MASS VERSUS ACCELERATION FOR PROPELLANT P421

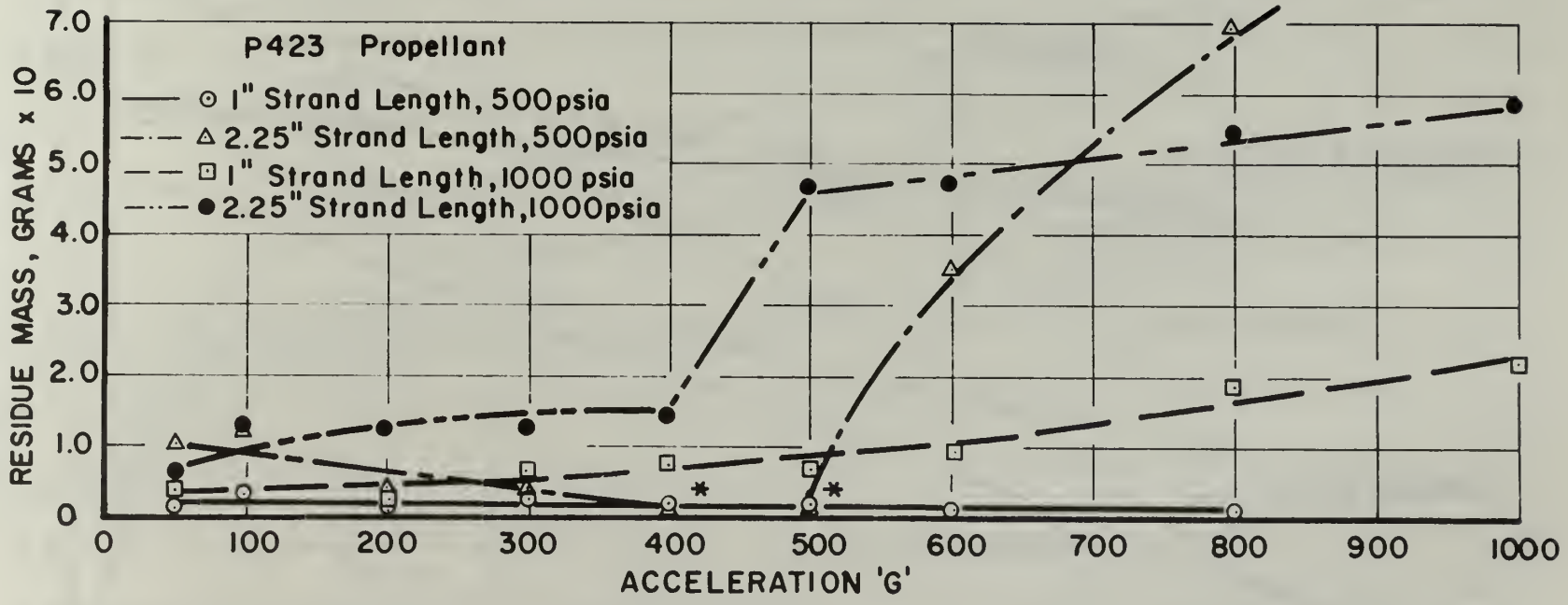

FIGURE 29 RESIDUE MASS VERSUS ACCELERATION FOR PROPELLANT P423

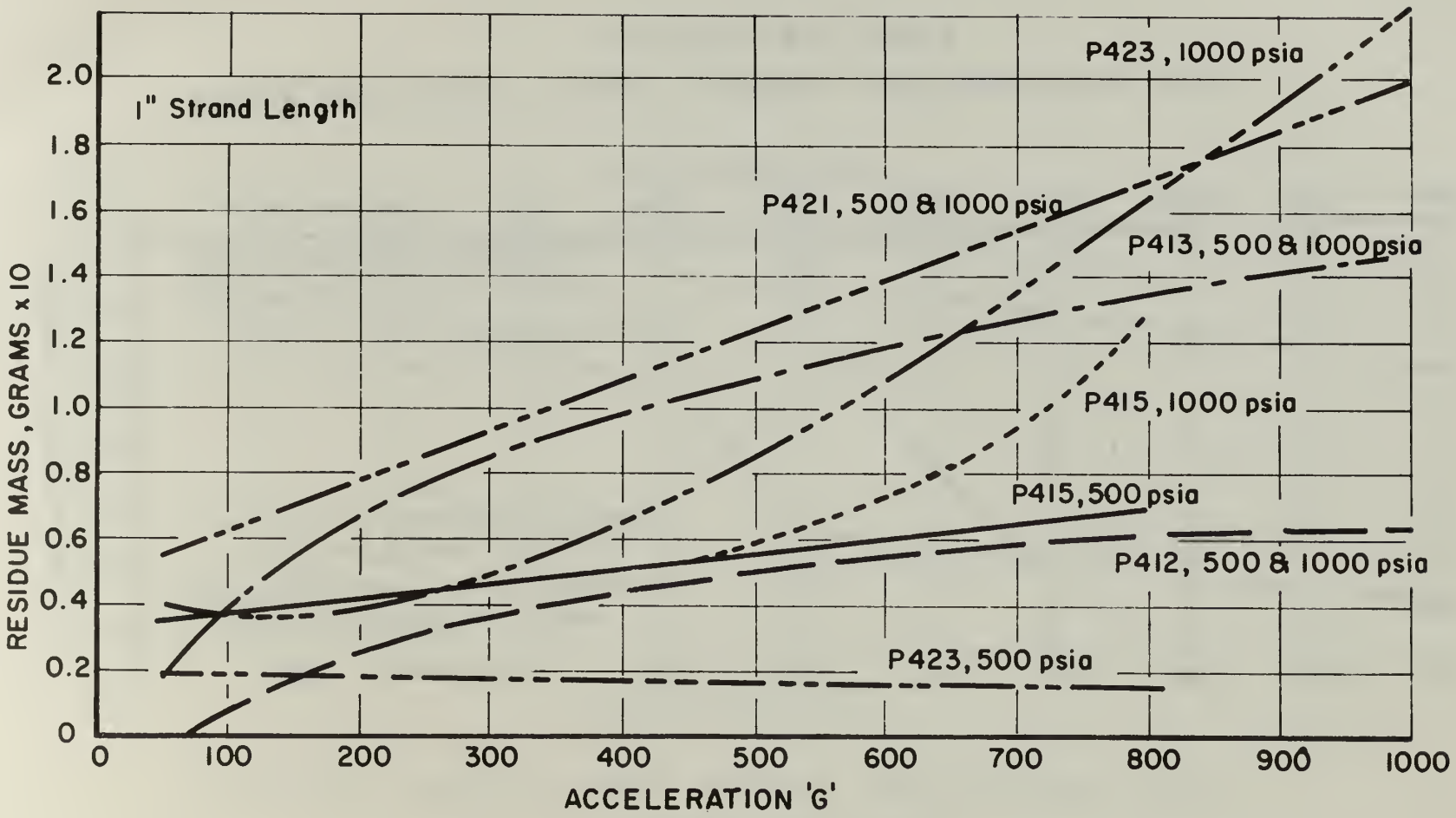

FIGURE 30 COMPARISON OF RESIDUE MASS VERSUS ACCELERATION FOR ONE INCH STRAND LENGTHS

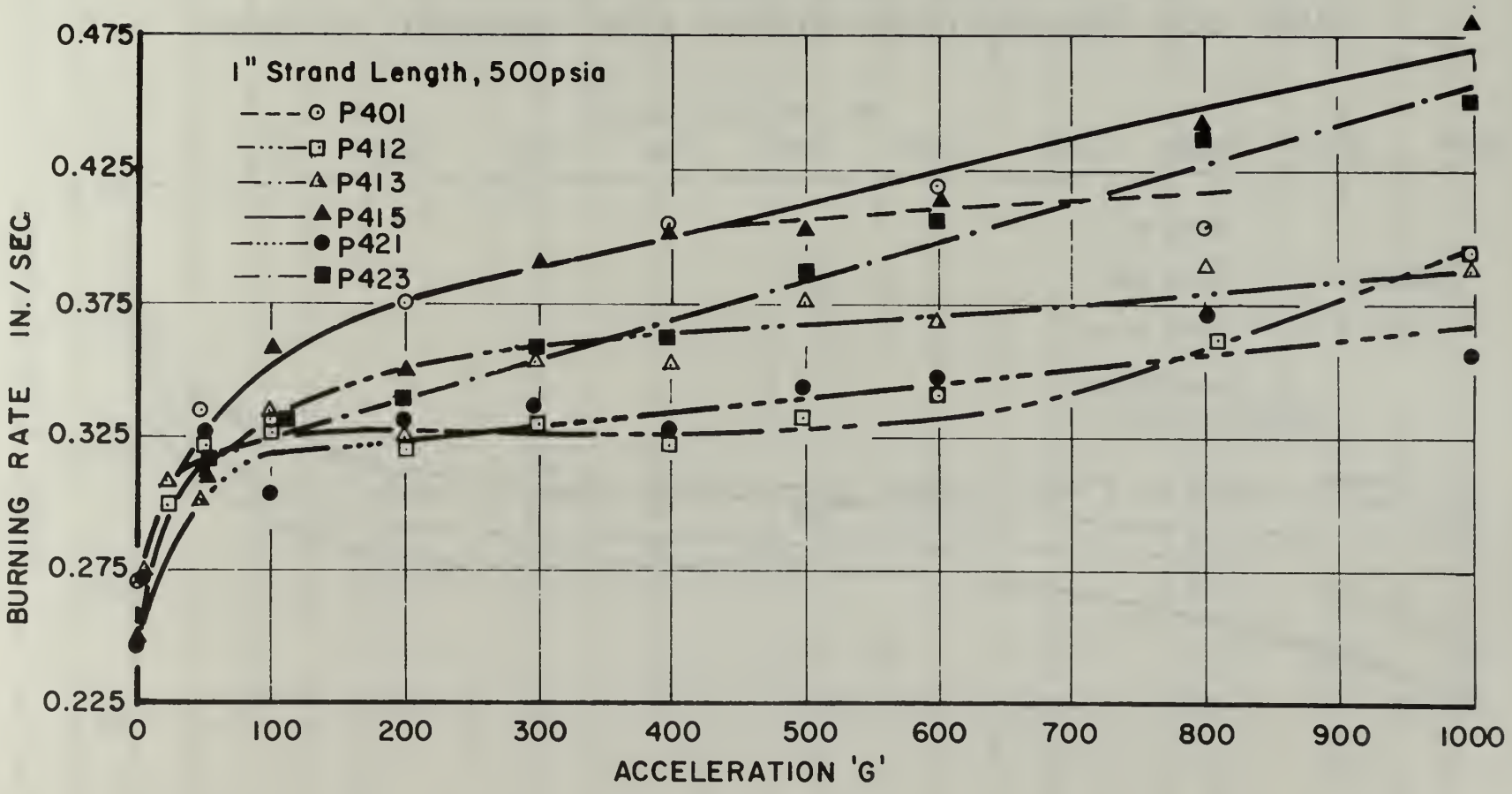

FIGURE 31 BURNING RATE VERSUS ACCELERATION FOR SIX ALUMINIZED PROPELLANTS AT 500 PSIA

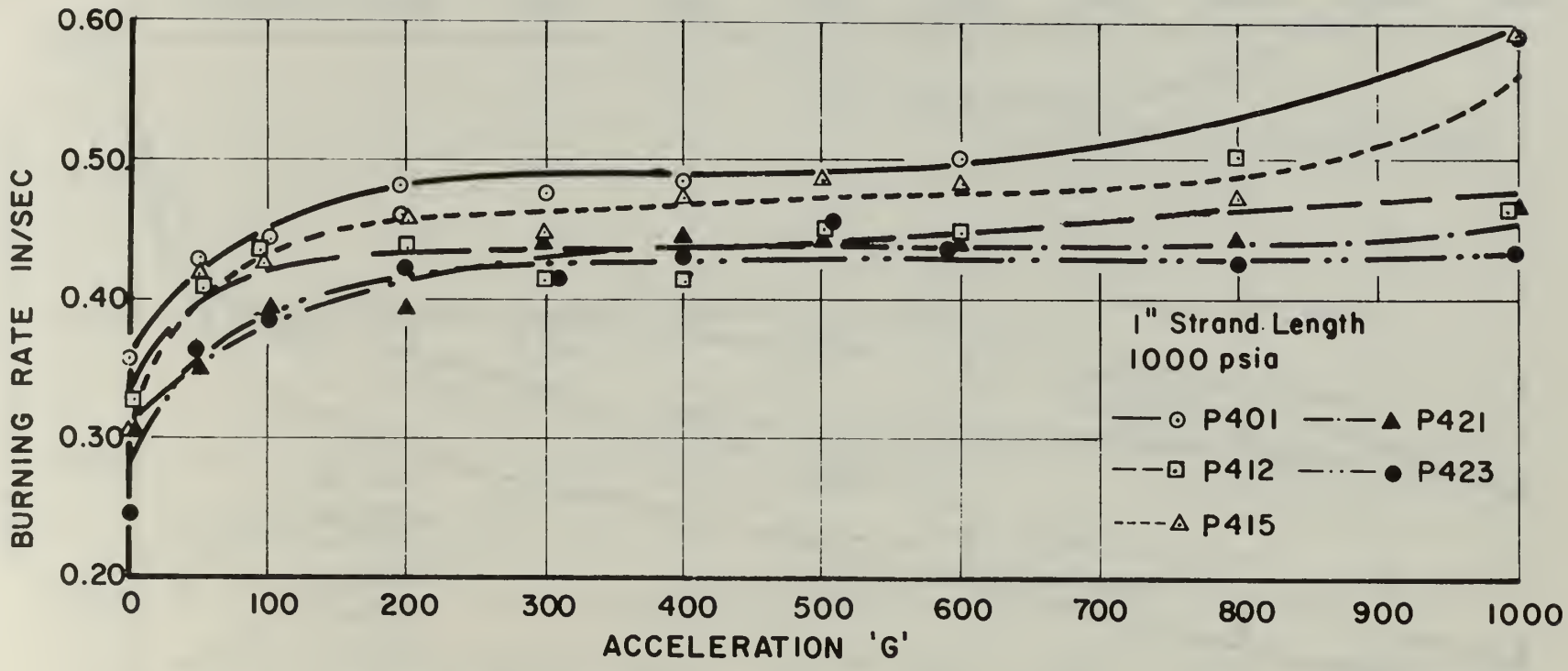

FIGURE 32 BURNING RATE VERSUS ACCELERATION FOR FIVE ALUMINIZED PROPELLANTS AT 1000 PSIA

the 0 G burning rate of a propellant. One might expect that the higher the burning rate and hence the gas evolution from the propellant surface, the more aerodynamic drag would tend to remove the aluminum from the propellant surface. The experimental evidence indicates that such a simple correlation is not valid.

The following observations regarding residue retention can be made based on the data in Figure 30. Propellants P421 and P423 contain the same Al, AP, and PBAN weight percentages and the same AP particle size distributions. The only difference between the propellants is the Al particle size distribution. Propellant P421 contains 10.6 μ mmd aluminum whereas P423 contains 28 μ mmd aluminum. Propellant P421 retained the greatest amount of residue at both pressure levels. In contrast, at 500 psia propellant P423 had the least residue retention of all seven metallized propellants. It appears that the size of the aluminum additive is an important parameter in controlling the amount of agglomeration and retention in an acceleration field. The smaller the aluminum additive size, the greater will be the amount of agglomeration, retention, and hence residue in a motor case. Data obtained in motor tests at United Technology Center (U.T.C.) indicated the same trend [1].

Propellants P413, P415, and P423 contain the same aluminum particle size distribution and weight percentage. The only differences between these propellants are in oxidizer size and weight percentages. Reference to the propellant formulations in Appendix IV shows that P413 and P423 differ only in the particle size of the coarse oxidizer particles, P413 having the smaller size. The only difference between P413 and P415 is in the weight percentage of coarse and fine oxidizer

particles, P415 having a higher weight percentage of fine size oxidizer. At 500 psia pressure there were significant differences in the amount of residue retained for these propellants as can be seen from Figure 30. Propellant P413 retained approximately twice as much residue as did P415 which in turn retained approximately twice as much as did P423. When the strands were burned at 1000 psia the differences in the amount of residue were not as well defined. Propellants P413 and P423 both retained a greater amount of residue than did P415. However, the relative amounts retained by P413 and P423 varied with acceleration level. Based on the behavior of these three propellants it is concluded that the amount of residue retained by bi-modal propellants can be reduced by increasing the weight percentage of the fine size oxidizer and increasing the size of the coarse size oxidizer.

Propellant P412 contained 5 per cent 28 μ mmd aluminum. The data in Figure 30 indicate that the amount of residue retained by propellant P412 was less than the amount retained by the 15 per cent aluminized propellants with the exception of P423 at 500 psia. Propellant P413 is the most similar in oxidizer particle size and weight percentage to P412. Since P412 contained one-third as much aluminum as did P413, one might expect that P412 would retain a proportionally less amount of residue. Again the experimental evidence indicates that such a correlation oversimplifies the situation. It was found that P412 retained approximately one-half the amount of residue as did P413.

The conditions which resulted in a decrease in the amount of residue retained in the inhibitor case of a 1.0 inch strand can be summarized as follows: 1) increasing the size of the aluminum additive from 10.6 μ mmd to 28 μ mmd, 2) increasing the size of the coarse

oxidizer particles from 94 μ mmd to 200 μ mmd, 3) increasing the weight percentage of the fine oxidizer particles, and 4) decreasing the weight percentage of the aluminum additive.

Figures 33 through 37 contain data which summarize the burning rate ratio and aluminum retention ratio (ARR) versus acceleration for propellants P412, P413, P415, P421, and P423. In calculating the ARR it was assumed that the residue consisted entirely of aluminum oxide. The ARR is equal to 0.529 x residue mass divided by the total mass of aluminum present in the propellant sample. Comparison of the data in the figures indicates that those propellants which over the acceleration range had the lower values of ARR (P415 and P423) exhibited the greatest sensitivity to acceleration. The behavior of P423 (Figure 37) is especially interesting. The ARR decreased with acceleration whereas the burning rate ratio increased with acceleration at 500 psia. The results at 1000 psia were quite different. At accelerations above 350 G the ARR increased rapidly with acceleration whereas the burning rate ratio attained a constant value. A possible cause for this behavior is propellant surface "flooding" which will be discussed in the following paragraphs.

As mentioned previously the experimental evidence indicates that there is a definite decrease in burning rate as the strand proceeds to burn. The decrease can be explained if one postulates that there are at least two distinct modes of combustion. In the first mode the aluminum agglomerates into discrete particles and interacts with the surface of the propellant at a finite number of points. The portion of the solid propellant surface under an agglomerate now pyrolyzes at a faster rate than it did prior to the imposition of the agglomerate

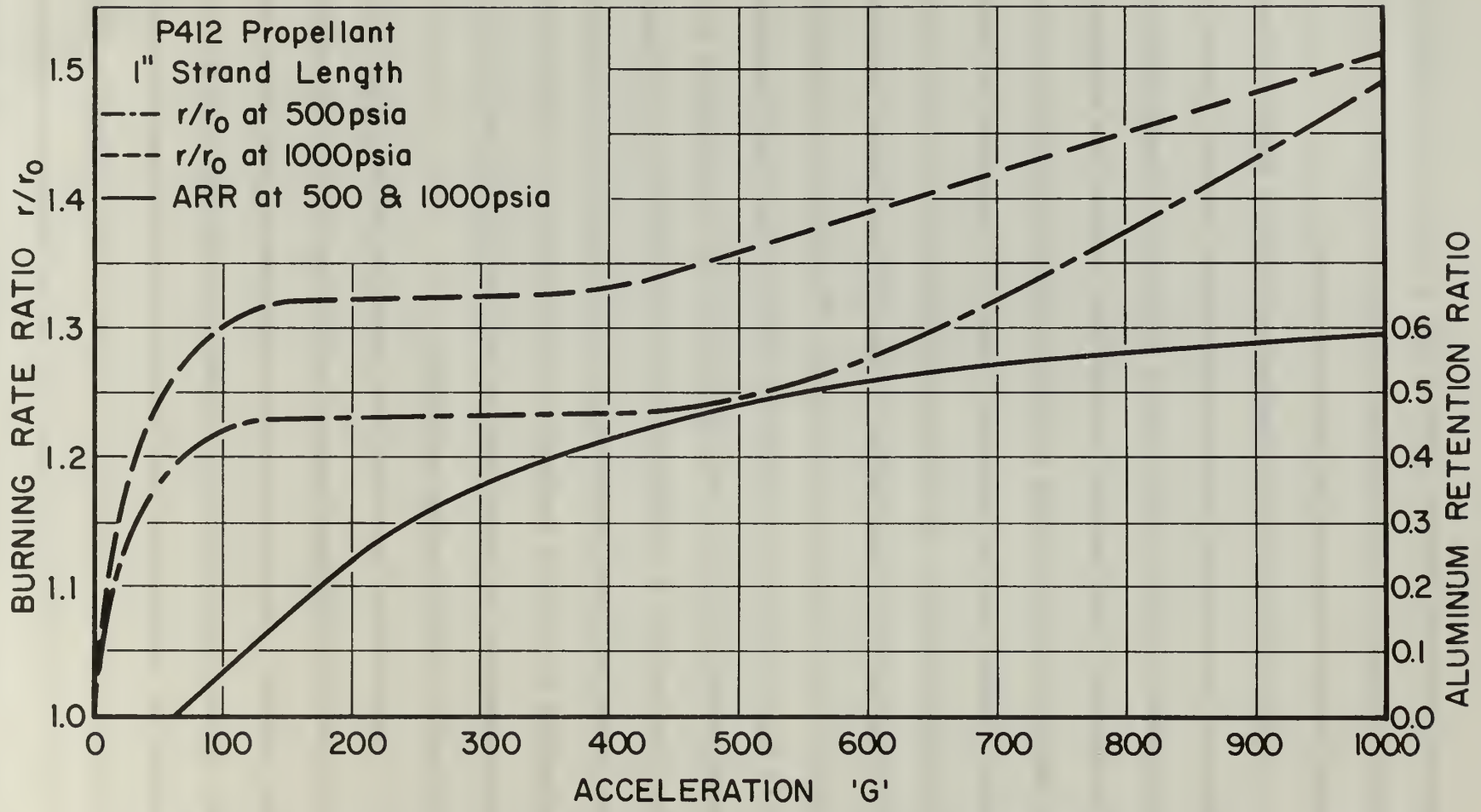

FIGURE 33 BURNING RATE RATIO AND ALUMINUM RETENTION RATIO VERSUS ACCELERATION FOR P412 PROPELLANT

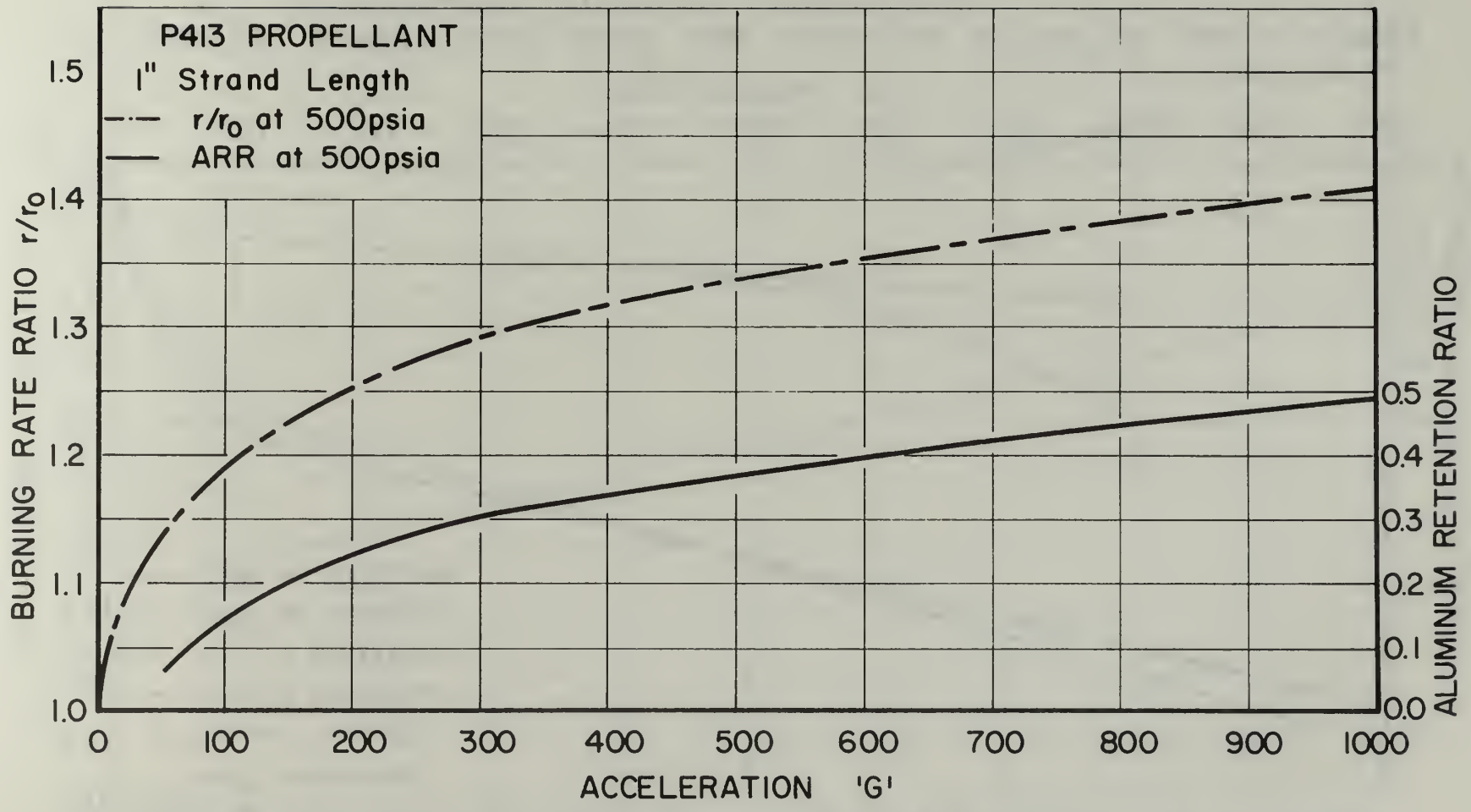

FIGURE 34 BURNING RATE RATIO AND ALUMINUM RETENTION RATIO VERSUS ACCELERATION FOR P413 PROPELLANT

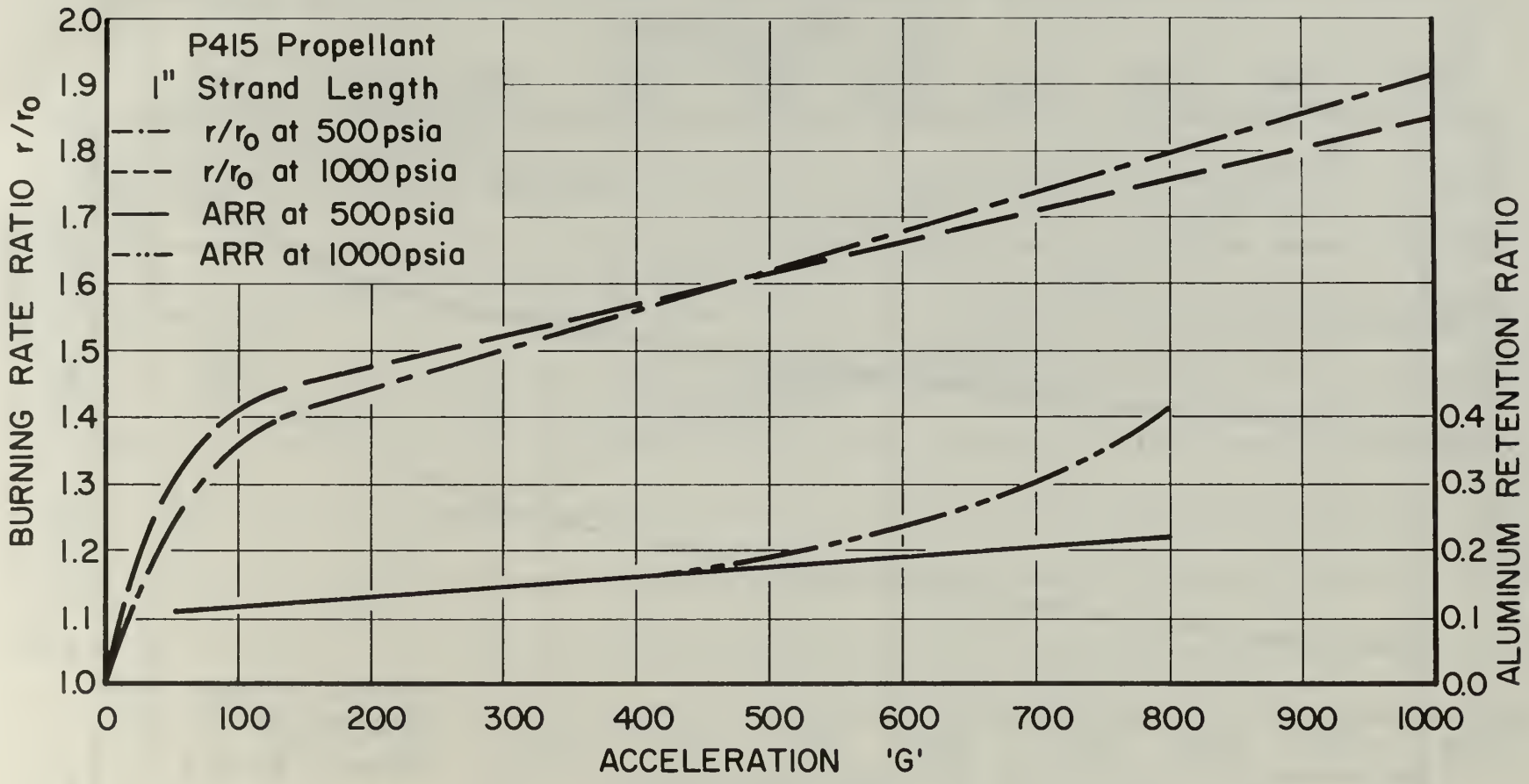

FIGURE 35 BURNING RATE RATIO AND ALUMINUM RETENTION RATIO VERSUS ACCELERATION FOR P415 PROPELLANT

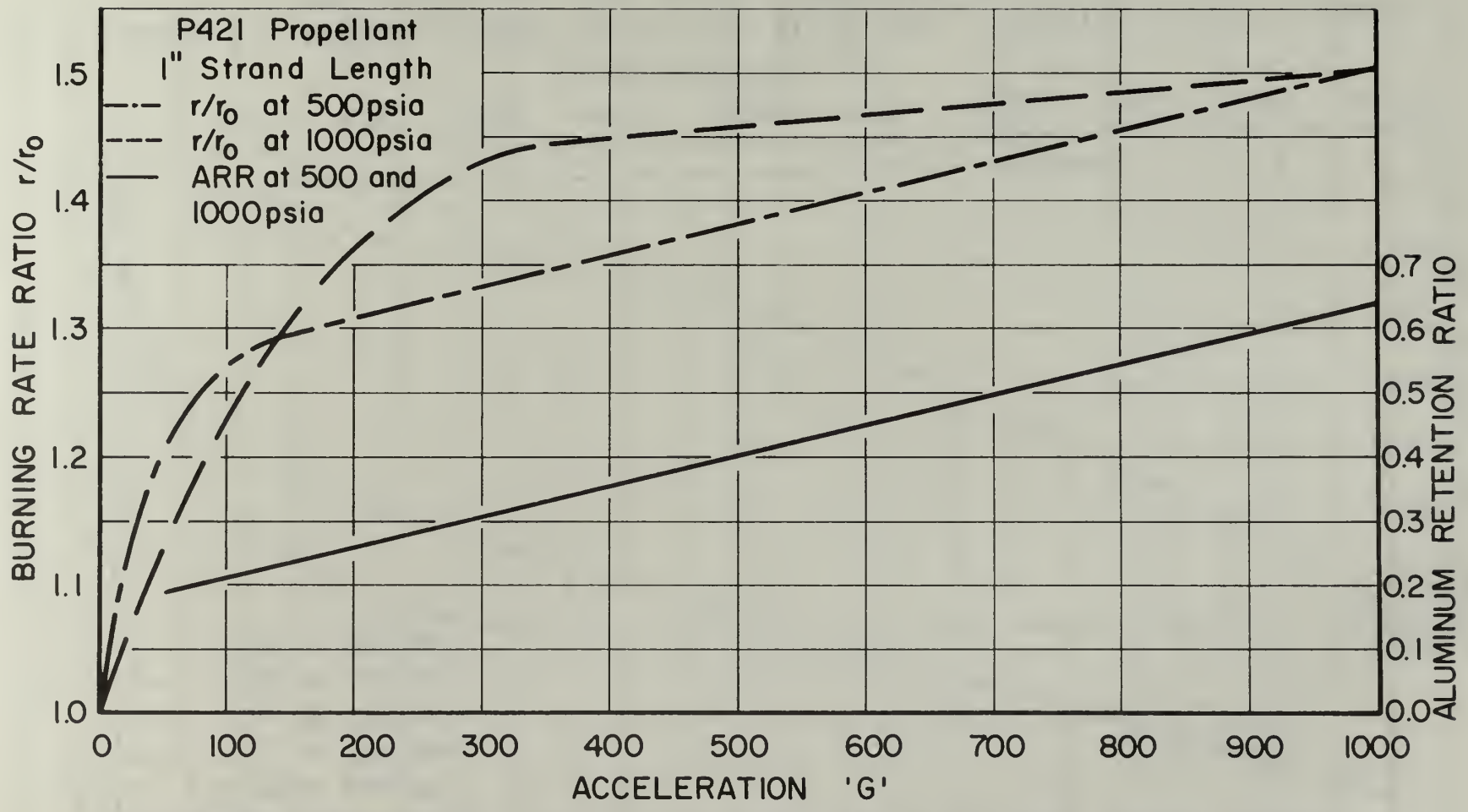

FIGURE 36 BURNING RATE RATIO AND ALUMINUM RETENTION RATIO VERSUS ACCELERATION FOR P421 PROPELLANT

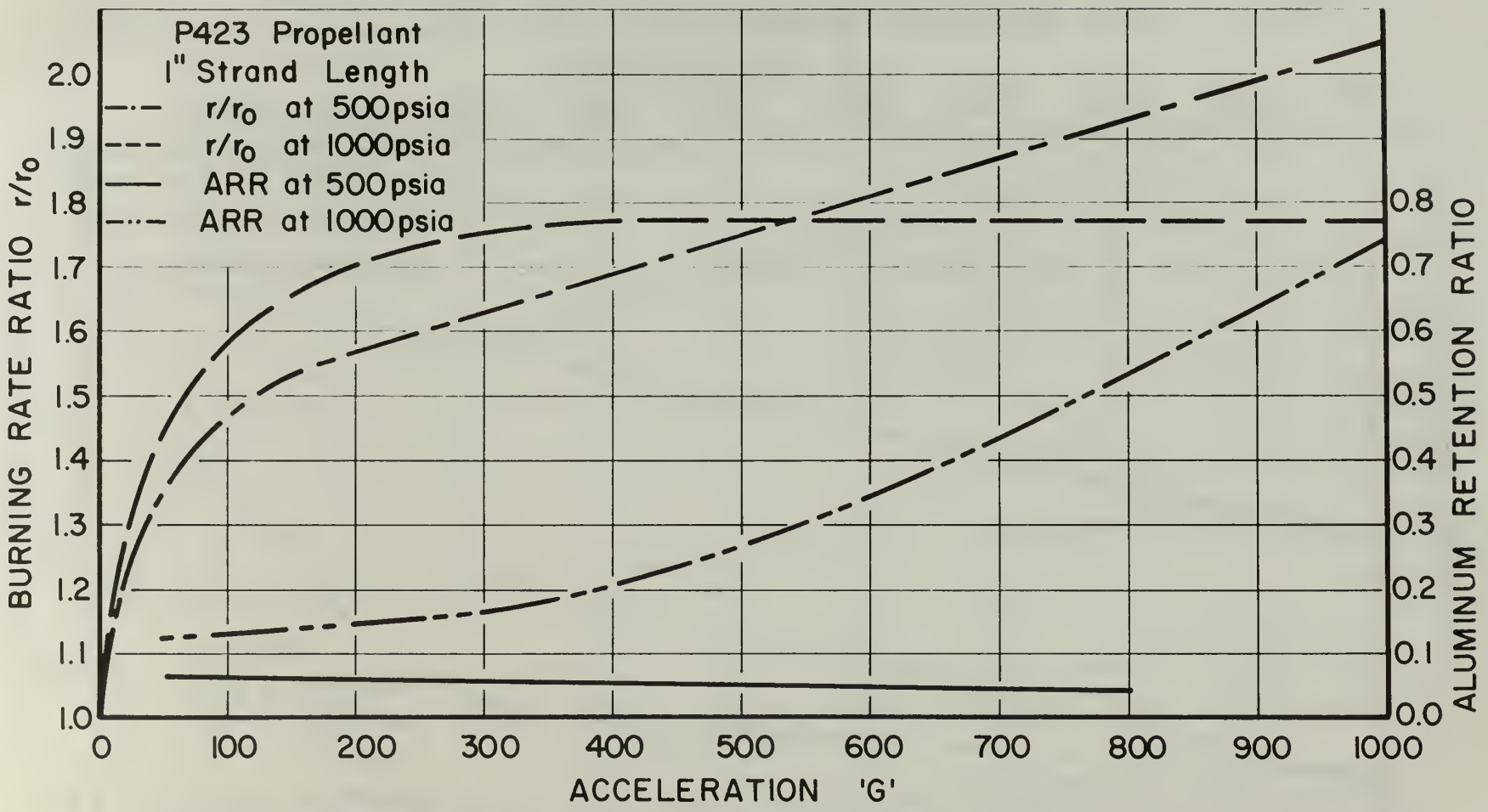

FIGURE 37 BURNING RATE RATIO AND ALUMINUM RETENTION RATIO VERSUS ACCELERATION FOR P423 PROPELLANT

between the flame zone and the propellant surface. This increased pyrolysis rate is probably caused by the combination of the release of chemical energy of metal combustion and the increased heat transfer from the flame zone to the propellant surface through the low thermal resistance agglomerate. An inverted cone-shaped pit with the agglomerate at the bottom is formed in the solid phase of the propellant. The rate at which the individual agglomerates in these pits proceed into the propellant solid phase controls the overall burning rate of the propellant.

As an agglomerate proceeds into the solid phase of the propellant, it undergoes combustion. Experiments conducted with individual aluminum particles at one G suggest that two distinct combustion mechanisms occur simultaneously [12]. Vapor-phase combustion is evidenced by a detached flame zone above the surface of an aluminum particle and by formation of a "smoke" of very fine oxide particles. Surface reaction is suggested by the blowing of oxide bubbles similar in size to the original aluminum particle and by the large amount of oxide associated with the parent particle in the quenched residues. High-speed motion pictures indicate that there is an asymmetrical buildup of aluminum oxide on the surface of an aluminum particle during combustion [13].

As the combusting aluminum agglomerate proceeds into the solid phase of the propellant, additional fresh aluminum mass is added to the agglomerate. The rate at which an agglomerate acquires mass (the sum of the rate of addition of new aluminum and the rate of retention of aluminum oxide from the aluminum combustion surface reactions) is greater than the rate at which the agglomerate loses mass through

vapor-phase aluminum combustion. Eventually the agglomerates become so large that they merge with agglomerates in adjacent pits. The surface of the propellant becomes covered with a continuous layer of aluminum and/or aluminum oxide and "floods." Once the surface of the propellant is "flooded," a second slower mode of combustion begins. The propellant surface is now relatively smooth compared to its condition in mode one. The parent aluminum particles no longer agglomerate as the regressing propellant surface uncovers them, but rather these particles are individually encompassed by the molten aluminum and/or aluminum oxide "flood" layer. These particles are then converted to aluminum oxide as the hot oxidizer gases bubble through the "flood" layer. The propellant burning rate is no longer dependent on the rate at which individual agglomerates penetrate the propellant. The burning rate becomes controlled by the heat transfer rate from the combustion processes taking place in the molten aluminum and/or aluminum oxide layer.

There exists experimental evidence that the aluminum agglomerates have the time dependent behavior outlined above. Crump [13] has taken high-speed motion pictures of the burning surface of aluminized propellants burning under standard acceleration conditions. The evidence indicates that individual aluminum particles accumulate and in a rapid sequence ignite locally, melt, draw up into a large burning sphere, and leave the burning surface as a large aluminum-aluminum oxide agglomerate. Crump pictured the parent aluminum particles as being contained in a binder "pocket" or "filament" between the oxidizer particles. As the burning progresses, the binder is pyrolyzed away and the original aluminum particles accumulate on the surface. Crump found experimentally

that: 1) The agglomerate size is determined by the pocket size (and hence by the AP size); 2) the agglomerate size is independent of the size of the original aluminum particles; 3) the agglomerate size decreases as the aluminum concentration decreases; and 4) the agglomeration in general is not a function of the binder type.

There is ample experimental evidence which indicates that the application of an acceleration force promotes agglomeration and causes these agglomerates to pit the propellant surface. Such evidence is indicated in the photographs shown as Figures 38 and 39. The photographs, made by N.W.C., are of a propellant grain which contained 19.5 per cent aluminum and was subjected to a radial acceleration of approximately 50 G. The propellant was extinguished 5.0 seconds after ignition when the motor case failed. Northam [11] also reported the presence of pits in his slab burning rate experiments which were done at acceleration levels up to 300 G.

The author was supplied with four castings made of the extinguished surface of an aluminized propellant by N.A.S.A., Langley, Virginia. The castings, made from RTV rubber impressions of the extinguished surface, represent exactly the extinguished propellant surface. The propellant, burned in a slab configuration using N.A.S.A. Langley's Centrifuge Test Facility, contained 17.7 per cent of 6.3 μ mmd aluminum additive. Four extinguishment experiments were conducted at accelerations of 20, 40, and 100 G. In all instances the propellant surface was completely covered with pits. The diameter of the average pit was approximately 1000 μ at 20 G, 2500 μ at 40 G, and 1750 μ at 100 G. In all instances the depth of a pit was approximately twice its diameter. The number of pits was approximately 240 per square inch

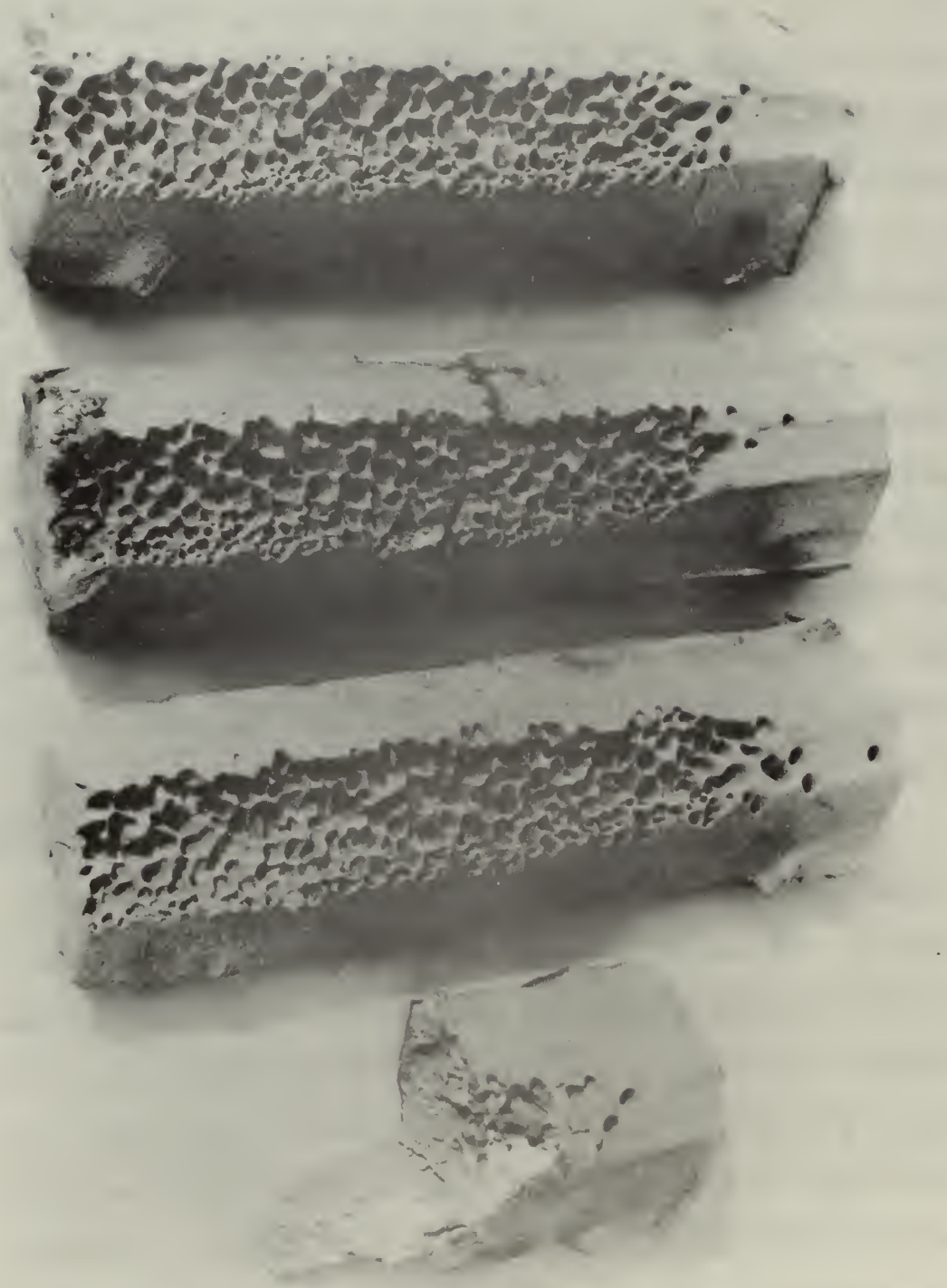

FIGURE 38 EXTINGUISHED PROPELLANT SURFACE

FIGURE 39 CLOSEUP VIEW OF EXTINGUISHED PROPELLANT SURFACE

at 20 G, 120 per square inch at 40 G, and 170 per square inch at 100 G acceleration. The propellant slab which was subjected to 20 G acceleration was extinguished 0.675 seconds after ignition whereas the propellant slab subjected to 100 G was extinguished after 1.0 seconds. Two experiments were conducted at 40 G. In one test the propellant was extinguished after 1.25 seconds, and the other, after 2.0 seconds. Unfortunately the propellants were burned at two different pressures so the tendency of the propellant to achieve a "flooded" condition cannot be fairly judged. However there is evidence in all the castings which indicates that what were initially two or three discrete agglomerates had merged into one larger agglomerate.

U.T.C. has conducted motor experiments in which the residue obtained the form of a solid continuous layer [1]. The burning rate of the propellants decreased during the test firings. The U.T.C. motors were fired at maximum acceleration levels of only 200 G and had web thicknesses of only 0.6 inches. Hence, there exists evidence that the propellant surface can become "flooded" after only 0.6 inches of burning at acceleration levels below 200 G and that this "flooding" resulted in a decreased burning rate.

Since the experimental data indicate that there exist at least two distinct modes of acceleration augmented combustion, it was decided to correlate the remainder of the strand data in a different manner. Since the residue data for the 1.0 inch strands indicate that the surface of the propellant was probably "flooded" at propellant burnout, it was decided to calculate the absolute burning rate of the propellant strands

in the second increment of strand length to determine if the various propellants burned at some common rate once they achieved a "flooded" condition.

The average burning rate in the second increment of strand length, r_{1-2}, was calculated using the equation

$$r_{1-2} = \frac{L_2 - L_1}{\frac{L_2}{r_2} - \frac{L_1}{r_1}} \qquad (2)$$

where:

L_1 = length of a nominal 1.0 inch length strand (inch)

L_2 = length of a nominal 2.25 inch length strand (inch)

r_1 = average burning rate of a nominal 1.0 inch length strand (inch/sec)

r_2 = average burning rate of a nominal 2.25 inch length strand (inch/sec)

Plots of burning rate in the second increment of strand length versus acceleration are shown in Figures 40 and 41.

The average amount of residue present on the propellant surface during the second increment of strand length, $m_{r_{1-2}}$, was calculated using the relationship

$$m_{r_{1-2}} = m_{r_1} + \frac{m_{r_2} - m_{r_1}}{2} \qquad (3)$$

where:

m_{r_1} = residue mass of a nominal 1.0 inch length strand (gm)

m_{r_2} = residue mass of a nominal 2.25 inch length strand (gm)

The resulting values are shown as a function of acceleration in Figures 42 and 43.

The burning rate data for the second increment of strand length in Figures 40 and 41 indicate that propellants P401 (coarse AP 68 μ) and

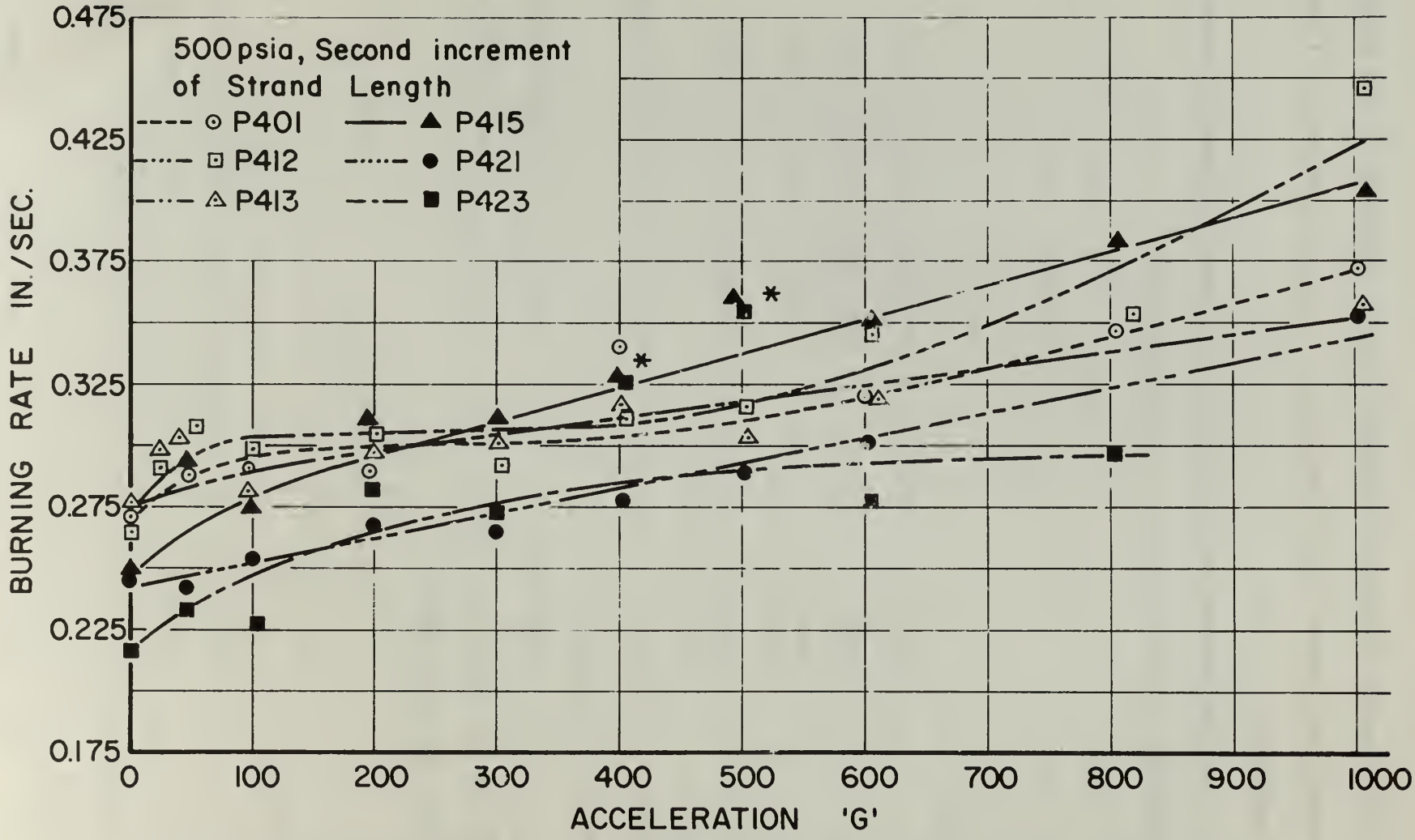

FIGURE 40 BURNING RATE VERSUS ACCELERATION FOR SECOND INCREMENT OF STRAND LENGTH AT 500 PSIA

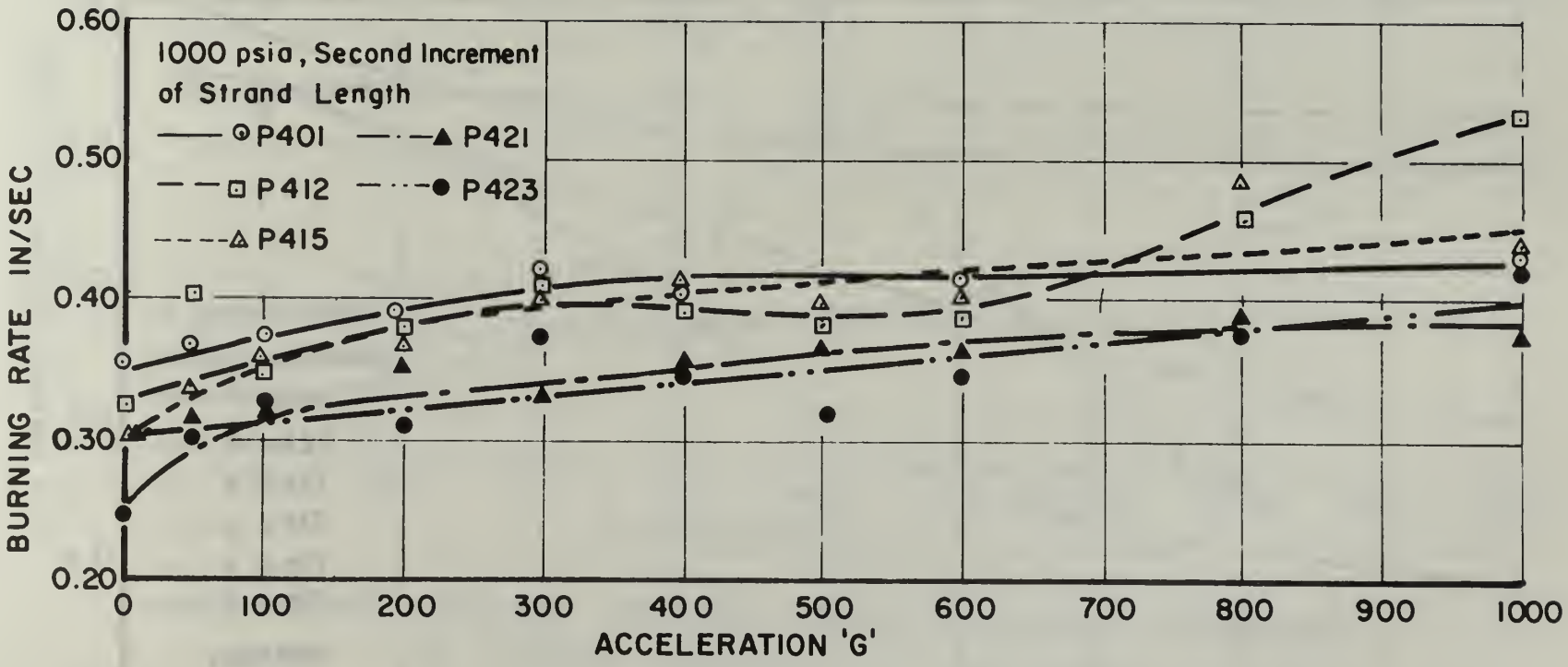

FIGURE 41 BURNING RATE VERSUS ACCELERATION FOR SECOND INCREMENT OF STRAND LENGTH AT 1000 PSIA

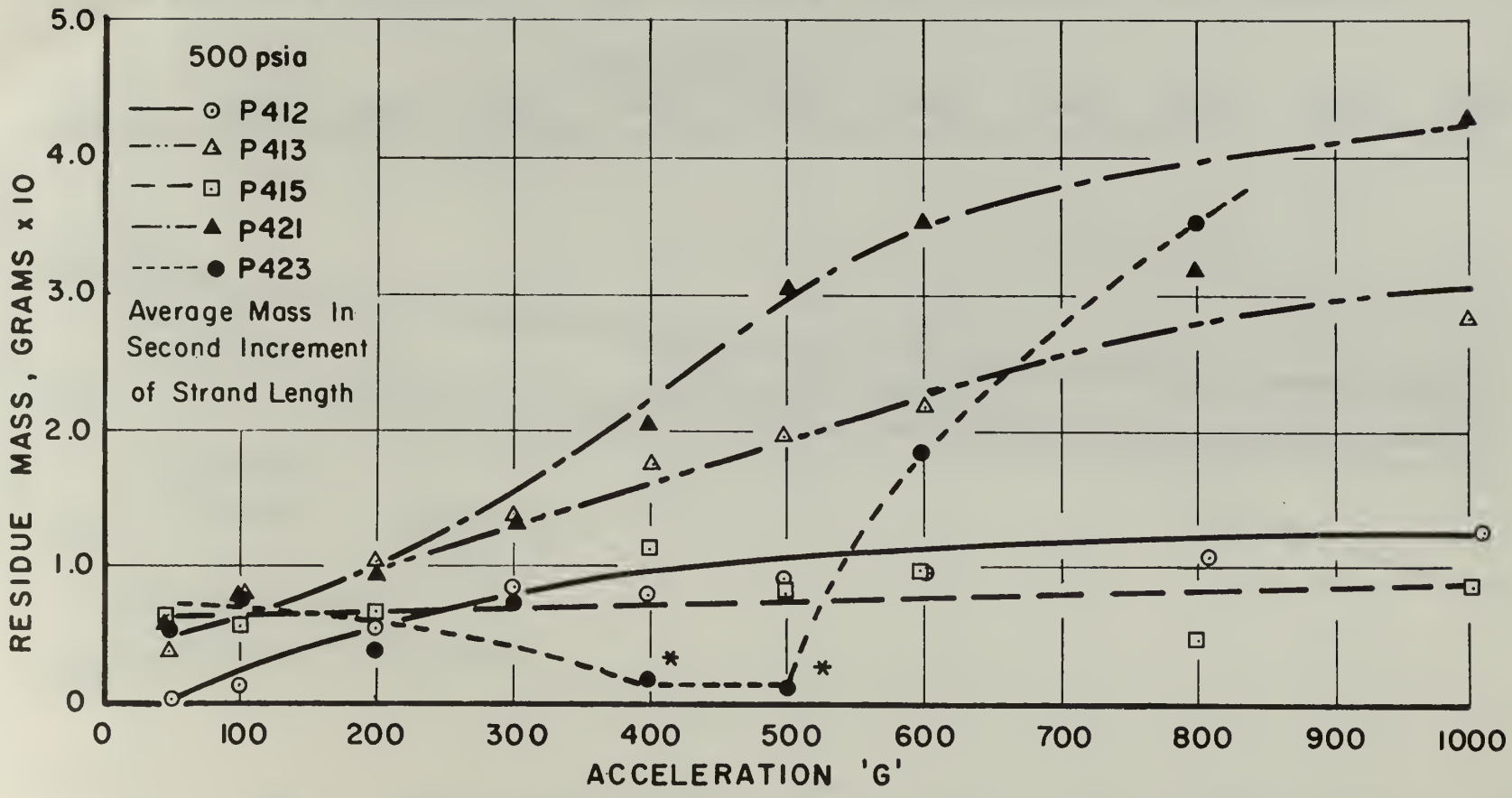

FIGURE 42 AVERAGE RESIDUE MASS IN SECOND INCREMENT OF STRAND LENGTH AT 500 PSIA

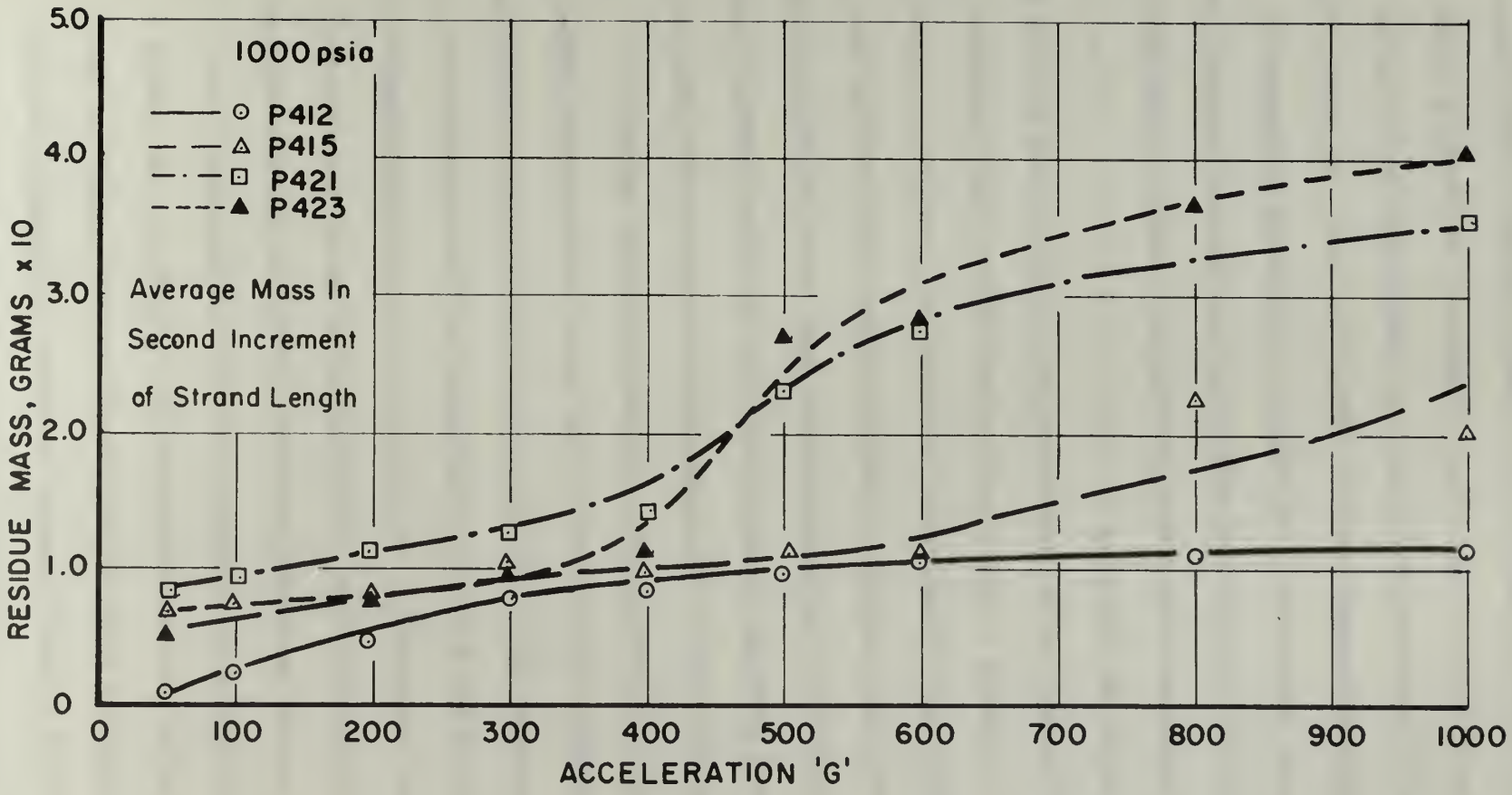

FIGURE 43 AVERAGE RESIDUE MASS IN SECOND INCREMENT OF STRAND LENGTH AT 1000 PSIA

P412, P413, and P415 (coarse AP 94 μ) have absolute burning rates which are very nearly equal to each other. Likewise, the burning rates of P421 and P423 (coarse AP 200 μ) are very nearly equal but somewhat less than the absolute burning rates of P401, P412, P413, and P415. The tendency of the absolute burning rates in the second increment of strand length to fall into two distinct groups is more clearly indicated by a comparison of the data in Figures 31 and 40 at 500 psia and Figures 32 and 41 at 1000 psia.

The tendency of the individual propellants within each of the two groups to achieve a common burning rate value seems reasonable when the following is considered. Once the propellant surface has attained a "flooded" condition, there no longer exist burning rate controlling individual agglomerates the sizes of which are probably a function of the physical composition of the propellant. There exists, however, a molten layer of aluminum and/or aluminum oxide which is feeding energy back to relatively similar propellant surfaces.

The data in Figures 20, 29, 40, and 42 indicate that propellant P423 exhibited an erratic behavior at 500 psia and acceleration levels of 400 and 500 G (data points marked with an asterisk). The propellant had an abnormally high burning rate and considerably less residue when compared to the corresponding values at 300 and 600 G. There is no apparent explanation for the anomalous behavior observed in these two experiments. However, the fact the abnormally small amounts of residue were retained when the burning rate was correspondingly abnormally high, lends credence to the assumption that at least two distinct modes of combustion exist. Apparently, as supported by the data in Figures 20 and 29, the two 2.25 inch strands

which were fired at 400 and 500 G burned in combustion mode one for the entire length of the strand.

Similar behavior was noted for propellant P412 at 500 psia (Figure 10). Three different burning rates were obtained for the three strands burned at 500 G acceleration. The strand that burned at the highest average rate, 0.355 inches/second, had 0.1130 grams of residue whereas the strand that burned at the lowest average rate, 0.321 inches/second, contained 0.1354 grams of residue. The same inverse relationship between burning rate and residue retention was found for the two strands burned at 800 G.

Anderson [3] found evidence that the heat transfer mechanism may be important in determining the burning rate behavior of metallized propellants in acceleration environments. He observed that the presence of a small amount of nichrome wire on a non-metallized propellant surface caused the burning rate to increase more than could be accounted for by the chemical energy released by the combustion of the nichrome wire. Additional evidence that heat transfer may be important was found by U.T.C. Experiments conducted at U.T.C. [14] indicated that propellants containing the refractory material tungsten exhibited burning rate augmentation in acceleration fields. Visual examination of the residue showed that no agglomeration had occurred and that there was no appreciable chemical reaction involving the tungsten.

Propellant P414 was formulated for comparison with propellant P412. The propellants differ primarily in that P414 contains 5 per cent aluminum oxide as the additive instead of 5 per cent aluminum. The formulation was conceived as an additional check on the possibility that heat transfer from the hot reaction gases through low thermal

resistance agglomerates (as compared to the combustion gases) may be an important mechanism in burning rate augmentation.

A comparison of the results obtained for propellants P412 and P414 is graphically presented in Figures 44, 45, 46, and 47. The data indicate that over most of the acceleration range the burning rate ratio of a propellant containing aluminum oxide (P414) was greater than that of a propellant containing aluminum (P412). It should be noted that the 0 G burning rates of P412 and P414 are within approximately 5 per cent of each other. This suggests that the aluminum oxide did not act as a burning rate catalyst. Moreover, since the aluminum oxide was believed to be chemically inert, the acceleration induced burning rate increase of P414 could not have been caused by chemical energy release at the propellant surface. This strengthens the assumption that heat transfer may be a very important if not the most important mechanism of acceleration induced burning rate augmentation. The data in Figure 14 indicate that the burning rate of P414 propellant did not vary with strand length. The large values of burning rate ratio suggest that propellant P414 was able to sustain mode one combustion and did not become "flooded" for the entire strand length.

Figure 46 shows the amount of residue retained for the propellants as a function of strand length and acceleration level. The aluminized propellant (P412) was found to retain approximately twice the residue weight as did P414 for a given strand length and acceleration level.

The residue data are also presented as solid retention ratio versus acceleration, see Figure 47. The solids retention ratio for

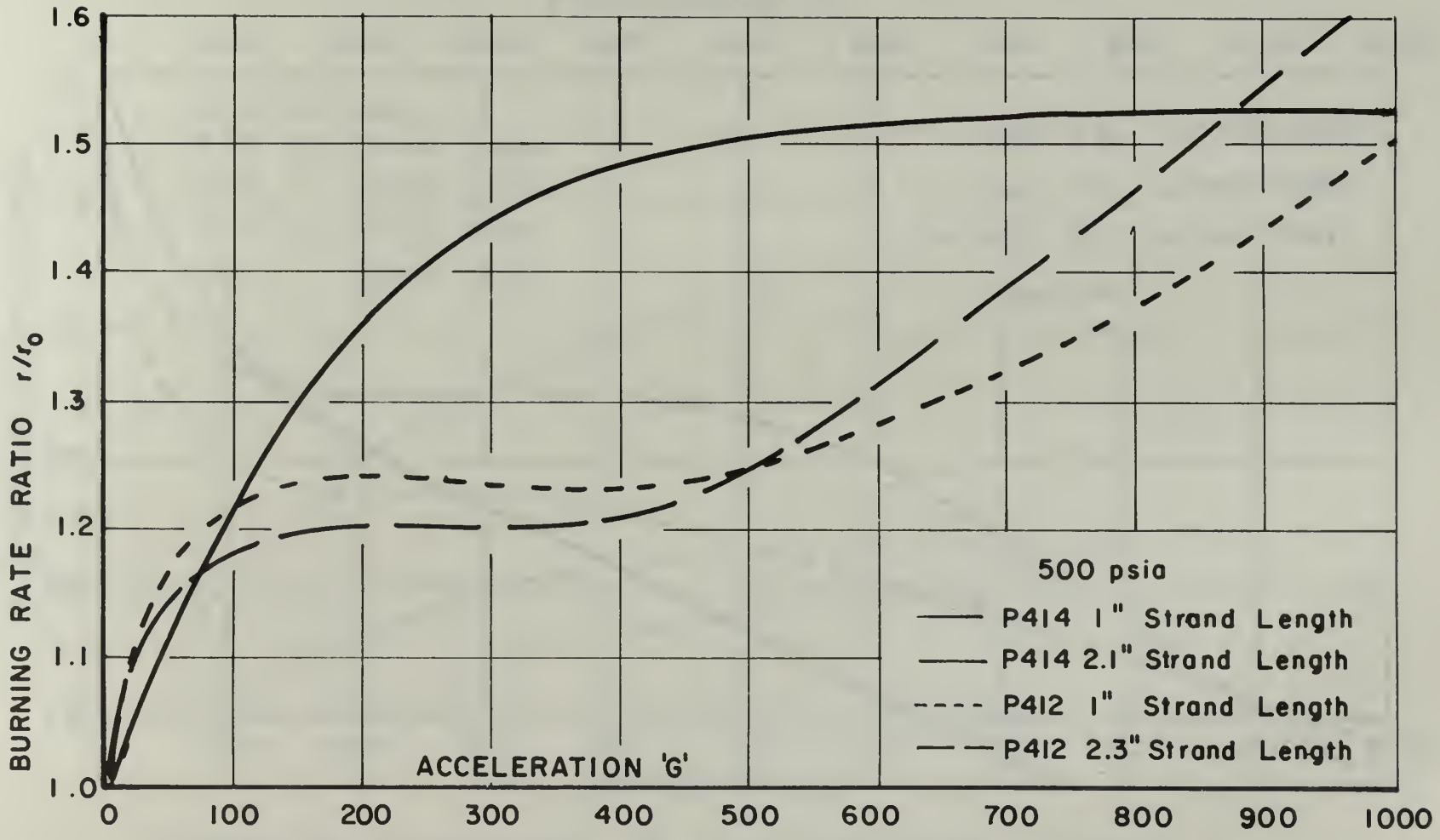

FIGURE 44 COMPARISON OF BURNING RATE RATIO VERSUS ACCELERATION FOR PROPELLANTS CONTAINING ALUMINUM AND ALUMINUM OXIDE AT 500 PSIA

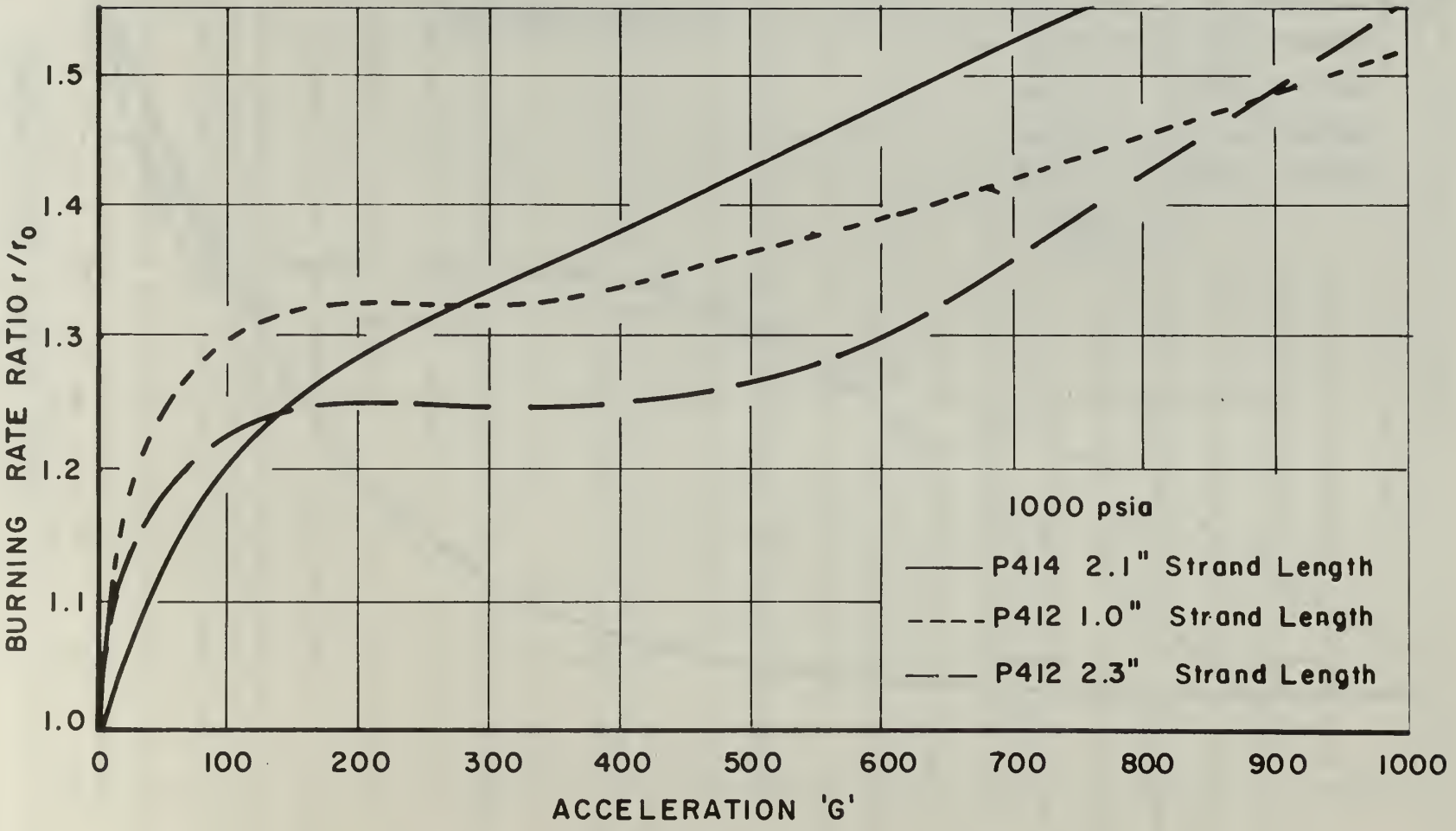

FIGURE 45 COMPARISON OF BURNING RATE RATIO VERSUS ACCELERATION FOR PROPELLANTS CONTAINING ALUMINUM AND ALUMINUM OXIDE AT 1000 PSIA

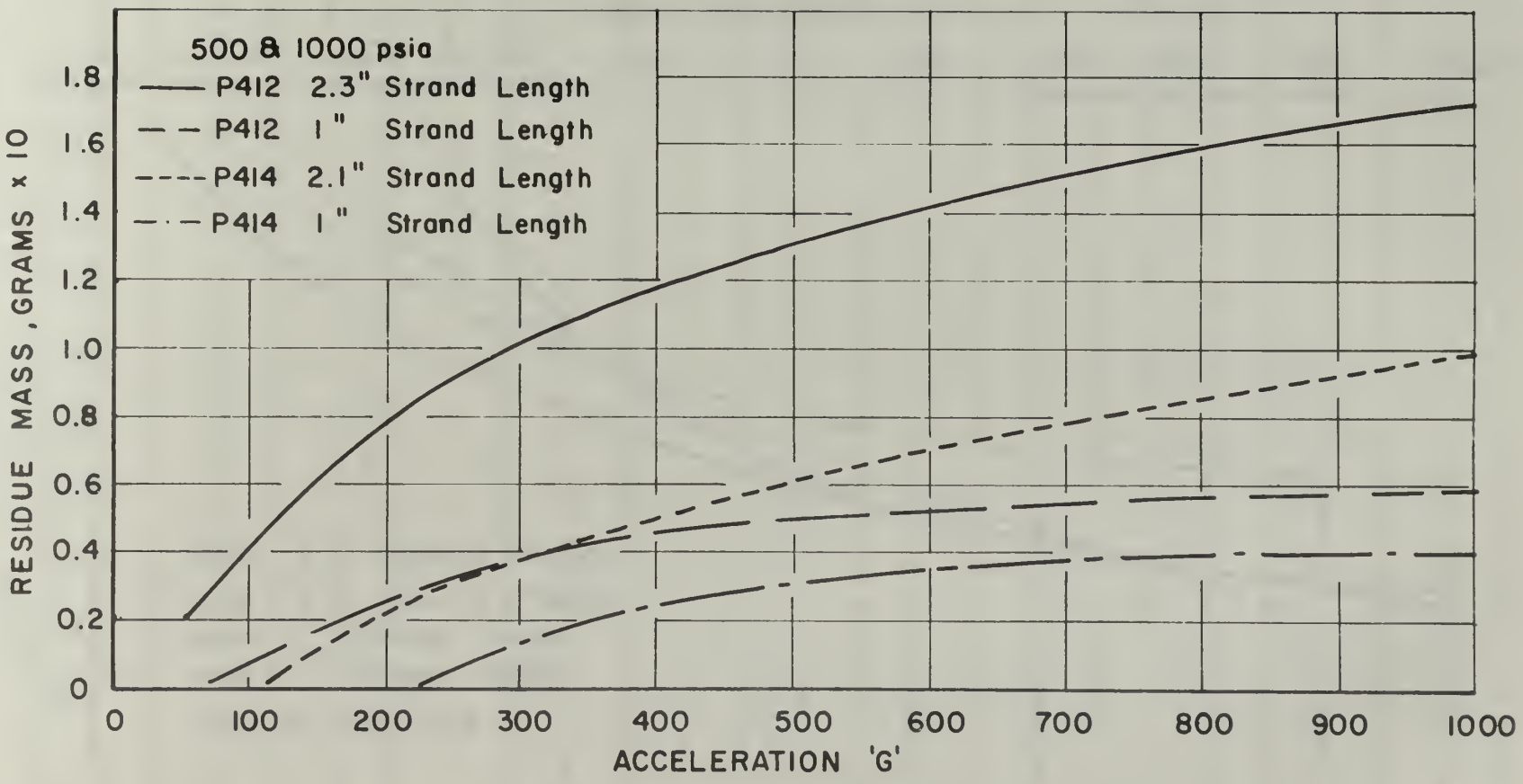

FIGURE 46 COMPARISON OF RESIDUE MASS VERSUS ACCELERATION FOR PROPELLANTS CONTAINING ALUMINUM AND ALUMINUM OXIDE

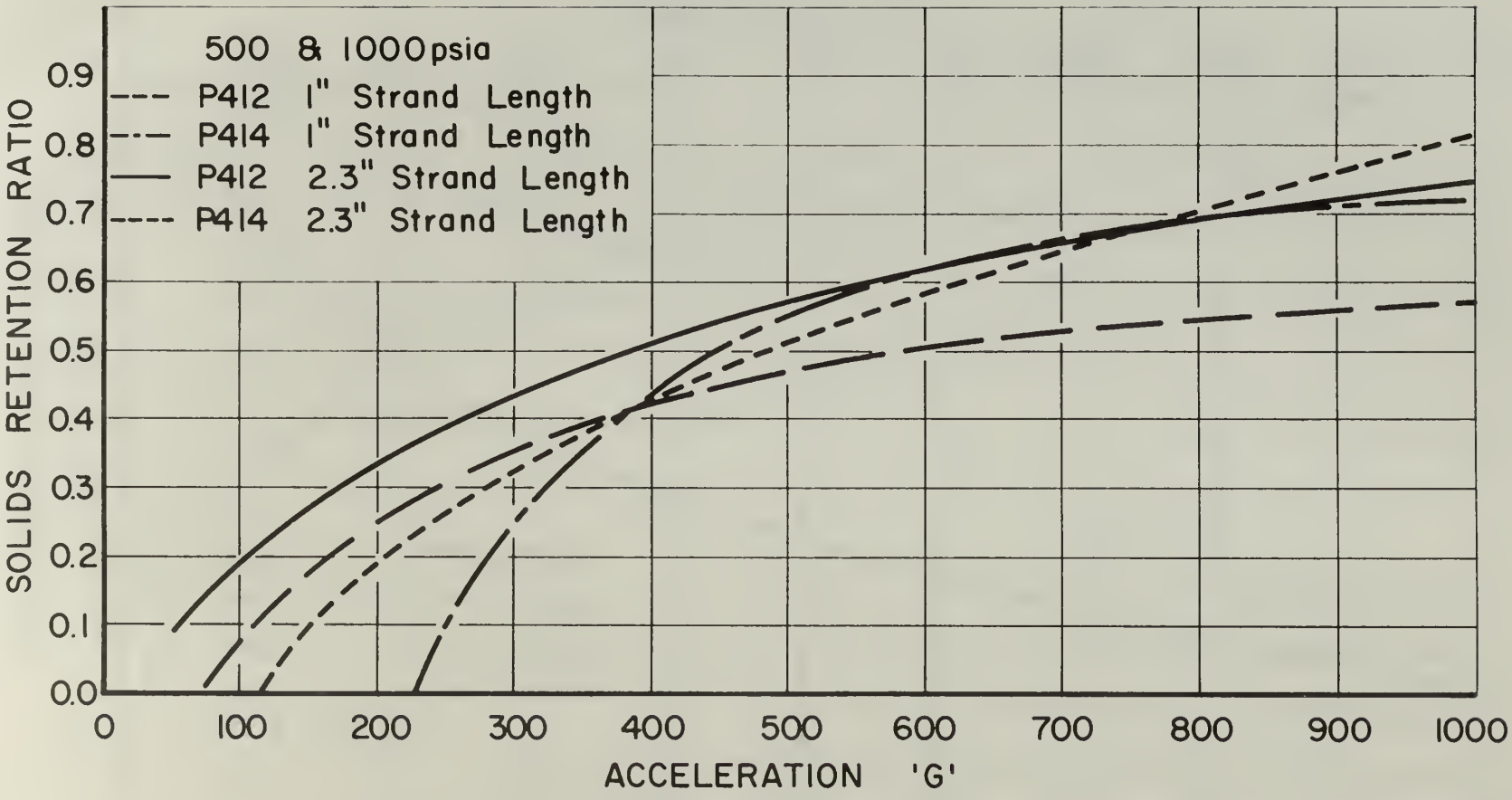

FIGURE 47 COMPARISON OF SOLIDS RETENTION RATIO VERSUS ACCELERATION FOR PROPELLANTS CONTAINING ALUMINUM AND ALUMINUM OXIDE

P412 propellant is the aluminum retention ratio. The solids retention ratio for propellant P414 is the ratio of the amount of aluminum oxide residue to the original amount of aluminum oxide present in the propellant strand. The data indicate that generally both propellants retained approximately the same percentage of the original aluminum (P412) or aluminum oxide (P414). One inch strand lengths of P414 below 350 G were an exception, as can be seen from the figure.

The retention of approximately equal percentages of original solids content seems to contradict the previous suggestion that the surface of the P414 propellant did not become "flooded." However, consideration of the nature of the residue removed from the P414 propellant with that removed from the aluminized propellants strengthens the view that P414 did not become "flooded" in the sense that the aluminized propellants became "flooded." The residue mass of P414 was porous and of low bulk density. It appeared as though individual particles had been bonded together (possibly with residue from the fuel binder). This is in contrast to the residue from the aluminized propellants which was not porous and had the appearance of a liquid which had been cooled and solidified.

Figure 48 contains the data obtained from elevated and ambient initial temperature experiments for P413 propellant. The data indicate that increasing the initial temperature of propellant P413 from 20° C to 66° C had no effect on the relative acceleration sensitivity of the propellant. At all acceleration levels the preheated propellant strands exhibited absolute burning rates about 4 per cent higher than those at 20° C. Thus the burning rate ratio was essentially independent of initial temperature for all acceleration levels.

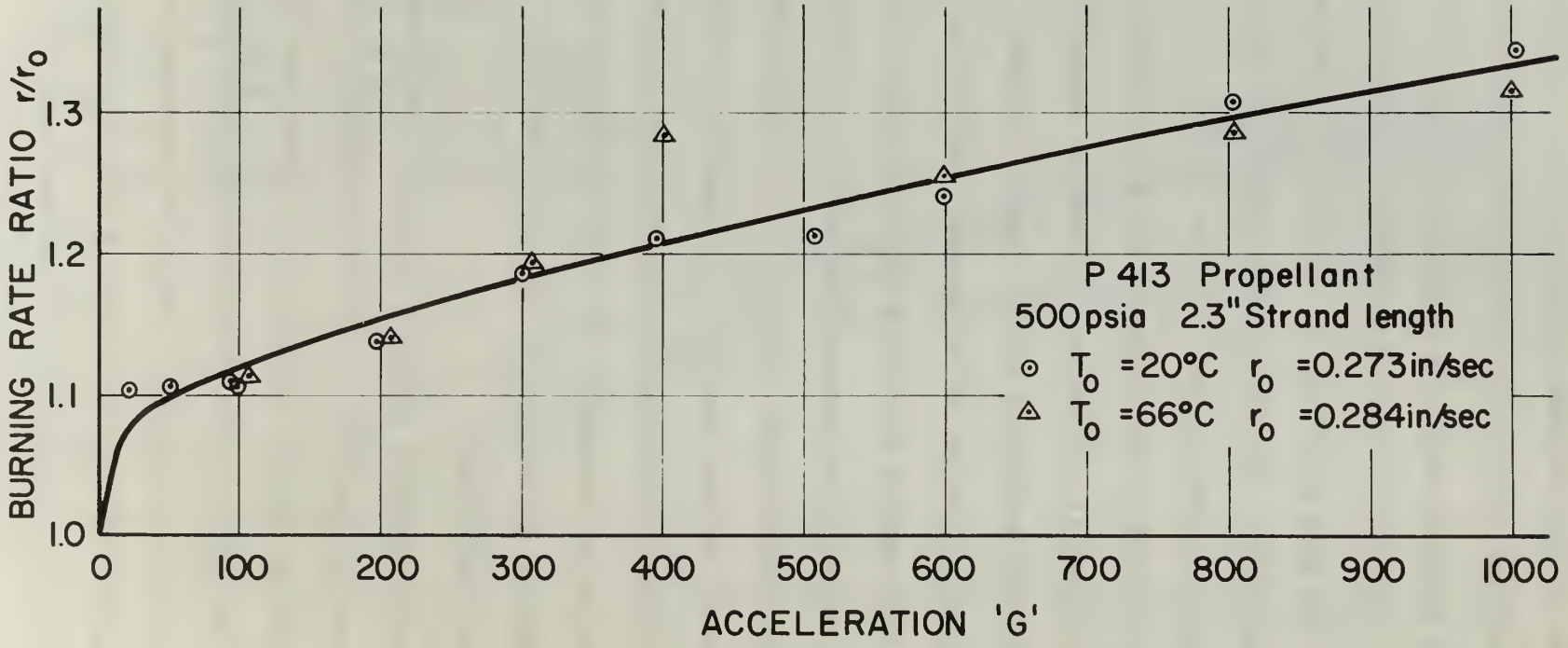

FIGURE 48 BURNING RATE RATIO VERSUS ACCELERATION AS A FUNCTION OF INITIAL PROPELLANT TEMPERATURE FOR PROPELLANT P413

The amounts of energy required to heat up and gasify a unit mass of propellant at an initial temperature of 20° C and a unit mass of the same propellant at 66° C are essentially equal. Furthermore, the gas phase processes would not be expected to change when the initial propellant temperature was increased from 20° C to 66° C. The experimental results indicate that the acceleration induced interaction between the gas phase and the propellant surface was not altered by increasing the initial propellant temperature from 20° C to 66° C.

The main conclusions derived from the experimental data can be summarized as follows. Aluminized propellants experience an increased burning rate when an acceleration field is imposed normal and into the burning surface. The burning rate commences to increase as the acceleration field is increased above 0 G and continues to increase monotonically for acceleration levels as high as 1000 G. The burning rate ratio exhibits no consistent pressure dependence but does exhibit a time dependence, decreasing as propellant burning proceeds. The initial temperature of the propellant does not affect the burning rate ratio at a given acceleration. The burning rate ratio and the aluminum retention ratio are inversely related. Less residue is retained when: 1) The aluminum particle size is increased from 10.6 μ mmd to 28 μ mmd; 2) the size of the coarse size oxidizer in bi-modal propellants is increased from 94 μ mmd to 200 μ mmd; and 3) the weight percentage of the small size oxidizer in bi-modal propellants is increased. As was the case for the burning rate ratio, there is no consistent pressure dependence for the amount of residue retained. Finally, the experimental data indicate that the heat transfer from the agglomerated aluminum particles to the propellant surface is an important mechanism

in the acceleration induced burning rate augmentation of composite solid aluminized propellants.

Comparison of Experiment with Existing Theories

In this section brief descriptions of the theoretical analyses of Crowe [9] and Glick [8] are presented. The theories are evaluated in light of the data obtained during the course of the experimental program.

Crowe's analysis was the first analytical approach to the phenomenon of burning rate augmentation of aluminized propellants in acceleration fields. Crowe reasoned that as the receding propellant surface uncovered an aluminum particle it would either be removed from the propellant surface by aerodynamic drag or be held on the surface by body forces. The disposition of a particular particle depended on the relative magnitude of the drag force and body force acting on it. If a particle were held on the propellant surface, the energy transferred to propellant surface would be increased by the release of the chemical energy from aluminum combustion. When the particle burned to a size such that the drag force became larger than the body force, the particle would leave the surface and no longer contribute to an augmented burning rate. If an aluminum particle were originally of such a size that the drag force was sufficient to overcome the acceleration induced body force, the particle would be removed immediately from the propellant surface and would not contribute to an augmented burning rate. Crowe expressed these assumptions mathematically by the equation

$$(r - r_o)\, h_v = r\, W_m\, L^*_H \qquad (4)$$

where r and r_o have their usual meanings and

h_v = energy required to heat and vaporize a unit mass of propellant (cal/gm)

W_m = propellant metal loading (weight percentage)

L^* = heat transferred to propellant per unit mass of aluminum particle burned (cal/gm)

H = fraction of particle mass consumed by combustion on the propellant surface

Solving Equation 4 for the burning rate ratio yields

$$\frac{r}{r_o} = \frac{1}{1 - \frac{W_m L^*}{h_v} H} \tag{5}$$

The parameter H is a function of acceleration, aluminum particle size distribution, and time. The time dependence of the function H arises from the necessary accumulation of particles on the propellant surface before a steady-state condition is achieved. Crowe derived the following expression for H by assuming that the aluminum particles had a log-normal size distribution and steady state conditions had been obtained:

$$H = \tfrac{1}{2}\,\mathrm{erfc}\left(\frac{\ln \xi_{p_c}/\xi_{p_m}}{\sigma}\right) - \exp\left(\frac{9}{2}\sigma^2\right)\left(\frac{\xi_{p_c}}{\xi_{p_m}}\right)^3 \mathrm{erfc}\left(\frac{\ln \xi_{p_c}/\xi_{p_m}}{\sigma} + 3\sigma\right) \tag{6}$$

where:

ξ_{p_c} = critical particle radius (micron)

ξ_{p_m} = mass mean particle radius (micron)

σ = standard deviation of the log-normal distribution

Crowe defined the critical particle radius as the radius of a particle for which the aerodynamic drag force was equal to the acceleration induced body force. It can be shown, by assuming Stokes drag law

is valid, that the drag on a spherical aluminum particle for a particular propellant is proportional to r/p where p is pressure. The body force on an aluminum particle is proportional to the acceleration force G. The critical particle radius is then a function of the factor Gp/r. Increasing Gp/r will decrease the critical particle radius. Decreasing the critical particle radius will increase the value of H and hence r/r_o. Thus increasing the pressure or acceleration or decreasing the burning rate of the propellant will result in higher values of r/r_o.

The analysis yields a dependence of burning rate ratio on acceleration as shown in Figure 49. The theoretical curves in Figure 49 resulted from use of the steady-state solution for H in Equation 5 and two values of the standard deviation of the aluminum particle size distribution, σ = 0 and 0.46. The burning rate was assumed to be increased by a factor of two when all the aluminum particles burned completely on the surface. Thus, the factor $W_m L^*/h_v$ equalled one-half.

The analysis predicts that the burning rate ratio will: 1) increase for a given propellant with increasing acceleration and pressure, 2) increase at a given acceleration with increased metal loading, 3) be unity for non-metallized propellants (i.e., $r/r_o = 1$ for $W_m = 0$), 4) be unity for propellants containing inert additives (i.e., $r/r_o = 1$ for $L^* = 0$), and 5) vary inversely with the burning rate of the propellant for a given metal loading, aluminum particle size distribution, pressure, and acceleration.

The general shape of the experimental curves of burning rate ratio versus acceleration obtained as a result of this investigation resembles the shape of the theoretical curves predicted by the analysis. The burning rate ratio increases as the acceleration is increased from 0 G and asymptotically approaches a limiting value as acceleration is increased.

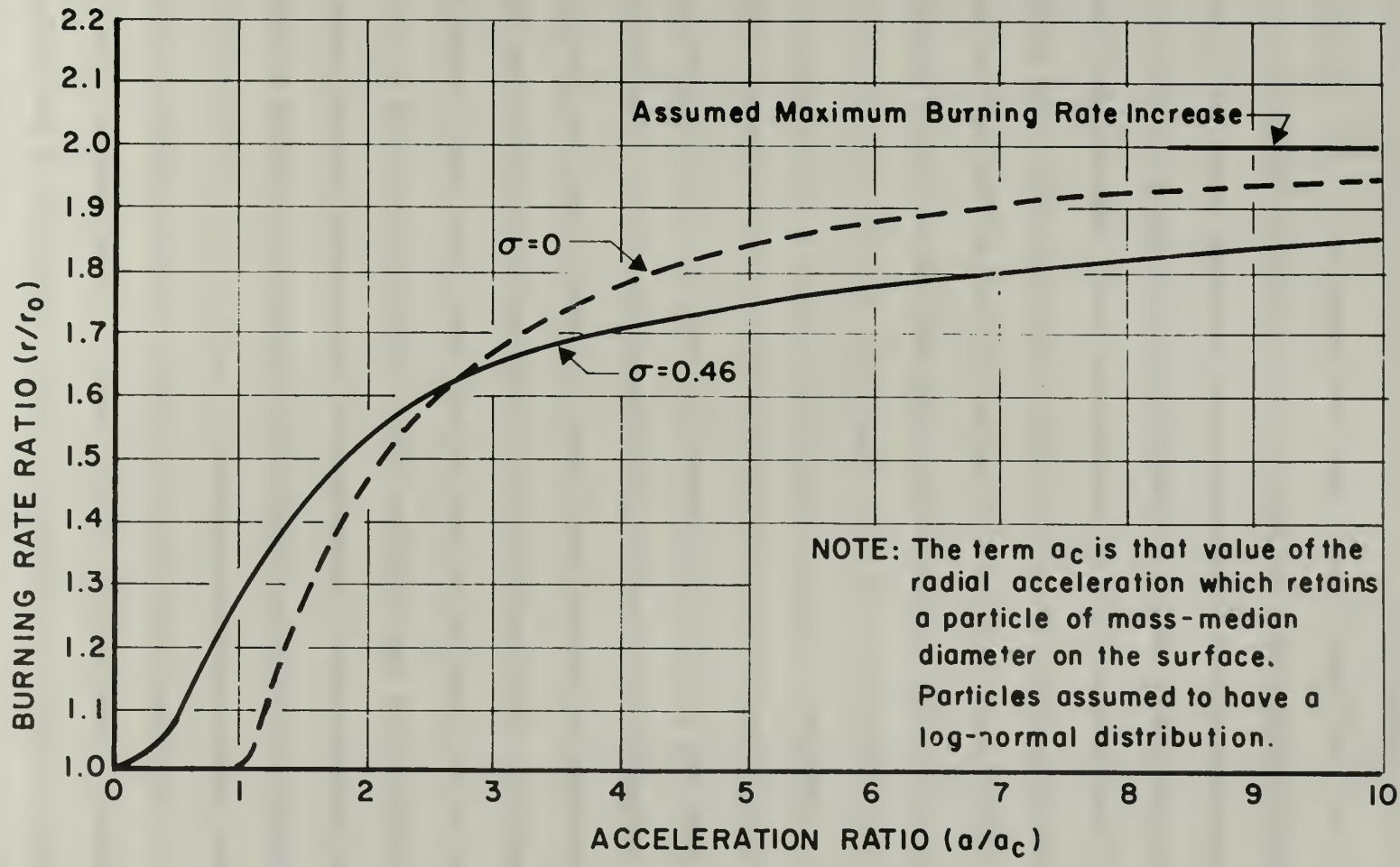

FIGURE 49 PREDICTED BURNING RATE RATIO VERSUS ACCELERATION RATIO FOR TWO PARTICLE SIZE DISTRIBUTIONS

Propellants P413, P415 and P423 all contained 15 per cent of a common aluminum particle size distribution, 67.15 per cent AP, and 17.85 per cent PBAN binder. Thus the parameters W_m, L^*, and h_v should be nearly equal for these propellants. The acceleration sensitivities of these propellants increased in the following order: P413, P415, and P423. The theory predicts (through the variation of H with O G propellant burning rate) that the acceleration sensitivity of the propellants in increasing order should be: P413, P415, and P423. The experimental data indicate that the theory correctly predicts the relative sensitivities of these propellants and thus is able to predict correctly the effect of increasing the basic propellant burning rate.

However, the propellants did not exhibit an increased burning rate ratio when the pressure was increased as is predicted by the model. No consistent pressure dependence was observed. The theory predicts that propellant P412 which was the only propellant to contain 5 per cent aluminum should have had the least acceleration sensitivity. However, it was found that propellant P412 exhibited approximately the same sensitivity to acceleration as did propellants P413 and P421, both of which contained 15 per cent aluminum. The theory predicts that non-aluminized propellants should be insensitive to acceleration. As indicated previously all three non-aluminized propellants exhibited a very definite acceleration sensitivity.

The behavior of propellant P414 containing aluminum oxide is contrary to the prediction of the theory. Since aluminum oxide can release no energy of combustion, a theory based solely on energy considerations is not able to correlate the burning rate behavior of propellant P414. The model does not take into consideration the

agglomeration of individual aluminum particles and the eventual "flooding" of the propellant surface. Nor does the model anticipate a decrease in burning rate as the propellant proceeds to burn.

Crowe's assumption that the drag on an aluminum particle is given by Stokes drag law introduces a source of error. Stokes drag law is valid for spherical particles without blowing in the low Reynolds number regime (1 > Re). An aluminum agglomerate does have blowing as there is a mass efflux from the particle surface due to metal combustion. In addition, as the agglomerates grow in size, their Reynolds numbers become larger than one. These two factors make the use of Stokes drag law somewhat in error.

Although the analysis is able to predict a qualitatively correct burning rate ratio dependence on acceleration and the effect of increasing the basic propellant burning rate, it is unable to correlate much of the other experimental evidence. The inability of the analysis to correlate the pressure dependence, the effect of lessening the amount of aluminum additive, and the behavior of non-metallized and aluminum oxide propellants casts doubt on the adequacy of the model.

Glick [8] proposed a modification of the model which took into account the agglomeration of the individual aluminum particles. In addition Glick accounted for the presence of pits on the propellant burning surface. He reasoned that since there were a finite number of cone shaped pits on the surface, the overall propellant burning rate was controlled by the rate at which the individual agglomerates at the base of these pits were able to proceed into the solid phase of the propellant. Glick made the following assumptions: 1) The phenomenon is steady in the mean; 2) particles evolved at the burning

surface remain or depart depending upon the magnitude of the viscous and inertial forces; 3) particles retained on the burning surface agglomerate and remain on the burning surface; 4) interaction between retained condensed phase material and the burning surface occurs at a limited number of points; 5) increased burning rates are caused by combustion of the condensed phase agglomerates; and 6) the line of descent of the agglomerated metal through the propellant is colinear with the acceleration force vector.

Figure 50 illustrates the analytical model employed. The figure shows conical pits in the propellant surface, the mean propellant surface, and the agglomerated metal particle, and illustrates some of the nomenclature.

The descent rate of a single agglomerated particle through the propellant was computed from an energy balance between the energy rate, $\dot{E}_r$, required to increase the burning rate above the base rate and the rate of energy supplied through metal combustion, $\dot{E}_s$. The energy rate required to increase the burning rate above the base rate is

$$\dot{E}_r = (r_a - r_o)\, h_v\, A_i \tag{7}$$

where r_a is the rate of descent of the agglomerate through the propellant, A_i is the effective interaction area of the particle with the propellant, and the other symbols have their usual meaning. A_i was assumed to be the area where the local burning rate was modified and is

$$A_i = \pi(\xi_a \cos \theta_c)^2 \tag{8}$$

where ξ_a and θ_c are defined in Figure 50.

However, $\cos^2 \theta_c = 1 - \sin^2 \theta_c$ and $\sin \theta_c = r_o/r_a$ so that

$$A_i = \pi\xi_a^2 [1 - (r_o/r_a)^2] \tag{9}$$

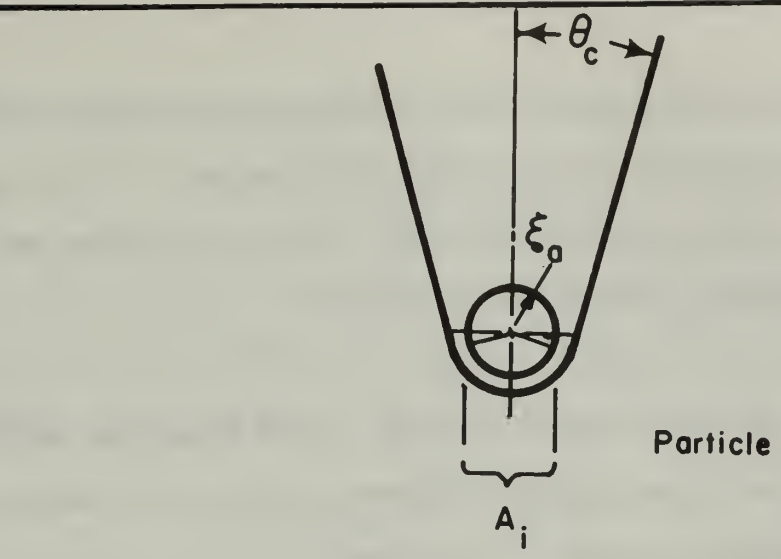

a) Individual Agglomerate

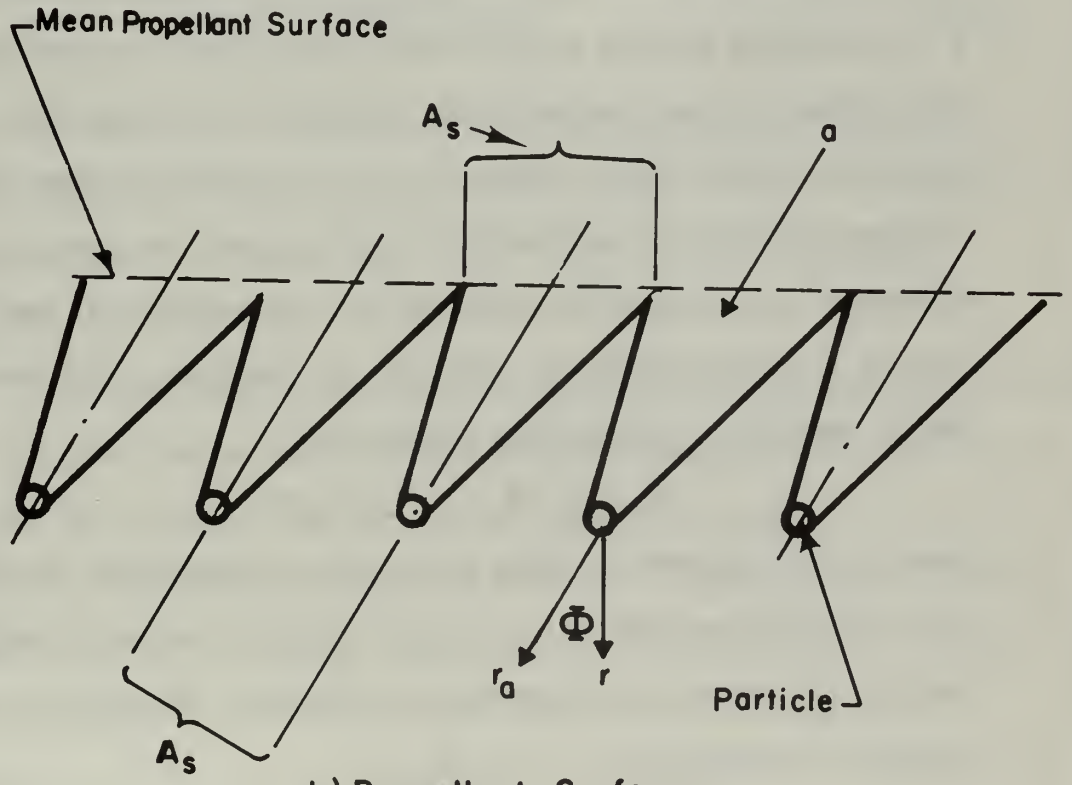

b) Propellant Surface

FIGURE 50 GEOMETRY OF GLICK'S ANALYTICAL MODEL

Since the propellant surface is pitted, any metal added to the agglomerated particle must originate within its own pit. If it is assumed that there are N_s pits per unit area of the mean burning surface, the effective area, A_s, swept by each pit is

$$A_s = N_s^{-1} \cos \Phi \tag{10}$$

where Φ is the angle between a normal to the propellant surface and the direction of the applied acceleration force. The metal added to the agglomerated particle in unit time, $\dot{m}_a$, is

$$\dot{m}_a = r_a \rho_s W_m [A_i + (A_s - A_i)H^*] \tag{11}$$

In Equation 11 it is assumed that all of the metal particles evolved in the interaction area, A_i, are agglomerated but only that fraction H^* of the metal evolved on the sides of the cone is agglomerated. Since the process has been assumed to be invariant with time, this metal must be burned in unit time. However, only the energy released in the clearance between the agglomerate and the propellant area, A_i, is effective in increasing the burning rate. Assuming that the energy release is uniform over the particle, the increase in the rate of energy feedback to the burning surface is

$$\dot{E}_s = \dot{m}_a \Delta H_c (1 - r_o/r_a)/2 \tag{12}$$

where ΔH_c is the lower heating value for the combustion of the metal in the products of combustion of the binder and oxidizer (cal/gm). The rate of descent of the particle obtained by Equations 7 and 12 and employing Equations 9, 10, and 11 is

$$r_a = r_o \left[\frac{1 - \Pi(1 - H^*)}{1 - \Pi[1 + (\beta-1)H^*]} \right]^{1/2} \tag{13}$$

where $\Pi = W_m \Delta H_c / 2h_v$ and $\beta = (N_s \pi \xi_a^2)^{-1} \cos \Phi$.

Examination of the vector diagram in Figure 50 shows that

$$r = r_a \cos \Phi \tag{14}$$

Therefore, the desired burning rate ratio becomes

$$\frac{r}{r_o} = \left[\frac{1 - \Pi(1 - H^*)}{1 - \Pi[1 + (\beta-1)H^*]} \right] \cos \Phi \qquad (15)$$

The function H^* is the fraction of metal evolved on the sides of the cone that is agglomerated and retained. Glick reasoned that H^* was simply the first term of Equation 6 or

$$H^* = \tfrac{1}{2} \operatorname{erfc} \left(\frac{\ln \xi_{p_c} / \xi_{p_m}}{\sigma} \right) \qquad (16)$$

Glick showed in a manner analogous to the method outlined on page 173 that for a given pressure

$$\frac{\xi_{p_c}}{\xi_{p_m}} = \left[(r/a)/(r/a)_c \right]^{\frac{1}{2}} \qquad (17)$$

where the subscript c denotes conditions which result in a particle of mass mean size being retained on the burning surface. The effect of acceleration on burning rate can be determined by employing Equations 15, 16, and 17.

The parameters β and Π can be considered as parameters concerned with agglomeration and propellant composition respectively. The terms involved in Π suggest that it is acceleration independent. Northam's data [11], the castings supplied by N.A.S.A. of extinguished propellant surfaces, and the "flooding" phenomenon observed during the course of this investigation indicate that the parameter β is acceleration dependent. Physically the reciprocal of β represents the percentage of the propellant surface which is shadowed from the combustion flame with aluminum agglomerate. Experimental observations indicate that a greater percentage of the surface becomes covered with aluminum agglomerate as the acceleration level is increased. Therefore, the value of β should decrease with increasing acceleration.

Glick's analysis does not include a method for estimating the values of β as a function of acceleration, so that an accurate prediction of the acceleration dependent burning rate behavior of a particular propellant prior to experimentation cannot be made.

The experimental results for a particular propellant can be used in conjunction with the analysis to obtain the variation of β with acceleration. The method is to estimate the value of $(r/a)_c$ for a given propellant and use the experimental results for burning rate, r, as a function of acceleration, a, in Equation 17 to obtain values of ξ_{p_c}, ξ_{p_m}. These values are then substituted into Equation 16 to obtain values of H^*. Values of H^* are then substituted into Equation 15 along with an estimate of Π to obtain values of β versus acceleration.

Glick used the experimental results of Anderson [3] in conjunction with the theory to obtain the variation of β with acceleration. He found that the value of β was large at low accelerations and decreased with increasing acceleration [15]. Thus the acceleration dependence of β required to correlate Anderson's experimental data was qualitatively correct.

It is believed that the model is an improvement over the model proposed by Crowe. The concept of aluminum agglomerates, located in discrete pits, penetrating the propellant surface at a rate which controls the overall propellant burning rate appears reasonable and is supported by experimental evidence. The assumption that equal amounts of aluminum are combusted and added to an agglomerate (i.e., that the phenomenon is steady-state) appears to be an over simplification. The fact that the propellant surface "floods" indicates that an agglomerate continues to grow in size as it penetrates the solid propellant.

The energy required to increase the burning rate at the interaction area between the agglomerate and the propellant surface was assumed to be supplied by metal combustion. As mentioned previously this assumption is not compatible with the behavior of propellants containing aluminum oxide and tungsten. For these reasons it is believed that a more sophisticated model is required to explain the observed experimental results.

III. FAST BURNING RATE PROPELLANTS

Two fast burning rate propellants supplied by the Thiokol Chemical Corporation were investigated at 1000 and 1500 psia. These propellants are designated 2A and J6. The only difference between the propellants was the size of the aluminum additive, propellant 2A having the larger size aluminum powder. Although the exact burning rates of the propellants are classified, it can be stated that the propellants burned at a rate very much higher than that of the propellants investigated in the basic parametric series.

Propellant J6 was photographed under standard acceleration conditions at 500 and 1000 psia by Crump of N.W.C., China Lake, California, using the high-speed motion picture technique outlined in Reference 13. The motion pictures show that no aluminum agglomeration took place. The aluminum particles burned as individual particles at both pressure levels.

Propellants 2A and J6 exhibited little or no burning rate augmentation at accelerations as high as 1018 G as can be seen from Figures 51 and 52. This negligible burning rate augmentation can be explained by the following considerations. The small size oxidizer

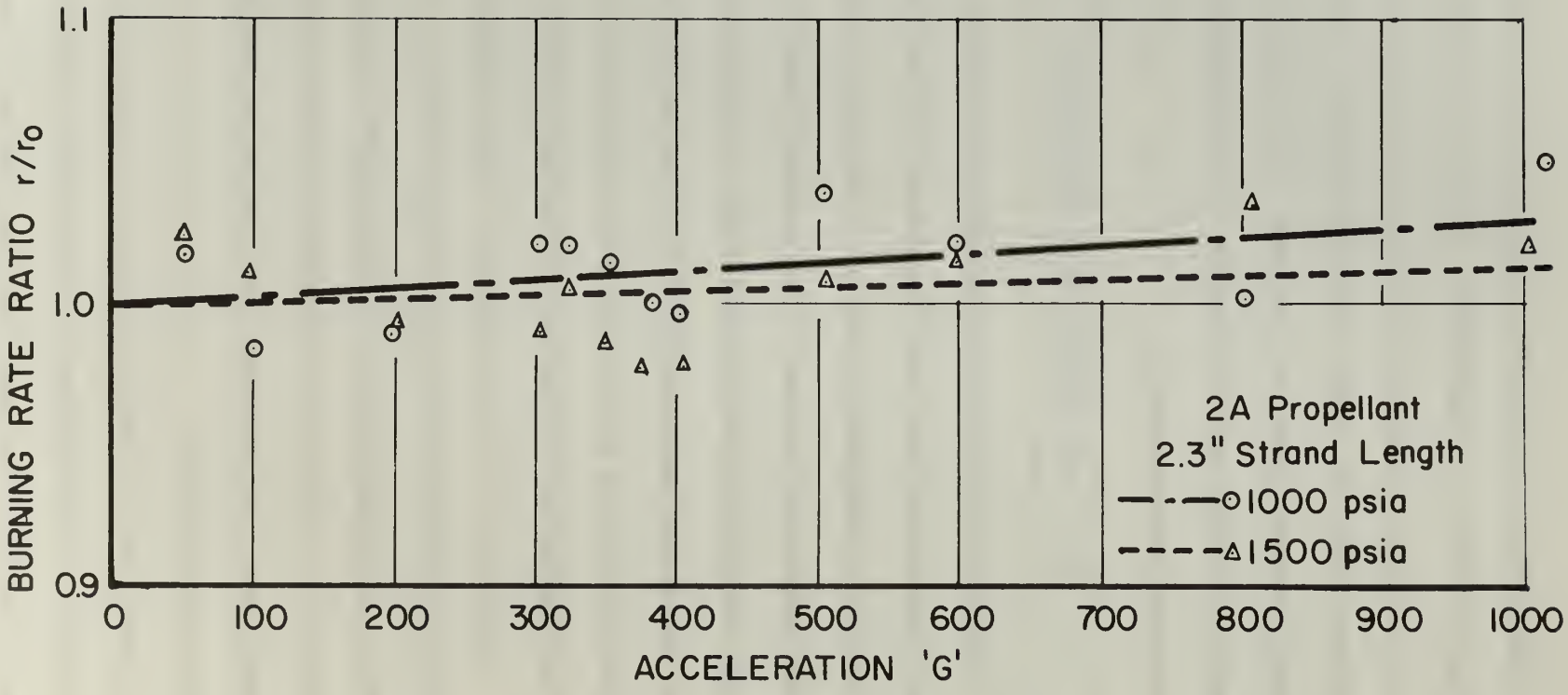

FIGURE 51 BURNING RATE RATIO VERSUS ACCELERATION FOR PROPELLANT 2A

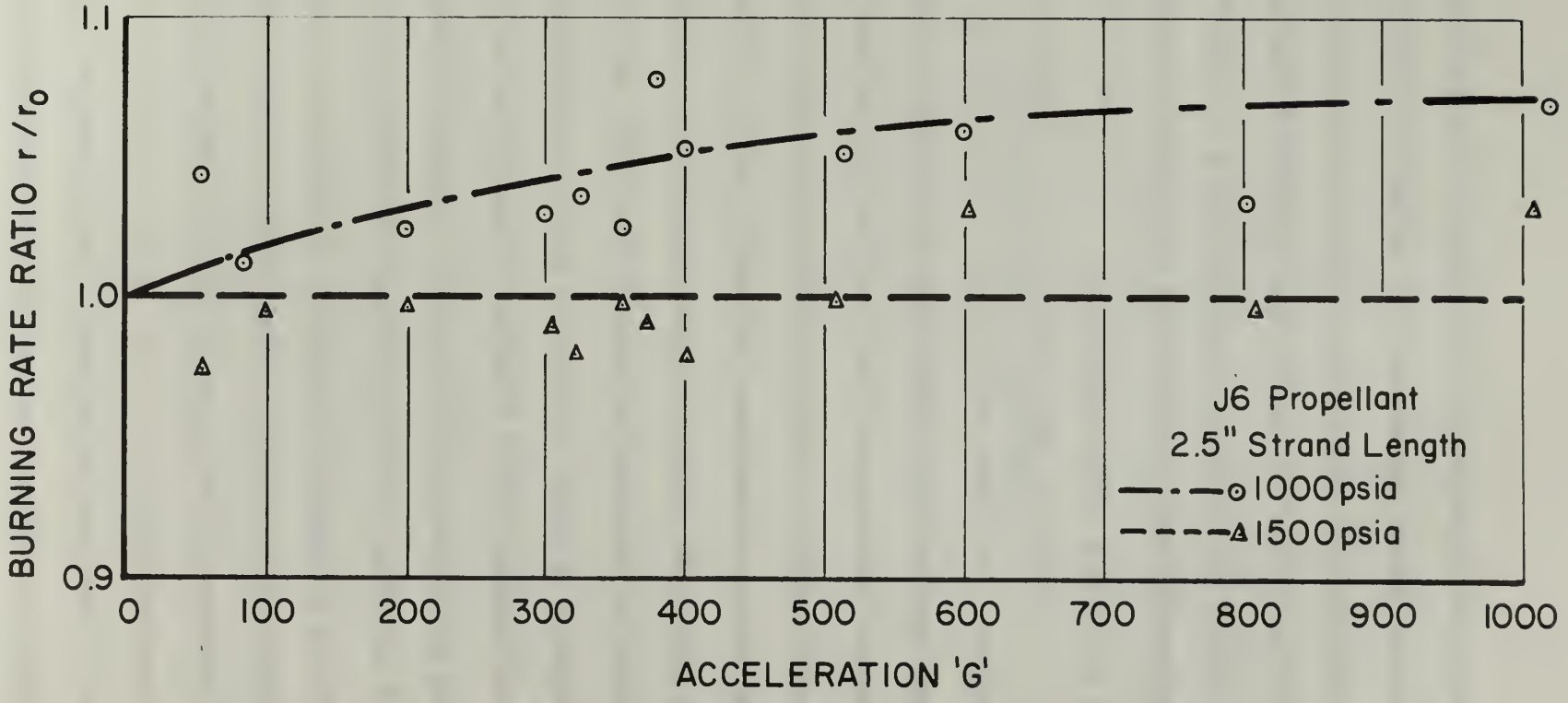

FIGURE 52 BURNING RATE RATIO VERSUS ACCELERATION FOR PROPELLANT J6

particles contained in the propellant probably resulted in very little or no aluminum agglomeration as evidenced by the motion pictures of J6 propellant and in accordance with Crump's pocket model. The high burning rate of the propellants produced a high gas velocity which provided the necessary aerodynamic drag to remove from the propellant surface whatever aluminum that did agglomerate. The result was little or no burning rate augmentation.

The spent inhibitor cases were investigated for possible residue. The sides and bottoms of the cases were covered with the same type of black carbon-like residue found in the basic propellant series. The amount of this residue was less than that found for the basic series of propellants, being only enough to blacken the sides and bottom of the cases. No single metal-like residue cap was found in any of the inhibitor cases. However, the cases of the J6 propellant burned at accelerations greater than 200 G and a pressure of 1000 psia contained a number of discrete aluminum oxide particles. The particles were examined with a 16 power microscope and an optical comparitor. They were spheroidal in shape and ranged in diameter from 8 μ to 160 μ. The particles were very difficult to separate from the carbon-like residue to facilitate weighing. Nevertheless, an attempt was made to weigh the oxide residue. The amount of oxide residue increased from approximately 0.01 grams at 200 G to approximately 0.05 grams at 1000 G acceleration.

The data in Figures 51 and 52 indicate that propellant J6 at 1000 psia exhibited the greatest sensitivity to acceleration. The fact that propellant J6 at 1000 psia was the only propellant to retain traces of aluminum oxide residue again demonstrates the dependence of

burning rate augmentation and retention of aluminum and/or aluminum oxide on the propellant surface. It is also interesting to note that it was the fast burning rate propellant with the small size aluminum particles, J6, which retained aluminum oxide residue. This correlates with the results obtained for the basic series which indicate that it is propellants with small aluminum powder which have the tendency to retain the greatest amount of residue.

IV. EROSIVE BURNING RATE EXPERIMENTS

The erosive burning rate experiments were conducted at 500 psia with a typical aluminized composite propellant. The experiments were conducted at four acceleration levels: 0, 100, 200, and 300 G with the acceleration vector directed into and perpendicular to the propellant burning surface. In addition experiments at 100 G were conducted with the acceleration vector directed outward from and perpendicular to the burning surface.

Generally two motors, each equipped with two timing wires, were fired at a given acceleration. These two motors provided four average burning rates at four different distances from the fore end of the motors. The burning rate values are shown in Figures 53a through 53e. The data at each acceleration level suggest that a good first approximation for burning rate versus distance from the fore end of the motor is a linear relationship. Accordingly, a linear least squares fit to the data at each acceleration level was made to obtain equations relating average burning rate to distance from the fore end of the motor. The form of these equations is

$$r_e = r_{x=o} + C_1 x \qquad (18)$$

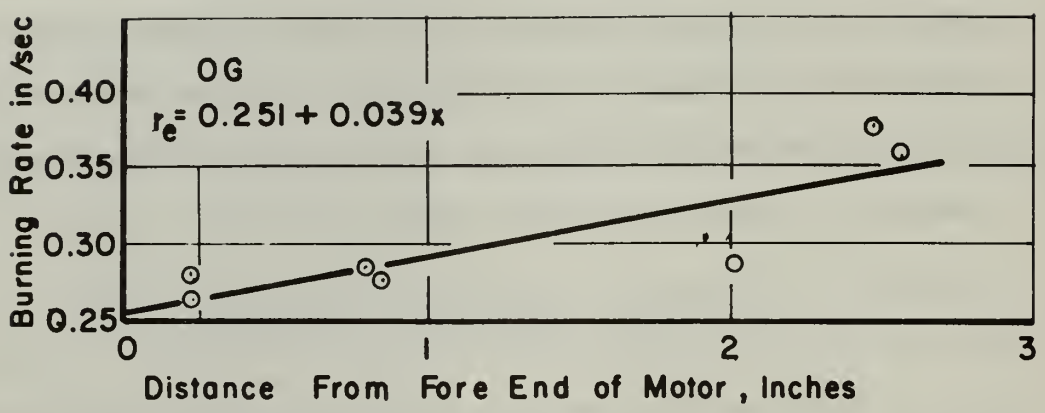

a) 0G

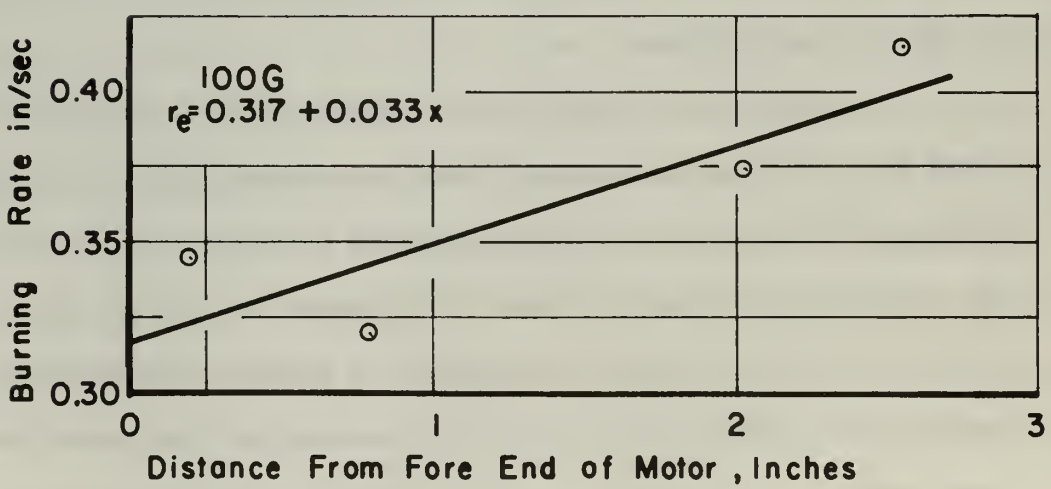

b) 100G

FIGURE 53 BURNING RATE VERSUS DISTANCE FROM FORE END OF EROSIVE MOTOR

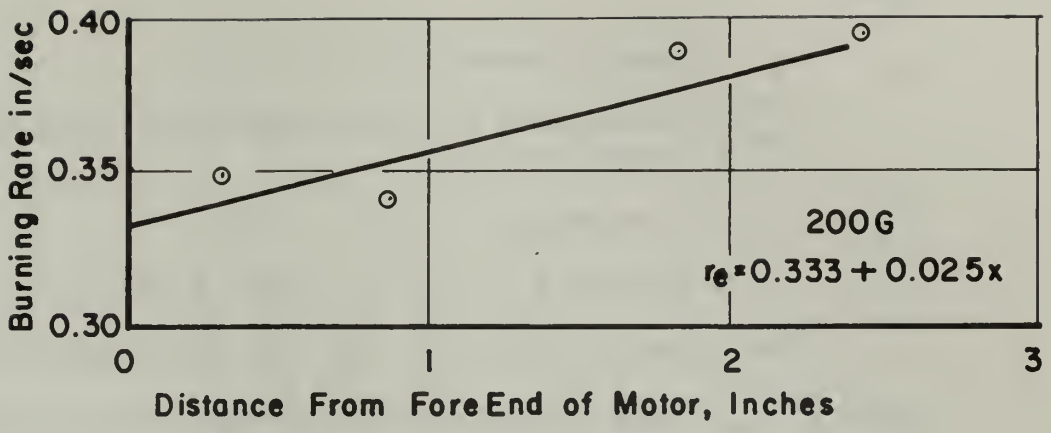

c) 200G

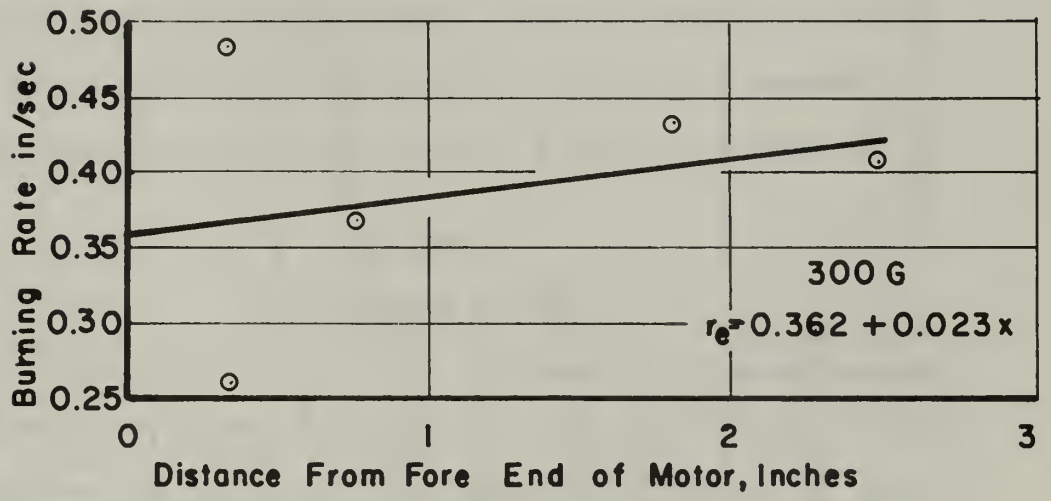

d) 300G

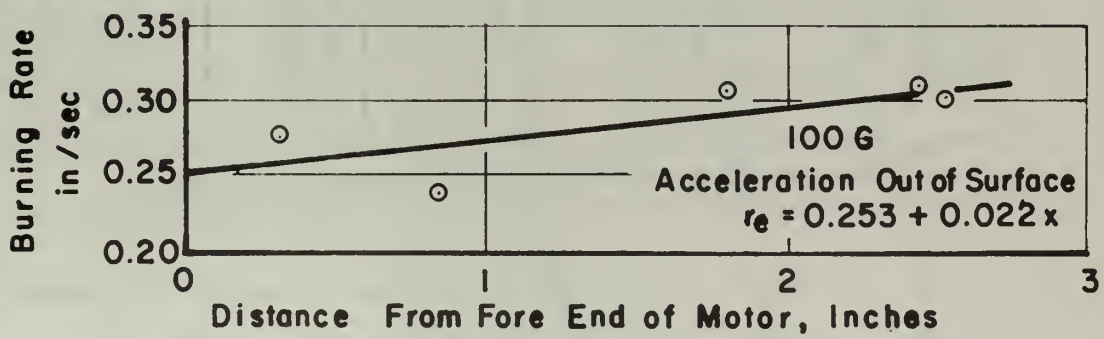

e) 100 G

FIGURE 53 BURNING RATE VERSUS DISTANCE FROM FORE END OF EROSIVE MOTOR

where:

r_e = erosive burning rate (inch/sec)

$r_{x=o}$ = burning rate at the fore end of the propellant strand (inch/sec)

C_1 = constant (sec^{-1})

x = distance from fore end of the propellant strand (inch)

The values of $r_{x=o}$ and C_1 vary with acceleration level. The values of $r_{x=o}$ compare very favorably with the burning rate values obtained from 0.7 inch length strands burned using the conventional strand-centrifuge technique. The comparison is shown in Table II. A comparison of absolute burning rate versus distance from the fore end of the erosive motor as a function of acceleration is shown in Figure 54.

TABLE II

EROSIVE BURNING DATA

Acceleration	r Strand	$r_{x=o}$	C_1	α	K
0	0.250	0.251	0.039	1.006	3.760
100	0.332	0.317	0.033	1.006	2.210
200	0.335	0.333	0.025	1.003	1.582
300	0.359	0.362	0.023	1.002	1.244
*100	-----	0.253	0.022	1.004	2.340
* Acceleration directed out of burning surface.					

The spent erosive motor cases were examined for possible residue. A black powdery residue was found on the sides and top of the motor cases. The bottoms of the motor cases which were burned at 0 G and 100 G (acceleration directed away from the burning surface) were smooth and showed no evidence of pitting or the presence of aluminum and/or

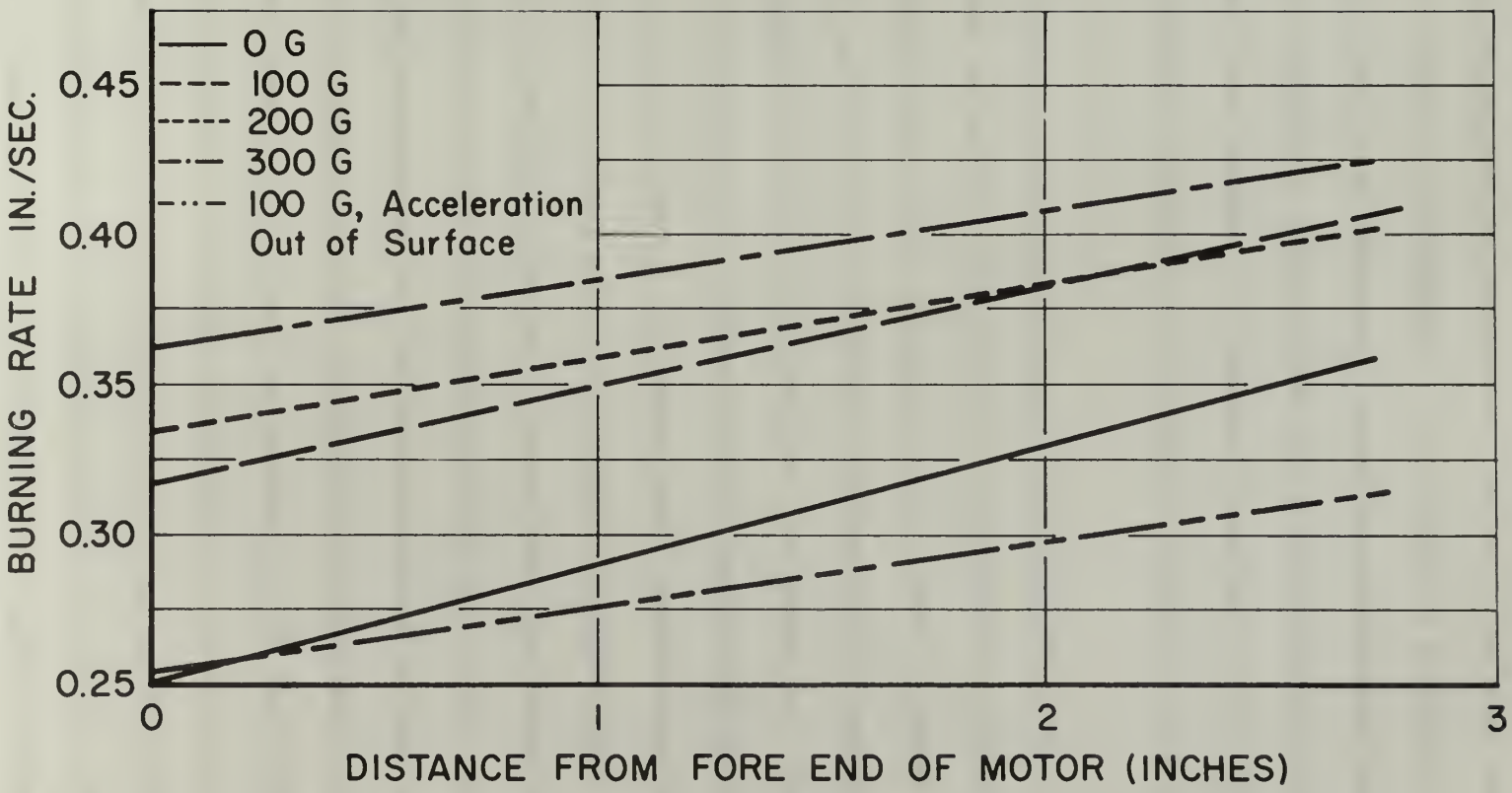

FIGURE 54 COMPARISON OF BURNING RATE VERSUS DISTANCE FROM FORE END OF EROSIVE MOTOR

aluminum oxide residue. The bottoms of the cases which were burned at 100, 200, and 300 G with the acceleration directed into the burning surface were badly pitted. The number of pits per unit area increased with increasing acceleration. The diameter and depth of an average size pit measured approximately 0.06 and 0.04 inches respectively and did not vary appreciably with acceleration. At 300 G the pits nearest the head end of the motor contained a spherical metal-like residue. No residue was found in the pits at acceleration levels of 100 and 200 G.

The available erosive burning rate data at one G can be correlated with a good degree of success by a number of analyses [16, 17, 18]. Common to all of these analyses is the assumption that combustion takes place in the boundary layer above the surface of the solid propellant. The propellant erosive burning rate is assumed to be dependent on the convective heat transfer rate to the propellant surface from the combustion products under conditions of transpiration.

One method of presenting erosive burning rate data is as a plot of erosive burning rate ratio, ε, versus combustion gas mass flux per unit port area. The erosive burning rate ratio is defined as the ratio of the burning rate at a motor position experiencing erosive burning to the basic non-erosive burning rate of the propellant. The mass flux per unit area, B, is a measure of the time average mass velocity per unit port area in the flow channel above the burning propellant surface. Mass velocity was chosen on the basis that it is the physically pertinent variable in the more familiar problem of convective heat transfer in uniform flow along a solid boundary. The method used to determine values of B from the burning rate data is presented in Appendix I.

Figure 55 contains plots of ε versus B as a function of acceleration level. Linear least squares fits were made to the ε versus B data to obtain equations of the form:

$$\varepsilon = \alpha + K\,B \tag{19}$$

The values for α and K determined for each acceleration level are presented in Table II. Since by definition $\varepsilon = 1$ for the condition of no mass flow over the propellant surface (i.e., B = 0), the value of α should be exactly one. The values of α in Table II are very close to the expected value.

The value of K decreases with increasing acceleration when the acceleration is directed into the propellant surface, indicating that the propellant becomes less sensitive to erosive effects as the acceleration level is increased. A probable explanation for the decreased erosive sensitivity is the following.

References 19 and 20 show that the erosive burning effect is more pronounced in slow burning propellants than in fast burning propellants. It is generally believed that the erosive effect is attributable to an enhanced rate of heat transfer to the solid propellant due to the presence of a gas flow parallel to the burning surface. Green [19] envisaged the inverse relationship between erosion sensitivity and basic burning rate as a boundary layer effect; the greater the velocity, the thinner the boundary layer and the steeper the temperature gradient from the hot core to the cooler solid surface. Thus a fast burning propellant would be expected to exhibit a relatively small erosion effect since the rapid evolution of gas normal to the burning surface would produce a thicker boundary layer (for a given parallel velocity) than would be obtained in the case of a slow burning propellant. Since

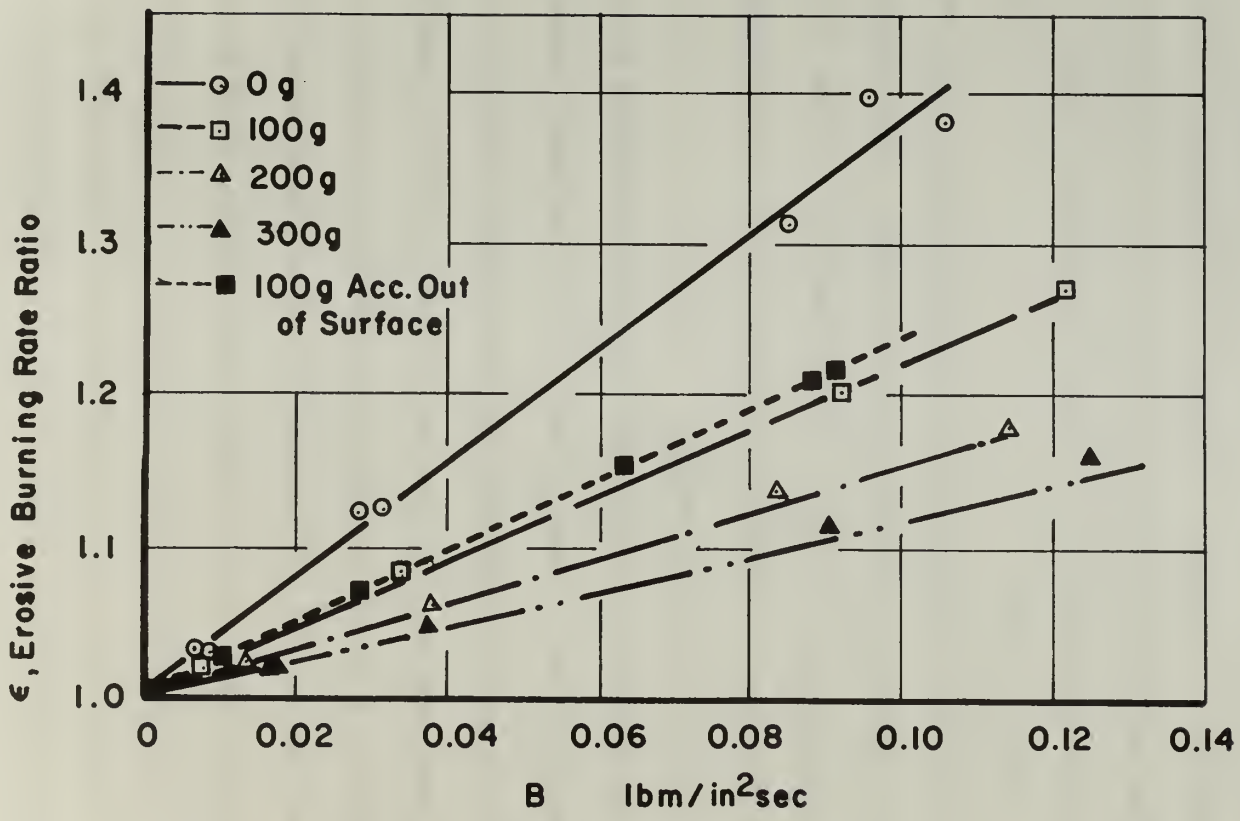

FIGURE 55 EROSIVE BURNING RATE RATIO VERSUS MASS FLUX AS A FUNCTION OF ACCELERATION LEVEL

increasing the acceleration level results in a faster basic non-erosive burning rate and hence less convective heat transfer to the propellant surface, it follows that the erosion sensitivity of the propellant should be decreased.

In Figure 56 are graphically presented values of K versus $r_{x=o}$. The inverse relation between K and $r_{x=o}$ is evident. Also shown for comparison in Figure 56 are values obtained by Green for eight different non-aluminized composite propellants. The values of K determined from Green's data are about four times less than the values obtained during the course of this investigation. The difference may be due to the addition of aluminum in the propellant under consideration in the present investigation. The presence of aluminum agglomerates on the surface of an aluminized propellant should enhance the heat transfer rate from the hot reaction gases to the propellant surface because of the presence of low thermal resistance paths which the agglomerates provide. Thus for a given value of mass flux parallel to the propellant surface the heat transfer rate to the surface would be greater for an aluminized propellant. The increased heat transfer rate would result in a higher erosive burning rate and hence a higher value of K for a given value of mass flux, B.

The data obtained from experiments conducted at 100 G with the acceleration directed outward from the propellant surface indicate that the propellant in this acceleration environment has a basic non-erosive burning rate equal to the 0 G non-erosive burning rate. However the value of K at 100 G was 2.340, which is 38 per cent less than the value of 3.760 obtained at 0 G acceleration. The data in Figure 56 suggest that for a given pressure the value of K is a function of $r_{x=o}$. Since

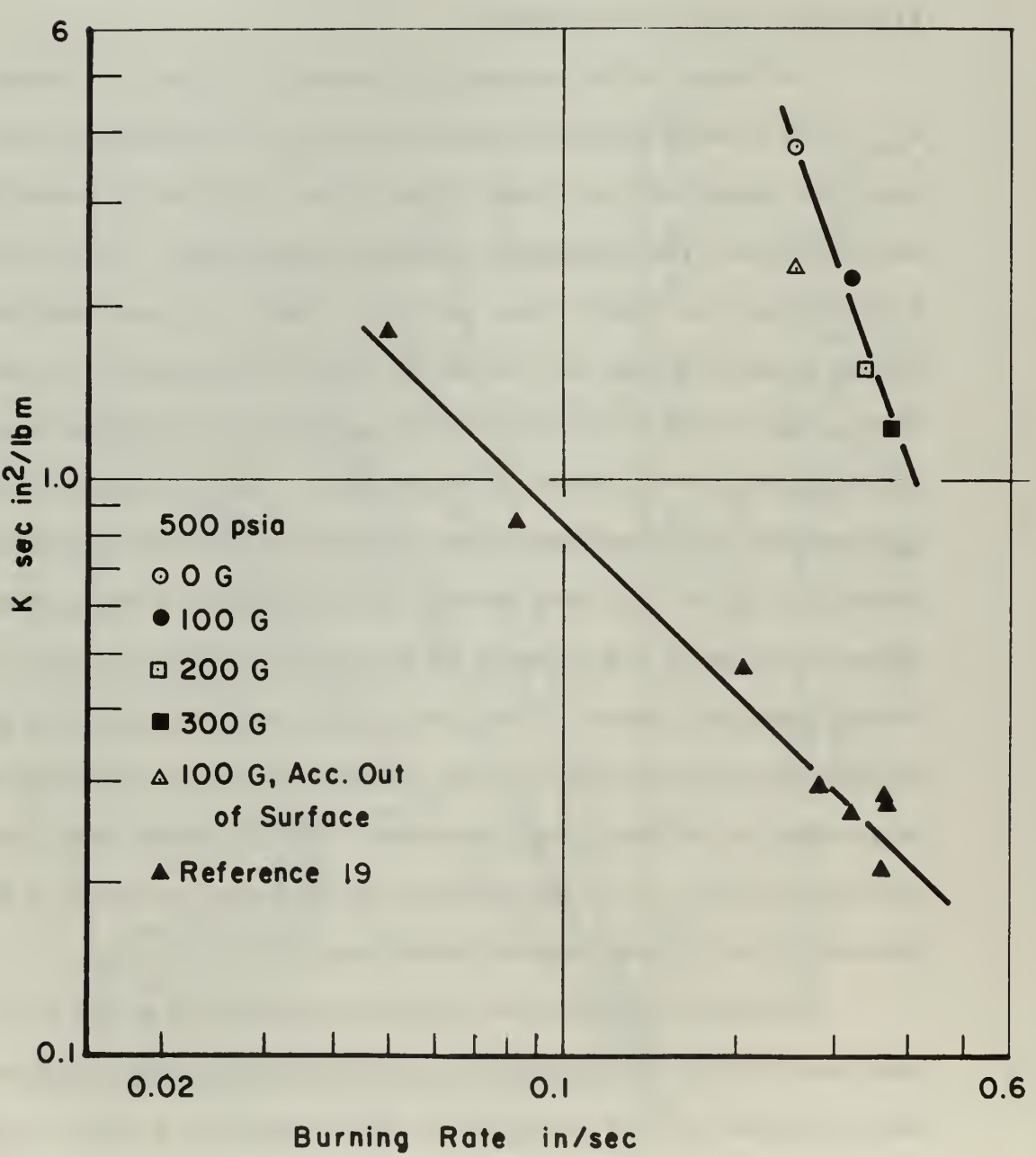

FIGURE 56 EROSIVE CONSTANT K VERSUS BURNING RATE

the basic non-erosive burning rates of the propellants under investigation were equal at 0 G and 100 G directed out of the propellant surface, the difference in the values of K cannot be explained by differences in the basic non-erosive burning rate and hence the boundary layer thickness. However, it is conceivable that with the acceleration field directed away from the surface the surface would be kept free of aluminum agglomerates, whereas at 0 G an aluminized propellant is known to have aluminum agglomerates present on its surface [13]. The absence of aluminum on the surface could account for the smaller value of K because of the diminished heat transfer rate. Thus the data obtained by directing the acceleration vector out of the propellant surface support the contention that the presence of aluminum on the surface yields higher values of K.

It is concluded that subjecting a propellant to an acceleration force directed into the propellant surface reduces the relative effects of erosion on the burning rate of the propellant. The reduction can be attributed to the increased evolution of gas normal to the burning surface resulting from the higher basic non-erosive burning rate. Directing the acceleration out of an aluminized propellant surface also results in a decreased erosion sensitivity. This is probably due to the removal of aluminum agglomerates from the propellant surface and the resulting diminished heat transfer rate from the hot reaction gases to the propellant surface.

CHAPTER V

A MODEL FOR NON-METALLIZED PROPELLANTS

General Background

In this section an analysis is developed based on an extension of a burning rate model for non-metallized composite propellants proposed by Fenn [21]. The results of the analysis are compared with the experimental data obtained during the course of this investigation. A method that enables the burning rate for a given propellant to be predicted as a function of pressure and acceleration is explained.

As indicated in Chapter IV the model proposed by Glick fails to correlate some of the experimental data obtained during the course of this investigation. Glick's analysis was based on an extension of Summerfield's granular diffusion flame model which has been used with a high degree of success in correlating a large amount of experimental data at one G. However, there exists certain experimental evidence which cannot be explained by Summerfield's model. This evidence includes the "bore-hole"[4] surface structure which has been observed in rapidly extinguished propellants, the "pressure extinguishment" of propellants which contain very small oxidizer particles when the pressure is raised to very high levels, and "plateau" effects (i.e., regions in which burning rate is invariant with or actually decreases with increasing pressure).

---

[4]The surface of propellants which have been extinguished by rapid depressurization has been observed to have the appearance of "burnt toast." The irregularities in the surface structure are composed of fuel, and no oxidizer particles are found.

Recently Fenn has postulated and developed a new model for the combustion of solid propellants that leads to the same burning rate dependence on pressure as does Summerfield's model:

$$r_o = p/(b_1 + b_2 r_o p^{\frac{1}{3}}) \qquad (20)$$

where b_1 and b_2 are experimentally determined constants. However, Fenn's model can be used to explain many of the experimental observations that the granular diffusion flame model cannot explain.

Fenn represents the flame as burning in a gaseous reaction zone centered between streams of fuel and oxidizer which are generated by the vaporization of each solid component. The reaction zone, shown schematically in Figure 57, is assumed to be comprised of two distinct regions, a premixed combustion region and a diffusion controlled combustion region. The premixed region is located at the base of the diffusion controlled region. The relative size of the two distinct regions is dependent on the pressure. At low pressures, where the rate of diffusion is greater than the rate of chemical reaction, the reaction zone is entirely a premixed combustion flame. At high pressures, where the chemical reaction rates are fast compared to the diffusion rates, the reaction zone is primarily a diffusion controlled flame. However, Fenn postulates that even at very high pressures there exists a microscopically small premixed region at the base of the reaction zone.

The reaction zone, centered above the interfacial region, is a "phalanx" which spearheads the attack of the hot reaction gases on the unburned solid. The vicinity of the interface between the two solid phases receives the greatest heat flux from the reaction zone, and solid component vaporization occurs most rapidly near the interface.

FIGURE 57
PHALANX FLAME
AT STEADY STATE

Fenn assumes that it is the rate at which this "phalanx" reaction zone proceeds into the propellant that is characteristic of the propellant burning rate.

It is important to note that according to the model the flame "phalanx" follows its penetration course along the interface between the fuel and oxidizer. The "phalanx" flame may proceed all the way around the oxidizer particle before the particle is completely consumed. The oxidizer particle would then become separated from the fuel matrix by a thin gas film. If the pressure suddenly dropped, as in extinguishment experiments, the oxidizer particles would be "blown out" of their cavities by the expanding gas layer leaving a "bore-hole" in the fuel matrix. Such "bore-holes" have been found in extinguished burning surfaces [22].

When the oxidizer particles are very small, it is conceivable that, having been surrounded by a gas film, they could be carried away by the drag forces produced by the normal gas flow from the gasifying surface. The particles would thus be removed from the immediate vicinity of the propellant surface. This effect could result in a depletion of oxidizer in and near the propellant surface. Fenn has shown that the penetration rate of the "phalanx" flame increases with increasing pressure. It is conceivable at high pressures that the increased "phalanx" flame penetration rate could result in an increase in the depletion of oxidizer at the propellant surface by the aerodynamic drag removal of small oxidizer particles. This depletion could cause a "plateau" or drop in the burning rate-pressure curve for the propellant as a whole and might even bring about "pressure extinguishment." Both of these phenomena have been observed, especially with small size oxidizer particles in fuel rich propellant compositions [22].

The possibility that a "phalanx" flame may burn completely around an oxidizer particle in the vicinity of the oxidizer particle-fuel matrix interface prior to the complete combustion of the oxidizer particle can thus explain certain experimental evidence that the granular diffusion flame cannot explain. It is this same possibility of the "phalanx" flame proceeding completely around an oxidizer particle prior to its complete combustion that can provide a basis for a model which will explain why acceleration forces will alter the burning rate of non-metallized propellants. Accordingly, Fenn's "phalanx" flame model will be extended to account for the effects of an acceleration field imposed on the propellant burning surface.

The Model

The possibility that oxidizer particles may become separated from the fuel matrix by a thin gas film, or in the extreme case may be removed from the near vicinity of the propellant surface by aerodynamic drag forces, leads to a consideration of the retention of the decomposing oxidizer particles on the propellant surface by centrifugal forces.

The acceleration force field will impede the motion of the oxidizer particles away from the surface. The body force, F_b, on a particle is

$$F_b = d_p^3 \rho_p a/6 \tag{21}$$

where the new symbols are defined by

d_p = particle diameter (cm)

ρ_p = particle density (gm/cm^3)

Assuming Stokes flow, the drag force, F_d, on a spherical oxidizer particle is given by

$$F_d = 3\pi\mu_g d_p V_g \tag{22}$$

where V_g is the gas phase velocity equal to $r\ \rho_s/\rho_g$ (cm/sec).

The condition

$$F_b = F_d \tag{23}$$

represents the condition in which the centrifugal forces balance the aerodynamic forces, and a given size oxidizer particle remains on the surface. When $F_d > F_b$, the particle will be removed from the surface. It is convenient to define a critical particle diameter, d_{p_c}, as the diameter of a particle for which $F_b = F_d$. Then, at a given acceleration, all those particles which have a diameter larger than the critical diameter will be retained on the surface while those particles which have a diameter smaller than the critical diameter will escape the surface. Substituting Equations 21 and 22 into Equation 23 and solving for d_{p_c} yields

$$d_{p_c} = 6\left[\frac{\mu_g\ r\ \rho_s}{2\ \rho_g\ \rho_p\ a}\right]^{\frac{1}{2}} \tag{24}$$

The magnitude of the critical diameter can easily be estimated as a function of acceleration by substituting representative values of the parameters in Equation 24. The following representative values for a non-metallized propellant were used:

$\mu_g = 1 \times 10^{-4}$ gm/cm sec

$r = 0.765$ cm/sec

$\rho_s = 1.65$ gm/cm^3

$\rho_p = 1.95$ gm/cm^3

$T_g = 1775°K$

$M = 22$ gm/gm mole

$R = 8.47 \times 10^4$ gm cm/gm mole °K

Assuming a perfect gas and defining $G = a/a_o$ where a_o = standard of gravity = 980 cm/sec^2, the following relations for pressures of 35.15×10^3 and 70.3×10^3 gm/cm^2 (500 and 1000 psia) were obtained:

$$d_{p_{c_{500}}} = 152\ [1/G]^{\frac{1}{2}} \text{ (microns)} \tag{25}$$

$$d_{p_{c_{1000}}} = 108\ [1/G]^{\frac{1}{2}} \text{ (microns)} \tag{26}$$

Equations 25 and 26 indicate that at a given acceleration the critical particle diameter is smaller at 1000 psia than at 500 psia. All particles larger than the critical size will remain on the surface and will decompose until they become equal to the critical size. Thus, at a given acceleration, the effect of raising the pressure will be to hold smaller particles on the surface, which in turn will result in more oxidizer mass being consumed on the propellant surface. These equations are plotted in Figure 58. Note that the critical particle sizes for acceleration levels above 10 G are of the same order of magnitude as small size oxidizer particles used in typical multi-modal propellants. For this reason and the fact that it is propellants with small size oxidizer particles which experience pressure extinguishment, the assumption will be made that acceleration induced burning rate increases are related to the acceleration induced retention of the small size oxidizer particles[5] on the surface of the propellant.

When a solid AP oxidizer particle decomposes, it partially reacts as a monopropellant. The oxidizer rich products of reaction subsequently burn with the fuel gases released by the pyrolysis of the fuel binder. The retention of small AP oxidizer particles on the surface of the

---

[5] Small size refers to particles which are the size of the magnitude of the critical particle sizes shown in Figure 58.

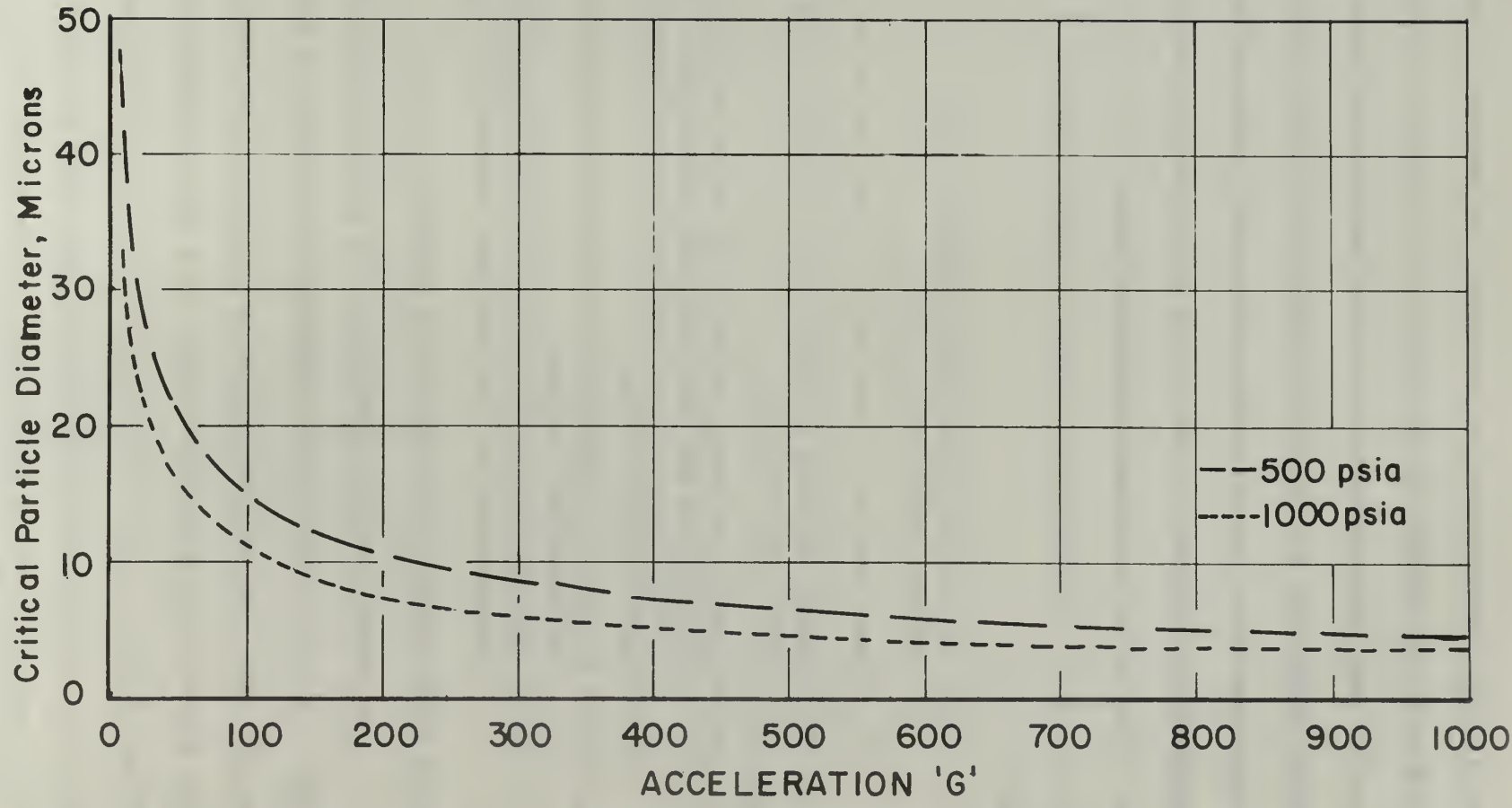

FIGURE 58 CRITICAL PARTICLE DIAMETER VERSUS ACCELERATION

propellant will make more of this oxygen rich decomposition product available at the surface of the propellant. This will increase the amount of fuel which is combusted in the immediate vicinity of the surface, which will result in additional heat transfer to the surface. The increased heat transfer to the surface will increase the rate of vaporization of the solid phase of the propellant and thus the burning rate. This can be expressed mathematically as

$$\Delta\dot{Q} = \rho_s(r - r_o)h_v = \rho_s r\, W_o h_c\, f\, J \qquad (27)$$

where:

$\Delta\dot{Q}$ = rate of additional heat transfer to the surface ($cal/cm^2 sec$)

W_o = mass fraction of small size AP oxidizer in the propellant

h_v = energy required to heat up and vaporize a unit mass of propellant (cal/gm)

h_c = quantity of energy released by the decomposition of the AP particles and the subsequent combustion of the oxidizer rich AP decomposition products and fuel vapor per gram of small size AP (cal/gm)

f = fraction of the energy release which is transferred to the propellant surface

J = fraction of small AP oxidizer particle mass released by decomposition on the propellant surface ($0 \leq J \leq 1$)

and the other symbols have their usual meaning.

The assumptions incorporated in the model can be summarized as follows: 1) The acceleration augmented burning rate is steady in the mean; 2) small AP oxidizer particles evolved at the burning surface become separated from the fuel matrix by a thin gas layer when the "phalanx" flame is able to burn completely around the AP particle-fuel matrix interface before the AP particle is consumed; 3) a particular size AP oxidizer particle will remain on the surface until it has decomposed to a size such that the aerodynamic drag force is able to

remove it from the surface; 4) the burning rate augmentation is related to the retention of these small sized AP oxidizer particles on the surface of the propellant; and 5) the burning rate increase is proportional to the amount of energy that is transferred to the propellant surface from the decomposition of the AP particles and the subsequent reaction of oxidizer rich AP decomposition products with the fuel vapor from the pyrolyzed fuel matrix.

Solving Equation 27 for the burning rate ratio, it is found that

$$r/r_o = \frac{1}{1 - \frac{W_o f h_c J}{h_v}} \qquad (28)$$

The use of Equation 28 to obtain quantitative predictions of the burning rate ratio as a function of acceleration would require knowledge of the values of h_c, f, h_v, and J as functions of acceleration and pressure. Such information is not known at the present time. However, the equation can be used to predict trends and the influence of parameters such as oxidizer particle size and loading, pressure level, and acceleration level.

As mentioned previously, when the oxidizer rich ammonium perchlorate particles in a propellant undergo decomposition, they liberate energy and oxidizer rich decomposition products. This oxidizer is then available for reaction with fuel vapor generated by the sublimation of the fuel matrix. The parameter h_c is a measure of the heat released by the combustion of this oxidizer rich decomposition product and fuel vapor. This parameter, as well as h_v and W_o, is a function of the particular propellant and not acceleration or pressure.

Examination of Equation 28 indicates that the term W_o f h_c J/h_v will determine the burning rate ratio. The larger this term, the larger will be the burning rate ratio. The terms in the factor W_o h_c/h_v suggest that it should be a function only of the particular propellant. For convenience in the discussion to follow, the factor W_o h_c/h_v will be designated η. If for two different propellants the values of f and J are equal, the propellant with the largest value of η will exhibit the greatest sensitivity to acceleration as indicated by Equation 28.

The parameter f represents the fraction of the energy released by the decomposition of the AP particles and subsequent combustion of the AP decomposition products and fuel vapor which will be transferred to the propellant surface. The value of f will depend on the temperature gradient in the gas phase above the propellant surface. That is, if the combustion of the oxidizer rich AP decomposition products and fuel vapor takes place at a relatively great distance from the propellant surface, the temperature gradient will be small and relatively little heat will be transferred to the propellant surface. If, however, the AP decomposition products and fuel vapor are combusted relatively close to the propellant surface, the temperature gradient and heat transfer to the propellant surface will be large.

The theories of both Summerfield and Fenn predict that at high pressures increasing the pressure will in effect move the combustion zone closer to the propellant surface at a rate proportional to the one-third power of the pressure (Equation 20). Thus f should increase at a rate proportional to the one-third power of the pressure. Referring again to Equation 28, it can be seen that increasing f while holding η and J constant will increase the burning rate ratio. Since increasing

the pressure increases f, it follows that increasing the pressure should result in a higher burning rate ratio.

Anything that will increase J will increase the burning rate ratio if η and f are held constant. The function J depends on the acceleration level, pressure level, propellant burning rate, particle size distribution, and the burning time of the oxidizer particles. The function has a minimum value of zero when none of the small size oxidizer particle mass is consumed directly on the propellant surface. This would occur at low acceleration levels where the critical particle diameter is large. At high accelerations all the small size oxidizer would be consumed directly on the surface, and the function J would have its maximum value of one.

The burning rate ratio of a particular propellant at a given pressure varies with acceleration through the parameter J. Knowledge of J as a function of acceleration is necessary to predict the actual shape of the burning rate ratio versus acceleration curve of a particular propellant. If it is assumed that steady state has been attained, it is possible to determine the acceleration dependence of J.

Once steady state burning has been achieved, the parameter J will depend on the small AP oxidizer particle size distribution and the acceleration level. The acceleration dependence of J is through the critical particle diameter. The fraction of the particle mass consumed on the propellant surface, J, will be equal to the mass consumed in all particles larger than critical size until those particles have burned to critical size. Thus, for a given critical particle diameter the value of J will depend on the particle size distribution; for if the particle size distribution is such that a very small percentage of the

particles are larger than the critical particle diameter, the value of J will be small. In contrast, if the particle size distribution is such that almost all of the particles are smaller than the same given critical particle diameter, the value of J will be relatively large.

Using Equation 24 and the perfect gas law, it is easily verified that

$$d_{p_c} = K_1 \left[r/Gp\right]^{\frac{1}{2}} \tag{29}$$

where

$$K_1 = 6 \times 10^4 \left[\frac{2.54}{70.3} \frac{\mu_g \rho_s RT_g}{2 \rho_p a_c M}\right]^{\frac{1}{2}} \text{ micron} \left(\frac{\text{lb}_f \text{ sec}}{\text{in}^2}\right)^{\frac{1}{2}} \tag{30}$$

The assumption that K_1 is a constant is equivalent to assuming that μ_g and T_g do not vary with acceleration. The factor $10^4 \times [2.54/70.3]^{\frac{1}{2}}$ is the conversion factor necessary to allow substitution of r in units of inches/second and p in units of psi (the units in which these two quantities are generally measured) in Equation 29 to achieve a value of d_{p_c} in units of microns (the unit in which d_{p_c} is generally measured).

Having expressed the critical particle diameter as a function of Gp/r, a prediction of J versus Gp/r can be made in the following manner. Given a value of Gp/r, the critical particle diameter can be calculated using Equation 29 and an estimate for K_1. Once the value of d_{p_c} is known, the small size oxidizer distribution can be used to obtain the value of J. A method of estimating J for a given size distribution and critical particle diameter is presented in Appendix II. A plot of J versus d_{p_c} obtained for the small size oxidizer particle size distribution shown in Plate 12 by the method Appendix II is shown in Figure 59.

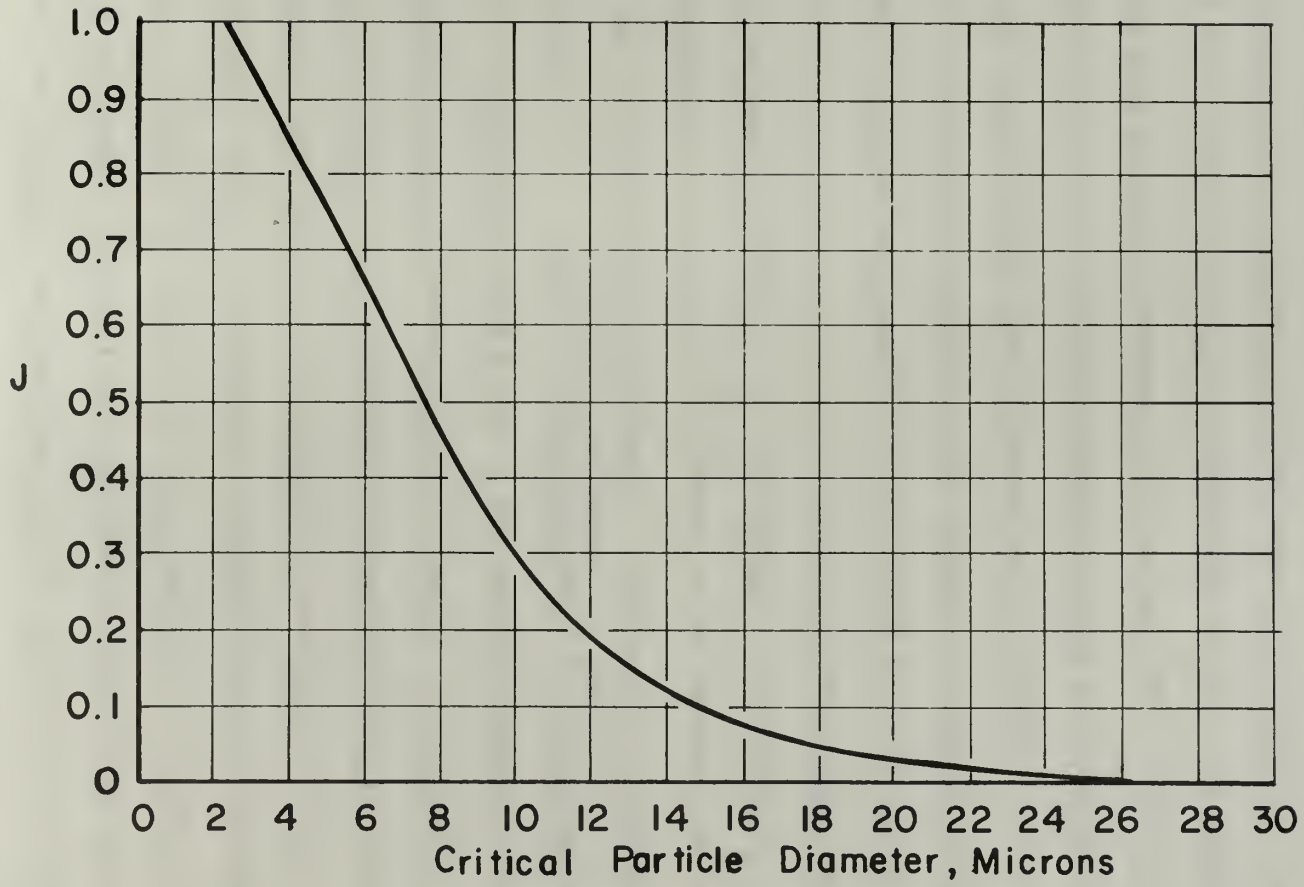

FIGURE 59 VALUES OF J VERSUS CRITICAL PARTICLE DIAMETER

The analysis can be used to predict the burning rate behavior of a particular propellant if prior knowledge of W_o, h_c, h_v, f, and J exists. The terms W_o, h_c, h_v are functions of the particular propellant and, with the exception of W_o, can only be determined approximately prior to experimentation. The term f is a function of pressure that appears to have to be determined by experiment. The acceleration dependence of J can be ascertained if K_1 and the small size AP distribution are known. The latter can be assumed to be known, whereas the former can only be determined approximately prior to experiment. Until more exact knowledge of the values of such factors as h_c, h_v, f, and K_1 becomes available, it appears that an accurate prediction of the acceleration and pressure dependence of burning rate requires experimental determination of these factors.

The analysis suggests that the following scheme be used to obtain the pressure and acceleration dependence of the burning rate of a particular propellant. Experimentally determine the burning rate of the propellant at three acceleration levels: 0 G, an intermediate G level of between 300 and 400 G, and a high acceleration level of greater than 600 G. Using the high acceleration limit burning rate, determine r/r_o and use Equation 28 with J = 1 to solve for W_o f h_c/h_v. Next use the burning rate obtained at the intermediate G level to form the quantity Gp/r and solve for the value of J using Equation 28. Prepare a plot of J versus d_{p_c} by the method of Appendix II for the particular small size AP oxidizer distribution. Enter this plot with the value of J obtained for the intermediate G level. The value of d_{p_c} obtained from the plot and the value of Gp/r determined experimentally are substituted into Equation 29 to obtain a value of K_1.

The burning rate ratio versus acceleration plot can then be constructed in the following manner. Pick representative values of Gp/r and solve for the corresponding values of d_{p_c} using Equation 29. Then use the prepared plot of J versus d_{p_c} to obtain values of J. Use these values of J in Equation 28 (with the value of $W_o\ f\ h_c/h_v$ determined from the high acceleration level experiment) to obtain values of r/r_o. The variation of r/r_o with Gp/r is now known. Since the pressure is known, it is then possible to calculate the values of r/r_o versus G. The method will be illustrated in the next section when the results of the experimental investigation are compared with the theory.

The pressure dependence is easily determined through the parameter f. Using the value of $W_o\ f\ h_c/h_v$ obtained from the experiment done at the high acceleration level at the original pressure level, calculate a new value of $W_o\ f\ h_c/h_v$ for the desired new pressure level from the expression

$$\frac{W_o\ f\ h_c/h_v\big|_{\text{pressure 1}}}{W_o\ f\ h_c/h_v\big|_{\text{pressure 2}}} = \left[\frac{(\text{pressure 1})}{(\text{pressure 2})}\right]^{\frac{1}{3}} \qquad (31)$$

Again pick a series of values of Gp/r and solve for the corresponding values of d_{p_c} using the value of K_1 determined at the original pressure level. Proceed in the manner outlined above for the original pressure level to obtain the value of r/r_o versus G. The pressure dependence through the parameter f should be valid over the pressure range for which the combustion zone thickness is diffusion rate controlled and hence proportional to the one-third power of the pressure.

In summary, the theory predicts that: 1) No burning rate augmentation will occur until a threshold acceleration level is reached (the threshold acceleration is that value of acceleration just sufficient

to hold the largest size AP particles in the small size AP particle distribution on the propellant surface); 2) the burning rate will increase with acceleration as more and more of the small size AP particle mass is consumed on the propellant surface; 3) a limit burning rate is achieved at high acceleration levels when all the small size AP particle mass is consumed on the propellant surface; 4) increasing the pressure will result in larger values of burning rate ratio for a given propellant; 5) increasing the weight percentage of the fine oxidizer particles in otherwise similar propellants will result in larger values of burning rate ratio; and 6) increasing the basic burning rate of a propellant will lessen the effect of acceleration on the burning rate of a propellant. The last two observations are somewhat interrelated since increasing the weight percentage of the fine AP particles generally results in a faster basic burning rate. The net effect on the acceleration sensitivity obtained by increasing the weight percentage of the fine AP particles would depend on how much the increased basic burning rate offsets the detrimental effect of increasing the weight percentage of the fine AP particles. If burning rate catalysts are used to increase the basic burning rate of the propellant and no change is made in the weight percentage of the fine AP particles, the theory predicts without reservation that the acceleration sensitivity of the propellant will be reduced.

Comparison of Experiment with Theory

The experimental results will be compared to the theory in three ways: 1) The relative acceleration sensitivities of the three propellants through the propellant parameter W_o will be considered; 2) the theoretical pressure dependence of acceleration sensitivity will be

compared to experiment; and 3) the theoretical acceleration dependence of burning rate ratio for all three propellants will be compared to experimental results.

An indication of how well Equation 28 is able to predict the relative acceleration sensitivities of the three propellants can be ascertained by considering the relative magnitudes of the high acceleration limiting burning rate ratio exhibited by the three propellants. The value of J will approach unity at high acceleration levels and the burning rate ratio will approach a constant value for a given pressure and propellant. The following values of η f shown in Table III were obtained by using Equation 28 and taking J=1 and r/r_o equal to the high acceleration (> 600 G) limiting burning rate ratio as shown in Figures 6 and 7.

TABLE III

NON-METALLIZED PROPELLANT DATA

Propellant Designator	500 PSIA		1000 PSIA	
	r/r_o max	η f	r/r_o max	η f
P410	1.230	0.187	1.285	0.222
P411	1.435	0.303	1.630	0.387
P420	1.286	0.222	1.440	0.306

Since the three propellants P410, P411, and P420 all contain the same oxidizer (AP) and the same binder (PBAN), the amount of energy that is released per gram of small size AP, h_c, should be the same for all three propellants. Furthermore, since propellants P410, P411, and P420 all contain 79 per cent AP and 21 per cent PBAN, they should have

approximately equal values of h_v. Therefore, for these propellants the individual propellant values of η ($= W_o\ h_c/h_v$) should vary directly as the weight percentage of the small size AP oxidizer particles, W_o. Since the value of f depends on pressure and not the particular propellant, it follows from the above considerations that values of η f at a given pressure should be in the same ratio as the values of W_o for the three propellants. Mathematically, for example,

$$\frac{\eta\ f\big|_{P410}}{\eta\ f\big|_{P411}} = \frac{W_o\ h_c\ f/h_v\big|_{P410}}{W_o\ h_c\ f/h_v\big|_{P411}} = \frac{W_o\big|_{P410}}{W_o\big|_{P411}} \qquad (32)$$

since $\quad h_c/h_v\big|_{P410} = h_c/h_v\big|_{P411}$ and $f\big|_{P410} = f\big|_{P411}$

if the pressure is held constant. A comparison of the ratios of the propellant parameter W_o and the ratios of η f calculated using Equation 28 and the burning rate data is shown in Table IV. The agreement between P410 and P411 propellants is excellent. The agreement between P420 and the two P410 series propellants is only fair. However, the experimentally determined η f ratios all trend in the correct manner.

TABLE IV

PROPELLANT COMPARISON

Propellant Comparison	W_o ratio	500 PSIA η f ratio	1000 PSIA η f ratio
P410/P411	0.577	0.617	0.574
P410/P420	1.000	0.843	0.725
P411/P420	1.731	1.365	1.265

The values of η f for a given propellant should increase with increasing pressure because of the factor f. The ratio of

$$\eta\ f\big|_{1000\ psia} \Big/ \eta\ f\big|_{500\ psia} \qquad (33)$$

for a given propellant should be approximately $(1000)^{1/3}/(500)^{1/3} = 1.26$ since f should vary as the one-third power of pressure and η is invariant with pressure. The experimentally determined ratios were: P410, 1.189; P411, 1.278; and P420, 1.378. These values are in good agreement with the expected value of 1.26. Thus Equation 28 is able to predict reasonably well the pressure dependence and the relative acceleration sensitivities of propellants P410, P411, and P420 at high acceleration levels.

The ability of the analysis to predict the acceleration dependence of the burning rate ratio can best be judged by constructing burning rate ratio versus acceleration curves for the three propellants and then comparing the predicted dependence with the experimental results. This was done for the three propellants at both pressure levels. The theoretical curves were constructed using the method outlined in the previous section. A detailed description of the construction of the curves in Figure 61 for propellant P411 will serve to demonstrate the procedure.

It was assumed that the burning rate had been experimentally determined at 500 psia and three acceleration levels, 0 G, 403 G, and 811 G (the data points marked with an asterisk in Figure 61). The burning rates at 811 G, 0.379 inches/second, and 0 G, 0.265 inches/second, were used to determine $r/r_o = 1.430$ at 811 G. Equation 28, with J = 1, was used to obtain a value of $W_o h_c f/h_v$ equal to 0.301. Next, the burning rate at 403 G, 0.356 inches/second, was used to obtain $r/r_o = 1.344$ at 403 G. This value was substituted into Equation 28 along with the value of $W_o h_c f/h_v$ to determine J = 0.850 at 403 G. The factor Gp/r at 403 G was then evaluated as 5.66×10^5.

The plot of J versus d_{p_c} shown in Figure 59 was constructed using the particle size distribution of the small size AP particles in propellant P411. (Note that this plot is good for propellants P410 and P420 also because all three propellants have the same small size AP oxidizer). This plot was entered with the value of J to obtain the corresponding value of 4.0 μ for d_{p_c}. This value of d_{p_c} and the value of Gp/r were substituted into Equation 29 to obtain the value of $K_1 = 3009$.

A series of values between 1.4×10^6 and 3×10^4 for Gp/r was then substituted into Equation 29. The corresponding values of d_{p_c} were then used to enter Figure 59 to obtain values of J. These values and the value of $W_o\ h_c\ f/h_v$ were substituted in Equation 28 to obtain values of r/r_o. The values of r/r_o versus G were then determined from the known values of r/r_o versus Gp/r.

The relationship between r/r_o and G for 1000 psia was then determined in the following manner. It was assumed that the 0 G burning rate had been experimentally determined as 0.309 inches/second. The value of $W_o\ h_c\ f/h_v$ obtained at 500 psia was multiplied by 1.26 to obtain the value of $W_o\ h_c\ f/h_v = 0.379$ at 1000 psia. A series of values for Gp/r from 2×10^6 to 3×10^4 was substituted into Equation 29 with $K_1 = 3009$ to obtain the corresponding values of d_{p_c}. The calculation then proceeded in exactly the same manner as outlined for a pressure of 500 psia.

The same method was used to construct the theoretical curves for the other two propellants. The results for all three propellants at both pressure levels are presented in Figure 60, 61, and 62. The data points marked with asterisks and the 0 G burning rates are the

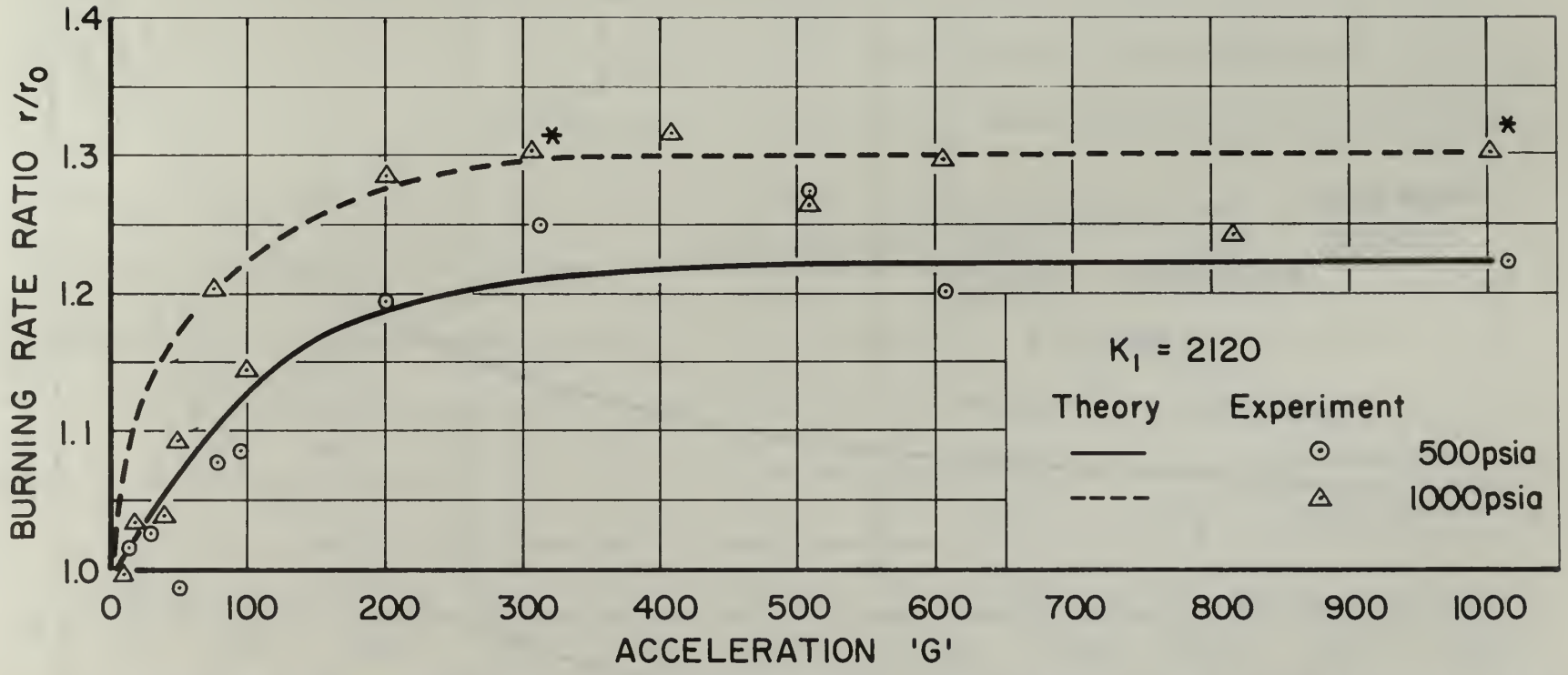

FIGURE 60 COMPARISON OF THEORY WITH EXPERIMENT FOR P410 PROPELLANT

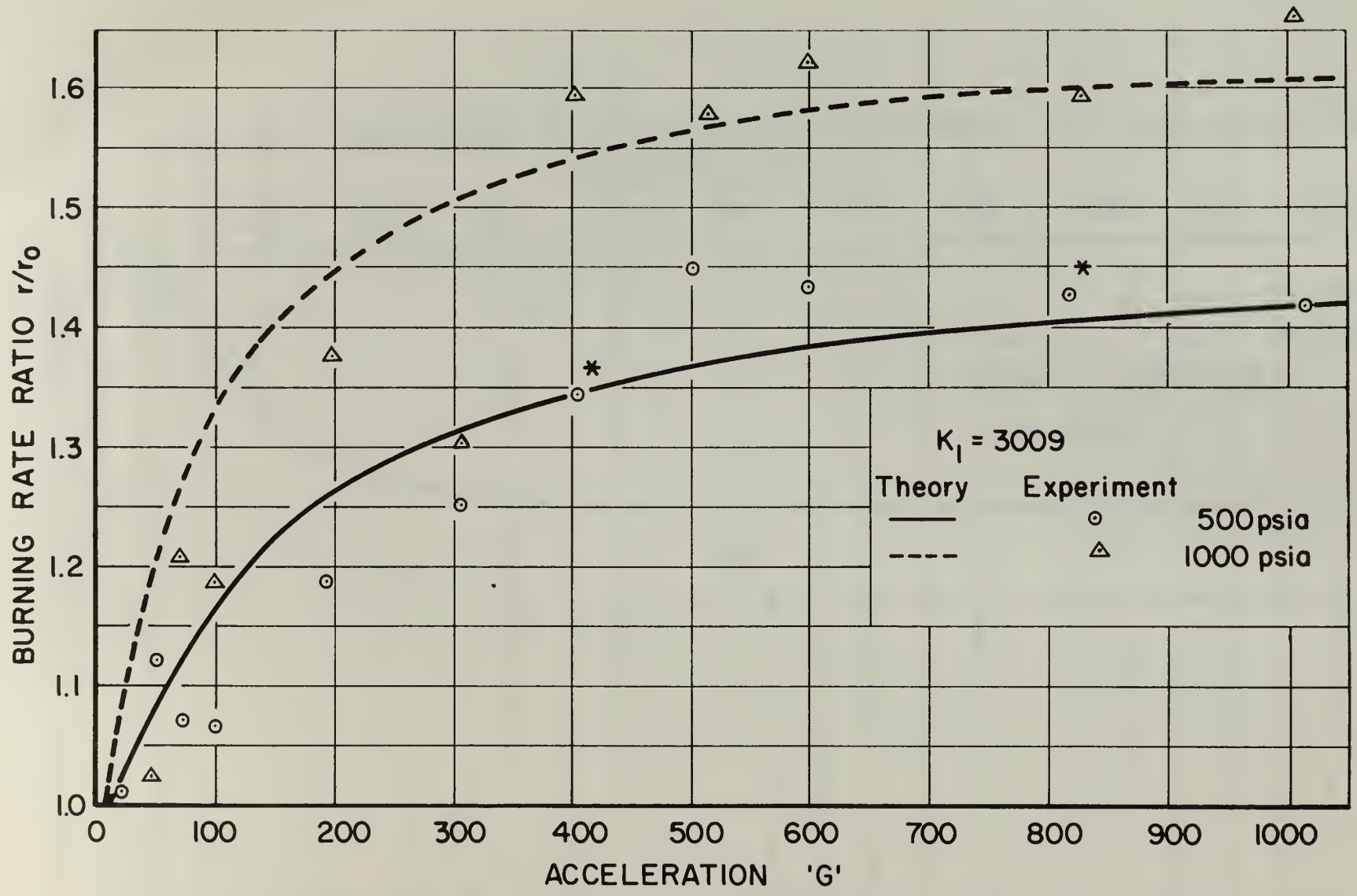

FIGURE 61 COMPARISON OF THEORY WITH EXPERIMENT FOR P411 PROPELLANT

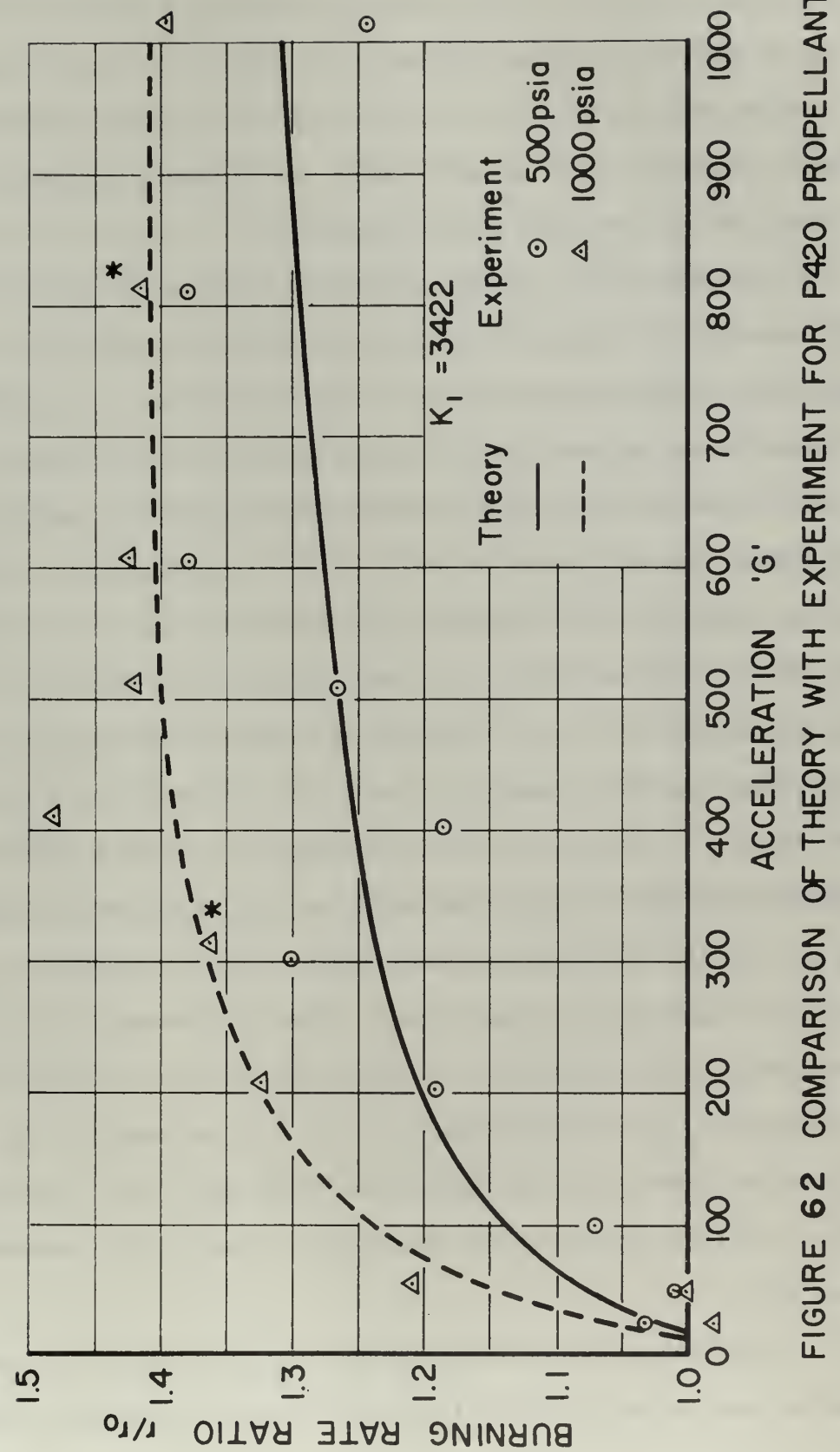

FIGURE 62 COMPARISON OF THEORY WITH EXPERIMENT FOR P420 PROPELLANT

experimental data that were assumed known and from which the theoretical curves were constructed. The other data points are shown in the figures to allow comparison of the experimental data with the theoretical curves. As can be seen from Figures 60, 61, and 62, the theory is able to predict reasonably well the acceleration and pressure dependence of burning rate ratio for all three propellants.

The values of K_1 used to construct the theoretical curves are about one-half the value of 6190 obtained if the values of the thermophysical properties listed on page 173 are substituted into Equation 30. It should be emphasized that the values listed on page 173 are only typical values and could be in error for the propellants under consideration. Another source of error is the assumption that Stokes drag law, Equation 22, is valid for the small oxidizer particles. Stokes drag law is valid for spheres with no mass flux from the surface at low Reynolds numbers ($1 > Re$). The small AP oxidizer particles are not true spheres and have a mass flux out of their surface since they are decomposing. It is known [23] that the drag on a burning particle is as much as an order of magnitude less than that predicted by Stokes drag law for the low Reynolds number range (< 10) encountered in small particle-low gas velocity conditions. Since the numerator of K_1 is proportional to the square root of the particle drag, it follows that the value of K_1 for a decomposing particle will be less than the value of K_1 for an inert particle which obeys Stokes drag law. Thus the theory is able to correlate the experimental results with reasonable values of K_1.

In addition to predicting the burning rate behavior of the propellants when the acceleration is directed into the burning surface, the

analysis predicts the experimentally determined behavior when the acceleration is directed out of the propellant burning surface. When the acceleration vector is directed outward from the burning surface the value of J should be zero. Thus, Equation 28 predicts that directing the acceleration out of the propellant burning surface will not alter the burning rate. The experimental results support this conclusion.

Finally, the theory is able to predict the correct qualitative behavior of the limit burning rate ratio when the initial temperature of the propellant is increased. An examination of the factors in Equation 28 suggests that the only parameter affected by the propellant initial temperature will be h_v. The higher the initial propellant temperature the lower will be the energy required to heat up and gasify a unit mass of propellant (h_v). Then, for a given propellant (W_o and h_c constant), and a given pressure (f constant) and at the high acceleration limit (J = 1), the effect of increasing the initial propellant temperature (and hence decreasing h_v) will be to increase r/r_o. This agrees with the experimental results presented in Figure 5.

CHAPTER VI

METALLIZED PROPELLANT CONSIDERATIONS

Analytical Considerations

As indicated in Chapter IV, the existing analyses [8, 9] for metallized propellants are unable to account for some of the more important experimental results obtained during the course of this and other investigations. The analyses incorporate, as do all analyses which attempt to analyze very complicated phenomenon, several simplifying assumptions to render the phenomenon amenable to mathematical analysis. The inability of the analyses to correlate some of the important aspects of the experimental evidence appears to stem from the use of invalid simplifying assumptions. In particular, the following assumptions appear to be serious oversimplifications: 1) The phenomenon is steady in the mean, and 2) the source of additional heat transfer to the propellant surface is the chemical energy of metal combustion.

The formulation of a new mathematical model to account for the effect of acceleration on the propellant burning rate does not appear possible due to lack of fundamental knowledge of several important aspects of the overall phenomenon. The discussion to follow will present a few considerations which it is hoped will shed some additional light on the phenomenon and point the way for further study.

The experimental evidence indicates that the process is not steady for conventional aluminized propellants (burning rates less than 0.5 inch per second). There appear to be at least two distinct modes of combustion. Shortly after ignition, no longer than 0.675

seconds as indicated by the extinguished propellants slabs supplied by N.A.S.A., there exist a finite number of discrete aluminum agglomerates on the surface of the propellant. These agglomerates increase the propellant burning rate in the local vicinity of the agglomerate and cause a pit to form. The burning rate of the propellant as a whole is controlled by the rate at which an agglomerate is able to penetrate the solid phase of the propellant as the following considerations indicate.

Referring to Figure 63a, assume that the conical surface of the pit recedes normal to itself at a rate r_o and that the agglomerate particle proceeds into the propellant at a rate r_a in a direction colinear with the applied acceleration force. The mass flow rate contributed by an area element under the agglomerate is $\rho_s r_a \, dA_p$ where dA_p is the projected area under the agglomerate parallel to the mean propellant surface. But $dA_p = dA \sin \theta_c$ and $r_a \sin \theta_c = r_o$. Therefore, $\rho_s r_a \, dA_p = \rho_s r_a \, dA \sin \theta_c = \rho_s r_o \, dA$ which is the mass flow rate contributed by the area element of the conical surface. Hence the increased mass flow from the propellant surface can be considered as due to an increased gas-solid interfacial area regressing at the O G burning rate of the propellant or an increased burning rate acting over the projected area of the propellant. Since the rate, r_a, at which an agglomerate proceeds into the propellant solid phase controls the pit geometry (and hence the gas-solid interfacial area increase), it is the rate r_a which is important and should be considered the burning rate controlling effect.

The experimental evidence indicates that heat transfer from an aluminum agglomerate to the propellant surface is important in determining the rate at which the agglomerate is able to penetrate the solid

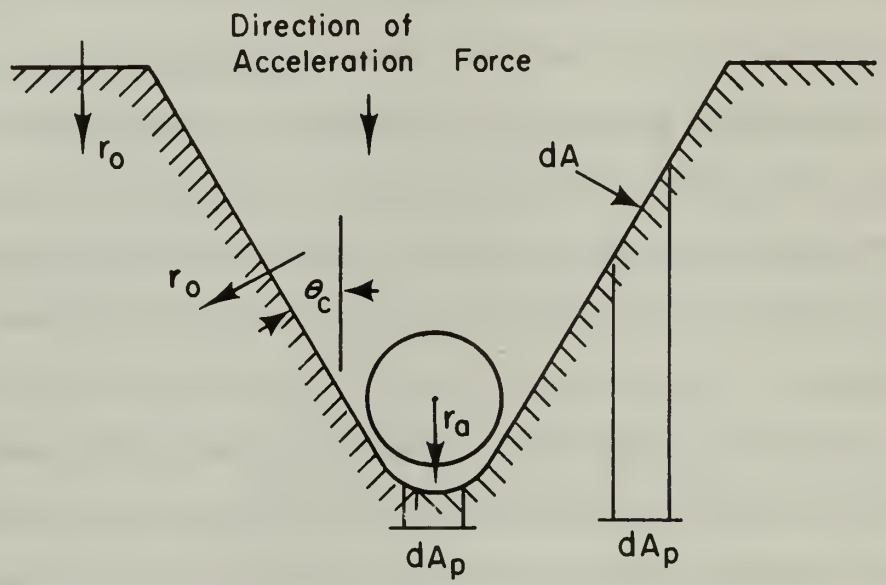

a. Agglomerate and Resulting Propellant Geometry

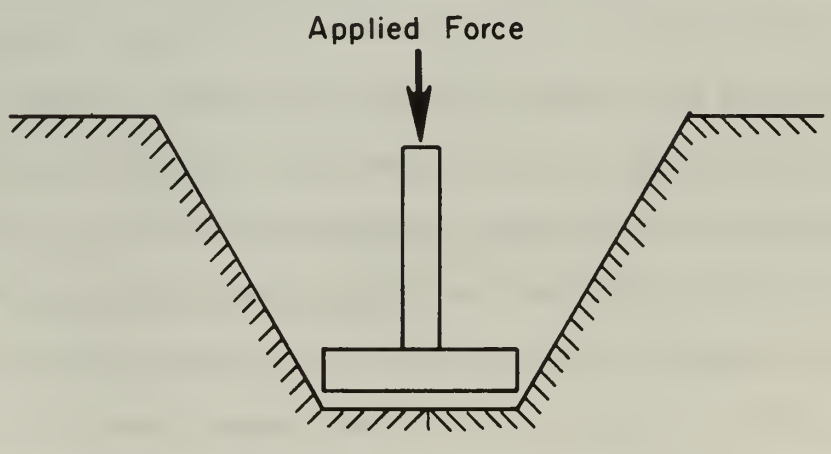

b. Mann's Ram and Resulting Propellant Geometry

FIGURE 63 COMPARISON OF AGGLOMERATE AND RAM GEOMETRICAL EFFECTS

phase of the propellant. The aluminum agglomerate can be considered as an axial, counterflow, conductive heat exchanger interposed between the flame zone and the solid propellant surface. Centrifugal forces press the agglomerate against, and cause it to move with, the regressing propellant surface. Heat is transferred radially to the agglomerate, passes through the gas film between the agglomerate and the propellant, and then is diffused into the solid. This increased heat transfer causes the burning rate to increase to the value r_a.

A comparison of the rate of heat transfer from the flame zone to the propellant surface with and without the interposition of an aluminum-aluminum oxide agglomerate can be made by using the following expression which is derived in Appendix III:

$$\frac{\dot{q}_{ag}}{\dot{q}_{prop}} = \frac{1}{2}\frac{K_{ag}}{K_g} \qquad \text{(III-28)}$$

where:

$\dot{q}_{ag}$ = heat transfer rate to the propellant surface under an agglomerate (cal/sec)

$\dot{q}_{prop}$ = heat transfer rate to the propellant surface in an area void of agglomerates (cal/sec)

K_{ag} = thermal conductivity of agglomerate (cal/cm sec° K)

K_g = thermal conductivity of the propellant gas phase (cal/cm sec° K)

A typical value of K_g is 4.2×10^{-4} cal/cm sec° K. Since the agglomerate probably consists of aluminum and aluminum oxide, it is difficult to estimate an overall value of K_{ag}. If the agglomerate is considered as entirely aluminum oxide (thermal conductivity 0.015 cal/cm sec° K), Equation III-28 yields a ratio of $\dot{q}_{ag}$ to $\dot{q}_{prop}$ equal to approximately 18. However, if the agglomerate is considered to be entirely aluminum (thermal conductivity equal to 0.450 cal/cm sec° K),

the ratio becomes 536. Nevertheless, it is obvious that the interposition of an agglomerate between the flame zone and the propellant surface will cause significant increases in the heat transfer to the local propellant surface.

Experimental evidence exists which indicates that a heat exchanger positioned between the flame zone and the propellant surface will cause the propellant burning rate to increase. Mann, et. al., [24] have used an axial, counterflow, conductive heat exchanger positioned between the propellant surface and the flame zone to control the burning rate of non-metallized propellants. The burning rate of a solid propellant grain was able to be adjusted at will to values up to seven times the basic burning rate when a refractory metal heat-exchanger "ram" immersed in the products of combustion was forced into the propellant surface. The rams were generally right circular cylinders of the order of 1.0 inch in diameter and 0.125 inches thick and were made of either copper, steel, or molybdenum. A typical ram and the resulting propellant surface geometry are shown in Figure 63b.

The burning rate increase was found to vary linearly with the force with which a particular ram was pressed into the propellant surface. Increased force on the ram provided more intimate contact between the ram and the propellant, thus lessening the thickness of the gas film between the ram and the propellant and providing more heat transfer from the ram to the propellant.

An aluminum agglomerate being pressed into the surface of a propellant by an acceleration force can be considered a miniature ram. If the aluminum agglomerate is considered to be primarily a heat exchanger and not a source of chemical energy, then the evidence for

the burning rate augmentation of propellants containing inert materials can be explained. The following analysis indicates that the heat transfer effect is at least as great as chemical energy release effect.

A comparison of the relative magnitudes of the rate of chemical energy release by an agglomerate and the conductive heat transfer rate through the agglomerate can be made as follows. The heat of combustion of aluminum is approximately 750 cal/gram. This value was calculated by assuming the reaction between aluminum and the oxidizer gases is

$$2\ Al + 1\tfrac{1}{2}\ O_2 \rightarrow Al_2O_3 \tag{34}$$

An estimation of the rate at which aluminum in an agglomerate is converted to aluminum oxide can be used with this value of 750 cal/gram to estimate the rate of energy release from an agglomerate.

As a first approximation it will be assumed that the rate of aluminum conversion to aluminum oxide in an agglomerate is equal to the rate at which a single aluminum particle burns in an oxidizer rich gas stream. Aluminum particle burning times, τ_b, are generally given empirically by [1, 25]

$$\tau_b = A\ \xi_a^{\ n} \tag{35}$$

where A and n are empirical constants. Using Equation 35 it can be shown that

$$dm/dt = -3m/An\ \xi_a^{\ n} = -4\pi\rho_a\xi_a^{\ 3}/An\ \xi_a^{\ n} \tag{36}$$

where dm/dt is the rate at which aluminum particle mass is converted to aluminum oxide by combustion. It is necessary to assign values to A and n to estimate dm/dt.

Davis [25] has measured the burning times of aluminum particles burning in a gas mixture of 85 per cent AP and 15 per cent paraformaldehyde. For combustion pressures above 1000 psia the following

empirical burning rate law can be derived from the data

$$\tau_b = 136\ \xi_a^{1.8} \tag{37}$$

where the units of τ_b and ξ_a are seconds and centimeters respectively. Substitution of A = 136, n = 1.8, ρ_a = 2.7 grams/centimeter^3, and ξ_a = 0.01 centimeters (100 μ) into Equation 36 yields an estimate of $dm/dt = 5.54 \times 10^{-4}$ grams/second. The resulting estimate for the rate of chemical energy release from a 200 μ diameter agglomerate is 0.415 cal/second.

The rate of heat transfer from the flame zone to the propellant surface through the same agglomerate can be estimated from the following equation derived in Appendix III:

$$\dot{q}_{ag} = \frac{1}{2} K_{ag}\ \pi\ \xi_a^{\ 2}\ dT/dy \tag{III-26}$$

Typically the flame and surface temperatures of an aluminized propellant are approximately 2800° C and 560° C respectively. If it is assumed that the flame zone is approximately 200 μ from the surface of the propellant and that the temperature gradient, dT/dy, between the propellant surface and the flame zone is constant, it follows that $dT/dy \simeq 11 \times 10^4$°K/centimeter. For a 200 μ diameter agglomerate it follows from Equation III-26 that

$$\dot{q}_{ag} = 17.3\ K_{ag} \tag{38}$$

As mentioned previously it is difficult to make an accurate estimate of the value of K_{ag}. If the agglomerate is assumed to be entirely aluminim oxide, K_{ag} = 0.015 cal/cm sec° K, the estimate of $\dot{q}_{ag}$ from Equation 38 is 0.25 cal/second. If the agglomerate is assumed to be entirely aluminum, K_{ag} = 0.450 cal/cm sec° K, the estimate of $\dot{q}_{ag}$ from Equation 38 is 7.8 cal/second. The smaller of these estimates is of the order of the estimate obtained for the rate of chemical energy

release from the agglomerate. Thus it appears that heat transfer effects are significant and should be taken into consideration in any mathematical analysis.

The experimental evidence indicates that the burning rate decreases once the propellant surface becomes "flooded" with aluminum and/or aluminum oxide. Instead of individual agglomerates causing increased localized heat transfer to the propellant surface, the molten aluminum and/or aluminum oxide "flood" layer becomes the burning rate controlling mechanism. The decrease in propellant burning rate perhaps is due to the decrease in efficiency of a continuous "flood" layer type "ram" as opposed to individual agglomerate type "rams."

Mann found experimentally that the geometry of the ram was very important in determining its effectiveness. Those geometries which provided maximum surface area in the flame zone and minimum contact area with the propellant surface proved to be the most effective at increasing the burning rate of the propellant. Thus by drilling as many as 19 small axial holes through a particular solid ram he was able to increase its effectiveness. It would seem that a continuous "flood" layer would not have as large a ratio of surface area in the flame zone to contact area with the propellant surface as would an individual agglomerate and hence would not be as efficient a heat exchanger as would be an individual agglomerate.

Design Considerations

The agglomeration and retention of aluminum particles on the propellant surface is the cause of the burning rate augmentation of aluminized propellants. It appears that once retention of agglomerated particles begins, the eventual result will be a continuous "flood" of

the propellant surface with molten aluminum and/or aluminum oxide. The obvious and most basic method of controlling the burning rate augmentation is to somehow keep the aluminum from agglomerating.

The results obtained during the course of this investigation for the fast burning rate Thiokol propellants indicate that using very small oxidizer particles to discourage aluminum agglomeration together with adding burning rate catalysts to increase the basic burning rate of the propellant is a very effective way of eliminating aluminum agglomeration and retention and thus controlling the burning rate augmentation. If the application is such that very high burning rates are acceptable, then employing very small oxidizer particles and burning rate catalysts would be the preferred method of controlling the acceleration effect.

Another approach would be to coat the aluminum particles with a substance which would eliminate or at least reduce the amount of agglomeration. Photographic studies of burning composite propellants have indicated that the substitution of dichromated[6] for standard aluminum powder results in a reduction in the size of the metal agglomerates formed on the surface during combustion [13]. Smaller agglomerates will result in less retention for a given basic burning rate. The result of the reduction in size of the agglomerates should be a decreased amount of burning rate augmentation at acceleration levels below which the body force on the agglomerate is less than the drag force on the agglomerate. Experiments conducted at U.T.C. [1] with propellants containing dichromated aluminum powders of 46 μ mmd

---

[6]Dichromated aluminum results from treating aluminum in a dilute chromic acid solution. This results in an oxide coating with some inclusion of chromate species.

indicated that the use of dichromated aluminum substantially reduced the acceleration effect at accelerations below 100 G. At high acceleration levels (G > 160) the burning rate augmentation was nearly equal to that of an analogous propellant which contained aluminum powder which had not been dichromated. The use of dichromated aluminum in applications in which the maximum acceleration level is maintained at low levels (of the order of 100 G) appears to be an effective way of reducing the burning rate augmentation.

If the application is such that the basic burning rate of the propellant must be maintained at a low value and the acceleration level must exceed low levels (G > 200), then the designer should use propellants which retain the least amount of residue and design the motor for the resulting acceleration dependent burning rate. This investigation indicates that the designer can reduce the amount of residue by: 1) using large size Al particles (~ 28 μ) in preference to small size Al particles (~ 10 μ), 2) increasing the size of the coarse oxidizer particles (from 94 μ to 200 μ), 3) increasing the weight percentage of the fine oxidizer particles, and 4) decreasing the weight percentage of the aluminum additive.

Recommendations for Future Work

In light of the results obtained thus far in this and other investigations, it is felt that additional studies of a fundamental nature should be undertaken to provide more detailed understanding of the processes occurring at the propellant surface. High-speed motion pictures of the propellant burning in an acceleration field appear to be a good technique for determining the nature of the aluminum combustion. Information could be obtained about: 1) the effects of

acceleration on agglomeration, 2) the ignition of the aluminum, 3) the burning characteristics of the aluminum, and 4) the unsteady aluminum accumulation on the surface.

An alternate method of obtaining the same type of information would be to photograph the burning surface of a propellant strand that was fed into a small fixed spherical aluminum ram. In addition to circumventing the many optical problems associated with photographing a rotating propellant surface, the ram technique would allow control over parameters such as initial ram size and propellant feed rate. This technique would also eliminate the erosive burning and gaseous vortex effects present in an actual motor.

Additional studies should be done with fast burning rate propellants to ascertain the relative importance of very small oxidizer sizes which discourage agglomeration and the addition of burning rate catalysts which increase the burning rate and hence the aerodynamic drag on the agglomerates. A series of propellants could be formulated with an identical aluminum content. Progressively greater amounts of burning rate catalyst would be added to the formulations to increase the burning rate.

The effect of varying the oxidizer to fuel ratio should be studied. This could be accomplished by preparing a series of propellants with identical aluminum size distributions and weight percentages but different weight percentages of oxidizer particles and fuel binder. Additional studies should be done with coupled erosive and acceleration effects. Other propellants should be investigated, and the acceleration vector should be placed at various other angles to the burning surface including parallel to the surface.

CHAPTER VII

CONCLUSIONS

The work reported here represents the results of a four-fold investigation. Three areas of the investigation concerned the acceleration induced burning rate augmentation of: 1) non-metallized propellants, 2) nominal burning rate aluminized propellants, and 3) fast burning rate aluminized propellants. The fourth area of the investigation concerned the burning rate behavior of a typical aluminized propellant subjected simultaneously to acceleration and erosive burning effects.

The main conclusions derived from the three non-metallized propellants can be summarized as follows. First, the burning rates of these propellants were found to be affected by accelerations greater than 50 G when the acceleration field was directed normal and into the propellant burning surface. Second, an acceleration field directed normal and out of the propellant burning surface was found to have no effect on the burning rate. Third, no time dependence was indicated by the average burning rates of 1.0 inch and nominal 2.1 inch strands. Fourth, increasing the pressure from 500 to 1000 psia was found to increase the acceleration sensitivity of the propellants. Fifth, strands which were preheated to 54° C exhibited an increased acceleration sensitivity as compared to strands initially at ambient temperature.

A mathematical model which attributes the increase in burning rate to the retention of the fine AP oxidizer particles on the propellant surface was developed. The model was successfully employed to correlate the experimental results obtained during the course of this

study. The model suggests that the acceleration effects can be minimized by decreasing the weight percentage of the fine AP particles in multi-modal propellants and increasing the basic burning rate of the propellant by the use of burning rate catalysts. As mentioned previously the use of a high percentage of fine oxidizer particles will have both an advantageous effect of increasing the basic burning rate of a propellant and a disadvantageous effect of increasing W_o. The net effect on propellant acceleration sensitivity will depend on the relative magnitudes of the two effects.

The main conclusions derived from the aluminized propellants are as follows: 1) Accelerations normal and into the burning surface of the nominal burning rate aluminized propellants were found to affect their burning rates; 2) the burning rate of an individual strand was found to decrease as the strand proceeded to burn; 3) the acceleration sensitivity of the aluminized propellants exhibited no consistent pressure dependence; 4) an increased initial temperature was not found to affect the acceleration sensitivity of the single propellant so investigated; and 5) the primary factor affecting the relative acceleration sensitivities of the aluminized propellants was the amount of aluminum and/or aluminum oxide retained in the spent inhibitor cases. There was an inverse relationship between the amount of burning rate increase experienced by a propellant and the percentage of the original aluminum retained on the surface of the propellant. This inverse relationship can be explained by postulating at least two distinct burning rate augmentation modes: 1) A relatively fast combustion mode in which distinct agglomerates determine the overall propellant burning rate, and 2) a slower combustion mode in which the surface of the propellant is covered

with a continuous "flood" layer. Those propellants which become "flooded" the soonest after ignition experience the least burning rate increase and the greatest aluminum retention, whereas those propellants which tend to remain in the discrete agglomerate combustion mode the longest after ignition experience the greatest burning rate increase and the least aluminum retention.

The primary factor affecting aluminum retention was found to be the aluminum particle size. Increasing the aluminum size from 10.6 μ mmd to 28 μ mmd in otherwise similar propellants was found to decrease the amount of aluminum retained on the propellant surface. It was also found that increasing the size of the coarse AP particles and increasing the weight percentage of the fine AP particles reduced the amount of aluminum retention. No consistent pressure or basic burning rate dependence was found for the amount of aluminum retention. Once the surfaces of the five propellants became "flooded," they burned at essentially equal absolute burning rates dependent primarily on the size of the coarse AP particles in the propellants.

A propellant formulated with aluminum oxide replacing aluminum was found to exhibit a greater acceleration sensitivity than the analogous aluminized propellant. This suggests that heat transfer is an important mechanism in the overall augmentation phenomenon.

Acceleration as great as 1018 G produced very little or no burning rate augmentation (< 6 per cent at most) for two fast burning rate propellants burned at 1000 and 1500 psia. This indicates that employing very small AP particles together with burning rate catalysts is an effective way to control burning rate augmentation.

The erosive burning rate experiments indicate that the erosive effect is inversely proportional to the acceleration level when the acceleration is directed into the propellant burning surface. It is also tentatively concluded on the basis of two experiments that directing the acceleration field away from the propellant surface results in a decreased erosive effect.

The models proposed by Crowe [9] and Glick [8] do not adequately predict the relative acceleration sensitivities of the basic series of aluminized propellants. The results of this investigation suggest that any new model will have to account for the unsteady accumulation of aluminum and/or aluminum oxide on the propellant surface and the heat transfer from the flame zone to the propellant surface through the low thermal resistance agglomerates on the propellant surface.

Investigations of a fundamental nature, as recommended in Chapter VI, are required to gain further understanding of the mechanisms involved.

REFERENCES

1. "Investigation of Performance Losses and Ballistics Effects in Solid Propellant Rockets," UTC 2197-FR (Naval Ordnance Systems Command Contract No. NOw 66-0444C), United Technology Center, Sunnyvale, California, April, 1967.

2. Vecchio, R., and Harnett, S., "Static Spin Testing of Solid Propellant Rockets," Bulletin of the First Meeting of ICRPG Working Group on Static Testing, CPIA Publication No. 24, October, 1963.

3. Anderson, J., "An Investigation of the Effect of Acceleration on the Burning Rate of Composite Propellants," unpublished Ph.D. thesis, Naval Postgraduate School, Monterey, California, August, 1966.

4. "Compilation of Spin Data Program, Technical Summary No. 1," Report No. 2122-1, Emerson Electric Co., St. Louis, Mo., January, 1967.

5. "Compilation of Spin Data Program, Technical Summary No. 2," Report No. 2122-2, Emerson Electric Co., St. Louis, Mo., May, 1967.

6. Anderson, J., and Reichenbach, R., "76-Inch Diameter Centrifuge Facility," Department of Aeronautics, Technical Note 66T-4, Naval Postgraduate School, Monterey, California, September, 1966.

7. Glick, R., "The Effect of Acceleration on the Burning Rate of Non-Metallized Composite Propellants" (paper presented at the ICRPG 3rd Combustion Conference, John F. Kennedy Space Center, October 17-21, 1966).

8. Glick, R., "An Analytical Study of the Effects of Radial Acceleration Upon the Combustion Mechanism of Solid Propellant," Thiokol Report No. 42-66, NASA Report No. 66218, Thiokol Chemical Corporation, Huntsville, Alabama, December, 1966.

9. Crowe, C., and Willoughby, P., "Effect of Spin on the Internal Ballistics of a Solid Propellant Motor," AIAA Paper No. 66-253 [presented at the AIAA Fourth Aerospace Sciences Meeting (West Coast), June 27-29, 1966].

10. Summerfield, M., et. al., "Burning Mechanism of Ammonium Perchlorate Propellants," Progress in Astronautics and Rocketry, Vol. 1, New York: Academic Press, 1960, p. 142.

11. Northam, G., "An Experimental Investigation of the Effects of Acceleration on the Combustion Characteristics of an Aluminized Composite Solid Propellant," Proceedings of the ICRPG/AIAA Solid Propulsion Conference, CPIA Publication No. 111, Vol. II, Washington, D. C., July, 1966, p. 129.

12. "Aluminum Particle Combustion Progress Report 1 April 1964-30 June 1965," Technical Progress Report 415, Naval Ordnance Test Station, China Lake, California, April, 1966.

13. Crump, J., "Aluminum Combustion in Composite Propellants," Proceedings of the Second ICRPG Combustion Conference, Aerospace Corp., El Segundo, California, November 1-5, 1965.

14. "Investigation of Particle Growth and Ballistic Effects on Solid Propellant Rockets," UTC 2128-FR (BuWeps Contract No. NOw 65-022f), United Technology Center, Sunnyvale, California, June 1966.

15. Glick, R., Hodge, B., and Caveny, L., "Effect of Acceleration on the Burning Rate of Composite Propellants," AIAA Paper No. 67-470 (presented at the AIAA Third Joint Propulsion Specialist Conference, Washington, D. C., July, 1967).

16. Miller, E., "Erosive Burning of Composite Solid Propellants," Combustion and Flame, 10 (1966), 330.

17. Corner, J., "The Effect of Turbulence on Heterogeneous Reaction Ratio," Trans Faraday Soc, 43 (1947), 635.

18. Lenoir, J., and Robillard, G., "A Mathematical Method to Predict the Effects of Erosive Burning in Solid Propellant Rockets," Sixth Symposium (International) on Combustion. New York: Reinhold, 1957. p. 663.

19. Green, Jr., L., "Erosive Burning of Some Composite Solid Propellants," Jet Propulsion, 24 (1954), 9.

20. Wimpress, R., Internal Ballistics of Solid Fuel Rockets. 1st edition. New York: McGraw-Hill Book Co., Inc., 1950.

21. Fenn, J., "A Phalanx Flame Model for the Combustion of Composite Solid Propellants," Project Squid Technical Report PR-114-P, April, 1967.

22. Bastress, E., "Modification of the Burning Rates of Ammonium Perchlorate Solid Propellants by Particle Size Control," Department of Aeronautical Engineering, Aeronautical Engineering Report No. 536 [ONR Contract Nonr 1858 (32)-NR 098-201], Princeton University, Princeton, New Jersey, March, 1961.

23. Eisenklam, P., Arunachalam, S., and Weston, J., "Evaporation Rates and Drag Resistance of Burning Drops," Eleventh Symposium (International) on Combustion. Pittsburg, Pennsylvania: The Combustion Institute, 1967, p. 715.

24. Mann, R., Marston, C., and Stokes III, B., "Control of Solid Propellant Combustion," Journal of Spacecraft and Rockets, 3 (1966), 1196.

25. Davis, A., "Solid Propellants: The Combustion of Particles of Metal Ingredients," Combustion and Flame, 7 (1963), 359.

APPENDIX I

DERIVATION OF AN EXPRESSION FOR B IN TERMS OF EROSIVE MOTOR PARAMETERS AND PROPELLANT BURNING RATES.

An expression for the mass flux per unit area, B, is derived based on the following assumptions:

1. The burning rate at a given distance from the fore end of the propellant strand can be expressed as $r_e = r_{x=o} + c_1 x$ where $r_{x=o}$ and C_1 are determined from a least squares fit to the experimental data.
2. The instantaneous burning rate at any x distance from the fore end of the propellant strand is constant and equal to the average burning rate at that x.

It follows from the first assumption that the propellant surface remains plane during burning. This allows geometric simplifications to be made in the determination of an expression for B. The second assumption was necessary because no practical way of determining instantaneous burning rate was available.

Let:

x = the distance of the timing wire from the fore end of the propellant strand (inch)

y = thickness of the propellant strand at the timing wire location (inch)

w = width of the propellant strand (inch)

h = channel height above the propellant strand (inch)

ρ_{s_e} = density of the propellant ($lbm/inch^3$)

$r_{x=o}$ = average burning rate at the fore end of the propellant strand (inch/sec)

c_1 = constant in the burning rate equation $r_e = r_{x=o} + c_1 x$ obtained from a least squares fit to the experimental burning rate data (sec^{-1})

t_w = $y/(r_{x=o} + c_1 x)$, burning time of the propellant at x as derived from the burning rate equation (sec)

B = cross-sectional-average mass velocity in the flow channel ($lbm/inch^2$ sec)

The depth, y_o, to which the fore end of the propellant strand has burned after time, t_w, is given by,

$$y_o = r_{x=o}\, t_w \qquad \text{I-1}$$

The mass of propellant, m, which has passed the cross-section at x in time, t_w, is given by,

$$m = \rho_{s_e}\, xw\left(\frac{y_o + y}{2}\right) \qquad \text{I-2}$$

The time average cross-sectional area, A, during propellant burning at the cross-section x is,

$$A = \frac{1}{2}\, w[h + (h+y)] \qquad \text{I-3}$$

Now defining $B = m/A\, t_w$ and using Equations I-1, I-2, and I-3, and the definition of t_w yield after simplification,

$$B = \frac{\rho_{s_e}\, x\, [2r_{x=o} + c_1 x]}{2h + y} \qquad \text{I-4}$$

APPENDIX II

DETERMINATION OF THE FRACTION OF OXIDIZER MASS CONSUMED ON THE PROPELLANT SURFACE AS A FUNCTION OF CRITICAL PARTICLE DIAMETER

Particle size distributions as shown in Plates 12 through 16 are described in terms of cumulative mass percentage. That is, the distribution curve starts with 100 per cent of the particles having a diameter less than the largest diameter present. From this point each location on the curve indicates the percentage by mass of the particles which are smaller than the diameter corresponding to that location. Finally a diameter is reached which is smaller than all particles present.

Given a particle diameter it is possible to use the particle size distribution to find what mass percentage of the particles are larger than the given particle diameter. Thus it is possible to ascertain the mass percentage of the distribution which is removed when all particles larger than a certain size are removed from the distribution. For instance, for the 9 μ mmd AP distribution shown in Plate 12, 40 per cent of the mass would be lost if all particles over 10 μ were removed from the distribution. Given two particle diameters it is possible to ascertain the mass percentage of the particles which have a size between the two given diameters. For instance, for the same AP distribution 28 per cent of the particle mass is contained in particles which have a diameter larger than 7 μ and smaller than 10 μ.

The particle size distribution cannot be used directly to ascertain the mass fraction which is removed from a distribution when all particles larger than a certain diameter are reduced to that diameter. For example, if the particles between 7 and 10 μ were all

reduced to 7 μ in diameter, the mass removed from the distribution would not be 28 per cent of the original mass as would be the case if these same particles were completely removed from the distribution. The amount of mass removed by reducing all the particles between the diameters of 7 and 10 μ to a diameter of 7 μ would only be a fraction of the original 28 per cent.

The mass fraction of the 9 μ mmd AP mass distribution removed by combustion at the propellant surface, J, as a function of critical particle diameter, d_{p_c}, was estimated in the following manner. The particles in the distribution were considered to be separated according to diameter into fifteen increments, each 2 μ's wide. The percentage of the entire distribution's mass contained in those particles in each 2 μ increment was obtained from the distribution curve shown in Plate 12. For example the distribution curve in Plate 12 shows that 3 per cent of the distribution's mass is contained in particles between 18 and 20 μ in diameter, whereas 8 per cent of the distribution's mass is contained in particles between 12 and 14 μ in diameter.

The assumption was made that the particles were homogeneous and spherical. Then for a given critical particle diameter that fraction of mass removed from a given 2 μ particle size increment was estimated by the equation:

$$m_f = 1 - \left(\frac{d_{p_c}^*}{d_{p_i}} \right)^3$$

where:

m_f = fraction of mass removed from a given 2 μ particle size increment

$d_{p_c}^* = d_{p_c} - 1$ (micron)

d_{p_i} = initial mean particle diameter within a given size increment (equal to the arithmetic mean of the end points of the size increment) (micron)

Multiplying m_f for a given size increment by the percentage of the particle distribution mass contained within that increment yields the fraction of the original particle mass contained in that increment which is removed from the distribution by reducing all particles in that increment to the given critical diameter. Then summing over all the 2 μ size increments yields the fraction of the distribution's mass removed when all the particles in the distribution are reduced to the critical size.

The calculation of three points on the plot shown in Figure 59 will serve to clarify the procedure. From the particle size distribution as reported by N.W.C. we have:

0.5 per cent by mass of the particles between 28 and 30 μ in diameter,

0.5 per cent by mass of the particles between 26 and 28 μ in diameter, and

1.0 per cent by mass of the particles between 24 and 26 μ in diameter.

Then for

$$d_{p_c} = 28\ \mu \quad J = 0.005\ [1 - (27/29)^3] = 0.00096$$

$$d_{p_c} = 26\ \mu \quad J = 0.005\ [1 - (25/29)^3] + 0.005\ [1 - (25/27)^3] = 0.002827$$

$$d_{p_c} = 24\ \mu \quad J = 0.005\ [1 - (23/29)^3] + 0.005\ [1 - (23/27)^3] + 0.01\ [1 - (23/25)^3] = 0.006628$$

The calculation was continued to account for all the particles in the distribution. The results are plotted in Figure 59.

APPENDIX III

DERIVATION OF AN EXPRESSION FOR THE HEAT TRANSFER RATE THROUGH AN AGGLOMERATE FROM THE FLAME ZONE TO THE PROPELLANT SURFACE

An expression for the heat transfer rate through an agglomerate is derived. The expression allows an estimate to be made of the heat transfer rate to the propellant surface with and without the interposition of an agglomerate between the flame zone and the propellant surface. In addition, the expression can be used to compare the relative magnitudes of the heat transfer rate through and the chemical energy release rate of an agglomerate.

An expression for the heat transfer rate is derived based on the following assumptions: 1) The process is steady-state; 2) the agglomerate is a homogeneous solid sphere with a constant thermal conductivity, K_{ag}; 3) heat is generated uniformly in the agglomerate at a rate q''' per unit volume; 4) polar symmetry exists in the agglomerate; 5) the agglomerate is imbedded in the solid phase of propellant to its equatorial plane; and 6) the temperature gradient in the gas phase, C_2, is constant between the propellant surface and the flame zone. Figure 64a illustrates the model and defines the nomenclature.

Making use of the first four assumptions, the governing differential equation for the temperature in the agglomerate, T, becomes

$$r^2 \frac{\partial^2 T}{\partial r^2} + 2r \frac{\partial T}{\partial r} + \frac{\partial^2 T}{\partial \theta^2} + \cot \theta \frac{\partial T}{\partial \theta} + \frac{q'''}{K_{ag}} = 0 \qquad \text{(III-1)}$$

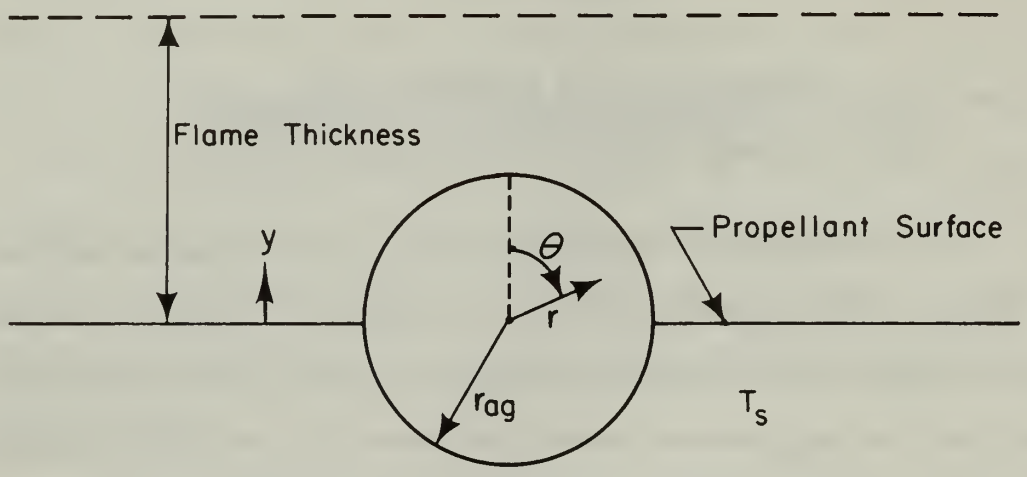

a. The Agglomerate Model and Nomenclature

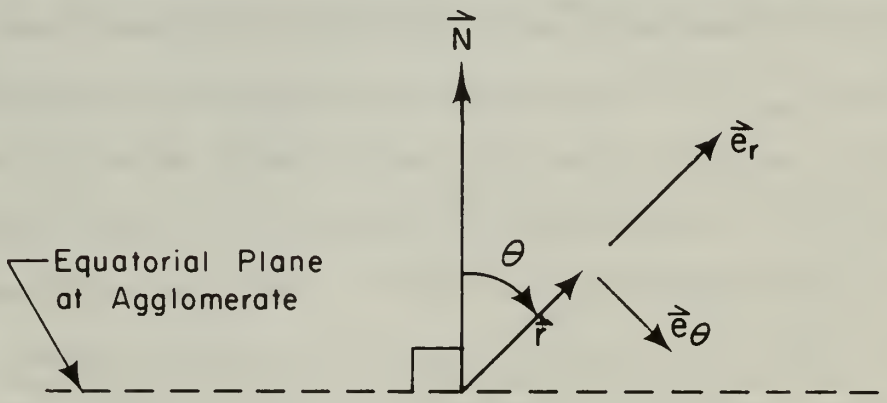

b. Vector Relations

FIGURE 64 THE AGGLOMERATE HEAT TRANSFER MODEL

The last two assumptions yield the boundary conditions

$$T(r_{ag},\theta) = T_s + C_2 Y = T_s + C_2\, r_{ag} \cos\theta \qquad 0 \leq \theta \leq 90° \qquad \text{(III-2)}$$

and

$$T(r_{ag},\theta) = T_s \qquad 90° \leq \theta \leq 180° \qquad \text{(III-3)}$$

Substitution of a new variable

$$T^*(r,\theta) = T(r,\theta) - T_s - \frac{q'''}{K_{ag}} (\ln r_{ag} - \ln r) \qquad \text{(III-4)}$$

into the governing differential equation yields

$$r^2 \frac{d^2T^*}{dr^2} + 2r \frac{dT^*}{dr} + \frac{\partial^2 T^*}{\partial\theta^2} + \cot\theta \frac{\partial T^*}{\partial\theta} = 0 \qquad \text{(III-5)}$$

and the boundary conditions become

$$T^*(r_{ag},\theta) = C_2\, r_{ag} \cos\theta \qquad 0 \leq \theta \leq 90° \qquad \text{(III-6)}$$

and

$$T^*(r_{ag},\theta) = 0 \qquad 90° \leq \theta \leq 180° \qquad \text{(III-7)}$$

Equations III-5, III-6, and III-7 represent the Dirichlet problem for the steady-state temperature in a uniform solid when the temperature on the surface is given. Using the standard separation of variables technique, assume that

$$T^*(r,\theta) = R(r)\,\Theta(\theta) \qquad \text{(III-8)}$$

then Equation III-5 becomes

$$r^2R''\Theta + 2r\,R'\Theta + R\Theta'' + \cot\theta\, R\Theta' = 0 \qquad \text{(III-9)}$$

Separation of variables yields the following equations

$$r^2 \frac{R''}{R} + 2r \frac{R'}{R} - \lambda^2 = 0 \qquad \text{(III-10a)}$$

and

$$\frac{\Theta''}{\Theta} + \cot\theta \frac{\Theta'}{\Theta} + \lambda^2 = 0 \qquad \text{(III-10b)}$$

Let $x = \cos\theta$ and $X(x) = \Theta(\theta)$, then Equation III-10b becomes after simplification

$$(1-x^2)X - 2xX' + \lambda^2 X = 0 \qquad \text{(III-11)}$$

Equation III-11 is Legendre's equation and has solutions [when $\lambda^2 = N(N+1)$, N a positive integer] of the form

$$X(x) = A_N P_N(x) \qquad \text{(III-12)}$$

where A_N are constants to be evaluated from the boundary conditions and $P_N(x)$ are the Legendre polynomials.

Equation III-10a is an equidimensional equation which has the solution

$$R(r) = C_3 r^{-\frac{1}{2}+\sqrt{\frac{1}{4}+\lambda^2}} + C_4 r^{-\frac{1}{2}-\sqrt{\frac{1}{4}+\lambda^2}} \qquad \text{(III-13)}$$

but $\lambda^2 = N(N+1)$, hence

$$R(r) = C_3 r^N + C_4 r^{-(N+1)} \qquad \text{(III-14)}$$

Since R (0) is bounded, $C_4 = 0$. Then, using Equations III-8, III-12, and III-14 and absorbing the constant C_3 into the A_N's, one obtains

$$T^*(r,x) = \sum_{N=0}^{\infty} A_N P_N(x) r^N \qquad \text{(III-15)}$$

The boundary conditions, Equations III-6 and III-7, can be rewritten in terms of the independent variable x (recall $x = \cos\theta$).

$$T^*(r_{ag},x) = C_2 r_{ag} x \qquad 0 \leq x \leq 1 \qquad \text{(III-6a)}$$

$$T^*(r_{ag},x) = 0 \qquad -1 \leq x \leq 0 \qquad \text{(III-7a)}$$

The constants A_N can be evaluated as follows. Rewrite Equation 15 as

$$\int_{-1}^{1} T^*(r_{ag},x) P_K(x)dx = \sum_{N=0}^{\infty} \int_{-1}^{1} A_N r_{ag}^N P_N(x) P_K(x)dx \qquad \text{(III-15a)}$$

It follows from the orthogonality of the Legendre polynomials, that the right hand side of Equation III-15a is 0 except when N = K. Then

$$\int_{-1}^{1} T^*(r_{ag},x) P_N(x)dx = A_N r_{ag}^N \int_{-1}^{1} P_N^2(x)dx = \frac{2A_N r_{ag}^N}{2N+1} \qquad \text{(III-16)}$$

or

$$A_N = \frac{2N+1}{2r_{ag}^N} \int_{1}^{1} T^*(r_{ag},x) P_N(x)dx \qquad \text{(III-17)}$$

Using Equations III-6a and III-7a in Equation III-17 yields

$$A_N = \frac{(2N+1)C_2\, r_{ag}^{N-1}}{2} \int_0^1 xP_N(x)dx \qquad \text{(III-18)}$$

The first few coefficients, A_N, were evaluated as:

$$A_o = \frac{C_2 r_{ag}}{4} \; ; \quad A_1 = \frac{C_2}{2} \; ; \quad A_2 = \frac{5C_2}{10r_{ag}} \; ; \quad A_3 = 0$$

$$A_4 = \frac{-9C_2}{96r_{ag}^3} \; ; \quad A_5 = 0 \; ; \quad A_6 = \frac{13C_2}{256r_{ag}^5} \; ; \quad A_7 = 0$$

The temperature distribution in the agglomerate, T, is given by combining Equations III-4 and III-15 and using the values of A_N. There results

$$T(r,x) = T_s + \frac{q'''}{K_{ag}} \ln \frac{r_{ag}}{r} + \frac{C_2 r_{ag}}{4} + \frac{C_2}{2} r\, P_1(x) + \frac{5C_2}{16r_{ag}} r^2\, P_2(x) - \frac{9C_2}{96r_{ag}^3} r^4\, P_4(x) + \frac{13C_2}{256r_{ag}^5} r^6\, P_6(x) + \ldots\ldots\ldots \qquad \text{(III-19)}$$

or upon substitution of the Legendre polynomials

$$T(r,\theta) = T_s + \frac{q'''}{K_{ag}} \ln \frac{r_{ag}}{r} + \frac{C_2}{4} r_{ag} + \frac{C_2}{2} r \cos\theta + \frac{5C_2}{32r_{ag}} r^2 (3\cos^2\theta - 1)$$

$$- \frac{9C_2}{768} \frac{r^4}{r_{ag}^2} (35\cos^4\theta - 30\cos^2\theta + 3) + \frac{13C_2 r^6}{4096r_{ag}^5} (231\cos^6\theta - 315\cos^4\theta$$

$$+ 105\cos^2\theta - 5) + \ldots\ldots \qquad \text{(III-20)}$$

The remaining terms in the series are all constants or even functions of cos θ.

The heat flux to the propellant surface in contact with the agglomerate is equal to the heat flux conducted through the equatorial plane of the agglomerate plus the heat generated in the lower hemisphere of the agglomerate. The heat flux through the equatorial plane of the agglomerate can be found by using Equation III-20.

In spherical coordinates with polar symmetry

$$\frac{dT}{d\vec{r}} = \frac{\partial T}{\partial r}\vec{e}_r + \frac{1}{r}\frac{\partial T}{\partial \theta}\vec{e}_\theta \qquad \text{(III-21)}$$

where the vectors $\vec{r}$, $\vec{e}_r$, and $\vec{e}_\theta$ are defined in Figure 64b. Let $\vec{N}$ be a unit vector perpendicular to the equatorial plane of the agglomerate. Then the temperature gradient perpendicular to the equatorial plane is given by

$$\vec{N} \cdot \frac{dT}{d\vec{r}} = \frac{\partial T}{\partial r}\cos\theta + \frac{1}{r}\frac{\partial T}{\partial \theta}(-\sin\theta) \qquad \text{(III-22)}$$

At the equatorial plane, $\theta = \frac{\pi}{2}$, the magnitude of the temperature gradient parallel to the vector $\vec{N}$ is

$$\left|\frac{dT}{d\vec{r}}\right| = \frac{1}{r}\frac{\partial T}{\partial \theta}\bigg|_{\theta = \frac{\pi}{2}} \qquad \text{(III-23)}$$

and the rate of heat flux through the equatorial plane, $\dot{q}_{ag}$, is

$$\dot{q}_{ag} = -K_{ag}\frac{\pi r_{ag}^2}{r}\frac{\partial T}{\partial \theta}\bigg|_{\theta = \frac{\pi}{2}} \qquad \text{(III-24)}$$

The minus sign is necessary because the direction of the heat flux is opposite the direction of the vector $\vec{N}$.

Differentiation of Equation III-20 with respect to θ and subsequent evaluation of the derivative at $\theta = \frac{\pi}{2}$ yields

$$\frac{\partial T}{\partial \theta}\bigg|_{\theta = \frac{\pi}{2}} = -\frac{C_2 r}{2} \qquad \text{(III-25)}$$

Only one term remains upon evaluation at $\theta = \frac{\pi}{2}$ because after differentiation of Equation III-20 every term except one contains $\cos\theta$ raised to some power greater than one. Therefore, recalling that C_2 is the temperature gradient in the gas phase ($C_2 = dT/dy$), there is obtained

$$\dot{q}_{ag} = \frac{1}{2} K_{ag} \pi r_{ag}^2 \, dT/dy \qquad \text{(III-26)}$$

Equation III-26 is the desired expression for the rate of heat flux from the flame zone to the propellant surface through an agglomerate. The total heat transfer rate to the propellant surface will equal the sum of $\dot{q}_{ag}$ and the rate of heat generation in the lower hemisphere of the agglomerate. The relative magnitude of these rates is considered in Chapter VI.

An equal area of propellant surface not covered by an agglomerate experiences a heat transfer rate equal to

$$\dot{q}_{prop} = K_g \pi r_{ag}^2 \, dT/dy \qquad \text{(III-27)}$$

where K_g is the gas phase conductivity. Combining Equations III-26 and III-27 yields for the ratio $\dot{q}_{ag}/\dot{q}_{prop}$

$$\frac{\dot{q}_{ag}}{\dot{q}_{prop}} = \frac{K_{ag}}{2 K_g} \qquad \text{(III-28)}$$

Equations III-26 and III-28 are the desired results.

APPENDIX IV

PROPELLANT FORMULATIONS

	P401	P410	P411	P412	P413	P414	P415	P420	P421	P423
10.6 μ mmd Al	14.0								15.0	
28 μ mmd Al				5.0	15.0		15.0			15.0
9 μ mmd AP		19.62	34.0	16.83	11.26	17.32	27.15	19.62	11.26	11.26
68 μ mmd AP	68.0									
94 μ mmd AP		59.38	45.0	58.22	55.89	57.73	40.0			
200 μ mmd AP								59.38	55.89	55.89
9.3 μ mmd Al_2O_3						5.0				
PBAN Binder	18.0	21.0	21.0	19.95	17.85	19.95	17.85	21.0	17.85	17.85

INITIAL DISTRIBUTION LIST

		No. Copies
1.	Defense Documentation Center Cameron Station Alexandria, Virginia 22314	20
2.	Library Naval Postgraduate School Monterey, California 93940	2
3.	Commander, Naval Ordnance System Command Department of the Navy Washington, D. C. 20360	1
4.	Chairman, Department of Aeronautics Naval Postgraduate School Monterey, California 93940	1
5.	Dr. Roy E. Reichenbach Room 1050, Bldg. 01 TRW Systems One Space Park Redondo Beach, California 90278	10
6.	Prof. Frank D. Faulkner Department of Mathematics Naval Postgraduate School Monterey, California 93940	1
7.	Dr. Allen E. Fuhs Department of Aeronautics Naval Postgraduate School Monterey, California 93940	1
8.	Dr. Paul F. Pucci Department of Mechanical Engineering Naval Postgraduate School Monterey, California 93940	1
9.	Dr. Louis V. Schmidt Department of Aeronautics Naval Postgraduate School Monterey, California 93940	1
10.	Dr. Michael H. Vavra Department of Aeronautics Naval Postgraduate School Monterey, California 93940	1
11.	Curricular Officer Aeronautical Engineering Programs Naval Postgraduate School Monterey, California 93940	1

		No. Copies
12.	Mr. Edward Michelson Department of Aeronautics Naval Postgraduate School Monterey, California 93940	1
13.	Dr. E. Lamar Naval Air Systems Command (Code 03C) Department of the Navy Washington, D. C. 20360	1
14.	Mr. I. Silver Naval Air Systems Command (Code 330) Department of the Navy Washington, D. C. 20360	1
15.	Mr. P. Fisher Naval Ordnance Systems Command (Code 03211) Department of the Navy Washington, D. C. 20360	1
16.	Mr. B. Drimmer Naval Ordnance Systems Command (Code 033) Department of the Navy Washington, D. C. 20360	1
17.	Mr. J. Murrin Naval Ordnance Systems Command (Code 0331) Department of the Navy Washington, D. C. 20360	1
18.	Dr. B. Wolfson Air Force Office of Scientific Research Arlington, Virginia 22202	1
19.	Dr. Billings Brown Institute for Defense Analyses 400 Army Navy Drive Arlington, Virginia 22202	1
20.	Mr. William D. Guthrie AMSMI - RKA Army Missile Command Bldg. 7120 Redstone Arsenal, Alabama 35809	1
21.	Dr. Martin Summerfield Department of Aerospace and Mechanical Sciences Princeton University Princeton, New Jersey 08540	1

		No. Copies
22.	Dr. John B. Fenn Department of Aerospace and Mechanical Sciences Princeton University Princeton, New Jersey 08540	1
23.	Mr. James P. Diebold Development Engineering Branch (Code 4571) Naval Weapons Center China Lake, California 93555	1
24.	Mr. James E. Crump Aerothermochemistry Group (Code 508) Naval Weapons Center China Lake, California 93555	1
25.	LCDR James B. Anderson, USN Operational Test and Evaluation Force, Pacific Naval Air Station, North Island San Diego, California 92135	1
26.	Dr. Clayton T. Crowe Physical Sciences Lab United Technology Center Sunnyvale, California 94088	1
27.	Mr. Melvin H. Lucy Mail Stop 498 NASA Langley Research Center Langley Station Hampton, Virginia 23365	1
28.	Mr. B. Hodge Aerothermodynamic Group Thiokol Chemical Corporation Huntsville, Alabama 35808	1
29.	Mr. Leo Manda Emerson Electric Company St. Louis, Missouri 63136	1
30.	Mr. Kenneth Johnson Missile and Information Systems Division Mail Stop 8C-76 The Boeing Company Seattle, Washington 98124	1
31.	Mr. L. Baxter Chemical Propulsion Division Hercules Incorporated Los Angeles, California 90005	1

		No. Copies
32.	Mr. R. Froelich Department 0735, Bldg. 2015 Aerojet-General Corporation Sacramento, California 95655	1
33.	Chairman, Department of Aeronautical and Astronautical Engineering The Ohio State University Columbus, Ohio 43210	1
34.	Dr. S. Penner Department of Aerospace and Mechanical Engineering University of California, San Diego La Jolla, California 92037	1
35.	Dr. Forman Williams Department of Aerospace and Mechanical Engineering University of California, San Diego La Jolla, California 92037	1
36.	Captain Charles Payne, USAF Air Force Rocket Propulsion Lab (Code RPMCP) Edwards Air Force Base, California 93523	1
37.	Captain R. Rowe, USN Strategic Offensive and Defensive Systems Office of the Chief of Naval Operations Navy Department Washington, D. C. 20360	1
38.	Mr. Robert Blaise Center for Naval Analyses Washington, D. C. 20360	1
39.	Dr. W. Rannie Guggenheim Laboratory California Institute of Technology Pasadena, California 91109	1
40.	LT Edward J. Sturm, USN Organization and Manpower Management Office (AIR 09B) Naval Air Systems Command Washington, D. C. 20360	6

DOCUMENT CONTROL DATA - R&D

(Security classification of title, body of abstract and indexing annotation must be entered when the overall report is classified)

1. ORIGINATING ACTIVITY *(Corporate author)*
Naval Postgraduate School
Monterey, California 93940

2a. REPORT SECURITY CLASSIFICATION
UNCLASSIFIED

2b. GROUP

3. REPORT TITLE
A Study of the Burning Rates of Composite Solid Propellants in Acceleration Fields

4. DESCRIPTIVE NOTES *(Type of report and inclusive dates)*
Thesis

5. AUTHOR(S) *(Last name, first name, initial)*
Sturm, Edward J., Lieutenant, USN

6. REPORT DATE	7a. TOTAL NO. OF PAGES	7b. NO. OF REFS
March 1968	226	25

8a. CONTRACT OR GRANT NO.

b. PROJECT NO.

c. Req. No. 17-7-5073

d.

9a. ORIGINATOR'S REPORT NUMBER(S)

9b. OTHER REPORT NO(S) *(Any other numbers that may be assigned this report)*

10. AVAILABILITY/LIMITATION NOTICES
[redacted]

11. SUPPLEMENTARY NOTES

12. SPONSORING MILITARY ACTIVITY
Naval Ordnance Systems Command
Navy Department
Washington, D. C.

13. ABSTRACT

The average burning rates of a series of composite solid propellants were measured in acceleration fields up to 1000 G using a combustion bomb mounted on a centrifuge. The propellants were burned at constant pressures of 500, 1000, and 1500 psia. Specially prepared motors allowed the study of the effect of simultaneous erosive and acceleration induced burning rate increases.

The burning rates of both the non-metallized and the majority of the metallized propellants were found to depend on acceleration. The effect of acceleration was found to depend on the basic burning rates of the propellants and the aluminum and oxidizer particle sizes and weight percentages. The burning rates of two very fast burning rate propellants were found to be essentially independent of acceleration. The erosion sensitivity of a propellant was found to decrease with increasing acceleration.

A model was developed which successfully correlates the experimental results obtained for the non-metallized propellants. The experimental results for the metallized propellants could not be correlated by either of two models proposed by other investigators. This result indicates that a more complex model is required to explain the observed acceleration effects for metallized propellants.

14 KEY WORDS	LINK A		LINK B		LINK C	
	ROLE	WT	ROLE	WT	ROLE	WT
Solid Propellant						
Burning Rate						
Acceleration						
Erosive Burning